CRISPR/Cas9 genome editing of Recessive Dystrophic Epidermolysis Bullosa (RDEB) mutation hotspot

Candidate:

Gaetano Naso

Supervisors:

Prof Waseem Qasim

Dr Anastasia Petrova

Great Ormond Street

Institute of Child health

University College London

A thesis submitted for the degree of Doctor of Philosophy

Declaration:

I, Gaetano Naso confirm that the work presented in this thesis is my own. Where information has been derived from other sources, I confirm that this has been indicated in this thesis.

Signature: Gaetano Naso

Date: May 2021

Abstract

Recessive dystrophic epidermolysis bullosa (RDEB) is a severe life-threatening skin adhesion disorder caused by loss-of-function mutations in the *COL7A1*-encoding type VII collagen (C7), a structural protein playing a crucial role in anchoring fibril (AF) formation at the dermal-epidermal junction (DEJ).

Combinatorial cell and gene therapies based on the addition of a full-length copy of *COL7A1* cDNA in RDEB keratinocytes, fibroblasts and skin equivalents have shown potential in preclinical and clinical settings although only modest and transient improvements have been reported. In parallel, induced pluripotent stem cells (iPSCs) are being investigated in preclinical studies for RDEB. iPSCs represent a valuable source of autologous patient material and can be differentiated into keratinocytes and fibroblasts for cellular therapy applications. Implementation of CRISPR/Cas9 and base editing-mediated gene correction in patient-derived iPSCs has allowed for the generation of autologous cellular models capable of overcoming barriers of conventional gene therapy.

In this regards, the work described in this thesis aims to evaluate the feasibility of genome-editing approaches using CRISPR/Cas9 and Cytosine Base editing (BE) platforms to correct a mutation hotspot (c.425A>G, p.Lysl42Arg) within exon 3 of *COL7A1* gene in patient-derived iPSCs. Gene repair by homology-directed recombination (HDR) following CRISPR/Cas9-induced double-strand breaks (DSBs) through viral and non-viral donor template deliveries resulted in a significant correction of the *COL7A1* locus on genomic level. To avoid concerns surrounding the generation of DSBs, seamless BE-based G:C to A:T conversion resulted in a high restoration of the wild type *COL7A1* sequence. Ultimately, capacity of gene- and base-corrected RDEB iPSCs to be differentiated in into keratinocytes (iKer) was evaluated *in vitro* and functional recovery of *de novo* C7 was assayed on protein level.

Overall, this study explored the potential of CRISPR/Cas9 and BE site-specific correction of *COL7A1* in RDEB-derived pluripotent stem cells. Furthermore, it demonstrated that gene-corrected iPSCs can be used as a source of epidermal

progenitors thereby confirming their potential for future cell therapies for skin disorders.

Impact statement

Over the past decades, correction of life-threatening inherited skin disorders by gene addition have shown significant potential for preclinical and clinical implementation with significant progress made for Recessive Dystrophic Epidermolysis Bullosa (RDEB). Advances in the field have allowed for the development of *ex vivo* cellular therapy approaches via delivery of a copy of full-length *COL7A1* transgene via retroviral and lentiviral vectors. Despite recent promising *ex vivo* gene therapy application for other forms of epidermolysis bullosa, clinical trials based on genetically corrected skin grafts for RDEB are hurdled by technical and biological limitations. On the other hand, targeted genome editing tools have the potential to overcome barriers associated with conventional gene addition approaches and several proof-of-concept studies have shown the feasibility of precise *COL7A1* restoration under its endogenous promoter.

This report describes investigations and evaluation of precise gene correction using the CRISPR/Cas9 and Cytosine Base genome editing systems, including in RDEB patient-derived induced pluripotent stem cells (iPSCs).

In the first instance, the study focused on the design of CRISPR/Cas9 and base editing strategies to target a specific *COL7A1* loss-of-function mutation hotspot (Chapter 3). In this regards, critical aspects of nuclease and donor template delivery by the means of viral or non-viral approaches were investigated. The second part of the study (Chapter 4) focused on investigating the feasibility of reprograming RDEB fibroblasts into induced pluripotent stem cells (RDEB-iPSCs) and evaluation of endogenous *COL7A1* repair by HDR-mediated donor templates and seamless C>T base correction using CB editors. Both systems have shown efficient and precise correction of *COL7A1* mutation hotspot in RDEB-iPSCs. In the final part of the project (Chapter 5) the ability of gene corrected iPSCs to be differentiated into keratinocytes was evaluated followed by the assessment of type VII collagen protein restoration *in vitro*.

Although this project reports the application of CRISPR/Cas9- and BE-mediated correction of a single point mutation, the gene targeting approaches described in this

manuscript would be suited to potentially correct a wide variety of *COL7A1* mutations involved in recessive (RDEB) and dominant dystrophic epidermolysis bullosa (DDEB).

Results of this study have contributed to a number of publications over the course of this PhD:

1. Naso G, Petrova A. Cellular therapy options for genetic skin disorders with a focus on recessive dystrophic epidermolysis bullosa. Br Med Bull; 2020, DOI: 10.1093/bmb/ldaa029.
2. Naso G, Petrova A. CRISPR/Cas9 gene editing for genodermatoses: progress and perspectives. Emerging Topics in Life Sciences; 2019,3:313:326, https://doi.org/10.1042/ETLS20180148
3. CRISPR/Cas9-Mediated in situ correction of COL7A1 splice-site mutation hotspot (2019) - Genome Engineering: Frontiers of CRISPR-Cas, Cold Spring Harbor – New York, USA
4. CRISPR/Cas9 genome editing of RDEB mutation hotspot (2018) - “The British Society of Gene and Cell Therapy” (BSGCT) – London, UK

Acknowledgements

This incredible opportunity would not have been possible without the supervision of Professor Waseem Qasim and Dr. Anastasia Petrova and for their priceless support throughout this project. All of my gratitude goes to them for believing in my capabilities and for their wise guidance. Over the course of my studies at UCL, they always offered me excellent support for my project giving me the opportunity to present my work at some of the most important national and international conferences of the field which I have truly appreciated.

I am also truly grateful to my funders Cure EB (formely Sohana Research Fund), the NIHR GOSH BRC doctoral training fund and the Synthego Genome Engineer Innovation Grant for their support of this project.

I would also say thank you for all the former and new members of the Qasim group for their amazing support, the friendship and trust matured over the course of my studies. My sincere thanks goes to everyone from the Molecular and Cellular Immunology group who have provided me with valuable advice, moral support and loads of laughs, important as well for completing this journey. I would particularly like to thank my old beloved friends Giada, Nicola, Giumy and Alessio for being my first port of call when I moved to London 4 years ago, and even more so for providing comic relief when most needed. On a more personal level, I am also deeply grateful to Barbara and for her constant patience, understanding and support especially while I have been writing my thesis. I feel so lucky that our paths crossed.

Finally, a very warm thank you goes to my family, for all the unconditional support and encouragement since my decision of moving in another country to start a new chapter of my life. No matter the distance between us, you have been always there for me. My biggest reward is making you proud and hoping that this life experience might be helpful for you, Eleonora, and for your bright future.

Table of contents

Figures

Tables

Abbreviations

2A self-cleaving peptides P2A

ABE ..... Adenine base editors

Anchoring fibrils ..... AFs

Ascorbic acid ..... AA

Base excision repair ..... BER

Basement membrane zone ..... BMZ

Base Editor ..... BE

Beta-2-Microglobulin B2M

Bone marrow transplantation ..... BMT

Bone morphogenic protein 4 ..... BMP-4

Cytidine Deaminase base editor ..... CBE

Clustered regularly interspaced short palindromic repeats ..... CRISPR

Complementary DNA ..... cDNA

CRISPR RNAs ..... crRNAs

CRISPR-associated protein 9 ..... Cas9

Deoxyribonucleic acid ..... DNA

Defined keratinocyte serum-free medium ..... DKSFM

Dermal-epidermal junction ..... DEJ

Dominant Dystrophic Epidermolysis Bullosa ..... DDEB

Dystrophic Epidermolysis Bullosa ..... DEB

Double stranded breaks ..... DSBs

Dulbeco's Modified Eagle Medium ..... DMEM

Dulbecco's Phosphate-Buffered Saline ..... PBS

Elongation factor1 alpha EF1α

Embryoid bodies ..... EBs

Embryonic stem cells ..... ESCs

Enhanced green fluorescence protein ..... EGFP

Epidermolysis Bullosa Simplex ..... EBS

Epidermolysis Bullosa ..... EB

Exon3-Distal guide Ex3D

Fluorescence activated cell sorting ..... FACS

Fluorescence *in situ* hybridization ..... FISH

Glycine-proline-hydroxyproline ..... Gly-X-Y

Good manufacturing practice ..... GMP

Hematopoietic cell transplantation ..... HTC

Hemidesmosome ..... HD

High fidelity SpCas9 ..... SpCas9-HF1

Homology directed recombination ..... HDR

Immunoepitope mapping ..... IFM

Immunofluorescence ..... IF

Induced pluripotent stem cells ..... IPSCs

Inference of CRISPR Edits ..... ICE

Insertions and deletions ..... InDels

Junctional Epidermolysis Bullosa ..... JEB

Keratin ..... K

Krüppel-like factor 4 ..... KLF-4

Meganuclease ..... MN

Mesenchymal stromal stem cells ..... MSCs

Messenger RNA ..... mRNA

Micrograms ..... µg

Microliters ..... µl

Monoclonal antibody ..... mAb

Multiplicity of Infection ..... MOI

Next generation sequencing ..... NGS

Non-collagenous domain NC-1

Non-homologous end joining ..... NHEJ

Non-integrating lentiviral vectors ..... NILV

Octamer binding transcription factor 3/4 ..... OCT3/4

Picomole ..... pmol

Polymerase chain reaction ..... PCR

Premature termination codon ..... PTC

Preintegration complex..... PIC

Primer binding site ..... PBS

Protospacer adjacent motif .....PAM

Quantitative polymerase chain reaction .....qPCR

Recessive Dystrophic Epidermolysis Bullosa.....RDEB

Retinoic acid .....RA

Rev responsive element..... RRE

Ribonucleoprotein complexes .....RNPs

Ribonucleic acid ..... RNA

RNA encapsidation signal..... Ψ

Self-inactivating.....SIN

Site directed mutageneis .....SDM

SRY (sex determining region Y)-box 2 .....Sox2

Skin equivalent.....SE

Single guide RNA .....sgRNA

Single nucleotide polymorphism .....SNP

Single-stranded oligonucleotides..... ssODNs

Synthesis-dependent strand annealing .....SDSA

Squamous cell carcinoma..... SCC

Stage-specific embryonic antigen-4..... SSEA4

Tracking of InDels by Decomposition..... TIDE

Trans-activating crRNA.....tracrRNA

Transcription activator-like effector nucleases ..... TALENs

Transient activating cells..... TA

Transmission electron microscopy ..... TEM

Transporter associated with Antigen Processing 1..... TAP1

Type VII collagen alpha 1 protein C7

Tumour recognition antigen ..... TRA

Uracil DNA glycosylase inhibitor ..... UGI

Uracil N-glycosylase ..... UNG

Vector copy number..... VCN

Vesicular stomatitis virus glycoprotein..... VSV-G

Wild-type..... WT

Woodchuck Hepatitis virus posttranscriptional regulatory element ..... WPRE

Zinc-finger nucleases..... ZFNs

Zinc-finger proteins..... ZFPs

Chapter 1 Introduction

1.1 Epidermolysis bullosa: overview

Epidermolysis bullosa (EB) constitutes a group of genetically heterogeneous skin disorders mainly characterized by chronic erosion and blistering of the skin and mucous membrane at birth or during the adulthood. Although main clinical manifestations involve skin and mucous membranes, extracutaneous manifestations affecting hair, nails, teeth and gastrointestinal and oesophageal tracts make EB a systemic disease. The outcome for patients affected by EB is correlated with the spectrum of phenotypic manifestation. Forms of EB range from mild, where life-long blistering has no impact on the overall longevity of patients, to severe life-threating conditions due to metabolic perturbations, dehydration and chronic infections of the blistered skin. In addition, some forms of EB are characterized by debilitating scarring leading to highly aggressive skin cancer, lethal by young adulthood. Currently, clinical management is still focused on reducing the symptoms of the disease. Wound care and daily dressing remain the cornerstone of treatment and the average annual cost per patients across the EU countries is estimated at € 31,3190 (Angelis et al., 2016).

Despite the broad phenotypic nature of EB clinical subtypes, at molecular level, most of the genes involved play key role in skin integrity and structural stability within the epidermis and between the epidermis and the dermis underneath. EB is known to result from mutations in 21 different genes (**Table 1.1**) expressed within the cutaneous basement membrane zone (BMZ) at the dermal-epidermal junction (DEJ) (Has et al., 2020). As a result of the mutations, the proteins produced in skin cells are either functionally impaired or absent. Expression of aberrant proteins corresponds to the presence of recurrent generalized or localized blisters, lesions and erosions of the skin and mucous tissues upon minor mechanical trauma with tendency for phenotype severity the deeper the cleavage occurs within the dermal-epidermal region. At the molecular level, the gravity of EB depends on the type of mutated gene, the localization of the corresponding protein within the cutaneous membrane zone at the DEJ and on the level of epidermal-dermal separation from the underlying basal

lamina. The genes involved can have either dominant or recessive inheritance. Since its first description based on electron microscopic features described in 1962 (Pearson 1962), traditionally, EB has been classified into four broad categories, determined by diagnostic transmission electron microscopy (TEM) of the BMZ and/or immunoepitope mapping (IFM).

Table 1.1 Summary table of molecular and clinical features of EB

EB Type	EBS			JEB		DEB		KS
Major EB subtypes	Suprabasal		Basal	Generalized	localized	RDEB	DDEB	Generalized
Subtype	Loc WC	Gen. Sev. DM	Gen. Int. nDM Koebner	Sev.(Herlitz) Int. (non-Herlitz)	inversa	Gen. Sev. Gen. Int. Localized	Gen.	
Inheritance	AR, AD			AR		AR	AD	AR
Most common clinical features	Blisters/erosions Crust Nail dystrophy Keratoderma Mechanical fragility Oral cavity erosions Growth retardation (occasional)			Blisters/erosions Crusts, Milia Dystrophic nails Atrophic scarring Granulation tissue (Herlitz), Scarring alopecia Mechanical fragility Oral cavity erosions Enamel hypoplasia severe growth retardation (Herlitz) anaemia (Herlitz) Gastrointestinal tract Involvement (Herlitz) Genitourinary tract (Herlitz) Ocular involvements (Herlitz)		Blisters/erosions Crust, Milia Dystrophic nails Atrophic scarring scalp abnormalities EB nevi (RDEB) Severe mechanical fragility anaemia (RDEB) Ocular involvements Gastrointestinal tract Growth retardation (RDEB) Squamous cell carcinoma (RDEB),		Blisters Atrophic scarring Dystrophic/ absent nails Granulation tissue, Keratoderma, Poikiloderma, Photosensitivity Colitis Esophagitis Squamous cell carcinoma (after age 30)
Death related to EB	None/uncommon			Common (Herlitz)		Common (RDEB)		Uncommon
Level of cleavage	Intra-epidermal			Lamina Lucida		Lamina densa		mixed
Genes involved	TGM5 PKP1 DSP JUP	KRT5, KRT14 PLEC1 EXPH5		LAMA3 LAMB3 LAMC2	LAMA3 LAMB3 LAMC2 COL17A1 ITGA3 ITGA6 ITGB4	COL7A1		FERMT1
Type of mutations	Spl, Del, NS, MS, In-frame InDels			MS, NS Ins, Spl		NS, Spl	MS, NS, Del, Ins	NS, Del, Spl, Ins, InDels

Summary table based on data collection from published data (Fine et al., 2014; Has et al., 2020) and from Dr. Christos Georgiadis (Georgiadis, 2016). Abbreviations: EBS, Epidermolysis Bullosa Simplex; JEB, Junctional Epidermolysis Bullosa; DEB, Dystrophic Epidermolysis Bullosa; KS, Kindler Syndrome; AR, Autosomal Recessive; AD, Autosomal Dominant; HD, Hemidesmosome; AF, Anchoring Fibril; KC, Keratinocyte; Spl, Splice site mutation; Del, Deletion; NS, Nonsense mutation; MS, Missense mutation; InDels, insertion/deletion; Gen, generalised; Loc, localised; Del, Deletion; NS, Nonsense mutation; MS, Missense mutation.

1.2 Structure and overview of the human skin

The skin is the largest organ in the human body and a first-order physical barrier against a wide range of environmental insults. Its functions include protection against pathogen invasion, chemicals, natural factors (e.g. UV light) and mechanical or environmental stress. Like every other organ, the skin is a dynamic tissue with a high adaptive response to external and internal signals. In this regard, it plays an important role in the immunologic surveillance, body fluid loss control, thermoregulation and sensorial functions. The complexity of its physiochemical and mechanical functions reflects a deeper complex network of different cell types which are finely regulated to co-work in different layers of the skin. The skin consists of three different layers as known as epidermis, dermis and the deeper subcutaneous fatty layer underneath, the hypodermis.

The epidermis is the outermost layer of the human skin and it comprises mainly of keratinocytes which are distributed in four distinct “strata” with an additional layer present in thicker skin found in the palms and soles (*strarum lucidum*) (**Figure 1.1**). The most external layer, the *stratum corneum*, consists of terminally differentiated enucleated cells, known as corneocytes, which essentially constitute the first line of separation and defence with the external environment. Corneocytes possess a flat cell morphology and are organized in a lipid-rich extracellular matrix which substitutes the cell-cell junctions present in the lowest layers. The barrier function is mainly supported by a process of cornification which keratinocytes undergo upon terminal differentiation.

The *stratum granulosum* is a thin layer of diamond-shaped cells mainly producing keratohyalin and lamellar granules which contain a wide range of keratins and glycolipids, respectively. Both those cellular products are secreted from keratinocytes and undergo towards biochemical modifications making a complex extracellular structure which keeps cells adherent together. Below, the *stratum spinosum,* contains irregular shaped keratinocytes due to their ability to contact neighbouring cells through desmosomes, and in the bottom layer, transient amplifying keratinocyte progenitors from the *stratum basale*, are found. In this last layer, active

keratinocyte stem cells are attached to the basement membrane and provide long-lived renewal of the epidermis around every 4 weeks. Additional other cell populations situated amongst the keratinocytes such as melanocytes, Merkel cells and Langerhans 'cells are distributed in different layers of the epidermis and are responsible for the pigmentation of the skin, mechanoreceptive and immune functions, respectively.

The importance of the human skin structure and all its different skin layer functions are two key factors that need to be carefully evaluated for clinical diagnosis for gernodermatoses and to assess the capacity of *ex vivo* transgenic keratinocyte stem cells to mimic a correct skin structure upon skin graft onto patients' wounds. Although progresses in translational research concerning the use of pre-clinical mouse models for skin wound healing and tissue regeneration, remarkable distinctions between the human and mouse skin morphophysiology make difficult to bridge the gap between preclinical and clinical studies. Nevertheless human and mouse skin have overlapping features, they greatily differs in skin thickness and cell number. Human skin is relatively thick and firm (> 100µm) whereas murine skin is thinner (>25 µm) and made by 2 to 3 layers of keratinocytes with a less pronounced cornified layer. Furthermore, a higher density of hair follicles could be seen in the murine epidermis compared to human skin where, in contrast, displays a sparse and uneven hair follicle distribution.

Underneath the epidermis, the dermis is a fibrous connective structure situated between the epidermis and the subcutaneous fat tissue, largely contributing towards water retention and tensile and supportive stability of the skin. It is made up of two different dermal layers called papillary dermis, in proximity to the epidermis, and a thick lower layer called reticular dermis. The cellular and extracellular composition of the two layers is different. The papillary dermis is mainly composed of loose connective tissue characterized by fibrous components released from fibroblasts and consists of collagen, specifically type I and III, elastic fibres, composed of elastin, fibrillin, microfibrils and polysaccharides. The main role of these components is to contribute to water retention and to support the epidermis with the tensile strength required upon mechanical stress from the environment. To a lesser extent, the

papillary dermis contains mast cells, localized in the perivascular areas of the dermis, which are involved in inflammatory reactions, wound healing and collagen remodelling (Wilgus and Wulff, 2014). The dermis also houses other cellular components such as histocytes which assist the skin immune system, blood vessels, contributing to thermoregulation and metabolic functions, nerve endings involved in sensorial perceptions and glands. The reticular dermis is made of dense connective tissue and constitutes the bulk of the dermis. The subcutaneous layers below the dermis offers insulation and energy storage but also has an active role in the hair follicle regeneration and wound healing (Kruglikov and Scherer 2016).

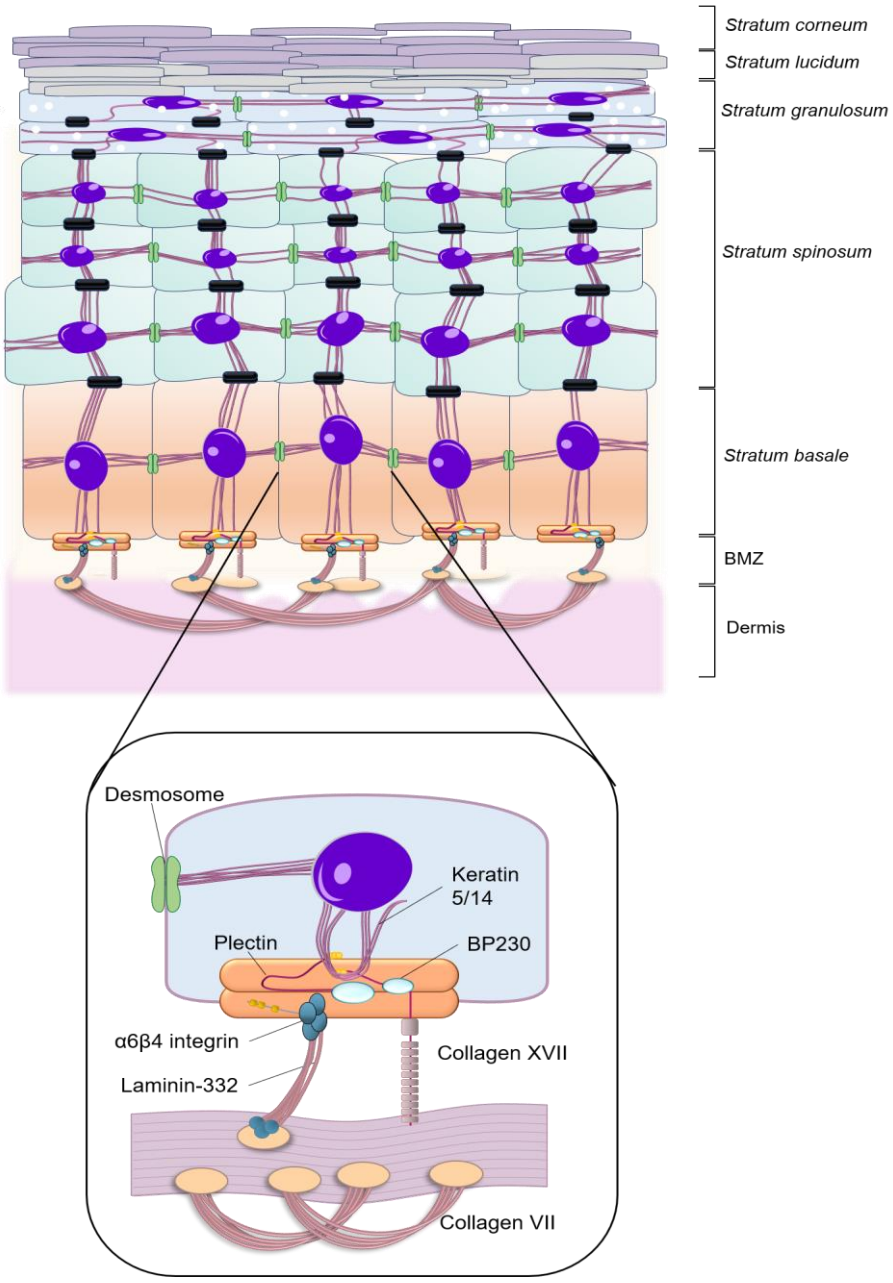

Figure 1.1 Schematic of human skin

Schematic of the epidermal-dermal architecture of the skin. The skin is composed of two main layers: the dermis and the epidermis, separated by a thin layer of extracellular matrix as known as basement membrane (BMZ). Above the BMZ is the stratum basale, consisting quiescent and high proliferating epidermal stem cells. Following vertical stratification, different epidermal layers are formed: *stratum spinosum*, *stratum granulosum, stratum lucidum* and *stratum corneum.* The main structural proteins involved within the BMZ and the stratum basale are listed in the figure magnification below.

1.2.1 The role of keratinocyte stem cells in human epidermis

Epidermal stem cells play a crucial role in the formation of the layered skin structure and its long-term homeostasis and repair following injury. The complete turnover of the epidermis is around 3 to 4 weeks and implies a "vertical" progression of keratinocytes towards terminal differentiation from the *stratum basale* to the outermost cornified layer. To accomplish its self-renewal process, the epidermis relies on the presence of stem cells, which retain high proliferative capacity and long-lasting self-renewal, and transient amplifying cells (TA). The latter, arise from stem cells but have a high proliferative rate only for a limited period of time, therefore, TA represent the largest group of dividing cells which undergo terminal differentiation (**Figure 1.2B**). To date, different epithelial stem cells have been found in different locations of skin which act as sheltered microenvironments or "niches" (**Figure 1.2A**). The niches harbour differentiated progeny and stem cells that coexists providing a fine regulation of stem cells maintenance and behaviour (Barrandon and Green 1987; Rochat et al., 1994; Hsu et al., 2011). Three different niches have been identified hosting epithelial stem cells. Using an approach of lineage tracing in stem cells (Lavker et al., 1982; Bickenbach et al., 1981; Boehnke et al., 2012; Hsu et al., 2014) epidermal stem cell have been identified in the basal layer of the epidermis (interfollicular epidermal stem cells -IFE), in the bulge area of hair follicles (HF) and in a region between the bulge and the sebaceous glands (SG). HF epidermal stem cell are multipotent *in vivo* and their commitment to a specific cell fate is determined by a finely orchestrated external signals and transcriptional factors such as Lef1 and Tcf3 (Merrill et al., 2001). For example, HF stem cells can migrate upwards for differentiation into sebocytes and downward to contribute to the formation of the inner root sheath, but were also shown to migrate towards the *stratum basale* and transiently contribute to the renewal of the epidermis after injury (Cotsarelis et al., 1990; Ito et al., 2005).

Of particular importance, the regeneration of the human epidermis is sustained by the basal interfollicular stem cells which reside in the basal layer of the epidermis and in the rete ridges which function as natural protective niches. Those cells are characterized by high clonogenic expansion *in vitro* (Barrandon and Green, 1987) and

their ability to generate functional skin sheets *ex vivo* which has become a gold-standard for cell therapies for burn patients (Langdon et al., 1988; Green 1991) or for novel new gene/cell therapy clinical treatments (Hirsch et al., 2017; Mavilio et al., 2006). Among interfollicular stem cells, *in vitro* colony-forming human epidermal cells shown heterogeneity in their capacity for sustained growth in culture. Analysis of such different single cell derived colonies showed that three different clonal cell types exist in human primary keratinocytes in culture with distincitive proliferation hallmarks and gene expression patterns: holoclone, paraclone and meroclone (Barrandon and Green 1987; Enzo et al., 2021) (**Figure 1.2C**). Holoclone is the epidermal stem cell with the highest proliferative potential and is considered by different research groups the prototypic keratinocyte stem cell (Jones and Watt 1993; Pellegrini et al., 1999; Green 1991). Upon grafting keratinocytes cultures containing holoclones can regenerate life-long epidermis, whereas cultures of meroclones and paraclones only can only transiently fulfil the regeneration of the epidermis (Gallico et al., 1984). A single holoclone, in fact, is able to undergo more than 140 doublings before senescence and represent only 5% of the epidermal stem cell populations (Hirsch et al., 2017). Those cells are mitotically active with a strong telomerase activity which determines the ability for permanent tissue regeneration from a single cell in animal models as well as in humans. The paraclone is generated by TA cells, and shows a very limited proliferative potential (~15 doublings) and usually gives rise to aborted colonies. The meroclone is a mixed cellular population with intermediated characteristics between holoclones and paraclones and mainly consists of a reservoir of TA cells. The clonal conversion from holoclone to meroclone and paraclone is unidirectional and results in a progressively reduced growth potential and stemness (Barrandon and Green, 1987). Various studies were conducted aiming to understand the mechanisms by which holoclones can be found either in resting or active proliferation state, thus being able to self-renew and to trigger terminal differentiation commitment. One model proposes that slow cycling cells are able to undergo an asymmetric division due to the polarization of key regulatory factors during mitosis resulting in the generation of two cell daughters, one with committed suprabasal and the other with proliferate basal cell fate (Lechler and Fuchs 2005).

Comprehensive efforts have been also made to molecularly identify and isolate human keratinocyte stem cells. Holoclones display high level of ΔNp63-α, a transcriptional factor which regulates the proliferative potential of keratinocyte stem cells (Pellegrini et al., 2001). The p63 transcription factor belongs to a family that includes two structurally related proteins such as p53 and p73 and plays a crucial role in the early epithelial morphogenesis in mice and humans (Yang et al., 1999; Mills et al., 1999; Senoo et al., 2007). Knockout of p63 showed absence of stratified epithelia or inability of ectoderm-derived cells to develop into epithelial lineages due to the lack of stem cells to fulfil a correct morphogenesis or renewal (Yang et al., 1999; Mills et al., 1999). The role of p63 has also been demonstrated in meroclones and paraclones with the presence of two different isoforms (ΔNp63-β and ΔNp63-γ, respectively) which are involved in epidermal differentiation (Pellegrini et al., 2001). Other isoforms of p63, characterized by the lack of the transactivational domain (TAp63), were shown to be involved in epithelial stratification and able to induce the formation of keratin 14-positive cells, marker of mature keratinocytes (Koster et al., 2004).

Alongside p63, keratin filaments such as keratin 5 (K5) and keratin 14 (K14) are also considered markers of epidermal stem cells (Webb et al., 2004). Keratin filaments consist of a large group of intermediate filaments providing mechanical and scaffolding support to the epidermis and accounting for 85% of the total mass of differentiated keratinocytes (Fuchs 1995). The keratins expression network is tightly regulated during squamous cell differentiation (Alam et al., 2011). Absence or mutation of these keratins can have detrimental impact on tissue integrity resulting in blistering disorders and tissue fragility (Coulombe et al., 2009). Mitotically active basal keratinocytes connected to the basement membrane have shown to express high concentrations of K14 and K5 expressed as heterodimeric pairs (Moll et al., 1982; Nelson and Sun 1983). K14 is also considered as a markers of epithelial stem cells. Its regulatory function in epithelial homeostasis has been shown in K14 knockout mice (Alam et al., 2011). $K14^{-/-}$ epithelial cells showed perturbation in proliferation and delay in cell progression. With the progression towards terminal differentiation, levels of K5 and K14 gradually decrease leading to an increased synthesis of K1 and

K10 in post mitotic keratinocytes within the suprabasal and spinous epidermal layers (Moll et al., 1982). In the uppermost layer (*stratum granulosum*) the synthesis of keratins is replaced with the production of filaggrin from the keratohyalin granules aiding to the water retention and skin barrier function. Loricrin is another protein secreted by cells from *stratum granulosum* and is subsequently used in terminally differentiated post mitotic corneocytes for strengthening the skin barrier.

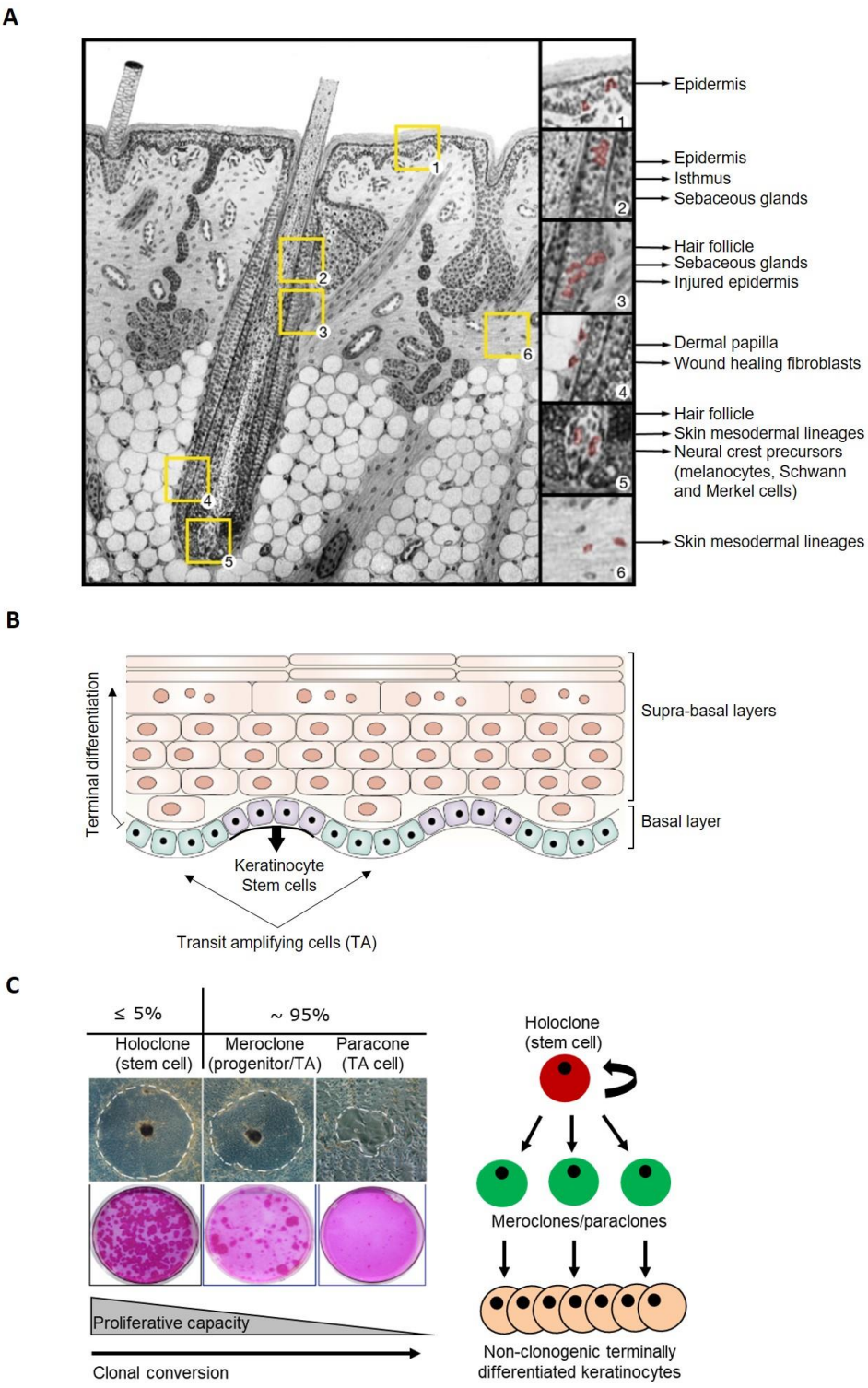

Figure 1.2 Localization of epidermal stem cells and clonal morphology of keratinocyte stem cells

Yellow squares and their magnifications on the right indicate different locations of epidermal stem cells within skin and their respective contributions to the maintenance of skin homeostasis **(A)**: 1. Interfollicular epidermal stem cells; 2. Bulge epidermal stem cells; 3. isthmus epidermal stem cells; 4. Hair follicle dermal-sheath stem cells; 5. Skin-derived

precursors; 6. dermal mesenchymal stem cells. (Figure taken from Petrova et al., 2010). Schematic of epidermal stem cells in the basal layer **(B)**. Self-renewal relies on quiescent slow-dividing stem cells (purple). Other stem cells generate transient actively dividing TA cells (green) which generate non-dividing, differentiated cells making the supra-basal layers. Clonal classification of keratinocyte stem cells (figure taken from Hsu et al., 2014)(Hsu et al., 2014) **(C)**. (Right) Holoclone stem cells (red) generate cell progeny that forms large progressively growing colonies (meroclones/paraclones in green) which progressively generate only colonies committed to terminal differentiation (yellow). (Top Left) Morphology of holoclone, meroclone and paraclone forming colonies under brightfiled microscope. (Bottom Left) Colony forming efficiency (CFE) assay is a common way of measuring the clonogenic ability of keratinocyte stem cells and estimating the number of holoclones in a biopsy and their growth potential (cells in purple) *in vitro*. Clones are scored according to their colony morphology. Holoclone represents ~5% of the clonogenic population and retains extensive proliferative potential. Mercolone/paraclone (~95%) show fewer colonies indicating clonal conversion and progressive loss of growth potential. (Figure modified from Hirsch et al., 2018) (Hirsch et al., 2018)**.**

1.2.2 The role of the basement membrane zone

The epidermal basement membrane zone (BMZ) is a distinct complex network of structural proteins and macromolecules secreted from keratinocytes and fibroblasts from the epidermis and dermis, respectively. On macroscopic level, the BMZ has a crucial role in anchoring the epidermis with the dermis and abnormalities in its composition result in blistering skin disorders such as epidermolysis bullosa. On ultrastructural level, the BMZ is composed of 4 different layers such as: the plasma membrane of basal keratinocytes (the *lamina lucida)*, *lamina densa* and the sub-basal lamina fibrous zone. Keratinocyte stem cell layer is attached to the BMZ by a complex cytoplasmic plaques known as hemidesmosomes (HDs). HDs are multiprotein complexes that facilitate the stable adhesion of the keratinocyte stem cell basal pole to the underlying basement membrane. The core of this complex comprises of 5 proteins with intracellular (BP230 and Plectin) and transmembrane localization (α6β4 integrin, type XVII collagen also known as BP180 and CD151) (Owaribe et al., 1990; Walko et al., 2015)(**Figure 1.3**). The mechanical stability of HDs rely on multiple interactions of several protein components that form a membrane-embedded tightly-ordered complex. Since HDs are required to bind the epidermis to the underlying dermis, their dissolution is implicated in blistering diseases and a variety of biological processes. For example, during terminal differentiation, basal

keratinocytes detach from the BMZ to allow for their migration toward the suprabasal epidermal layers. During this process, cells disassemble their HDs in order to loosen their tight attachment to the BMZ and become migratory (Hopkinson et al., 2014). On the intracellular level, the transmembrane α6β4 integrin interacts with the keratin intermediate filaments consisting of basal keratins-5 and -14 through the association with two members of the plakin family such as plectin and dystonin (230kDa BPAG1e, BP230) at the inner hemidesmosomal plaque (Walko et al., 2015). On the extracellular level, however, the α6 integrin extracellular domain binds the BP180, CD151 and Laminin-332 passing through the *lamina lucida* and *densa* (Hopkinson et al., 1998). Another main component playing a crucial role in the epidermal-dermal adhesion is type VII collagen which forms U-shaped, "wheat stack" shaped loop structures called anchoring fibrils (AFs). Type collagen VII is secreted from keratinocyte and, to a lesser extent, from fibroblasts. The terminal (NC1)-domain of type VII collagen indirectly binds with hemidesmosomal α6β4 integrin via the bridging activity of laminin-332 in the *lamina densa* (Rousselle et al., 1997). In human skin, AFs protrude from the BMZ to the "anchoring plaques" made of type I and III collagen in the underlying dermal papillae elements before terminating back in the *lamina densa* (Shimizu et al., 1997).

The integrity and mechanical resistance to external stress is mainly given by the extracellular membrane (ECM) composition of the BMZ. Mutation in the HD compartment or in other main BMZ components in between the *lamina lucida* and *densa*, such as collagen VII, collagen XVII, α6β4 integrin or laminin-332, can also lead to the formation of intercellular or epidermal-dermal blisters characteristic of junctional (JEB) and dystrophic epidermolysis bullosa (DEB). Although originally the BMZ components were thought to have only a physical supportive role in the skin, it was also shown that they interplay in the regulation of cell growth, self-renewal of keratinocyte stem cells, migration and apoptosis (Gumbiner 1996; Aumailley and Smyth 1998; De Rosa et al., 2019). Dynamic changes in cell adhesion participate in the skin morphogenesis and homeostasis which require finely tuned interactions between adhesion molecules, the cytoskeleton of the basal cells and the network of signalling pathways coming through the dermis and epidermis (Hsu et al., 2014;

Gumbiner 1996). Furthermore, signals generated locally by adhesion junctions can interact with classic signal transduction pathways to help control cell growth, differentiation and migration. An example of cell growth regulation was recently shown in JEB and in wild type keratinocyte stem cells by single-cell trancriptomic analysis (De Rosa et al., 2019; Enzo et al., 2021). Mutation occurring in laminin-332 was shown to lead depletion of JEB holoclones through the dysregulation of the laminin-332 adhesion dependent YAP/TAZ pathway in keratinocyte stem cells (De Rosa et al., 2019). Moreover, dysregulation of laminin-332 is also implicated in tumour progression through the modulation of cell adhesion and migration following upregulation of the phosphoinositol-3-kinase (PI3K) (Katayama and Sekiguchi 2004; Waterman et al., 2007). Similarly to Laminin-332, the α6β4 integrin was shown to have a significant impact on signalling molecules that stimulate migration and invasion through PI3K and Rho GTPases. In epithelial carcinoma, abnormally migrating carcinoma cells showed enhanced stimulation of actin protrusions and stimulation of the α3β1 focal adhesion integrin (Mercurio et al., 2001). Together α3β1 and α6β4 integrin are the major epidermal integrin in the ECM of the BMZ. In human epidermis, high expression of β1 integrin is seen in slow-cycling keratinocyte stem cells and their ablation in mice models cause defects in the BM assembly and impaired proliferation (Raghavan et al., 2000). Moreover, selection of β1+ human keratinocyte basal cells produces a high concentration of colony-forming cell when cultured *in vitro*, thus confirming that this cell population retains a high stem cell potential (Jones and Watt 1993). Similarly, α6β4 integrin is also involved in proliferation of basal cells through its signalling network with a small GTPase known as Rac1 (Benitah et al., 2005).

Collectively all these studies demonstrated that the BMZ is a crucial niche component for keratinocyte stem cells in the basal layer.

1.2.3 Fibroblasts and role of human dermis in epidermal homeostasis

Another essential niche component of basal epidermal stem cells is constituted by fibroblasts in the dermis. The dermis is located below the BMZ and it is divided in two layers: the uppermost dermal papillae and the lower reticular dermis. Dermal fibroblasts represent the most important population in the dermis, however, different subpopulation have been identified in papillary and reticular dermis harbouring different biological and functional characteristics (Schafer et al., 1985). Fibroblasts from the papillary area, in conjunction with keratinocytes, have shown to contribute to the scaffolding and organization of the basement membrane (Marinkovich et al., 1993). Types IV and VII collagen and a subset of laminin are actively synthetized and deposited at the BMZ. As previously mentioned in section 1.2.2, absence of collagen VII results in blistering at the dermal-epidermal junction, however, cell and gene therapies to correct collagen VII in DEB patients can be addressed by targeting either keratinocytes or fibroblasts. Other collagen types, such as types I and III collagens, are mainly expressed by fibroblasts and play a key role in maintaining the epidermal-dermal structural integrity through their interaction with the AFs. To a lesser extent other subtypes of collagens (types V, VI, XII, XIV and XVI) are also synthetized and co-interact with the surface of collagen type I and III (Blum and Ruggiero 2005).

Co-culture of fibroblasts and keratinocytes have shown to co-regulate each other through cell-cell contact or paracrine release of grow factors and cytokines. It was shown that fibroblasts regulate the expression of collagen VII by keratinocytes through TGF-β signalling (König and Bruckner-Tuderman, 1992; Strassburg et al., 2010). Through paracrine and autocrine interactions fibroblasts can engage with the epidermis during homeostasis (Gilchrest et al., 1983; Werner and Smola 2001) or wound healing upon injury (Smith et al., 1997; Moulin 1995). Different studies highlighted the importance of dermal fibroblasts-derived growth factors in the regulation of keratinocyte colony formation *in vitro* and in mice models through the release of mitogens, such as insulin-like growth factors (IGFs), keratinocyte growth factors (KGF-1), fibroblasts growth factor-7 (FGF-7) and -10 (FGF-10) epidermal growth factors such as EGFR ligands (Rheinwald and Green 1975; Lewis et al., 2010).

Similarly, evidence of paracrine support of the fibroblasts matrix on the epidermis homeostasis has been observed in embryonic stem cells-derived keratinocytes (Lewis et al., 2010). Accordingly, the use of lethally irradiated mouse fibroblast mesenchymal cells has shown to support the growth of adult human keratinocytes paving the way for their serial culture *in vitro* for regenerative medicine applications (Rheinwald and Green, 1975). The use of lethally irradiated 3T3-2 murine fibroblasts nowadays is considered a standard method for the production of graftable epithelia for clinical *ex vivo* applications (Hirsch et al., 2017; Mavilio et al., 2006).

1.3 Molecular characterization of epidermolysis bullosa types

1.3.1 Epidermolysis Bullosa Simplex (EBS)

EBS is the most generalized severe subtype of EB. In accordance to the National Epidermolysius Bullosa Registry, the overall prevalence is estimated about 11.07 per million population (Fine 2016). Clinical hallmarks of EBS are blisters occurring in clusters with inflammatory appearance following exposure to mechanical friction or trauma. In most of the case, EBS has an autosomal dominant inheritance leading to deleterious dominant negative effects in basal keratin genes, *KRT5* and *KRT14* (**Figure 1.3**). Aberrations in cytoskeletal keratins-5 and -14 proteins result in the disruption of the intermediate filament network in the basal keratinocyte layer and within the dermal-epidermal junction leading to cell fragility and non-scarring blisters.

1.3.2 Junctional Epidermolysis Bullosa (JEB)

In junctional epidermolysis bullosa (JEB) the tissue separation occurs within the dermal-epidermal junction, primarily within the lamina lucida. Two different subtypes of JEB have been classified: the Herlitz type (lethal) and the non-Herlitz form (non-lethal). The classic clinically devastating Herlitz JEB (H-JEB) is frequently lethal during the first years and is characterized by premature termination codon (PTC) mutations leading to truncated non-functional proteins within the dermal-epidermal junction whereas the non-Herlitz form has a milder prognosis associated with life-long blistering. Despite their differences in clinical severity, both forms are inherited in autosomal recessive pattern. Most of the newborns affected by JEB show blisters

covering large part of the skin body surface including mucosal membranes, such as the respiratory and digestive tracks, leading to respiratory issues and malnutrition. The blister occurs at the level of the hemidesmosome complexes within the basal keratinocytes involving four principal genes. Up to 70% of JEB mutations involve complete or partial loss of function in the laminin-332 trimer (*LAMB3*) and, with lesser extent, *LAMA3*, *LAMC2*, integrin alpha6beta4 (*ITGA6*, *ITGB4*) and *COL17A1*, thus all proteins essential for the integrity of the epidermal layer or the dermis underneath (**Figure 1.3**).

1.3.3 Dystrophic Epidermolysis Bullosa (DEB)

Alongside Herlitz JEB, dystrophic EB is one of the most severe form of EB resulting in generalized blistering accompanied by high mortality rate in young adulthood. To date, incidence of DEB has been estimated to affect 6 out of 100000 patients worldwide with over 815 pathogenic mutations including missense, nonsense, splicing, small insertions or deletions reported (Kowalewski et al., 2011). Clinical phenotypes in patients affected by DEB include localized or generalized skin fragility after minimal mechanical trauma, scarring blisters and erosions on the whole body surface. As in JEB, internal mucosae are also involved. Typical consequences of severe blistering encountered by DEB patients are joint contractures of limbs or hand deformities including progressive digital fusion (pseudosyndactyly), flexion contractures and adduction contracture of the thumb leading to life threatening skin carcinomas. Patients suffering from DEB have been associated with a 70% chance of developing squamous skin carcinomas by adulthood with a 90% of mortality rate. DEB is inherited in autosomal dominant (DDEB) or autosomal recessive (RDEB) inheritance pattern. The gene responsible of DEB clinical manifestations is the COL7A1 gene encoding for type VII collagen alpha 1 (C7) protein. Type VII collagen is the major component of fibrous structures called anchoring fibrils (AFs) with a key role in preservation of the structural integrity of the skin creating a biologic “velcro” between the epidermis and the underlying dermis at the BMZ (**Figure 1.3**). Loss of function in the COL7A1 gene leads to the lack of functional AFs within the lamina densa of the dermal-epidermal basement membrane zone, thus leading to the formation of deep blisters involving the papillary dermis.

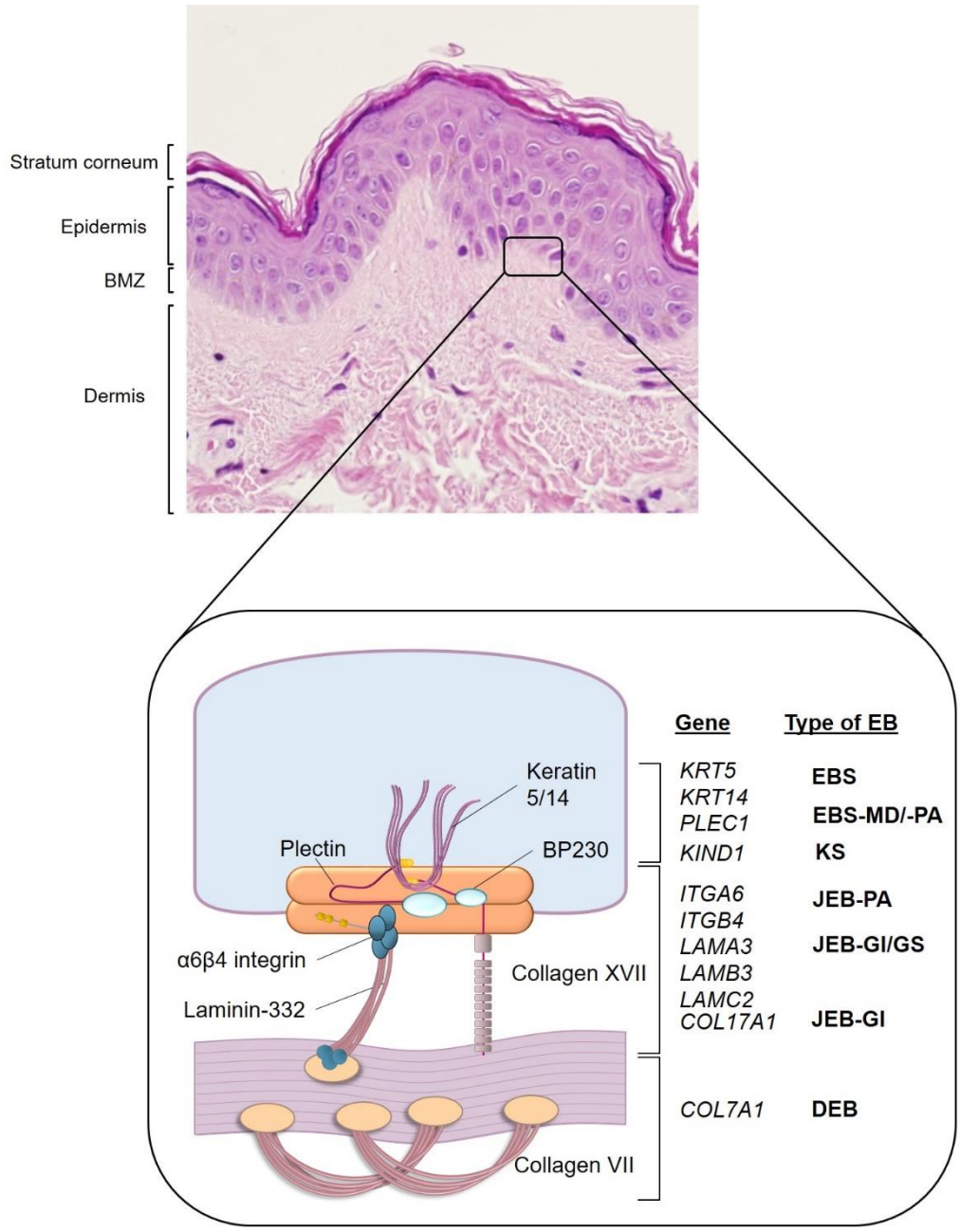

Figure 1.3 Molecular basis of Epidermolysis bullosa

The left figure shows a haematoxylin and eosin staining of normal skin. The right figure is a schematic of molecular architecture of the basement membrane zone (BMZ) and the structural proteins involved in different types of EB. Abbreviations: EBS, epidermolysis bullosa simplex; MD, muscular dystrophy; KS, Kindler syndrome; JEB, junctional epidermolysis bullosa; PA, pyloric atresia; GI, generalized intermediate; GS, generalized severe; DEB, dystrophic epidermolysis bullosa. (Picture taken from Naso and Petrova, 2019).

1.4 Type VII collagen

Type VII collagen plays a key role in the maintenance of the epidermal-dermal integrity and is the major component of AFs in the BMZ. Firstly discovered in 1983 (Bentz et al., 1983), and cloned in 1994 (Christiano et al., 1994b), extensive functional studies of type VII collagen have been conducted due its clinical correlation with dystrophic epidermolysis bullosa (DEB). Type VII collagen is encoded by the *COL7A1* gene and its chromosomal linkage analysis which was carried out in 1991 mapped the gene in the short arm of chromosome 3 at the locus 3p21 (Parente et al., 1991) (**Figure 1.4A**). The *COL7A1* gene consists of 118 exons in approximately 31,132Kb of the human genome from its transcriptional start site to the polyadenylation one (Christiano et al., 1994b). The corresponding mRNA is compact, 9Kb size, and codes for 2944 amino acids encoding for a 350kDa proα1(VII) polypeptide. C7 is produced and secreted extracellularly by keratinocytes and dermal fibroblasts. Type VII collagen belongs to a large family of non-fibrillar collagens and is characterized by heterogeneous supramolecular organization (Christiano et al., 1994a). A characteristic structural feature of type VII collagen is the presence of a 1530 amino acid protein domain in triple-helical conformation which provides structural stability and is used as structural building blocks for the formation of AFs (Ramshaw et al., 1998; Christiano et al., 1994b). This structural protein domain spans the central portion of the proα1 polypeptide and the characteristic collagenous triple-helical domain fold is made up of Gly-X-Y repeats from exon 29 to exon 112. The central collagenous domain is flanked by a 145kDa non-collagenous amino-terminal globular domain (NC1) and by a 20kDa carboxy-terminal globular domain (NC2) (**Figure 1.4B**). In details, the amino-terminal NC1 domain starts with the 5' untranslated region consisting of a signal peptidase cleavage site encoded by the first exon of *COL7A1* and is critical for the release of C7 pre-proteins from the cytoplasm into the extra-cytoplasmic location (Christiano et al. 1994b). The NC1 domain also encodes for three sub-modules with significant homology to adhesive proteins including cartilage matrix domain CMP (38.8%), from exon 2 to 5, fibronectin type III-like domains FN-III (23.2%), from exon 6 to 23, and to the von Willebrand factor A domain (21.1%) (Christiano et al., 1994b). The two final NC1 exons, 27 and 28, encode for a cysteine

proline rich domain with no homology sequence described so far. The triple-helical domain consists of 84 exons (29-112) flanked by the two non-collagenous domains. The region is made up of Gly-X-Y repeats with a 39 amino acid interruption forming the hinge region. The NC2 domain, exon 113 to 118, is placed on the C-terminal of the proα1 chain and has a segment with homology to the Kunitz protease inhibitor, however, its function has not been yet established**.**

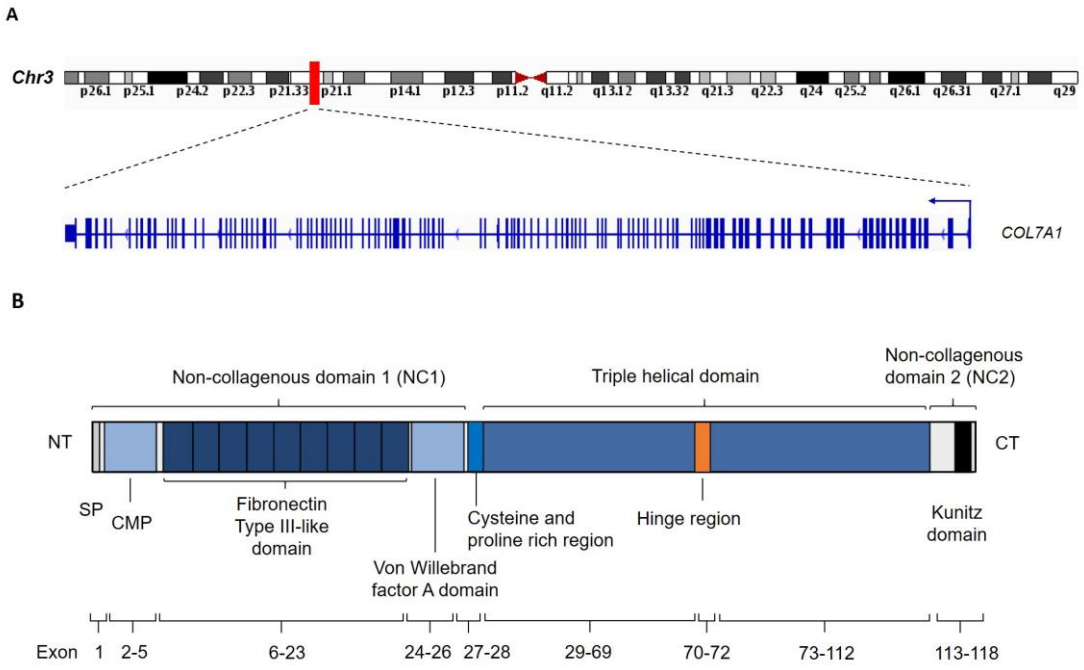

Figure 1.4 Schematic of human chromosome 3 and *COL7A1* gene

Magnified view of the chromosome 3 and localization of the *COL7A1* gene (3p21.31) and its 118 exons **(A)**. Schematic representation of the structural organisation of the type VII collagen proα1(VII) polypeptide exons **(B)**. The N terminus of the amino acid sequence codes for a 5' UTR signal peptide which is followed by a non-collagenous domain (NC1) spanning across 26 exons, approximately 145kDa in size, and consisting of sub domains with homology to known adhesive molecules. These are a cartilage matrix protein (CMP) like domain, followed by nine consecutive fibronectin type III modules, a von Willebrand factor A, domain and a cysteine, proline rich region. The triple–helical domain (84 exons) flanked by the two non-collagenous regions is made up of Gly-X-Y repeats with a large 39 amino acid interruption forming a collagenous hinge region (orange box). The polypeptide ends with the second non-collagenous domain (NC2) made up of seven exons and about 30kDa in size containing a segment resembling the Kunitz protease inhibitor molecule. Organization into anchoring fibrils.

Type VII collagen is one of the main component of AFs. Together with the hemidesmosomes, AFs are involved in the reinforcement of the dermal-epidermal attachment. The essentiality of such structure is supported by the observation of ultrastructural aberrations in patients affected with dystrophic epidermolysis bullosa (DEB). During intracellular processing of C7, three proα1 chain fold together through their carboxy-terminal ends and collagenous domains, into a homotrimeric type VII collagen monomer acquiring the typical triple helical conformation. Upon secretion, type VII collagen homotrimers, also known as procollagens, assemble in an antiparallel dimers through their overlapping C-terminal ends following proteolytic cleavage of the NC2 domain, hence promoting the stability of the dimer (**Figure 1.5**). Subsequently, multiple dimers laterally aggregate to form cross-banded, centro-symmetrical AF structures with the NC1 domains at both ends (Bächinger et al., 1990). Transmission electron microscopy shows that both ends of AFs fall within the *lamina densa* where the NC1 domains bind key macromolecules such as the β3 chain and γ2 chain of laminin-332 guaranteing the adhesion of AFs to basal epidermal cells. The flexibility of the AFs is conferred by the highly conserved discontinuities within the Gly-X-Y repetition in each proα1 chains and the creation of a “U-shapes” which secure the entrapment of type I and III collagens in the papillary dermis (Christiano et al., 1994a; König and Bruckner-Tuderman, 1992). Validation of new synthesis and deposition of AFs at the dermal-epidermal junction through electron microscopy is used to determine the functional level of type VII collagen upon gene and cell therapy for DEB patients.

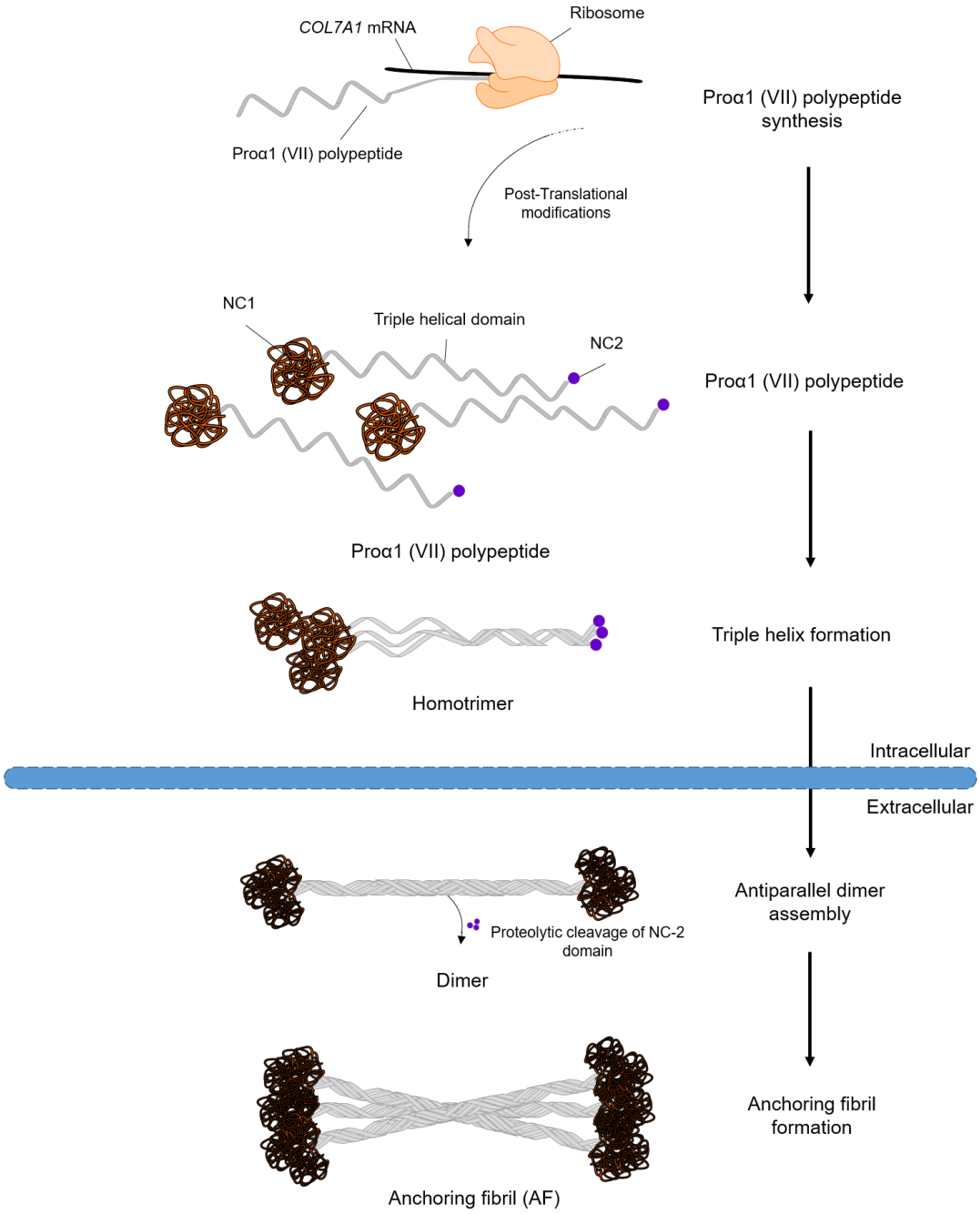

Figure 1.5 Organisation of type VII collagen into anchoring fibrils

Three monomeric proα1(VII) procollagen polypeptides are synthetized and assembled into a triple helix (as known as homotrimer) acquiring a characteristic triple helical conformation. Upon homotrimers secretion into the extracellular space, triple helical type VII collagen molecules form antiparallel dimers followed by proteolytic cleavage of the NC2 domain. Subsequently, several dimer molecules laterally assemble to form cross-striated, centro-symmetric anchoring fibrils (AFs).

1.4.1 Type VII Collagen involvement in Epidermolysis Bullosa and squamous cell carcinoma

Mutations in the *COL7A1* gene lead to severe clinical consequences on integrity of the skin. Immunofluorescence and transmission electronic microscopy analysis of skin sections from DEB patients shows absence or significant reduction of collagen VII epitopes and alteration of the BMZ due to malformation or complete absence of AFs, respectively. Cloning of the *COL7A1* gene and the determination of the function of every single domain paved the way for in-depth studies on the involvement of collagen VII in blistering diseases (Christiano et al., 1994a; Christiano et al., 1994b). To date more than 800 distinct mutations, including nonsense, missense splicing, insertion or deletions in the *COL7A1* gene have been reported, spanning all over the 118 exons (Wertheim-Tysarowska et al., 2012) (**Figure 1.6**). Consequently, genotype-phenotype correlations have been observed and different combinations of mutations determine a different degree of disease manifestation. In recessive DEB (RDEB) patients, the presence of premature termination codon (PTC)-causing mutations in both alleles result in complete absence of type VII collagen with severe mutilating scarring and blistering. On the other hand, combinations of a PTC mutation with a more subtle missense mutation can result in milder RDEB forms. Dominant DEB (DDEB) is mostly due to mutations which result in glycine substitution in the Gly-X-Y repeat sequence within the triple-helix central domain. Collectively, the precise degree of severity of DEB reflects the combinations of mutations in *COL7A1* and their mRNA and protein levels, combined with the effects of modifier genes on the individuals' genetic background and the exposure to environmental trauma (Chung and Uitto 2010; Christiano and Uitto 1996).

Therefore, loss of the structural function of C7 in RDEB patients is associated with chronic lifelong blistering, scarring and impaired wound-healing. Chronic wounds are typically characterized by increased bacterial colonization, fibrosis and inflammation which in turn can predispose patient into squamous cell carcinoma (SCC) development. Of note, RDEB-associated SCCs (RDEB-SCCs) have been reported as more aggressive than common skin SCCs of different etiology (e.g. UV-mediated epithelial SCCs) and characterized by high morbidity and mortality (Condorelli et al.,

2019). According to the The USA National EB Registry, the incidence of developing in RDEB-SCCs increases with age and it is currently 67.8% by age 35 and up to 90.1 (Tang et al., 2021; Fine et al., 2009).

One of the causes associated with the development of SCC relies on the inverse correlation between the severity of the RDEB and the levels of PTC truncated collagen VII expression in patients. This hypothesis was initially corroborated by Ortiz-Urda et al., due to the reported high incidence of RDEB-SCCs in patients retaining the amino-terminal noncollagenous domain NC1 (Ortiz-Urda et al., 2005). More precisely, the fibronectin-like sequences within the residual NC1 domain was shown to overexpress Ras-driven Skin SCC development and promote tumour cell invasion in a lamimin-332-depended manner (Ortiz-Urda et al., 2005). This obserevation was also corroborated upon the clinical observation that RDEB patients with absent levels of type VII collagen failed to develop SCC (Ortiz-Urda et al., 2005). By contrast, in a second study involving a different cohort of RDEB patients, it was reported that even the complete lack of C7 expression can promote the development of SCC without the detection of any Ras-activating events (Pourreyron et al., 2007). Although the uncertain ethiology of C7 role in the develpoment RDEB-SCC, other molecular associated factors such as hypermethylation of p16INK4a, low expression of growth factor binding protein 3 and elevated levels of matrix metalloproteinase (MMP7) have been frequently linked to SCC in RDEB patients (Kivisaari et al., 2008).

More recently, the identification of mutational signatures in RDEB SCC has provided more insight into the underlying genetic cause of skin cancer development. Whole-exome, whole-genome, and RNA sequencing of 27 RDEB SCC tumors has displayed patterned mutations in several genes (CASP8, TP53, NOTCH1, NOTCH2, CDKN2A, HRAS, and FAT1) previously identified as potential drivers in multiple aggressive skin SCC sequencing studies (Cho et al., 2018; Li et al., 2015; Pickering et al., 2014). In order to identify the genetic cause that could lead to the early-onset of skin cancer in RDEB patients, a recent study from Cho *et al*., found APOBEC (apolipoprotein B mRNA-editing enzyme catalytic polypeptide–like) -driven mutation signatures due to recurrent C>T and C>G somatic conversions in RDEB-SCC-associated driver genes such as HRAS, NOTCH1 and TP53 (Cho et al., 2018). Although APOBEC signatures were

already found to a different extent in several cancer types, in RDEB-SCC the amount of mutations determined by the APOBEC deaminase activity is significantly higher than that detected in non-RDEB SCCs (1.7–2%) or HPV-induced head and neck squamous cell carcinoma SCCs (HNSCC) (30%) (Inman et al., 2018; Cho et al., 2018; Condorelli et al., 2019). In support of these findings, up-regulation of different human APOBEC members such as, APOBEC3A, APOBEC3B and APOBEC3H, has been observed particularly prominent in areas of RDEB chronic tissue damage (Cho et al., 2018). All together, these recent findings helped to better understand the biological and molecular etiology of RDEB-SCC and could shed the light to the development of genomically-driven treatments, such as anti-APOBEC therapies.

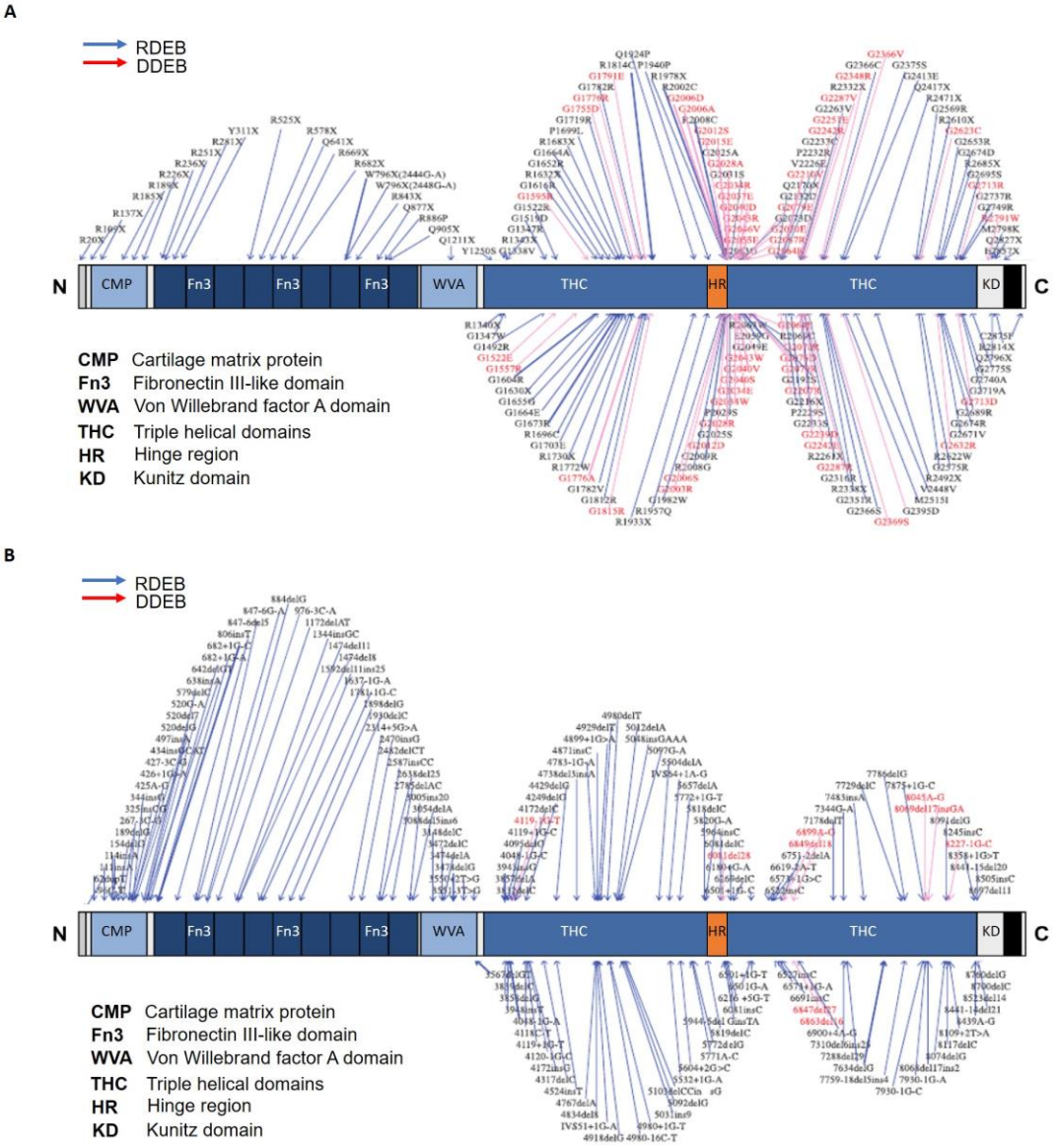

Figure 1.6 *COL7A1* mutation types reported in RDEB and DDEB patients.

Missense and nonsense mutations **(A)** and *COL7A1* deletions, insertions, splice site mutations **(B)** in dystrophic epidermolysis bullosa (DEB) patients. Red and blue arrows correspond to dominant (DDEB) and recessive (RDEB) dystrophic epidermolysis bullosa mutations, respectively. Figure taken from (Dang and Murrell, 2008).

1.5 Cell therapy for DEB

1.5.1 Therapy for DEB skin disorders: cell therapy

To date, the main treatment option for patients with DEB is extensive daily wound dressing of skin chronic wounds combined with nutritional supplements or gastrostomy in severe cases, for lesions of the mucosal membranes. Although a long lasting and effective treatment is yet to be found for DEB, in the past decades various cell and gene therapy approaches have been evaluated. For cell therapy applications, different cell types have been shown to be effective to alleviate local and systemic RDEB complications (**Figure 1.7**). For RDEB, C7 producing cells such as keratinocytes and fibroblasts have been widely used in gene and cell therapies in preclinical and clinical settings. Although keratinocytes and fibroblasts contribute to the synthesis of extracellular matrix components of the BMZ, the former have shown to retain a higher proliferative potential, secrete larger amount of C7 and able to sustain the adhesion of the epidermis to the dermis (Chen et al., 2002). An example of cell therapy involving *ex vivo* generation of autologous epidermal grafts been shown to be applicable for EB patients affected by revertant mosaicisms (Gostyński et al., 2014a; Gostyński et al., 2014b). In particular for RDEB, revertant mosaicism has been reported in 36% of patients mainly affecting keratinocytes (Jonkman and Pasmooij, 2009), although rare cases of reversion has been documented in patient's fibroblasts (Twaroski et al., 2019). Clinically, patients with different forms of EB have shown small patches of normal skin due to a spontaneous correction of the inherited mutation with a second somatic mutation which deplete the EB-causing one. Although mechanisms of reversion have not been fully elucidated, cell therapy using naturally revertant keratinocytes has been reported in two JEB patients with germline mutations in *COL17A1* (Gostyński et al., 2014b) and *LAMB3* (Gostyński et al., 2014) genes. In both patients, modest re-epithelization was observed although a gradual reduction of revertant cells have been reported within the grafts. Such decrease, was hypothesized to be related to the different behaviour of revertant and non-revertant cells in culture due to the activation of NF-Kb pro-inflammatory pathways which confers clonal selection of the latter over the former (Gostyński et al., 2014a). To

circumnavigate the issue of non-revertant cell proliferation during cell expansion, revertant JEB and RDEB cells were shown to be converted into induced pluripotent stem cells (iPSCs) and subsequently differentiated into naturally gene-corrected keratinocytes (Umegaki-arao et al., 2014; Tolar et al., 2014). Another constraint of natural cell therapy is related to the small number of revertant cells that can be expanded from single punch biopsies. As shown by a recent study of Hirsch and colleagues, approximately 1888 holoclones/cm^2 were required to achieve therapeutic longevity of transgenic keratinocyte grafts in a paediatric patient with JEB (Hirsch et al., 2017). However, although "natural" cell therapy using revertant cells has shown some potential in patients with JEB, only proof-of-concept applications using patient-derived iPSCs have been reported for RDEB (Tolar et al., 2011; Umegaki-Arao et al., 2014). On the other hand, retroviral and lentiviral vectors encoding for a copy of the *COL7A1* cDNA, fully described in **section 1.6**, have been widely used to transduce and correct RDEB patients' keratinocytes.

1.5.2 Allogeneic fibroblasts therapy

Although keratinocytes are the main contributors of collagen VII in the skin, injections of dermal fibroblasts showed to actively sustain collagen expression in RDEB along with a critical role in wound healing (Stanley et al., 1985; König and Bruckner-Tuderman, 1992). Previously, potential of allogeneic fibroblast-based approaches was tested in a preclinical RDEB model (Kern et al., 2009). In this study, $20x10^6$ EGFP+ new-born-derived murine fibroblasts were injected intradermally into immunocompetent hypomorph RDEB mice expressing only baseline (10%) C7 at dermal-epidermal junction (Kern et al., 2009). Intradermally injected fibroblasts showed slight lateral migration from the point of injection, and up to 35% of *COL7A1* mRNA and *de novo* C7 protein were detected 100 days post injection. First reported clinical study of singular injection of allogeneic fibroblasts in 5 RDEB patients carrying different mutations showed a short-term increase of C7 at the dermal-epidermal junction (Wong et al., 2008). However, contribution of *de novo* C7 from donor's fibroblasts was only partial, and the increase in patients 'own *COL7A1* mutant mRNA, and subsequent formation of aberrant AFs, was also observed. Accordingly, most marked C7 deposition at DEJ following intradermal injections was seen in patients

with reduced and not absent baseline expression of C7, suggesting that such therapy would be most beneficial in patients with residual protein expression. The mechanism underlying the increase of endogenous C7 and wound healing was proposed to be related to the elevated expression of heparin binding EGF-like growth factor (HB-EGF) at the site of injection (Nagy et al., 2011). Consequently, a phase II double-blinded randomised vehicle-controlled trial in 5 RDEB patients showed that injections of either allogeneic fibroblasts or suspension solution alone encouraged healing of chronic wounds at a comparable level (Venugopal et al., 2013). Overall, data collected from patients suggested that only short term benefits can be achieved following allogeneic fibroblasts injections. This limitation of allogeneic fibroblast-based therapy was reported in two different clinical trials (Petrof et al., 2013; Venugopal et al., 2013) where significant clinical response was limited to up to 1 month post injection, after which there was no discernible difference with the placebo treatment.

1.5.3 Bone marrow transplantation of allogeneic cells

Taken into consideration the systemic manifestations of DEB, significant efforts have been made in evaluating cell types that can address its systemic nature. Initial research in animal models showed that bone marrow and hematopoietic cell transplantation (HTC) of non-haematopoietic (mesenchymal stromal stem cells, MSCs) or haematopoietic stem cells (multipotent HSCs and progenitors) contributed to wound healing in the skin (Badiavas et al., 2003). Proof-of-principle study carried out in chimeric mice models transplanted with EGFP-bone marrow cells, demonstrated that skin wound healing was promoted by migration of EGFP-derived cells from the site of the injury (Fathke et al., 2004; Badiavas et al., 2003). Interestingly, two subpopulations of bone marrow-derived cells including 15-20% of non-haematopoietic CD45- cells and a small percentage of haematopoietic CD45+ cells have been detected in the injured skin sites (Fathke et al., 2004; Badiavas et al., 2003). Systematic evaluation of wounding-stimulated bone marrow cells engraftment in the skin was observed by Tolar *et al.* by congenic bone marrow transplantation (BMT) in a *COL7A1*$^{-/-}$ knockout RDEB mouse model (Tolar et al., 2009). Moreover, BMT mice demonstrated that infusions of high doses of allogeneic bone

marrow-derived cells enriched in signalling lymphocytic activation molecule (SLAM) CD150+ and negative for CD48- in new-born *COL7A1*$^{-/-}$ irradiated mice were at least in part responsible for cellular homing to the injured skin. In particular, deposits of *de novo* C7 and development of rudimentary anchoring fibrils were detected in mice demonstrating improved survival rates in 15% of the transplanted CD150+/CD48− animals (Tolar et al., 2009). Following the effectiveness of BMT in murine RDEB, the first in-human study has been developed (Wagner et al., 2010). Six RDEB children received HLA-matched allogeneic transplantation of unfiltered bone marrow or umbilical cord stem cells under immunomyeloablative chemotherapy regime (Wagner et al., 2010). Clinical improvements of chronic wounds and decreased mucocutaneous blisters were observed within 100 days post transplantation. Increasing *de novo* C7 deposition was seen in 5 out of 6 patients between 30 and 100 days after transplantation followed by deposition of rudimental anchoring fibrils detected by transmission electronic microscope. FISH and PCR of polymorphic variable-number tandem repeat regions to determine the percentage of chimerism in BMT patients confirmed homing of bone marrow-derived cells to the recipient's wounded skin confirming observation from preclinical animal model studies (Tolar et al., 2009). Although data showed by Wagner *et al.* demonstrated a proof of concept of potential effectiveness of HCT in RDEB patients, side effects of aggressive myeloablative conditioning used in this study can put patient's life at high risk. Moreover, the precise mechanisms as well as the characterization of BM-cellular subpopulations which play a role in epithelial regeneration are still unclear.

1.5.4 Mesenchymal stromal stem cells

In parallel with HCT therapies, different groups investigated the potential of mesenchymal stromal stem cells (MSCs) to migrate to injured skin tissues and stimulate wound healing in RDEB skin injuries (Sasaki et al., 2008; Petrof et al., 2015; Perdoni et al., 2014; Igoucheva et al., 2011). Contribution of MSCs in natural healing process relies on their ability to be recruited to wound sites by paracrine signalling from the injured skin as well as the secretion of different collagen proteins such as III, VII and XVII improving the wounding healing process (Fujita and Shimizu, 2010). Moreover, the ability of MSCs to transdifferentiate into fibroblastic-like phenotype

cells when in co-culture with fibroblasts suggested that cell-cell interactions and/or secreted factors (such as IL-6 and IL-10) play a key role in the differentiation of MSCs towards fibroblast-like fate, thereby contributing to re-epithelization of chronic and acute wounds (Igoucheva, Alexeev, and Uitto, 2011). Intradermal injection of high concentration ($0.1\text{-}5x10^6/cm^2$) of human MSCs in *COL7A1* $^{-/-}$ mouse model demonstrated migration of MSCs to the wounded skin with cells adopting fibroblast-like morphology leading to the restoration of 15% of C7 protein within the BMZ compared to the wild type levels (Kühl et al., 2015). Molecular analysis at 1 week post injection showed dose-dependent contribution of MSCs to *de novo* C7 deposition at the dermal-epidermal junction. As previously shown in BMT for RDEB patients (Wagner et al., 2010), production of *de novo* C7 promoted the formation of functional but rudimentary anchoring fibrils for up to 3 months (Kühl et al., 2015). However, long term engraftment of MSCs in the dermis did not occur as demonstrated by apoptosis assays (Kühl et al., 2015). First reported clinical use of MSCs in two RDEB patients was demonstrated by Conget *et al.* where $0.5x10^6$ of allogeneic MSCs were injected intradermally in chronic wounded sites (Conget et al., 2010). Similarly to preclinical animal models, deposition of new C7 at the BMZ followed by re-epithelization of the blistering sites led to clinical benefits for up to 4 months post injection. Short term amelioration of RDEB symptoms after intravenous infusions of BM-MSCs were recently reported in 10-patients clinical trial (Petrof et al., 2015) and in a double-blinded clinical study conducted by El-Darouti *et al*. where allogeneic MSCs were administered intravenously into 14 RDEB patients (El-Darouti et al., 2016). To increase the release of MSC-derived C7, Petrova *et al*., designed a gene therapy approach on MSCs using self-inactivating lentiviral vector expressing codon-optimized *COL7A1* under expression of phosphoglycerate kinase (PGK) constitutive promoter in humanized skin model *in vivo* (Petrova et al., 2020). *Ex vivo* graft of transduced MSCs and RDEB fibroblast and keratinocyte grafted on NOD-SCIDIL2Rgammanull mice showed absence of blisters at dermal-epidermal junction with expression of human coC7 and anchoring fibril composition at the basement zone comparable with WT grafts. Deposition of sparse C7 sufficient to improve functional adhesion at the dermal-epidermal junction was observed upon intradermal injection of human engineered MSCs. By contrast, systemic delivery of

coCOL7A1 MSCs via intravenous route showed significant migration in the lungs and next to the injection site. No deposition of C7 detected in the graft confirmed the absence of migration to the blistered skin areas. In contrast with the observation of short-lived MSC after 28 days post administration in C7-hypomorphic mice (Kühl et al., 2015), this study showed persistence of Ki-67^{+} cells at 30 days post injection, albeit MSCs appeared to actively proliferating and expanding in the human graft (Petrova et al., 2020). Despite the absence of evidence of long-lasting clinical improvement in MSC-mediated wound healing, molecular mechanisms of MSC migration to acute and chronic blistered skin have not been completely characterized. In this context, some insight in activation and migration of bone marrow-derived cells towards the damaged skin tissues has been gained with the discovery of PDGFRα+ bone marrow cells contributing to epithelial regeneration in mice (Tamai et al., 2011). Tamai *et al*. reported that the release of high mobility group box 1 (HMBG1) factor in hypoxic environment of RDEB epidermal blisters was the main factor for recruiting and mobilization of non-haematopoietic cells from bone marrow (Tamai et al., 2011). By grafting *COL7A1*$^{-/-}$ skin onto the back of irradiated mice with EGFP-BM transplant, the authors demonstrated that the release of HMBG1 into the circulation led to the mobilization and recruitment of BM-derived epithelial progenitors of non-hematopoietic lineage (Lin-) positive for the platelet-derived growth factor receptor alpha (PDGFR-alpha). At 4 weeks post-engraftment EGFP+/PDGFR-alpha+/Lin- cells expressing both keratin 5 (marker of keratinocyte lineage) and C7 were detected by immunofluorescence and FACS analysis. Transplantation of dermal MSCs expressing ATP-binding cassette B5 (ABCB5+) in *COL7A1*$^{-/-}$ mice resulted in increased survival compared to the untreated controls, although no *de novo* C7 or infused ABCB5+ cells were detected in the skin. Nevertheless, the immunomodulatory activity of ABCB5+ MSCs and their ability to suppress inflammatory infiltration of myeloid derivatives led to the development of an early phase clinical trial of systemic administration of allogeneic ABCB5+ cells for treatment of RDEB (NCT03529877). Perdoni *et al*. showed that cytokine pre-conditioning of murine MSCs with TGFβ and TNFα for 48 hours induced simultaneous 8-fold, 4-fold and 2.2-fold increase in *COL7A1*, (TNFα)-stimulated protein 6 (Tsg6) and CXCR4R expression, respectively, compared to wild-type MSCs. Pre-conditioning

effects, however, have yet to be assessed therapeutically in humans (Perdoni et al., 2014).

1.5.5 Induced pluripotent stem cells (iPSCs)

The importance of the discovery that somatic cells can be induced to be reprogrammed back to pluripotent cells (iPSCs) through the ectopic expression of reprogramming factors (Takahashi and Yamanaka, 2006) has paved the way for the development of novel allogeneic and autologus treatment optitions for rare disorders. Similarly to embryonic stem cells (ESCs), iPSCs can be expanded indefinitely and can be differentiated into all three germ layers (mesoderm, ectoderm and endoderm) which can be used for the development of corrective therapies. Importantly, the use of autologous iPSCs in regenerative medicine can potentially overcome any ethical concerns and clinical obstacles associated with the use of primary cells or ESCs thus offering a possibility to treat patients with their own cells without the need of immunosuppressive drugs to prevent tissue rejection. Despite their tremendous potential application for cell-based therapies and disease modelling, the reliability of cell reprogramming, the development of robust protocols for the differentiation of iPSCs into relevant adult cell lines and their further translation for clinical applications are still under investigation although few clinical trials have been already launched (Deinsberger et al., 2020).

The combination of intracellular factors involved in the pluripotency reprograming network was firstly discovered in 2006 by Yamanaka *et al.* (Takahashi and Yamanaka 2006). In this study, 24 putative reprograming factors were analysed for their previous reported ability in ESCs to individually contribute to induce pluripotency in murine somatic cells (Cartwright et al., 2005; Niwa et al., 1998; Boyer et al., 2005; Niwa et al., 2000). Consecutive rounds of screening led to the discovery that only 4 ectopic factors were sufficient to reprogram somatic cells into embryonic-like state when co-delivered by retroviral vectors. These factors, Oct3/4 (also known as POU5F1), sex determining region Y (SRY)-box2 (Sox2), Krüppel-like factor 4 (Klf4) and c-Myc, collectively called OKSFM factors (Takahashi and Yamanaka 2006), have become the focal point of reprograming manipulation. Fibroblasts-derived iPSCs

showed ESC-like morphology, *in vitro* expression of ESC markers such as NANOG and SSEA-1 and were able to generate teratomas *in vivo* when injected into immunodeficient mice (Takahashi and Yamanaka 2006). Subsequently, iPSCs have been derived from a number of different species, including humans (Takahashi et al., 2007; Park et al., 2008), rats (Li et al., 2009) and rhesus monkeys (Liu et al., 2008) by expression of the four Yamanaka factors, demonstrating that fundamental features of the transcriptional network governing pluripotency remain conserved during evolution. Similarly, iPSCs have been derived from other skin cell populations, such as keratinocytes (Aasen et al., 2008; Maherali et al., 2008) and melanocytes (Utikal et al., 2009) or from somatic cells like neural cells (Eminli et al. 2008), stomach and liver cells (Aoi et al., 2008), pancreatic β cells (Stadtfeld et al., 2008) and terminally differentiated lymphocytes (Eminli et al., 2009). Advances in the area of iPSCs generation permitted the development of different combinations of factors able to induce pluripotency suggesting that an indefinite number of other molecular factors is implicated in the reprogramming process towards pluripotency. These modulators of the iPSCs state include transcription factors (Sox1 and Kfl2 (Nakagawa et al., 2008)), chromatin regulators (such as histone deacetylase (HDAC) inhibitor with valproic acid (VPA) (Huangfu et al., 2008), growth factors receptors (Yu et al., 2007) as well as miRNAs (Yu et al., 2007). However, it has been shown that expression of Yamanaka's factors is only essential in the initial steps of reprogramming and undesired silencing of the exogenous factors might occur by epigenetic factors such as DNA and histone methyltransferases (Stadtfeld et al., 2008). Reprograming blocks were also observed when constitutively active lentiviral vectors were used (Brambrink et al., 2008; Sommer et al., 2010). Overexpression of the reprograming factors such as c-Myc led to increased tumourigenicity in chimera mice (Nakagawa et al., 2008; Takahashi and Yamanaka 2006). Successful reprograming, albeit with a reduced efficiency and speed, was also achieved without the expression of exogenous c-Myc (Nakagawa et al., 2008; Marson et al., 2008) or with the use of inducible and polycistronic lentiviral vectors (Sommer et al., 2009). To circumvent the possible harmful effects, such as insertional mutagenesis and leaky transgene expression, of reprogramming through integrating vectors, integration-free techniques to generate iPSCs have been developed. These include non-integrating

vectors such as Sendai viruses (Fusaki et al., 2009), polycistronic vectors with Cre-lox system (Kaji et al., 2009), modified mRNA expressing reprogramming factors (Warren et al., 2010), transposons (Soldner et al., 2009) and proteins (Zhou et al., 2009).

Another important key factor to achieve high efficiency and quality of reprograming is the starting somatic cell population. Different somatic cells lineages showed variable reprogramming capacities depending on their origin, differentiation stage (progenitors or terminally differentiated cells) and gene expression profile predisposition. Furthermore, although genome-wide transcriptomic analyses comparing human iPSCs and hESCs showed no significant differences in their global gene expression, DNA methylation and histone patterns (Guenther et al., 2010), iPSCs displayed to have propensity for differentiation towards specific cell lineages. Remnants of epigenetic imprinting from the donor tissue, known as “epigenetic memory”, have been shown to predispose iPSCs to differentiation to the cell type of origin. For example, iPSCs derived from foreskin keratinocytes and umbilical cord blood have been shown to have a much higher differentiation potential for their respective cell lines as their tissue of origin (Kim et al., 2010). Subsequently, molecular analyses of the iPSCs-methylation patterns confirmed the presence of differentially methylated loci depending on their tissue of origin. These findings suggest that human iPSCs do not efficiently silence the expression patterns of the somatic cells from which they are derived. Different studies indicate that early-passage iPSCs are most likely to retain transient epigenetic signatures and fail to induce certain genes expressed in undifferentiated and highly proliferative hESCs. The supplementation of epidermal-derived iPSCs with exogenous cytokine such as WNT3A was shown to increase their blood-forming colony, thus suggesting that epigenetic marks can be overcome by manipulating the culture conditions (Kim et al., 2010). Although iPSCs can overcome the limitations associated with ESCs and offer a promise of personalized treatment, recent studies have shown increased genomic instability, epigenetic abnormality, and immunogenicity of iPSCs, raising safety concerns of iPSC-based cell therapy (Sebban and Buganim, 2016). Safe and successful application of iPSCs in cell and gene therapy requires a pure population of fully differentiated cells. In addition, standardized and efficient protocols for cell

reprogramming need to be established. Therefore, despite significant advances in the field of iPSCs technology, crucial criteria for their manufacturing and safety need to be met before their clinical use.

1.5.5.1 Application of iPSCs in dermatology

In dermatology, iPSCs have already been investigated for *in vitro* disease modelling and for generation of *de novo* keratinocytes for repair strategies when patients' cells are not available. Unlike primary keratinocytes and fibroblasts, iPSCs are more amenable to genetic manipulation both by the means of classic gene therapy or the novel gene and base editing strategies. Access to EB patient's keratinocytes is not always possible due to the young age of the patient and the severity of the disease. In severe forms of RDEB, where patient's skin is under chronic inflammation as a result of persistent blistering, keratinocyte stem cells might become depleted and cannot be cultivated or expanded *in vitro* prior to gene correction. Additionally, extensive manipulations of primary keratinocytes and clonal selection of single gene-corrected cell might also interfere with their self-renewal capacity leading to exhaustion and senescence (Siprashvili et al., 2016; Latella et al., 2017; De Rosa et al., 2019). Furthermore, because the epidermis is continuously renewed by keratinocyte stem cells in the proliferative basal layer, any permanent genetic correction must target this stem cell population. Although *in vitro* clonal analysis might be required in gene-corrected RDEB-iPSCs, they can in theory provide an inexhaustible supply of *COL7A1* functional cells due to their indefinite self-renewal capacity. So far, various skin cell types, such as fibroblasts, keratinocytes and melanocytes, have been used for reprogramming into iPSCs (Aasen et al., 2008; Utikal et al., 2009). Keratinocytes and melanocytes showed higher reprogramming efficiency compared to fibroblasts and their residual epigenetic memory may allow for easier differentiation back into the corresponding original cell type for cell replacement. To date, human iPSCs have been used to generate multi-lineages cell types populating the skin, including keratinocytes (**Table 1.2** and **Table 1.3**), folliculogenic human epithelial stem cells (Yang et al., 2014), fibroblasts (**Table 1.4**) and melanocytes (Ohta et al., 2011; Liu et al., 2019). The use of iPS-derived skin cells combined with the development of 3D scaffold systems resulted in the generation of cellular models for several

genodermatoses including different forms of epidermolysis bullosa, such as EBS (Bilousova and Roop, 2014), JEB (Tolar et al., 2013) and DEB (Itoh et al., 2011; Tolar et al., 2011), p63 mutant ectrodactyly, ectodermal dysplasia (Shalom-Feuerstein et al., 2013), epidermolytic hyperkeratosis (Bilousova et al., 2011), dyskeratosis congenita (DC) (Agarwal et al., 2010; Batista et al., 2011) and ichthyosis (Petrova et al., 2014; Kolundzic et al., 2019). Despite significant advances in the field of iPSCs, crucial criteria for their manufacture and safety need to be met before their clinical use. Moreover, elucidation of the long-term skin regeneration capacity and safety profile of cells derived from iPSCs is required before safe and efficacious clinical translation can take place.

1.5.5.2 Differentiation of pluripotent stem cells into keratinocytes

The main prerequisite that has to be met when manipulating cell fate of a pluripotent stem cell *in vitro*, is a thorough understanding of the embryonic morphogenesis of a given tissue, in order to achieve efficient production of the desired cell type. Over the last decades, significant advances in the field of pluripotent stem cells (PSCs) and epidermal stem cells biology have contributed towards the generation of keratinocytes derived from ESCs and iPSCs. One of the first reported evidence of keratinocyte-like derivation from murine ESCs (mESCs) was shown by Bagutti *et al.* in 1996 (Bagutti et al., 1996) alongside molecular studies on the role of β1 integrin in the epidermal differentiation process (Bagutti et al., 2001). *In vitro* cellular aggregates, known as embryoid bodies (EBs) (Doetschmanet al., 1985), from wild type mESCs cultured on de-epidermized human dermis (DED) with human dermal fibroblasts showed the formation of a small group of cells expressing common keratinocyte stem cell markers such as cytokeratin 14 (K14) and adhesion protein like α6β4 integrin. In accordance with the contribution of feeder layer in the epidermal cell maintenance *in vitro* (Green et al., 1979; Rheinwatd and Green 1975), the paracrine signalling promoted by fibroblasts in culture lead to the release of growth factors such as FGF10, TGFα and KGF that are capable of promoting growth and maturation of ESC-derived epidermal stem cells into multi-layered skin (Bagutti et al., 1996).

An important milestone in understanding the molecular network in the *in vitro* epidermal differentiation from ESCs was achieved by Kawasaki and colleagues as part of the study on generating neuronal stem cells from mESCs (Kawasaki et al., 2000). Upon gastrulation, the ectodermal germ layer has the potential to differentiate towards surface ectoderm and neuroectoderm which ultimately specify into the skin epithelium and the nervous system, respectively (Hemmati-Brivanlou and Meltont 1997). *In vitro*/*in vivo* fate-mapping and gene-knockout studies of the genesis of the epidermis have shown that bone morphogenic protein 4 (BMP-4), a member of the transforming growth factor β (TGFβ) ligand superfamily, can influence the commitment of ESCs into ectodermal-epidermal fate over ectodermal-neuronal one (Hemmati-Brivanlou and Meltont 1997; Baker et al., 1999; Davis et al., 2004; Troy and Turksen., 2005).

The importance of BMP-4 for keratinocyte derivation was confirmed by the study by Coraux *et al.*, where K14+ progenitor cells able to produce multi-layered epidermal tissue in organotypic culture models were obtained (Coraux et al., 2003). Histology and immunofluorescence staining of the generated epidermis revealed the expression of further keratinocyte markers, such as collagen IV, VII, laminin-332 and α6β4 integrin at the *stratum basale,* as well as the expression of epidermal differentiation markers in the outermost layers. Transmission electron microscopy of the BMZ of the reconstituted skin displayed formation of hemidesmosomes and AFs, thus confirming that mESCs-derived keratinocytes can correctly recapitulate keratinocyte phenotype and skin architecture and structure.

Alongside BMP-4, retinoic acid (RA) exhibits stage-specific effects on epithelial differentiation from hESCs. RA is a pleiotropic potent regulator of cell proliferation and modulator of cell differentiation highly involved in embryonic stem cells (Gudas and Wagner., 2011), as well as skin morphogenesis (Fisher and Voorhees., 1996). Addition of RA to primary human keratinocytes was shown to inhibit the terminal differentiation of keratinocytes *in vitro* by modulating the expression of ΔNp63 (Bamberger et al., 2002), a master key regulator of keratinocyte proliferation and epidermal stratification (Mills et al., 1999; Yang et al., 1999). Accordingly, it has been shown that RA increases the frequency of hESC-derived epithelial cells expressing

p63, K14, laminin332, and involucrin (IVN) and cytokeratin 10 (K10) in the outermost epithelial-like layers in organotypic culture (Metallo et al., 2010; Metallo et al., 2008).

Consequently, several studies confirmed that synergic induction of BMP-4 and RA in hESCs mimics the commitment of the surface ectoderm derived from pluripotent stem cells into single-layered epithelium expressing early epidermal markers such as cytokeratin 8 (K8) and 18 (K18) (Lingyu Li et al., 2013; Metallo et al., 2008; Aberdam et al., 2008; Selekman et al., 2013). Cultivation of ESC-derived K18+ epidermal progenitors on stromal fibroblast layer drove epidermal lineage maturation, consisting of cell death, migration, and epithelial colony formation of p63+/K14+ hESC-derived basal keratinocytes (Aberdam et al., 2008). In support of such findings, in depth molecular and epigenetic understandings of keratinocyte development from pluripotent stem cells have been developed. High-throughput RNA sequencing and chromatin landscape organization during lineage-specific commitment into keratinocyte, revealed key transitions master regulators of lineage initiation and maturation of keratinocytes (Lingjie Li et al., 2019). Three major stages of epigenetic landscapes and associated-gene expression patterns changes have been described as the sequential transition between pluripotent stem cell, characterized by OCT4 (POU5F1), surface ectoderm progenitor (initiation), typified by K8 and K18 expression upon BMP-4 and RA treatment and mature keratinocyte (maturation) corresponding to the emerging expression of p63

Despite the accepted role of RA/BMP-4 in the earliest epidermal commitment, significant variability between all the studies on PSC-differentiation into epidermal cells can be explained by the differences in the composition of matrix and media used, often resulting in variable differentiation efficiencies and poor reproducibility. Therefore, multiple studies have addressed the role of cell-cell and cell-matrix interactions in epithelial and epidermal differentiation. The importance of cell-matrix interaction was observed in β1 *null* mESCs which were unable to differentiate towards epidermal lineages (Bagutti et al., 2001). The absence of the β1 integrin, in fact, lead to the lack of molecular networks between the cells and growth factors, expressed by the ECM *in vivo* or surrogate matrix *in vitro*, leading to impaired keratinocyte differentiation (Bagutti et al., 2001). Serial cultivation of hESCs on

stromal fibroblast layer showed an enriched and stable population of K18/K8 positive epithelial cells derived from the ectodermal lineage (Aberdam et al., 2008). In addition, cell density during the commitment phase in RA-based epithelial differentiation protocol is critical. It has been estimated that cell density of at least 4500 cells/cm^2 is necessary to achieve an almost pure population of committed K18+ simple epithelial cells (Selekman et al., 2013). Moreover, hESCs can be differentiated, either as EB aggregates or adherent cells, on different ECMs, such as collagen I, (Metallo et al., 2010; Metallo et al. 2010), collagen IV (Bilousova et al., 2011) or commercial coating matrices with variable collagen/laminin ratio such as Matrigel® (Shinkuma et al., 2016), Geltrex® (Kogut et al., 2013), StemAdhere and Synthemax (Selekman et al., 2013).

High variability has been also observed in the media composition. Similarly to normal human keratinocyte culture, a co-culture system consisting of ESCs and irradiated feeder layers and use of optimized media (such as FAD) containing insulin, fibroblast growth factor (FGF), and epidermal growth factor (EGF) provided a suitable molecular environment for ESCs differentiation into epidermal cells (Guenou et al., 2009; Haase et al., 2007; Aberdam et al., 2008; Green et al., 2003). However, different rates of epidermal cell-derivation, abnormal colony formation of keratinocyte-like cells and short-cell doubling were observed in all the studies.

Abnormal colony morphology of iPSCs-derived keratinocytes was postulated to be related to ambiguity of markers to identify epithelial cells derived from PSC cells as “keratinocytes” and the fact that FAD medium equally supports the growth of epidermal subtypes from other stratified and non-stratified epithelia of both endodermal and ectodermal origin (Pellegrini et al., 1999). For example, p63 and K14 were also reported as general markers of endodermal commitment during development (Dabelsteen et al., 2009). Cells from epidermal tissues such as urothelial and tracheobronchial share the same markers with epidermal keratinocytes, including p63/K14 in the basal layer and involucrin/K10 during their commitment to terminal differentiation (Dabelsteen et al., 2009). The short-lived progeny of epidermal-derived cells was shown to be related to impaired regulation of the p16INK4A and p14ARF-dependent senescence mechanisms (Dabelsteen et al., 2009;

Iuchi et al., 2006) or due to an incomplete epidermal differentiation *in vitro.* Use of more defined keratinocyte medium (such as DM and DKSFM) in ESCs showed significant level of epidermal enrichment with higher number of p63/K14 expressing cells compared to FAD medium (Metallo et al., 2010; Itoh et al., 2013). Similarly, in iPSCs the highest rate of p63+/K14+ keratinocytes derivation was achieved when cells were cultured in DKSFM with up to 44.7% of p63+/K14+ cells obtained after the 30-days of differentiation and over 70% after the first passage, indicating that K14+ population can be enriched by culture conditions (Itoh et al., 2013). Furthermore, enrichment of K14 cells is feasible by flow sorting the cells expressing high levels of integrin α6 (ITGA6) and β4 (ITGB4) in order to obtain a pure keratinocyte population for downstream studies (Itoh et al., 2013).

Alongside the capacity of PSC-derived keratinocyte to stratify and recapitulate the skin architecture in 3D models *in vitro* and *in vivo*, iPSC-derived epidermal stem cells were shown to form *de novo* hair follicles, sebaceous glands and interfollicular epidermis hence confirming the multipotent capacity of PSC-derived epidermal stem cells (Yang et al., 2014; Bilousova et al., 2011). Yang study has also shown that fine temporal control of EGF, RA and BMP signalling leads to the expression of intracellular and surface markers of epithelial stem cells from the hair follicle bulge, including cytokeratin 15 (K15) and CD200+/ITGA6+, with as a similar gene expression levels in hiPSC-derived epidermal stem cells as in human hair follicles (Yang et al., 2014). Human iPSC-derived cells were shown to be capable of generating all hair follicle lineages including the hair shaft, and the inner and outer root sheaths in skin reconstitution assays.

In the context of EB, significant effort has been put into the development and validation of differentiation protocols for obtaining keratinocytes and other relevant cell types from iPSCs for a potential cell therapy application (Itoh et al., 2011; Umegaki-arao et al., 2014; Bilousova et al., 2011). Several research groups have demonstrated the feasibility of generating iPSC-derived keratinocytes from patients with various forms of EB (Umegaki-arao et al., 2014; Tolar et al., 2011; Webber et al., 2016; Shinkuma et al., 2016; Jacków et al., 2019; Osborn et al., 2020). First examples of potential application of iPSCs technology in EB were described by Umegaki *et al.*

and Tolar *et al.*, with the generation of iPSCs from keratinocytes and fibroblasts obtained from patients who presented with revertant mosaicism for JEB and RDEB, respectively (Umegaki-Arao et al., 2014; Tolar et al., 2011). These iPSCs were then differentiated into keratinocytes, which exhibited similar global gene expression profile as the original somatic revertant keratinocytes and showed upregulated expression of *COL17A1* or *COL7A1* compared to the mutant, non-revertant cells (Umegaki-Arao et al., 2014; Tolar et al., 2011). C17 and C7 proteins were also detected in the basal layer in xenograft mouse models (Umegaki-Arao et al., 2014; Tolar et al., 2011).

In the absence or revertant mosaicism, several research groups have successfully combined cell reprogramming and differentiation with gene and base editing strategies to produce functional, gene corrected cells (Shinkuma et al., 2016; Jacków et al., 2019; Sebastiano et al., 2014; Osborn et al., 2020). *COL7A1*-corrected iPSC-derived keratinocytes were shown to share morphological and biological features of primary human keratinocytes, including the ability to produce epidermal sheets expressing functional C7 resulting in AF formation *in vivo* (Shinkuma et al., 2016; Jacków et al., 2019). To assess the potential of iPSC-derived keratinocytes in cellular therapy for RDEB, molecular analysis from 2D cultures confirmed the expression of full length of secreted mature collagen VII as well as its deposition at the basement membrane zone and anchoring fibrils formations in 3D skin equivalents *in vivo* (Shinkuma et al., 2016; Jacków et al., 2019).

1.5.5.3 Differentiation of pluripotent stem cells into fibroblasts

In contrast to keratinocyte differentiation, established protocols for generating dermal fibroblasts from ESCs/iPSCs have not been fully defined yet. Elucidation of the protocols for dermal fibroblasts differentiation has been hindered by insufficient knowledge in the developmental biology of mesodermal tissues and a lack of specific markers of fibroblasts maturation. Spontaneous differentiation of ESCs-derived embryoid bodies (EBs) into fibroblast-like spindle-shaped cells has been observed in different studies (Chen et al., 2009; Xu et al., 2004; Togo et al., 2011).

Studies of Hewitt *et al*. have reported simultaneous generation of multiple skin cell lineages, including keratinocyte- and fibroblast-like cells from ESCs and iPSCs (Hewitt et al., 2009, 2011; Shamis et al., 2012). PSCs were differentiated into heterogeneous mix of epithelial and fibroblast cells using FAD medium, feeder layers and BMP-4, components widely used for generating epithelial cells from ESCs/iPSCs. In these studies, both iPSCs/ESCs-derived fibroblasts shared similar cell morphology characterized by elongated and polygonal cell shapes with proliferative potential between 10-18 doublings (Hewitt et al., 2009, 2011; Shamis et al., 2012). During differentiation, progressive loss of pluripotency markers in both hESCs and iPSCs was observed alongside increasing co-expression of mesenchymal stromal stem cell associated antigens (CD73, CD10, and CD13) and endothelial adhesion molecules (such as CD105) with levels of expression similar to parental fibroblasts. In addition, overlapping patterns of fibroblasts-related genes and methylation profiles of promoters associated with ECM (such as collagens I and IV) production, were observed. Supplementation with ascorbic acid, known to increase collagen synthesis (Pinnel, 1987), resulted in greater production of proα1 (I) (COL1A1), proα1(IV) (COL4A1), proα1(III) (COL3A1) and pro-α1(V) (COL5A1) collagens in fibroblast-like cells compared to the parental ones (Shamis et al., 2012). PSC-derived-fibroblasts were also shown to deposit *de novo* ECM-forming basement membrane interface when co-cultivated with foreskin-derived keratinocyte *in vitro,* thereby mimicking the crosstalk between stromal and epidermal skin compartments required for tissue development.

Based on the evidence of ascorbic acid (Franceschi 2009; Keller 2005) and TGFβ family members (Kumar and Sun 2005; Watabe and Miyazono 2009) contribution to mesodermal development from ESCs, Itoh *et al.* developed a different method of deriving pure fibroblasts from iPSCs (Itoh et al., 2013). IPSC-derived cells expressed mesodermal and fibroblast inductions markers such as CD73, CD90 alongside multiple types of collagens, including type I, III, IV and VII. As with PSC-derived keratinocytes, iPS-derived cells with features of fibroblasts may present an important source for future therapeutic applications in RDEB. In this direction, PSCs-derived fibroblasts and keratinocytes were shown to be successfully co-cultivated on matrix

supports in order to generate skin equivalents (SEs) for RDEB and other skin disorders (Itoh et al., 2013; Kim et al., 2018). SEs are composed of both keratinocytes and fibroblasts and, hence, have a potential to combine the positive effects of both cell types. Several studies showed that SEs, composed of healthy or gene corrected RDEB iPSCs-derived keratinocytes and fibroblasts, were able to deposit ECM-forming basement membrane interface and sustain significant *de novo* C7 expression at the BMZ when grafted onto immunodeficient mice (Itoh et al., 2013; Kim et al., 2018). Potential of such application in RDEB resides on the fact that SE are currently under evaluation in clinical trials. Despite the rapid progression towards the clinical use of iPSCs, further elucidation on the molecular features that define these iPS- and ES-derived fibroblasts following differentiation must be taken to fine-tune the engineering of specific types of fibroblasts that function in the development of organs and tissues.

Collectively, hESCs and hiPSCs offer a potential to generate all relevant cell types that can be used in gene and cell therapy for EB. Despite the advances in establishing the protocols for epidermal and dermal differentiation from ESCs and iPSCs, major roadblocks remain. To meet clinical demands for the various cell types that can be generated from hPSCs, it is necessary to employ reproducible differentiation systems with fully defined cell culture and matrix components. To this end, dissecting genome-wide regulatory landscape during differentiation remains critical for understanding lineage commitment in epidermal and dermal development.

Table 1.2 Differentiation of ESCs into keratinocytes

Ref.	Cell Line	Method	Matrix	Media+IF	Markers	Comments
Bagutti et al. 1996	mESC D3 mESC (G-201) (β1-)	EBs	Feeder layer Gel.Coating	CM EM	K14,α6β4int, K10,K8,K18,K19	Keratinocytes No terminal differentiation (K1- /Involucrin-)
Bagutti et al. 2001	mESC (D3) mESC (G-201) (β1-)	EBs	HDF DED	CM *FGF,KGF,FGF10,TGFα,TGFβ1, HGF*	K5,K14,α6β4int,K10	Cysts resembling stratified squamous epithelia (D3)
Kawasaki et al. 2000	mESC (EB5)	Ad	PA6 feeder	EM (*+ BMP-4, 2-βME*)	K14	Epidermal differentiation only
Coraux et al. 2003	mESC (CGR8)	Ad	HNFs/NIH-3T3	EM (+ *BMP-4 or AA*)	K14, K10, ColIV/VII, α6β4int, lamα3, filaggrin	Stratification and formation of BMZ Cutaneous epidermal cells
Green et al. 2003	hESC (H9)	- EBs -Teratoma	NIH-3T3	FAD	K14, p63, involucrin, basonuclin	General keratinocytes of squamous epithelium Sparse stratification (involucrin+) ~15 doublings
Selekman et al. 2013	hESC (H9)	Ad	StemAdhere Synthemax ®	UCM (+ *RA*) DKSFM	K18,K14,P63,filaggrin, involucrin, K10	K14+/p63+ keratinocyte progenitor Cell doubling depending on the substrate
Aberdam et al. 2008	hESC (H9)	Ad	PA6feeder/ NIH-3T3	FAD (*+ BMP-4*)	K8/K18 intermediate K14, p63, lamα3	~60 doublings for K8/K18+cells
Metallo et al. 2008, 2010	hESC (H1,H9)	EBs/Ad	Gel.coating	DKSFM *+RA* (for EB) DKSFM *+RA+BMP-4* (Ad)	K18, K14, p63, involucrin, filaggrin	~10 doublings Keratinocyte progenitors
Hewitt et al. 2009	hESCs (H9)	Ad	MEF (day0-14) Plastic (14-21) Col-I (21)	NHK (day0-7) NHK (+BMP-4) (Day4-7) SCES (day 7-14) NHK (14-onwords)	K18	>20 passages

Guenou et al. 2009	hESC H9, SA01	Ad	NIH-3T3/ColI	FAD *(+ BMP-4 + AA)* KGM2	p63, K5, K14, K10, involucrin, α6β4int, laminin332, filaggrin, ColVII	Long replicative lifespan of p63/K14 + cells (~40-60 doublings) Epidermal keratinocytes
Huang et al. 2008	mESCs (KM,DS3,CJ7)	Ad	MEF	EM + MEF EM only	K14,K18,K10, involucrin	Variable cell doubling (10-30) Keratinocyte-like cells
Haase et al. 2007	mESC (CCE)	EBs	ColI	FAD	K14, involucrin	Epithelial cells, no long-term culture No successful cell passaging

Summary table compiled based on published data of PSCs differentiation into keratinocyte lineages discussed in section 1.5.2.2. To note: due to the high variability and complexity of all the differentiation protocols cited in this thesis, a simplified representation of the most important characteristics of each study are reported in the table. Abbreviations: column "**cell line**": mESC, Mouse embryonic stem cells; hESCs, human embryonic stem cells; in brackets are the names of the cell lines used in every study. Column "**Method**": EBs, Embryoid bodies; Ad, adherent cells. Column "**Matrix**": HDF, human dermal fibroblasts; DED, de-epidermized dermis; HNF, human normal fibroblasts; NIH-3T3, Todaro and Green 3T3 mouse embryonic fibroblast line; Col, collagen; MEF, mouse embryonic fibroblasts; column "**Media + inducing factors (IF)**": CM, conditioned medium; EM, various versions of Eagle's medium; ESCM, Embryonic stem cell culture medium; FAD: serum and growth factor supplemented Rheinwald/Green medium widely used for keratinocyte growth; KGM2, keratinocyte growth medium; RA, Retinoic Acid; BMP-4, Bone morphogenetic protein 4; AA, Ascorbic acid. Column "**markers**" (epidermal markers detected on protein level by immunostaining or Western blot analysis): K14, keratin 14; K5; Keratin 5; K10, keratin 10; K8; Keratin 8; K18, keratin 18; col-VII, collagen VII; Col-XVII, collagen XVII; p63, TP63 transformation-related protein 63; α6β4int,integrin alpha6 beta4.

Table 1.3 Differentiation of iPSCs into keratinocytes

Ref.	Cell Line	Method	Matrix	Media + IF	Markers	Protocol duration	Note
Bilousova et al., 2011	miPSC	EBs	ColIV	ESCM (Initiation) *+ RA/BMP-4* DKSFM (Maturation) *+Ca^{++}*(terminal differentiation)	K14, K5, p63, K1, loricrin	>14 days	*De novo* keratinocyte Hair, Sebaceous glands *(in vivo)* ~18 doublings
Itoh et al., 2011, 2013	hiPSCs (RDEB/WT)	Ad	Matrigel®	ESCM (Initiation) *+ RA + BMP-4* DKSFM (Maturation) DKSFM(Terminal differentiation) *+ Ca^{++}*	K14, K5, α6β4int, K10	>30 days	~ 5 passages Epidermal keratinocytes Increase of K14+/p63+ upon rapid attachments
Kogut et al., 2013	hiPSCs	Ad	Geltrex®/ColIIV ColI/ColIV-rapid attachment	DKSFM (Initiation) *+ RA + BMP-4* DKSFM (Maturation) CnT07 (Maturation/Propagation)	K14, p63	>24 days	Pure K14+ population after 3 Rapid Attachments
Tolar et al., 2013	hiPSCs (JEB)	EBs	Low attachment, Gel Coating	DKSFM *+ RA + BMP-4*	K5, K1, Col-VII, Col-XVII	nr	Keratinocyte cells
Sebastiano et al., 2014	hiPSCs	EBs	Gel.coating ColI (propagation)	FAD (initiation) *+ RA + BMP-4* N2 (commitment) *+ RA + BMP-4* DKSFM (maturation)	K14, p63, K10, laminin-332, α6int, Involucrin, Dsg3	>60 days	Keratinocyte cells
Webber et al., 2016	hiPSCs (RDEB)	Ad	Geltrex® ColI/ColIV-rapid attachment	DKSFM (initiation) *+ RA + BMP-4* DKSFM (maturation) CnT07 (Maturation/propagation)	K14, p63, K5	>24 days	Keratinocyte cells

Kim et al. 2018	hiPSCs	EBs	ColIV	EM *(+ RA + BMP-4)* -Initiation EM*(+ RA + BMP-4)*- Maturation EM *(+ EGF + BMP-4)*-Maturation	K14, p63, K5, involucrin, loricrin	>30 days	Keratinocyte cells similar to primary keratinocytes in morphology and gene expression
Yang et al. 2014	hiPSCs	EBs	3T3-feeder	EM (Initiation) *+ BMP-4* DKFSM (maturation) *+ RA + BMP-4* *KSFM/DKSFM (maturation)* *+ BMP-4 + RA + EGF* KSFM (propagation) *+ EGF*	CD200, α6int, K18, K5, K14, K15, P63	>40 days	iPSCs-derived EpSCs able to reconstitute the epithelial components of the hair follicle and interfollicular epidermis
Jacków et al. 2019	hiPSCs (RDEB)	Ad	Vitronectin	PSCM (Initiation) *+ RA + BMP-4* DKSFM (Maturation/Propagation)	K14, p63, K10, loricrin	>60 days	Keratinocyte cells Stratified epidermis from human skin equivalent *in vivo*
Petrova et al. 2014	hiPSCs/hESCs	Ad	Matrigel® HDF-ECM ColIV	PSCM (Initiation) *+ RA + BMP-4* EM (Selection) *+ RA + BMP-4* DKSFM (Maturation) *+ RA* EpiLife®(Propagation)	K14, p63, K18, filaggrin, loricrin, involucrin	>28 days	Stratification and formation of BMZ-like structure

Summary table compiled based on published data of PSCs differentiation into keratinocyte lineages discussed in section 15.2.2. To note: due to the high variability and complexity of all the differentiation protocols cited in this thesis, a simplified representation of the most important characteristics of each study are reported in the table. Abbreviations: column "**cell line**": miPSCs, Mouse induced pluripotent stem cells; hiPSCS, human induced pluripotent stem cells; (RDEB), studies that used RDEB-iPSCs. Column "**Method**": EBs, Embryoid bodies; Ad, adherent cells. Column "**Matrix**". Different matrix and media are used according to the differentiation stage. Typically, the commitment of pluripotent stem cells into epidermal cells is classified in three stages: *initiation*, cells are

committed towards ectodermal differentiation, *maturation* and *propagation* of fully mature PSC-derived keratinocytes. Abbreviations: HDF, human dermal fibroblasts; DED, de-epidermized dermis; HNF, human normal fibroblasts; NIH-3T3, Todaro and Green 3T3 mouse embryonic fibroblast line; Col, collagen; MEF, mouse embryonic fibroblasts. Column "**Media + inducing factors (IF)**": CM, conditioned medium; UM, unconditioned medium; EM, various versions of Eagle's medium; ESCM, Embryonic stem cell culture medium; FAD: serum and growth factor supplemented Rheinwald/Green medium. DKSFM/KSFM, Defined/keratinocyte serum-free medium; CnT07®, EpiLife®, are proprietary media used for keratinocyte cultivation; RA, Retinoic Acid; BMP-4, Bone morphogenetic protein 4; AA, Ascorbic acid. Column "**markers**" (epidermal markers detected on protein level by immunostaining or Western blot analysis): K14, keratin 14; K5; Keratin 5; K10, keratin 10; K8; Keratin 8; K18, keratin 18; K15, keratin 15, colVII, collagen VII; Col-XVII, collagen XVII; p63, TP63 transformation-related protein 63; α6β4int, integrin alpha6 beta4.

Table 1.4 Differentiation of ESCs/iPSCs into fibroblasts

Ref.	Cell Line	Method	Matrix	Media + IF	Markers	Protocol duration	Note
Itoh et al., 2013/ Jacków et al., 2019	hiPSCs (RDEB/WT)	EBs	Gel coating Plastic	DMEM + 20%FBS *+ AA + TGF- β2* DMEM *+20%FBS* DMEM *+10%FBS*	ColIII, ColI, vimentin, CD-90,CD-73	>30 days	Morphology of spindle-shaped iPSC-derived fibroblasts was observed after several passages. RDEB-induced fibroblasts able to produce colVII and fulfil epidermal stratification in SE
Kim et al., 2018	CBMC-iPSCs	EBs	Matrigel® coating plastic Coll coating	EM1 *+EGF (+BMP-4)* EM2	Fibronectin, vimentin, CD-73, CD-105, CD-90, ColI, ColIII	>30 days	Fibroblasts cells Derived fibroblasts supports development and maturation of keratinocytes in SE
Hewitt et al., 2009, 2011; Shamis et al., 2012	iPSCs/hESCs (H9)	Ad	MEF (day0-14) Plastic (14-21) ColI (21)	NHK (day0-7) NHK (+BMP-4) (Day4-7) SCES (day 7-14) NHK (14-onwords)	K18, CD73, CD-10,CD-13,CD-105, CD166,ColI,ColIII,colIV,ColV vimentin	>30 days	proliferative potential between 10-18 doublings Derived fibroblasts supports development and maturation of keratinocytes in SE Production of ECM in the BMZ

Summary table compiled based on published data of PSCs differentiation into fibroblasts discussed in section 15.2.3. To note: a simplified representation of the most important characteristics of each protocols are reported in the table. Abbreviations: column "**cell line**": hiPSCs, human induced pluripotent stem cells; CMBC, Cord blood mononuclear cells; ESCs, embryonic stem cells. Column "**Method**": EBs, Embryoid bodies; Ad, adherent cells. Column "**Matrix**": ColI, type I collagen; MEF, mouse embryonic fibroblasts. Column "**Media + inducing factors (IF)**" EM, various versions of Eagle's medium for different stage of iPSCs-derived fibroblast derivation; DMEM, Dulbecco's Modified Eagle Medium: FBS, fetal bovine serum; AA, ascorbic acid; TGF-β2, Transforming growth factor-beta 2; BMP-4, Bone morphogenetic protein 4; EGF, epidermal grow factor. Column "**markers**" (Mesenchymal/fibroblasts markers are detected on cDNA and protein level): colI, collagen I; colIII, collagen III; colIV, collagen IV, colV, collagen V, col VII, collagen VII.

1.6 Gene therapy for RDEB

Despite the potential of cell therapy protocols for RDEB, their long-term efficacy and safety are still unclear. With the advent of gene therapy, correction of patient`s cells by adding a wild type copy of the affected gene by viral vectors offers a promising potential for skin diseases. Like fibroblasts, human keratinocytes are a useful cell type for clinical applications in DEB. Thanks to the pioneering work by Barrandon and Green, primary epidermal stem cells (also known as holoclones) can be cultured *in vitro* while preserving their self-renewal, proliferative potential and differentiation-stratification properties (Barrandon and Green, 1987; Pellegrini et al., 1999). Although their cultivation *in vitro* can be challenging, keratinocytes showed to be a suitable target for viral gene therapies allowing the creation of autologous keratinocyte sheets that could be grafted on DEB patient wound beds.

1.6.1 Gamma-retrovirus based therapies for RDEB

In the last decades gamma-retroviruses have been converted into efficient DNA carriers for gene addition therapies by inserting a copy of the wild type gene within the retroviral genome. To take advantage of a virus for vector development, retroviral backbones were engineered and all genes encoding for structural, replication and envelop retroviral proteins, *gag pol env*, respectively, were divided into separate plasmids to reduce the likelihood of replication competent retrovirus (RCR) in gene-modified cells (Sakuma et al.,2012). The resulting retroviral backbone can accommodate a copy of a therapeutic cassette expressed from the viral 5' long terminal repeat (5'LTR). Retroviral vector have been adapted for RDEB gene therapy. Despite recent promising results in *ex vivo* skin gene therapy trial, where over 80% of patient`s body surface affected by JEB was replaced by autologous *LAMB3*-corrected skin grafts regenerating a long-term fully functional epidermis, addition of a normal copy of the *COL7A1* gene remains one of the biggest hurdles setting back the development of human gene therapy protocols for RDEB. To overcome limitations associated with the large size of the *COL7A1* cDNA (8.9Kb) and hence the inability to accommodate the full-length gene inside a gamma retroviral vector as well as the presence of repetitive sequences encoding for the Gly-X-Y collagenous central

domain, a *COL7A1* minigene lacking exons 70-104 which was able to mimic C7 trimerization was designed by Chen *et al*. (Chen et al., 2000) RDEB keratinocytes gene-corrected by retroviral mediated gene transfer showed persistent production of the reduced 230kDa monomer by western blot and enhanced cell adhesion and proliferative potential confirming that "minicollagen VII" had similar functional characteristics as the full-length C7. An alternative strategy to accommodate the transgene was developed by Murauer *et al.* using a trans-splicing repair mechanism of cell's spliceosome to recombine endogenous *COL7A1* pre-mRNA in RDEB keratinocytes along with an exogenously delivered RNA molecule called pre-trans-splicing molecule (PTM) (Murauer et al., 2011). Specifically, full-length *COL7A1* gene was replaced with 3.3Kb of wild type coding sequence from exon 65 to 118 and incorporated with 3' trans-splicing element including 224bp coding sequence complementary to the last nucleotides of the *COL7A1* intron 64 pre-mRNA and 36 nucleotides of exon 65. Correction was achieved *in vitro* in patient cells with a mutation in exon 106 with no signs of truncated C7 produced.

Based on previous investigation in canine RDEB keratinocytes which demonstrated the ability to accommodate the full-length *COL7A1* cDNA into two different retroviral vectors backbones (namely, pLZRS and pMSCV) and achieved correction of the RDEB phenotype *in vitro* (Baldeschi et al., 2003), Gache *et al.* showed the feasibility of pMSCV in human primary RDEB keratinocytes (Gache et al., 2004). Despite low transduction efficiency (40%), sufficient amount of clonogenic keratinocytes could be transduced to produce transplantable epithelia with a self-renewal capacity. Genetically corrected cells in skin equivalents maintained their proliferative potential and reverted the RDEB phenotype by producing 50 times more intra- and extra-cellular C7 than that produced by wild-type keratinocytes. Genetically corrected skin equivalents engrafted onto the back of 6-week old NOD/SCID mice showed deposition of anchoring fibrils at the dermal-epidermal junction 6 months post grafting. Sustained treatment of keratinocytes and fibroblasts *in vivo* with full-length *COL7A1* cDNA (LZRSE-COL71) under long terminal repeat (LTR), was developed by Siprashvili *et al*. (Shukla et al., 2010) Although the large cDNA size of *COL7A1* has a negative impact on virus packaging, causing a reduction in viral titre that hampers the clinical development of this type of vector-based gene therapy, Siprashvili and

co-workers were able to achieve a high viral titre by designing a gibbon ape leukemia virus (GALV) envelope. *In vivo* grafting experiments in immunodeficient mice of *COL7A1*-transduced RDEB keratinocytes resulted in a self-renewing epithelia for more than 12 epidermal turnovers cycles *in vivo* and deposition of human C7 at the basement membrane zone. Following the promising results of the preclinical testing, a phase-I clinical trial treating 4 patients affected by severe RDEB forms was conducted (Siprashvili et al., 2016). Autologous keratinocytes isolated from biopsies were transduced with Good Manufacture practice (GMP) grade LZRSE-*COL7A1*. Although no serious adverse events were reported, in 67% of the grafts generated the presence of self-renewing genetically-corrected keratinocytes was low with faint detection of *de novo* anchoring fibrils at the grafted sites. Variable response in wound healing was observed 1-year post engraftment. Similarly, a 1/2a open-label long-term study using the same retroviral vector has been reported including the 4 patients previously enrolled for a total of 7 patients (Eichstadt et al., 2019). Interestingly 95% of the treated areas showed around 50% or greater (75%) healing progression at 3 and 6 months and stable persistent healing in the grafted areas up to three years post grafting. For some participant, robust wound healing was evaluated up to 5 years. Skin reconstitution determined the presence of C7 and anchoring fibrils in 3 out of 7 patients at 12 months. Notably, a phase 3 trial is anticipated to start in late 2019 (EB-101) (NCT04227106). It is possible that, unlike JEB, limitations of gene therapy for RDEB could be associated to the low viability of skin stem cells and holoclones in DEB patients. Moreover, the use of gamma-retroviral vectors pose additional challenges for RDEB gene therapy due to the fact that retrotranscription of highly repetitive sequences might be more prone to genetic recombination leading to formation of non-functional recombinant C7 (Siprashvili et al., 2016). Furthermore, the use of viral long-terminal repeat (LTR) containing a strong enhancer located in the U3 region to drive transgene expression, was previously associated with a higher risk of insertional mutagenesis (Hacein-bey-abina et al., 2008; Howe et al., 2008; Ott et al., 2006). In fact, insertional mutagenesis has always been one of the biggest concerns in the development of human gene therapy protocols due to the capacity of integrating viral vector to integrate into or in the proximity of proto-oncogenic transcriptional units. Serious adverse events have been reported and described for

lymphoproliferative disorder in patients treated for X-linked Severe Combined Immunodeficiency (X-SCID) (Hacein-bey-abina et al., 2008; Howe et al., 2008) and X-linked Chronic Granulomatous Disease (X-CDG) (Ott et al., 2006).

Therefore, new strategies have emerged aiming to replace the classical gamma-retrovirus-based approach with self-inactivating (SIN) retroviral vectors. To minimize the risk of oncogenic events, Titeux *et al.* developed a minimal self-inactivating (SIN) retroviral vector able to accommodate the full-length *COL7A1* cDNA under the control of the EF1-α promoter used for preclinical studies (Titeux et al. 2010). Both keratinocytes and fibroblasts were transduced with high multiplicity of infection (MOI) two times within 24 hours with a transduction efficiency around 30-80% and 38-70%, respectively. An average copy number of integrated transgene of around 1-3 copies per cell was detected. Despite rearrangement of the proviral *COL7A1* sequence upon retrotranscription, expression of both full-length and recombinant truncated C7 did not hinder the expression and the stability of functional anchoring fibrils at the dermal-epidermal junction of genetically corrected skin equivalents grafted onto immunodeficient mice. Based on encouraging preclinical data and improved biosafety of SIN-gamma-retroviral vector observed *in vivo*, a clinical trial which aims to produce genetically corrected RDEB skin equivalents suitable for transplantation in patients will launch this year (Genegraft) (Gaucher et al., 2020).

1.6.2 Lentiviral-based therapy for RDEB

To overcome the raised concerns in biosafety associated with use of retroviral vectors due to LTR-driven oncogenes and their reversion to a virulent state, 3rd generation replication defective self-inactivating lentiviral vectors based on the human immunodeficiency virus (HIV) have been developed. In contrast to gamma-retroviral vectors, lentiviral vectors are: 1) able to infect both proliferating and non-proliferating cells, 2) can accommodate a larger therapeutic transgene (up to 9.7Kb), 3) have a reduced LTR-driven oncogene expression due to the partial deletion of the U3 region of the 3'LTR which is transferred upon reverse transcription and proviral integration to the 5'LTR (Sakuma et al., 2012). First example of full-length *COL7A1* cDNA encoded in a lentiviral-vector was demonstrated by Chen *et al.*(Chen et al.,

2002). Aiming to improve vector's biosafety, a modified murine leukaemia MND promoter driving the transgene was designed to reduce potential promoter inactivation by cellular methylations. RDEB patient keratinocytes and fibroblast showed long-term expression *in vitro* (5 months). Skin equivalents using either both gene-corrected RDEB keratinocytes and fibroblasts or gene-corrected keratinocytes and RDEB fibroblasts grafted onto immunodeficient mice showed deposition of C7 at dermal-epidermal junction identical to normal control cells (Chen et al., 2002). Nearly all the new deposited C7 was derived from keratinocytes (90-97%) and only 3-10% from fibroblasts. Another means of delivery was shown by Woodley and co-workers where a single intradermal injection of SIN-lentiviral vector into immunodeficient mice provided stable C7 expression at the BMZ for 3 months (Woodley et al., 2004). In contrast to the study by Chen *et al.,* (Chen et al., 2002) investigation whether fibroblasts could solely secrete C7 showed that human skin equivalent made by gene-corrected RDEB fibroblasts and parental RDEB keratinocytes or intradermal injection of gene-corrected fibroblasts in nude mice resulted in linear C7 deposition at the dermal-epidermal junction with a pattern identical to the wild type controls (Woodley et al., 2003). However, the small diffusion radius of intradermally injected cells and the generalized presence of blisters all over the body of the patients hamper the use of such route of administration for clinical therapies. Alternative delivery of lentivirally-corrected fibroblasts through intravenous injection was investigated by Woodley *et al.* (Woodley et al., 2007) Injected fibroblasts appeared to promote wound healing after homing to the wounded skin and secretion of human C7 at the BMZ. Recruitment of the fibroblasts from the circulation was shown to be specific to skin wounds since the cells were not detected in other organs. As with bone marrow cell therapy, molecular mechanisms underlying homing of fibroblasts to the wounded skin is still unknown. Recently, Georgiadis *et al*. developed a therapeutic grade SIN-lentiviral vector encoding codon optimized *COL7A1* transgene driven by phosphoglycerate kinase promoter (PGK) to transduce autologous RDEB fibroblasts (Georgiadis et al., 2016). Despite low transduction efficiency, expression of recombinant full-length C7 was confirmed *in vitro* and in human:murine xenograft *in vivo* showing the presence of anchoring fibrils at the dermal-epidermal junction. Notably, single cell clonal analysis of codon optimized-transduced fibroblast showed

low-level recombination events during reverse transcription linked to truncated sized protein previously observed by Titeux et al. (Titeux et al., 2010). GMP production of engineered fibroblasts enabled their use in phase-I clinical trial with the enrolment of 4 RDEB patients followed 3 intradermal injection of COL7A1-modified autologous fibroblasts in non-blistered skin (NCT02493816) (Lwin et al., 2019). All the 4 patients tolerated the intradermal injections without the presence of adverse events and no immune response to the newly synthetized full-length C7. Overall variable increase of C7 expression was observed at different time points (2 weeks, 3 months 12 months) in the injected areas however, in 2 subjects, no mature anchoring fibrils were detected in the injected skin areas nor proviral coCOL7A1 detected. Despite the limitation of the study due to the small number of patient enrolled, explanations of the lack of AF and no detection of the therapeutic COL7A1 cDNA in skin biopsies are still not clear.

1.6.3 Alternatives to lentiviral/retroviral gene delivery

Finally, alternative full-length *COL7A1* cDNA delivery approach by sleeping beauty T2 (SB) transposon system was developed in RDEB patient keratinocytes *ex vivo* (Latella et al., 2017). To transpose the cassette in primary clonogenic RDEB cells combination of three adenoviral (AdV) vectors has been used. Delivery platform consisted in a helper dependent AdV carrying the transposon cassette flanked by flippase recognition target, a second generation AdV encoding for flippase to mediate linearization of the FRT-flanked transposon and a first-generation vector encoding for the SB100X transposase. Despite multiple infections, the cell population retained clonogenic hallmarks exhibiting similar population doublings as normal keratinocytes. Notably, single cell clonal analysis in engineered keratinocytes showed that 85% of clones were positive for p63 and C7. The ability of engineered keratinocytes to sustain fully corrected C7 was verified *in vivo* based on xenotransplantation of skin equivalents onto immunodeficient mice. Another example of classic gene therapy application was demonstrated by Sebastiano *et al.* in 2014 showing that gene corrected iPSCs from patients with RDEB can differentiate into keratinocytes and generate skin sheets repairing the affected skin areas (Sebastiano et al., 2014). In this study, patient fibroblasts and keratinocytes were

used to generate different patient-specific iPSCs using lentiviral reprogramming vectors under GMP conditions. An adeno associated vector (AAV) carrying a donor template with asymmetric homology arms (8.8kb and 4.4kb) covering 31 exons and a central neomycin and thymidine kinase cassette for gene-correct cell selection. Gene correction by HDR, showed a target efficiency of 11% and 3% in the bulk population and 26% and 75% upon clonal selection *in vitro*. To address limitations related to safety of viral vectors and challenges to accommodate the entire size of *COL7A1* gene, alternative non-viral based gene therapy approaches have been developed over the years. Ortiz-Urda *et al*. developed a ϕC31 Phage-mediated platform to deliver a full-length *COL7A1* cDNA driven by CMV promoter and blasticidin gene selection into primary keratinocytes from RDEB patients (Ortiz-Urda et al., 2002). Advantages of using ϕC31 bacteriophage integrase include its ability to accommodate large insert of DNA (more than 10Kb) and to integrate without additional co-factors into targeted chromosomes due to the recognition of speudo-*attP* sequences within genomes by *attB* sequences flanking the therapeutic donor. Despite the lower transfection efficiency (45.6%) compared to the viral-deliveries, 99% of cells expressed normal levels of C7 after short-term drug selection. *In vivo* analysis of human RDEB skin equivalent grafted onto immunodeficient mice showed short-term expression of progenitors bearing the plasmid and the absence of epidermal-dermal separation. The same platform was used in parallel to correct patient-derived RDEB fibroblasts which were subsequently injected intradermally into human RDEB skin xenografted mice (Ortiz-Urda et al., 2003). Along with gene addition, gene silencing strategies by RNA interference were used to silence mutant alleles (Pendaries et al., 2012a; Goto et al., 2006; Turczynski et al., 2016). In an *in vitro* study carried by Pendaries *et al*., a targeted allele-specific RNA interference for a dominant in-frame skipping of exon 87 was employed (Pendaries et al., 2012b). Modest knockout of 65% and 52% was observed in DDEB patient-derived fibroblasts and keratinocytes, respectively. Another RNA-based methodology designed to induce skipping of the mutant exons by modulating the splicing of the pre-messenger RNA was developed using 2'-O-methyl antisense oligoribonucleotide (AONs) (Goto et al., 2006). Specifically, an AON targeting a PTC point mutation in exon 70 showed the ability to induce exon skipping in 6.2% of DEB keratinocytes. Turczynski *et al*.

designed two AONs targeting exonic splicing enhancer located at the 5' end of exon 73 and 80 of *COL7A1* leading up to 50%-95% of exon skipping in RDEB keratinocytes *ex vivo* and resulting in 36% of C7 re-expression (Turczynski et al., 2016). Proof of principle of such technology *in vivo* led to restoration of anchoring fibrils in xenografted mice following subcutaneous injections of antisense ribonucleotide at different doses (400ug to 1mg). A phase I/II clinical trial is currently testing AON targeting mutations in exon 73 of *COL7A1* (QR-313, Wings Therapeutics Inc.) through topical gel application onto patients wounds (NCT03605069). Another method relied on applying spliceosome-mediated RNA trans-splicing strategies (SMaRT) to address target mutations at a post transcriptional level (Gruber et al., 2013; Hainzl et al., 2017; Tockner et al., 2016). Although RNA-based therapies for DEB showed to overcome safety concerns associated with viral gene addition, their low efficiency limit immediate clinical translation. More recently, proof of concept of DNA-based therapy approaches designed to deliver a copy of the *COL7A1* gene into skin cells using multifunctional poly(β-amino ester) polymers (LPAEs) for RDEB has also shown promising results *ex vivo* (Zeng et al., 2019). Rational design of a 12 kb-length minicircle DNA encoding ∼9kb full-length *COL7A1* (MCC7) complexed to optimized high branched poly(β-amino ester) polymers (HC32−122), exhibited higher cell uptake efficiency (96.4%) and excellent physiochemical properties to facilitate the navigation of multiple extra- and intracellular barriers associated with keratinocyte gene transfections (Zeng et al., 2019). HC32−122/MCC7-transfected RDEB keratinocytes showed significant transcriptional *COL7A1* mRNA and robust recombinant C7 expression on protein level. Of note, in contrast with the current manufacturing and safety requirements for viral development for gene cand cell therapy, the manipulation, process, and storage stability of polymeric nanoparticles could have a practical advanatge for bench-to-bedside translations. The formulation of the HC32−122/MCC7 complex, has demonstrated to be facilely manipulated, lyophilized and stored for RDEB gene delivery (Zeng et al., 2019). Therefore this nanoparticle-based delivery has potential to be administered in combination with unguents to patients skin by topical aplication. Of note, an example of polymer-based topical gene therapy delivery platform for RDEB is currently in phase-I clinical trial (AP103, Amryt Pharma, PLC).

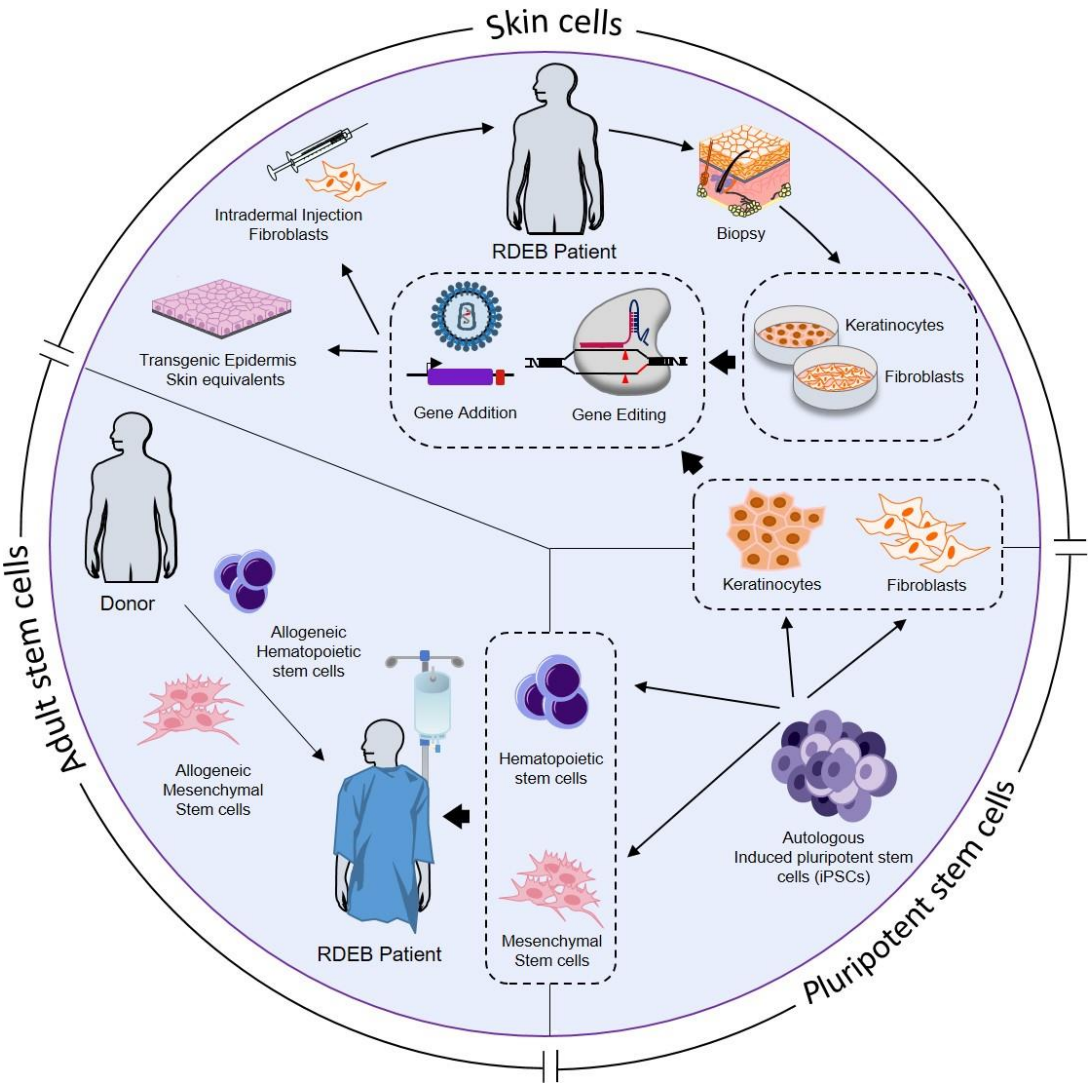

Figure 1.7 Illustration of combinatorial gene, cell therapies for RDEB treatment

Summary of current and potential gene and cell therapies for localized and systemic treatment of RDEB (Picture taken from Naso and Petrova, 2020).

1.7 Genome editing

The development of engineered endonucleases programmed to make highly precise changes within the genomic DNA at a nucleotide resolution has been driving an incredible revolution in gene therapy approaches. Despite the broad use of viral vectors for gene therapy applications, the ability to induce site-directed modification without perturbing the surrounding cellular environment is a critical concept for clinical applications. The discovery that naturally occurring DNA double-strand breaks (DSBs) can contribute to genome modifications and the subsequent development of engineered endonucleases, paved the way for the use of genome editing strategies in gene therapy. In the last decades, investigation of engineered platforms aimed to induce targeted DSBs in the region of interest have been developed. Two main DNA repair pathways are involved in gene-editing strategies. The fast but error-prone DNA repair process called non-homologous end joining (NHEJ) is frequently used to introduce insertions or deletions (InDels) or frameshift mutations resulting in the knockout of the gene (Lieber, 2010). On the other hand, in the presence of a therapeutic donor template flanked by homology arms homologous to the cleaved DNA ends triggers a slow but precise homology-directed repair (HDR) process resulting in gene correction or gene knockout depending on the strategy adopted (San Filippo et al., 2008). The main core technology of gene-editing tools is based on the use of engineered chimeric nucleases made by sequence-specific RNA or DNA-binding domains able to guide nonspecific DNA endonucleases to cut at a precise site within the genome. Four standard endonuclease platforms such as meganucleases (MN), Zinc Finger nuclease (ZFNs), transcription activator-like effector nuclease (TALENs) and clustered regularly interspaced short palindromic repeats/CRISPR-associated (CRISPR/Cas9) have been used in gene-editing so far. Although pioneering works on MNs showed promising results (Silva et al., 2011; Rouet et al.,1994), their translation into clinic is yet to be achieved. Engineering MNs to specificity target a chosen sequence has proven quite problematic and labour intensive due to their long DNA binding sites, thus reducing the number of genes that could be targeted by this tool (Grizot et al., 2010; Porteus et al., 2016). Unlike MNs, ZFN and TALENs are widely used in genome editing applications. The establishment of currently used zinc-fingers

nucleases platform was achieved by fusion of the non-specific cleavage domain of type II restriction enzyme *FoKI* to the C-terminus of a zinc finger array responsible for site-specific nuclease activity (Kim et al., 1996; Urnov et al., 2010). Conjecture behind the use of Zinc finger proteins (ZFP) as DNA-binding domains for ZFNs relies on their broad nature in mammalian transcription factors and their capability of binding three nucleotides per ZFP, thus making them a good tool for site-specific genome editing (Kim et al., 1996). However, arrays of ZFN motifs have to be assembled for targeting novel sequences. This approach, known as "modular assembly", generates candidate zinc-fingers for a given target sequence by identifying fingers for each component triplet and linking them into multi-finger peptide (Urnov et al., 2010; Carroll, 2011). While ZFNs are limited in the choice of the target sequence due to their modular assembly requirement, the modular assembly of "1 repeat to 1 base" of TALEN DNA binding domains makes TALEN a more accessible and more customizable tool for gene-editing strategies (Boch et al., 2009; Mussolino et al., 2012). However, the highly repetitive sequences of each TALE DNA-binding domain hinders generation of novel TALEN arrays as well as their delivery in viral vectors (Doudna and Charpentier 2014). Although ZFN and TALENs have been reported safe and efficient in different clinical trials, limitations in their design for a given DNA sequence and the hurdles associate with their production or delivery hamper their broad application in gene-editing settings. By contrast, the easy adaptability of CRISPR/Cas9 tools to "edit and correct" or to change a single DNA base in a targeted way can be employed to target various pathogenic mutations with unmet clinical need.

1.7.1 CRISPR/Cas9: a novel tool for genome-editing

The development of the CRISPR/Cas system (Clustered Regularly Interspaced Short Palindromic Repeats along with CRISPR associated protein) as a tool for therapeutic genome editing evolved after the first identification in *Escherichia coli* in 1987 described as series of short constant repeated elements interspaced by spacers of 32 nucleotides able to accommodate different sequences of exogenous DNA (Ishino et al., 1987). Although comparative studies based on genomic sequencing of CRISPR arrays showed the presence of short regularly spaced repeats in different species of bacteria and archaea (Mojica et al., 2000), its

biological relevance in adaptive immunity against the invasion of foreign nucleic acids, such as bacteriophages and plasmids, was discovered only in 2005 (Bolotin et al., 2005; Mojica et al., 2005). The CRISPR system adaptive immunity strategy can be divided into three stages: adaptation, expression, and interference (Barrangou and Marraffini 2014; Van der Oost et al., 2014) (**Figure 1.8A**). In the adaptation stage, foreign DNA fragments (also known as protospacers) are integrated into the "spacer" region within the CRISPR arrays. CRISPR arrays consist of repeated sequences interspersed with variable protospacer sequences that encode and are found with Cas genes within CRISPR loci. CRISPR arrays are transcribed during the expression stage into a long precursor CRISPR RNA (pre-crRNA) and loaded onto a Cas protein expressed by the Cas gene. The pre-crRNA is subsequently processed into mature crRNA by Cas proteins and host factors. Mature crRNA can direct the Cas protein to recognize invading sequences by Watson and Crick base pairing with the sequence previously integrated within the spacer region. Current data obtained by bioinformatics studies suggests that invading DNA fragments incorporated into the CRISPR loci are not randomly chosen (Ishino et al., 1987; Sander and Joung, 2014). In fact during the interference stage, the Cas protein directs the silencing by degradation of the foreign sequence only when the invading DNA, recognized by the protospacer sequence, is flanked on its 5' or 3' end by short sequences known as "protospacer adjacent motif" (PAM) (Sander and Joung, 2014; Ishino et al., 1987). Although similar mechanisms of action were reported in all organisms, three different classes of CRISPR/Cas systems have been identified according to CRISPR locus organization and molecular mechanisms involved in generating crRNA and Cas proteins, maturation of the crRNA and cleavage (Jinek et al., 2012; Chylinski et al., 2013).

1.7.2 Type II CRISPR/Cas9 for gene-editing

Among all different classes, class II type 2 CRISPR system is by far the most molecularly characterized and used for gene-editing strategies due to the simplicity of the system (Cho et al., 2013; Cong et al., 2013). To date, the commonly used CRISPR/Cas9 gene-editing tool is based on the type II CRISPR locus from *Streptococcus pyogenes*. In nature, only four elements are required to achieve

targeted sequence cleavage (Cho et al., 2013; Cong et al., 2013). Once class II CRISPR loci are transcribed in pre-crRNA, a second RNA structure from a genomic locus upstream the CRISPR locus known as trans-activating CRISPR RNA (tracrRNA) hybridizes with the repeated sequences in the pre-crRNA making a tracrRNA:pre-crRNA duplex. The RNA duplex triggers double-stranded RNA-specific endoribonuclease RNase III to proceed with the maturation of the double-stranded RNA filament. The fully mature RNA duplex is able to associate with the Cas9 protein, creating an active ribonucleoprotein complex (RNP) able to recognize the invading DNA flanked by a short 5'-NGG-3' PAM motif. Mechanistic studies showed that the PAM sequence is critical for initial DNA binding (Chen and Doudna 2017). Upon recognition of the PAM by the Cas9:cRNA:tracRNA complex, two critical residues of arginine (Arg1333 and Arg1335) interact with the PAM GG dinucleotide determining a conformational change in the Cas9-phosphate lock loop which is able to interact with the phosphate group of the DNA backbone immediately upstream the PAM sequence. The interaction of the DNA backbone phosphate with the Cas9 results in a local strand separation of the two DNA strands and consequential base pairing between the displaced DNA strand with the first 10 to 12 nucleotides of the crRNA (also known as seed sequence). After interrogation of the unwrapped DNA region by the crRNA, further unwinding of the DNA leads to full accommodation of the Cas9 protein based on the annealing of the 20bp nucleotide spacer sequence with the target DNA. The DNA cleavage results from the action of two different catalytic domains. The HNH catalytic domain cleaves the target strand which is complementary to the 20-nucleotide sequence of the crRNA, whereas the non-target strand is cleaved by the RUV-C like domain. The two catalytic domains create a double strand break at 3bp upstream the 5' of the PAM resulting in a blunt-end cleavage of the DNA. After initial characterization of molecular basis of type II CRISPR/Cas9, different research groups tried to exploit this system for genome editing in human cells (Cho et al., 2013; Cong et al., 2013) . Further simplification of the type II CRISPR/Cas9 system was obtained by Jinek and colleagues by fusing the dual crRNA:tracrRNA into a single chimeric guide (sgRNA) of 100nt long avoiding the need of RNAse III for guide RNA maturation (**Figure 1.8B**). The new sgRNA retains two critical features: 1) the first 20bp at the

5’end of the sgRNA that determines the binding to the target site and 2) the double RNA:RNA structure at the 3’ end which is critical for Cas9 cleavage (Cong et al., 2013). This further simplification led to the creation of a two-component system: a Cas9 protein and a single guide RNA where the first 20bp at the 5’end of the sgRNA can be designed to program the CRISPR/Cas9 system to cut at the desired locus. In contrast to other engineered endonucleases, such as MNs, ZFNs and TALENs, where the nature of the DNA binding domains needs to be modified on protein level, the CRISPR/Cas9 system is easier to manipulate and requires only a change in the RNA sequence.

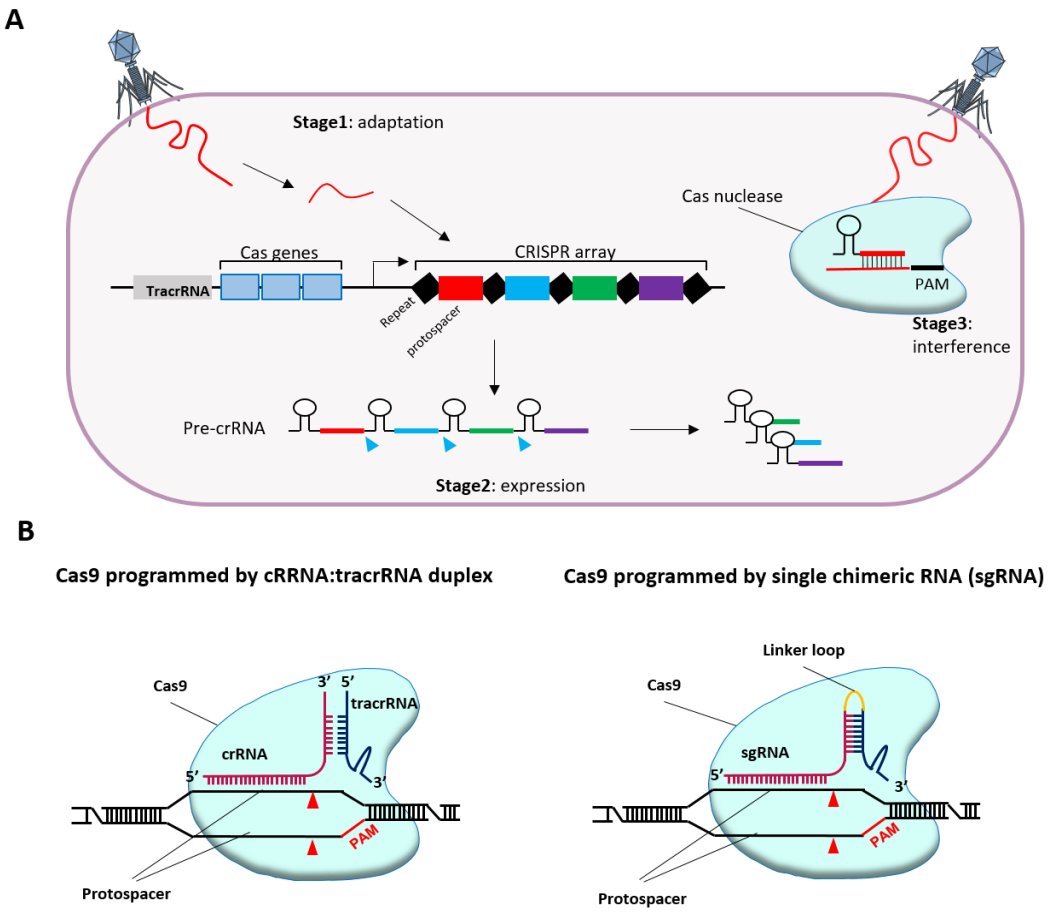

Figure 1.8 Overview of the CRISPR/Cas system.

General mechanism of CRISPR/Cas9 adaptive immunity **(A)**. In stage 1 (adaptation), acquisition of the endogenous DNA intro the CRISPR locus. From left to right: tracrRNA cassette, Cas nuclease genes and CRISPR array made of short repeats (black) flanked by different protospacers (red, blue, green and purple). In stage 2 (expression) transcription of the CRISPR array in pre-crRNA and further maturation in single crRNA each bearing one protospacer sequence. In stage 3 (interference) silencing/degradation of foreign DNA by CRISPR/Cas element. Black line: protospacer adjacent motif (PAM) recognized by Cas nuclease. Type II CRISPR/Cas9 system **(B)**. Left: Cas9 is guided by a dual guide RNA made by tracrRNA (blue) and mature crRNA (red) to cleave site-specific target DNA (protospacer). Red triangles represent Cas9 cutting sites. Right: chimeric single guide RNA (sgRNA) generated by fusing the 3'end of crRNA with the 5' of tracrRNA with a linker loop (yellow). Figure adapted from Jinek *et al.* (Jinek et al., 2012).

1.7.3 Strategies to increase CRISPR/Cas9 specificity

Despite the potential of broad application of the CRISPR/Cas9 system and its precise site-specific gene-editing activity, several factors could interfere with its efficacy and specificity. The specificity of the CRISPR/Cas9 system is determined by the uniqueness of the genomic target and the rational design of the sgRNA. To assess sgRNA-DNA specificity several groups created sgRNA variants containing 1 to 4 nucleotide mismatches within the protospacer and examined the ability of mismatched sgRNAs to direct on-target Cas9 activity in human cells (Sander and Joung, 2014). These studies showed that mismatches in the Watson and Crick base pairing within sgRNA and target DNA are generally tolerated at the 5' end (proximal end) of the protospacer over the 3' end (distal end) suggesting that the 8–12bp immediately upstream the PAM sequence (also known as the 'seed' sequence) are crucial for target recognition (Sander and Joung 2014; Ran et al., 2013). On the other hand, unwanted mutations within the sgRNA can potentially increase off-target Cas9 cleavage throughout the genome (Ran et al., 2013). Although sgRNA sequences are designed to have a perfect homology to the target DNA, the short 20bp protospacer sequence can potentially have additional sites throughout the genome with partial homology. Ran *et al*. showed that extension of the length of the 5' end of the sgRNA from 20 to 30bp had no impact on Cas9 target specificity (Ran et al. 2013). Northern blots, however, showed that the extended 5' sgRNAs were cleaved in cells from host RNAses suggesting that Cas9 protein can protect only the first 20bp of the sgRNA sequence (Ran et al., 2013). On the other hand, Fu Y *et al*. showed that truncation of the 20bp target sequence to 19bp, 18bp or 17bp can decrease undesired off-targeting events up to 5000-fold while retaining a cutting sensitivity similar to the untrimmed guide RNAs (Fu et al., 2014). By contrast, Zhang *et al*. showed that on-target Cas9 events using a 17bp truncated sgRNA decreased by 10%-20% compared to non-trimmed sgRNA in iPSCs (Zhang et al., 2016).

In addition to modifications of the protospacer, structural optimizations of the sgRNA scaffold region have also been studied. Truncation at the 3' end of the tracrRNA from 85bp to 67bp, 54bp or 48bp showed a drastic drop in target specificity levels due to impairments in sgRNA transcription and stability once

expressed inside cells (Hsu et al., 2013). By contrast, extension of the sgRNA hairpin by 5bp resulted in enhanced stability of the sgRNA-Cas9-DNA complex (Dang et al., 2015; Chen et al., 2013). Interestingly, replacing the fourth consecutive thymine with cytosine/guanine immediately downstream of the protospacer, showed increased sgRNA transcription in cells due to the disruption of the pause signal recognized by the RNA polymerase III (Dang et al., 2015; Chen et al., 2013). Based on these results combination of the two modification of the sgRNA backbone resulted in improved guide RNA production and stability in cells, therefore showing increased knockout over the unmodified guide RNA scaffold (Dang et al., 2015; Chen et al., 2013). Although these two structural adaptations of sgRNA showed to be efficient when the guide RNA is delivered by lentiviral vector, different modifications have been studied when sgRNAs are delivered as RNA instead. The studies showed that 2'-O-methyl 3'phosphorothioate (MS) chemical modifications at both 5' and 3' termini in the ribose-phosphate backbone of the sgRNA scaffold can induce high levels of genome editing while maintaining high on-target activity (Hendel et al., 2015; Osborn et al., 2016). Interestingly, Hendel *et al.* studies showed up to 50-fold increase of indel and HDR frequencies using different chemically modified sgRNAs designed for different endogenous targets (Hendel et al., 2015).

Strategies for reducing genome-wide off-targets have been directed towards improved engineering of Cas9 protein. Wild type SpCas9 contains two nuclease domains referred to as RuvC and HNH. The RuvC domain cleaves the single stranded DNA that is non-complementary to the sgRNA, while the HNH domain cleaves the complementary DNA strand. A different variant of Cas9 has been generated through rational mutagenesis of the RuvC catalytic domain (D10A) thus creating a new version of Cas9 protein (Cas9 nickase or nCas9) which creates a single nick at 3-4 nucleotides proximal to the PAM in the complementary strand (Nishimasu et al., 2014; Jinek et al., 2012). Although nicking of a single DNA strand is generally repaired by the non-mutagenic base-excision repair (BER) pathway, Cas9 nickases can be employed for precise genome editing. Co-delivery of two nCas9 with sgRNA appropriately oriented to target opposite strands can effectively generate overhanding DSBs within the target DNA increasing the target specificity (Jinek et al., 2012). Kinetics and

interactions during the formation of the Cas9-sgRNA-DNA complex have also been studied (Anders et al., 2014; Nishimasu et al., 2014). Kleinstiver *et al.* observed that the energy barrier used to complex the wild type SpCas9 with the sgRNA is higher than the amount required to make on-target DNA cleavage. This difference in terms of energy is enough to allow off-target cleavages in DNA templates with mismatches (Kleinstiver et al., 2016). To reduce off-targets, rational engineering based on the disruption of the Cas9 residues which interact with the phosphate backbone of the target DNA strand was developed (Kleinstiver et al., 2016). The so called high fidelity SpCas9 (SpCas9-HiFi-1) showed to have frequencies of InDels comparable with the wild type SpCas9 in more than 85% of target sites with decreased or absent off-target events (Kleinstiver et al., 2016).

1.7.4 Delivery of CRISPR/Cas9 Reagents

There is a variety of methods used to deliver the CRISPR/Cas9 components into target cells. Most widely used viral and non-viral systems to deliver CRISPR/Cas9 reagents are: messenger RNA (mRNA) Cas9/sgRNA, Cas9 protein complexed with sgRNA (ribonucleoprotein or RNP), or DNA plasmids/viral vectors expressing both Cas9 and sgRNA (**Figure 1.9**). Despite the simplicity of the type II CRISPR/Cas9 system, requiring only two components to make an amenable tool for genome editing, factors such as the large size of the Cas9 cassette, temporal expression of Cas9-sgRNA components, cell type and experimental design may affect gene-editing efficiencies. Most common and inexpensive non-viral delivery reported in literature involves transfection of DNA expression plasmid encoding for both sgRNA and Cas9 components. However, the main limitation of this approach is its unsuitability for hard-to-transfect primary cells. Moreover, long-lasting expression of Cas9 nuclease through plasmid DNA increases the amount of possible off-target effects that could be detrimental for clinical translations (Kim et al., 2014). Alternative delivery methods have been developed. Delivery of *in vitro* transcribed (IVT) or synthetic guide RNAs along with Cas9 mRNA or Cas9 protein (RNP) showed increased on-target fidelity over plasmid DNA delivery due to the rapid degradation of the nuclease (Hendel et al., 2015; Kim et al., 2014). Moreover, differences in nuclease persistence lead to different timings in Cas9-mediated DNA cleavage activity which is crucial when gene correction by donor

template is required. Frequency of RNP-mediated InDels was shown to reach a plateau within 24 hours post Cas9-sgRNA administration, whereas it took 72 hours to reach the equivalent amount of DNA cutting by plasmid transfection(Kim et al., 2014). Viral delivery of CRISPR/Cas9 reagents is more challenging as it raises more safety and technical issues. Although AAV-based vectors are ideal for somatic gene therapy due to their mild immune or adaptive response, broad tropism and ability to target both dividing or non-dividing cells, their application in gene-editing is limited due to the large size (~4.2Kb) of SpCas9 and sgRNA expression cassette. However, AAV-based CRISPR/Cas9 delivery can be accomplished by cloning Cas9 from different bacterial species. SaCas9 from *Staphylococcus aureus* which has a coding sequence roughly 1kb shorter than the common SpCas9 can be easily packaged into AAV-vectors retaining similar gene-editing efficiency (Friedland et al., 2011; Ran et al., 2015). Adenoviruses as well as lentiviruses have been reported for CRISPR/Cas9 application due to their ability to infect both dividing and non-dividing cells. Unlike adenoviruses, long-term expression of Cas9 nuclease due to proviral integration of lentiviral vectors increases cellular toxicity and off-target effects. In order to overcome these limitations, strategies such as non-integrating lentiviral vectors (NILV) expressing Cas9-sgRNA components (Izmiryan et al., 2018) or pre-packing Cas9 protein within lentiviral particles in their capsid (Cai et al., 2016) have been developed. An alternative strategy of lentiviral CRISPR/Cas9 delivery was shown by Marienne *et al*., who developed an inducible self-inactivating system for transient nuclease expression after lentiviral integration (Merienne et al., 2017). The so called KamiCas9 vector encodes an additional sgRNA (called sgCas9) expressed under the control of a weak promoter (7SK) able to target the Cas9 start codon in order to block its translation. Stable expression of sgCas9 showed a steep and long-term drop in Cas9 expression within 2 weeks post infection, thus preventing off-target activities. A combination of hybrid viral and non-viral CRISPR/Cas9 system delivery was designed by Georgiadis *et al*., where the nuclease was delivered separately as mRNA after lentiviral transduction with the vector encoding for guide RNA (Georgiadis et al., 2018). The particular design of the third-generation lentiviral vector used (called “Terminal CRISPR”) guaranteed a double expression of the U6-sgRNA expression cassette due to its integration within the U3-deleted region of the 3’LTR. Upon retro-

transcription of the viral backbone guide duplication and incorporation within the 5'LTR led to an increased gRNA expression.

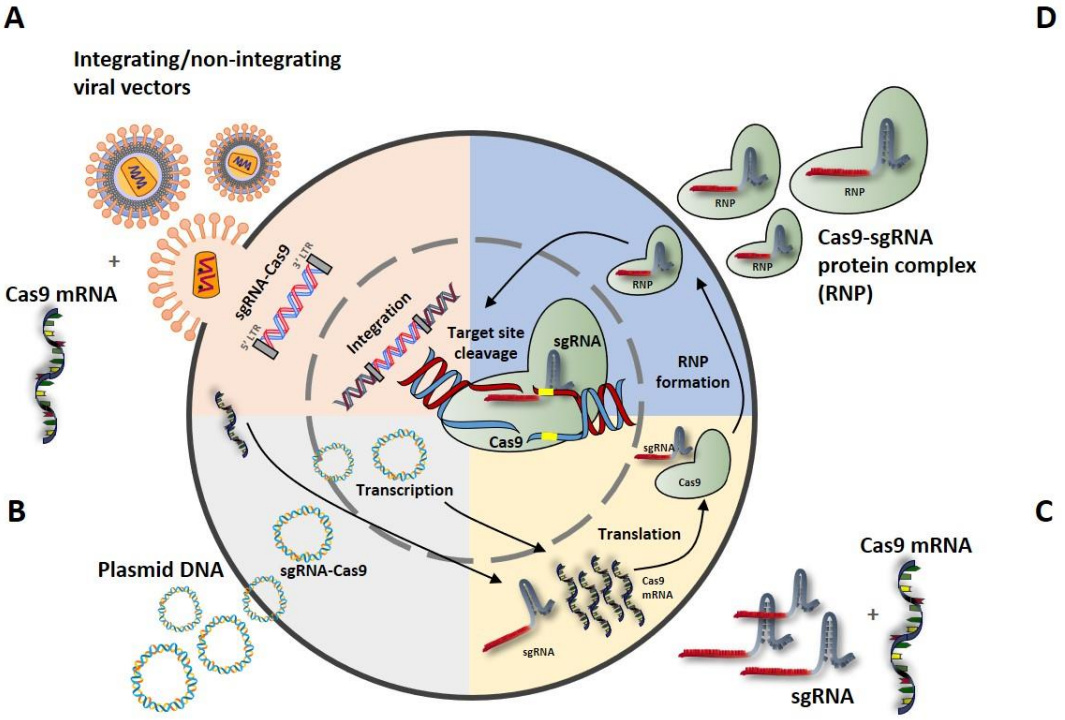

Figure 1.9 Delivery strategies and formats of CRISPR/Cas9 reagents

A. Viral vectors encoding sgRNA and SpCas9 or combination of guide RNA expressing vectors in combination with SpCas9 mRNA can be delivered to a variety of cell types by viral transduction of the former and by electroporation of the nuclease. In case of integrating vectors, stable integration into the target cell genome permits long term constitutive expression of CRISPR/Cas9 components. By contrast, prologued expression can be achieved with non-integrating vectors. sgRNA is transcribed by RNA polymerase III promoters, and mRNA SpCas9 transcribed by an RNA Pol II promoter before undergoing translation. Assembly of sgRNA and Cas9 determine the formation of Ribonucleoprotein (RNP) complexes that can be trafficked into the nucleus for targeted genomic cleavage. **B.** Plasmid DNA expressing either sgRNA, SpCas9 or both can be delivered by transfection or electroporation protocols. Plasmid DNA remains episomal, and it tends to diluted out over the course of cell divisions providing a route for transient delivery. **C.** For shorter expression, *in vitro* transcribed or *in silico* synthesised sgRNA and SpCas9 mRNA can be by transfection or electroporation. SpCas9 mRNA is translated into protein, which forms RNP complexes that are able to enter the nucleus and edit the target sequence. **D.** Pre-complexing of SpCas9 protein and synthesized sgRNA forms RNPs that can be delivered by transfection or electroporation. RNPs will traffic to the nucleus where they cleave target sequence. (Figure adapted from Dr. Roland Preece's PhD thesis, 2020).

1.7.5 Detection of off-target CRISPR/Cas9-mediated genome editing

Precise genome editing using CRISPR-Cas9 has shown promising therapeutic avenue for genetic diseases, although the risk of genotoxicity caused by off-target editing remains a significant safety concern. Different studies have reported the detection of small insertion or deletions (InDels) or large Cas9-depenedent chromosomal aberration such as translocations or inversions in the off-target loci. As detailed in **section 1.7.3** and **1.7.4**, much efforts have been invested in the past years in increasing the safety profile of genome editing tools: from the optimization of the guide RNA structure (e.g truncated protospacer (Fu et al., 2014; Zhang et al. 2016), alternative crRNA scaffold structure (Y. Dang et al. 2015)), to the rational engineering of high-fidelity Cas variants (Kleinstiver et al. 2016; Nishimasu et al. 2014; M. Jinek et al. 2012) or the use of novel of base editors for seamless corrections (Komor et al., 2017a; Gaudelli et al., 2017).

Alongside the previously described structural improvements of the CRISPR/Cas9 safety profile, *in silico* computational algorithms have recently emerged for selecting and validating sgRNA design (high sensitivity) and predicting potential DSBs in off-target loci (high specificity). These tools are generally based on sequence alignment methodologies and more complex physical/chemical parameters including RNA thermodynamics, sequence similarity and DNA or RNA bulges that would have a pivotal role on CRISPR–Cas9 efficiency and selectivity. More recently, development of predictive tools using machine-learning models or deep-learning techniques, such as CRISTA (CRISPR Target Assessment) (Abadi et al., 2017) and DeepCRISPR (Chuai et al., 2018), aim to increase their prediction accuracy.

To investigate the computationally predicted off-target sites, deep sequencing methods such as next-generation sequencing (NGS) are commonly employed for the detection of Cas9-induced double strand breaks. However, *in silico* off-target detection tools have shown predictive limitations such as differences in algorithms and can be associated with high false-positive rates (Wilson eta., 2018; Chuai et al., 2018).

To overcome the current limitations of *in silico* predictions, combinatorial approaches using *in vitro* cell-based methods that rely on high throughput sequencing of genomic DNA have also been developed allowing to detect CRISPR off-target effects in an unbiased, genome-wide fashion. These include Digenome-seq (digested genome sequencing)(Kim et al., 2015), CIRCLE-seq (circularization for *in vitro* reporting of cleavage effects by sequencing) (Tsai et al., 2017), SITE-seq (selective enrichment and identification of tagged genomic DNAends by sequencing) (Cameron et al., 2017), BLESS (Breaks Labeling In Situ and Sequencing) (Crosetto et al., 2013) or Guide-seq (genome-wide, unbiased identification of double strand breaks enabled by sequencing) (Tsai et al., 2015).

Nevertheless, studies suggest that *in vitro* genome wide methods tend to overestimate the number of relevant off-target sites or do not meet all the criteria for clinical assessment because of their low or unknown sensitivity, semiquantitative nature, and a partially biased analysis that identifies only particular types of genomic aberrations (Turchiano et al., 2021). Although there is no gold standard method for prediction and detection of off-target events so far, studies in clinically relevant cell products have opted to combine different assays based on different modalities of off-target detection in order to increase the detection of possible adverse effects (Georgiadis et al., 2018). Further efforts to develop standardized methods to carefully monitor and screen for the potential genetic changes are essential for safe clinical application of genome editing tools.

1.8 Mechanisms of double-stranded break (DSB) repair

Since its discovery, CRISPR/Cas9 gene-editing tool has been used for different targeted genome editing strategies in human cell types. One of the primary approaches developed in genome editing with engineered nucleases is the knockout of a mutated gene as a consequence of unrepaired or incorrectly repaired DSBs by NHEJ DNA repair pathway. Insertions and deletions (InDels) introduced by NHEJ-mediated gene repair result in a permanent gene knockout or in the restoration of a disrupted open reading frame by frameshift mutations. On the other hand, to repair or substitute a mutated gene, the homologous directed recombination (HDR) is the desired DNA repair mechanism that could be triggered by engineered nucleases along with the presence of a template DNA with homology arms complementary to the flanked DSB. Although the development of gene targeting by HDR was extensively reported, its application is limited by low efficiency in mammalian cells (Liang et al., 1998).

1.8.1 Non Homologous End Joining (NHEJ)

NHEJ occurs outside the S phase, when no nearby homology donor sequences are available and three different steps have been identified (Lieber et al., 2010). The first protein involved in the NHEJ process is Ku80 (**Figure 1.10A**). This heterodimer protein, formed by Ku70 and Ku86, recognizes DNA ends at the breakpoint sites and aligns the DNA ends protecting them from further degradations. Once loaded, the Ku complex undergoes conformational changes in its structure allowing the recruitment of the DNA-dependent protein kinase (DNA-PKcs) around the damaged sites. DNA-PKcs is a serine/threonine kinase required for the activation by phosphorylation of nuclear proteins such as Artemis, DNA ligases IV and XRCC4 involved in the NHEJ repair (Lieber et al., 2003). Terminal processing of the DNA ends is required before ligation of the two strands can occur. Blunt ending involves a metallo-beta-lactamase protein called Artemis which, upon previous phosphorylation and binding by DNA-PKcs, dictates trimming of single-stranded 5` and 3` overhangs (Lieber et al., 2010; Lieber et al., 2003). After the remodeling of the DSB ends, the XLF:XRCC4-DNA ligation IV complex is recruited to restore DNA integrity. The XLF:XRCC4-DNA ligase

IV complex permits ligation of the juxtaposed DNA ends. Once the DSB is repaired, all the components in the NHEJ complex are released from the DNA.

1.8.2 Homologous Directed Recombination (HDR)

Homologous directed recombination is a highly accurate DNA repair process which provides high-fidelity template-dependent DNA repair using homologous sequences in the genome such as sister chromatid or exogenous homologous sequences when provided. The canonical HDR mechanisms can be conceptually divided into three stages: pre-synapsis, synapsis and post-synapsis. While pre-synapsis and synapsis are initial common phases, the post-synapsis stage leads the repair of the damaged DNA by two different pathways: the double-strand break repair (DSBR) and synthesis-dependent strand annealing (SDSA). After DNA damage, DSB ends are protected by the MRE11/RAD50/NBS1 (MRN) complex (**Figure 1.10B**). Once bound, CtIP endonuclease generates long 3'-OH single-stranded protruding ends (ssDNA) which are covered by single-strands DNA binding proteins like replication protein A (RPA), essential for eliminating secondary structures and protection of single-strand overhang from enzymatic degradation. During the pre-synapsis phase, RAD51 and RAD52 are loaded on the ssDNA 3' overhangs forming a pre-synaptic filament which, with the aid of several accessory factors including RAD54/RAD54B/RDH54, promotes the DNA-invasion step allowing the search for donor template sequences with appropriate homology to the DNA break site. After a successful homology search, strand invasion occurs forming a synaptic complex with the homologous DNA joint also known as the displacement (D)-loop structure. Strand invasion is ensued by DNA synthesis from the invading 3' ssDNA overhang using the original homologous sequence as template, thus obtaining the so-called Holliday Junction (HJ). After DNA elongation, two main post-synaptic pathways have been described. 1) In Double-strand break repair (DSBR) model, the second DSB 3` end can be involved to form a second Holliday Junction intermediate structure. After gap-repair DNA synthesis and ligation, the intermediate HJ complexes can be resolved by specialized resolvases into non-crossover or crossover product according to the axis of cleavage. Thus, regardless of the mechanism by which the HJs are resolved, this process results in a mutual exchange of genetic information by sister chromatids of homologous

chromosomes. Alternatively, in synthesis-dependent strand annealing (SDSA) model, the first HJ obtained during the synapsis phase does not lead to the second end capture by the second ssDNA 3' overhang. DNA synthesis of the invading 3' overhang is ensued by DNA polymerase extension until a strand displacement event corresponding to the unwrapping of the HJ and annealing with the second ssDNA-DSB end before gap-filling DNA synthesis and ligation. The repair product from SDSA is a non-crossover product. The described process could be exploited for gene correction or addition of a desired exogenous DNA molecule after DSB induction by several engineered endonucleases (Capecchi 1989; Gaj et al., 2014; Liang et al., 1998).

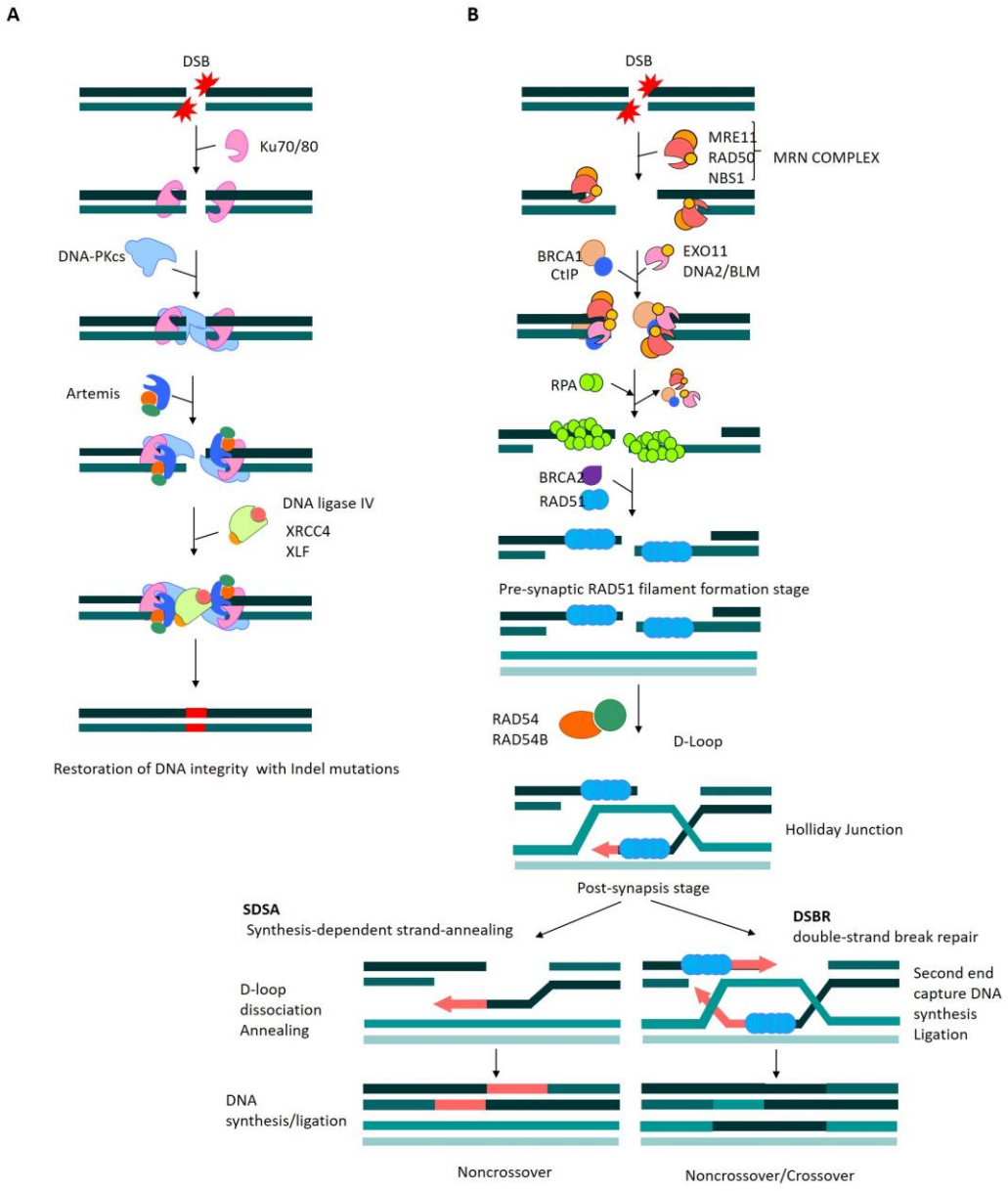

Figure 1.10 Repair of DSBs by NHEJ and HDR.

(A) Each DNA end at the extremity of the break is loaded with Ku70/80 heterodimer which subsequently recruits the DNA-dependent protein kinase catalytic subunit (DNA-PKcs)**.** End processing activity of the break extremities is recruited by PKcs**.** DNA integrity restoration occurs by the Ligase IV enzyme with XRCC4 and XLF cofactors. **(B)** Pathways of DNA double-strand break repair by homologous recombination. First, the break extremities are reprocessed, forming 3' single-strand DNA overhangs. After DSB formation, the DNA ends are resected to yield 3' single-strand DNA (ssDNA) overhangs, which become the substrate for the HR protein machinery to execute strand invasion of a partner chromosome that forms a nascent D-loop structure. In the DSBR pathway the second 3' overhang invades the homologous sequence and an intermediate structure bearing two Holliday Junctions is formed. Resolution of the intermediate is through either a crossover or non-crossover events. In the SDSA pathway, the D loop is unwound and the freed ssDNA strand anneals

with the complementary ssDNA strand that is associated with the other DSB end. The reaction is completed by gap-filling DNA synthesis and ligation. Only non-crossover products are formed. Picture modified from Davis et al. (Davis and Maizels 2014)).

1.9 Gene-editing for dystrophic epidermolysis bullosa

Although stem cell and *ex vivo* gene therapy approaches for DEB have shown some improvements of DEB symptoms, there is currently no definitive cure for patients. Graft versus host complications due transfusion of allogenic cells and aggressive conditioning regimen are the main hurdles associated with cell therapy approaches. Gene therapy, on the other hand, still retains concerning risks due to random integration profile of viral vectors. Furthermore, conventional therapy through gene addition is not feasible for treatment of dominant forms of DEB where dominant negative mutations result in an abnormal gene product which affects the wild type allele. In such a scenario, application of precise gene-editing tools have a potential to overcome these hurdles. Gene-editing tools can be designed and engineered to target and repair a specific defined region of the DNA, thereby alleviating genomic toxicity and maintaining endogenous gene expression control.

1.9.1 Previous generation of gene-editing tools for DEB

Despite their limitations for clinical applications, proof-of–concept of feasible gene-correction using meganucleases (MN) was firstly described by Izmiryan *et al.* for two *COL7A1* mutation hotspots in exon 2 (c.189delG; p.Lys6Trp*40) and 3 (c.425A > G; p.Lys142Arg) (Izmiryan et al., 2016). Despite *COL7A1* correction by non-integrating lentiviral vector (NILV) delivery of donor template, the low frequency of MN-mediated HDR (3%-7%) hampers their potential *ex vivo* applications. Proof-of-concept of TALEN-mediated gene correction was achieved by Osborn *et al*., addressing gene-editing-mediated *in situ* correction of a PTC mutation (1837 C>T) in RDEB patient fibroblasts (Osborn et al., 2013). To restore the expression of wild type *COL7A1*, a couple of TALENs were delivered as mRNA or plasmid DNA along with a plasmid donor template flanking exon 12 to 15 expressing a puromycin cassette (Osborn et al., 2013). To facilitate clonal selection of gene-corrected cells, fibroblasts

were sorted by puromycin selection. Gene-corrected fibroblasts were then reprogrammed into iPSCs and tested in an *in vivo* model for their capacity to deposit C7 at the dermal-epidermal junction (Osborn et al., 2013). By the use of TALENs delivered by adenoviral vector, Chamorro *et al.* demonstrated the feasibility of possible *ex vivo* gene correction of patient immortalized RDEB keratinocytes harbouring a highly recurrent c.6527InsC mutation in exon 80 by NHEJ-mediated exon skipping or by HDR when an AAV-DNA donor template was provided (Chamorro et al., 2016). Protein restoration in gene-corrected clones by HDR or NHEJ-restored reading frame was verified *in vitro* by immunofluorescence and western blot. Interestingly, *in vivo* assessment in immunodeficient mice of NHEJ-corrected cell clones showed restoration of C7 expression and correct deposition within the DEJ suggesting that long-term regeneration from reframed single gene edited epidermal stem cells clones is achievable (Chamorro et al., 2016). Two years later, translation of such donor-free genome editing strategy from immortalized RDEB cell line to primary keratinocytes showed efficient long-term skin regeneration from gene-edited stem cell clones in skin equivalents grafted onto immunodeficient mice (Mencía et al. 2018). NHEJ-edited *COL7A1* cell clones showed expression of edited forms of C7 with variable mechanical resistance to minor trauma, and correct deposition of C7 at the BMZ (Izmiryan et al., 2018).

1.9.2 Current status of CRISPR/Cas9 gene-editing for EB: Knockout gene strategies

As previously demonstrated by RNA-based gene therapies for RDEB or by TALEN-gene-editing settings, exon skipping or "reframing" strategies for *COL7A1* are possible for exons encoding Gly-X-Y repeats within the collagenous domain responsible for the structural triple helix C7 region (Bremer et al., 2016; Turczynski et al., 2016; Goto et al., 2006). Recently, different examples of exon skipping or reframing using the CRISPR/Cas9 system for *in vitro* or *in vivo* application have been reported. Moreover, novel bioinformatics tools able to predict *in silico* distribution of NHEJ-CRISPR/Cas9-mediated InDels can be used to design corrective strategies of disease-associated mutations by frame shifting or exon skipping (Allen et al., 2018; Shen et al., 2018). Similarly to Chamorro and Izmiryan works, Bonafont and co-

workers showed a highly efficient non-viral exon skipping approach using a dual-guide RNA Cas9 strategy for deletion of *COL7A1* exon 80 in RDEB patient keratinocytes (Bonafont et al., 2018). Despite the lack of specificity in NHEJ repair, a broad variety of re-joining events between intron 79 and 80 resulted in the expression of functional collagen VII variants. Unlike only 1% of epidermal stem cell clones with frame-restoration by NHEJ was observed with TALENs, the described CRISPR/Cas9 strategy resulted in up to 85% of reframed polyclonal primary keratinocytes. Using the same exon skipping strategy designed by Bonafont *et al*., an alternative non-viral delivery of RNP complexes using highly branched poly(beta-amino ester), HPAE-EB, demonstrated to achieve targeted genomic deletion of exon 80 in up to 40% of the treated RDEB keratinocytes with preserved cell viability above 85% upon Cas9 delivery (O'Keeffe Ahern et al., 2021). Feasibility of targeted skipping approach *in vivo* was demonstrated by Chen *et al.,* where RNPs were delivered through electroporation into postnatal mut/mut RDEB mice (Wu et al., 2017). Two guide RNAs in antisense orientation were designed within intron 79-80 resulting in the deletion of the entire exon 80. Upon demonstration of successful deletion at genomic and mRNA level *in vitro*, *in vivo* delivery of CRISPR/Cas9 reagents in mice resulted in intact epidermis and dermis with correct deposition of C7 at the BMZ (Wu et al., 2017). Exploiting the NHEJ pathway in its activity to repair DSBs by introducing random changes in the reading frame, Takashima *et al*. developed a CRISPR/Cas9-based reframing strategy to restore *COL7A1* reading frame from a recurrent heterozygous frameshift mutation in exon 70 (c.5819delC) (Takashima et al., 2019). For this purpose, co-transfection of plasmids carrying Cas9 and an allele-specific guide RNA targeting the mutant *COL7A1* allele was evaluated in RDEB primary fibroblasts. After monoclonal expansion, 34% of *COL7A1*-reframed cells showed partial restoration of *COL7A1* mRNA, protein expression *in vitro* and functional anchoring fibrils *in vivo* (Takashima et al., 2019). In contrast to exon skipping or reframing to rescue C7 expression, Shinkuma *et al.* showed the feasibility of CRISPR/Cas9 NHEJ-mediated genome editing to treat a dominant-negative mutation (c.8068_8084delinsGA-exon 109) in DDEB patient-derived iPSCs (Shinkuma et al., 2016). In order to leave the wild type *COL7A1* allele intact, an allele-specific sgRNA exclusively targeting the mutation site was designed (Shinkuma et al., 2016). Clonal

analysis of 4 different gene-edited *COL7A1* clones after keratinocyte and fibroblast differentiation showed frameshift or in-frame mutations in mRNA transcripts leading to premature termination codon (PTC) which did not interfere with the wild type *COL7A1* gene expression

Another important application of CRISPR/Cas9 knockout strategies for DEB is the development of *in vivo* mouse models. Although immunodeficient mice models are commonly used for gene-corrected xenograft (Chamorro et al., 2016; Shinkuma et al., 2016; Izmiryan et al., 2018), transgenic mice models for DEB are lacking. Recently, Tolar's group developed a *COL7A1*$^{-/-}$ NOD/SCID IL2rγcnull immunodeficient mouse embryos (NSG) by CRISPR/Cas9 reagents microinjections (Webber et al., 2017). It was shown that bi-allelic knockout of exon 1 of *COL7A1*, resulted in marked loss of C7 protein at the dermal-epidermal junction. However, complete C7 knockout hinders the evaluation of long term gene-correction therapies due to severe skin conditions of NSG mice and their premature death after birth. Mono-allelic knockout, which was achieved by lowering the dose of CRISPR/Cas9 reagents in mice embryos, increased the survival rate of RDEB animals suggesting that knockout targeting frequency was dose-dependent (Webber et al., 2017).

1.9.3 Current status of CRISPR/Cas9 gene-editing for EB: Knock-in gene strategies

Feasibility of functional *ex vivo* HDR-mediated CRISPR/Cas9 application was demonstrated by Izmiryan *et al*., where a donor template to correct a causative null mutation within exon 2 (c.189delG; p.Leu64Trpfs*40) was designed (Izmiryan et al., 2018). Both CRISPR/Cas9 reagents and donor template, were co-delivered by NILV vectors. Gene correction was evaluated in primary keratinocytes and fibroblasts resulting in 11% and 15.7% of corrected *COL7A1* mRNA expression by droplet PCR, respectively. Skin equivalents from human:murine xenograft mice model were analysed at 4 and 10 weeks post-grafting and showed up to 26% of *COL7A1* restoration following deposition of C7 and anchoring fibrils within the dermal-epidermal junction. Notwithstanding the challenge of developing an efficient non-viral delivery strategy for keratinocytes, the use of non-viral plasmid offers an

increased safety profile which would be crucial for clinical application of genome editing. In this direction, Koller *et al*. designed a completely non-viral based *ex vivo* homology-directed gene repair in RDEB primary cells (Hainzl et al., 2017). Here primary keratinocyte bearing c.6527insC mutation within exon 80 were co-transfected with one plasmid expressing both sgRNA-Cas9 elements and a donor template with an inserted mRuby/puromycin to facilitate clonal selection (Hainzl et al., 2017). Despite the advantage of clonal selection of gene-corrected cells *in vitro*, the inclusion of the selection cassette required subsequent Cre-recombinase treatment to remove the selection cassette which could influence the cis-splicing pattern at the target region. Up to 17% and 24% of gene correction was reported with wild type Cas9 and Cas9 nickase, respectively. Skin grafts from *COL7A1*-corrected cells showed correct deposition of C7 within the dermal-epidermal junction along with epidermal differentiation and stratification comparable with normal keratinocyte 8 weeks post transplantation onto immunodeficient mice. Although the isolation of gene-corrected cells might be plausible *in vitro*, plasmid DNA transfections in primary cells are too inefficient for any clinical setting. Similar strategy was developed by Tolar *et al*., designing a non-viral gene-correction platform for primary RDEB fibroblasts carrying c.4317delC mutation (Webber et al., 2016). Fibroblasts were gene-corrected using Cas9 nickase along with double-stranded DNA donor template carrying a floxed puromycin resistance cassette for subsequent Cre-recombinase-mediated removal. After puromycin selection, gene-corrected cell clones were reprogrammed into iPSCs and subsequently differentiated into keratinocytes *in vitro.* Importantly, gene-corrected iPSC-derived keratinocytes expressed epidermal stem cell markers (K5, K14 and p63), thus confirming that gene-editing by Cas9 nuclease did not interfere with the differentiation. Gene-corrected iPSCs were also differentiated into MSCs and CD34+ HSPCs (Webber et al., 2016). Gene correction in RDEB-iPSCs using CRISPR/Cas9-mediated HDR to repair 2 point mutations in exon 19 (c.2470inG) and exon32 (c.2470insG/c.3948insT) without drug selection was shown to be feasible with the use of single stranded oligos (ssODNs) (Jacków et al. 2019). More recently, a similar non-viral gene correction approach using single stranded donor template in patient-derived immortalized keratinocytes

and primay keratinocytes (c.425A>G) demonstrated up to 14% and 37% of C7 restoration, respectively (Kocher et al., 2021).

Osborn *et al*. investigated the potential of gene-editing strategies of systemic BMT cell-therapy for RDEB (Osborn et al., 2018). In particular, a transcriptional element upstream of the start codon site of the *COL7A1* gene was inserted by gene-editing in order to upregulate endogenous production of collagen VII in umbilical cord HSCs and peripheral blood T-cells (Osborn et al., 2018). A guide RNA targeting in proximity of the *COL7A1* start codon and a donor template carrying a UMET transcriptional element were designed. The UMET element consisted of a ubiquitous chromatin opening element (UCOE) with a hybrid MND promoter and a downstream truncated non-signalling epidermal growth factor receptor (tEGFR) in frame with the endogenous *COL7A1* exon 1, allowing for subsequent screening. Donor template was delivered by AAV-6 serotype in CD34+CD133+ HSC after electroporation of the Cas9 RNP complex. Expression of the tEGFR was found in 10% and 60% of the treated HSCs and T cells, respectively. Importantly, cells expressing the tEGFR marker for correct *in situ* integration of donor template, resulted in 15-fold and 3.5-fold increase in *COL7A1* mRNA by qRT-PCR in HSCs and human T cells, respectively, compared to normal keratinocytes.

1.10 New emerging promising applications in DEB therapies: base editors

Current CRISPR/Cas9 genome editing for the generation of knockout or integration of donor templates is only possible due to the exploitation of either NEHJ or HDR pathways upon DSBs. Despite significant breakthrough of the technology, these genome editing strategies still suffer from two major safety drawbacks making the use of Cas9 nuclease for clinical applications challenging. DNA repair processes like NHEJ result in an uncontrolled random introduction of InDels or unwanted chromosomal DNA rearrangements at the sites of the DSB that might be detrimental for cellular viability and molecular functions. On the other hand, HDR is relatively low in primary cells for therapeutic purposes, thus clonal isolation of gene-corrected cells is the only way to use patients 'cells for autologous/allogenic therapies. In contrast, base editing tools involve DSB-free site-specific modifications mediating either C to T

or A to G conversions without double stranded DNA cleavage (Gaudelli et al., 2017a; Komor et al., 2016). Currently at their 4th generation, base editor BE4 combines a D10A Cas9 nickase linked with the rat APOBEC1 (rAPOBEC1) cytidine deaminase which converts cytidine into thymidine on the sgRNA target site with a catalytic 5bp-window activity between the 4th and the 8th base of the non-target strand of the sgRNA (**Figure 1.11**). In order to overcome the limitation in base editing conversion in mammalian cells due to repair of the intermediate mismatched U:G-BE mediated pairing, an uracil DNA glycosylase inhibitor (UGI), which prevents Uracil-N-Glycosylase (UNG) from altering DNA inadvertently, was introduced. Based on BE structure and mechanisms of action many different base-editing systems have been developed with different deaminases (targetAID) (Nishida et al., 2016) and *Streptococcus Aureus* (Sa) Cas9 BE3 and BE4 (Kim et al., 2017; Komor et al., 2017).

Additionally, chimeric adenine base editors (ABE) have been developed by Gaudelli and co-workers to convert adenosines to guanosines (Gaudelli et al., 2017a) (**Figure 1.11**). Protein engineering resulted in the seventh-generation ABEs (last one ABE7.10) which combines a D10A Cas9 nickase with a tRNA adenosine deaminase (TadA) from *E. coli*. This deoxyadenosine deaminase is able to convert adenosine to inosine on single-stranded DNA thus converting A-T base pairs to G-C (Gaudelli et al., 2017a). Since the majority of single base genetic variants are associated with disease, base editors can be clinically relevant to introduce disease-suppressing mutations and to correct pathogenic mutations in human cells. According to ClinVar database for Base editor applications, 47% and 14% of all known pathogenic single nucleotide polymorphisms (SNPs) can be corrected with ABE and BE, respectively. In fact many clinically relevant EB pathogenic gene variants could in principle be corrected by base editors. In DEB, approximately 76.3% of registered mutations are SNPs. Out of those *COL7A1* pathogenic variants approximately 9% are A>G (5%) or T>C (4%) SNPs and 52% are G>A (32%) or C>T (20%) SNPs which can potentially be corrected with BEs or ABEs, respectively. For dominant forms of DEB, base editors can be used to selectively inactivate the mutant allele by precisely converting one of the four triplets (CAA, CAG, CGA, and TGG) into STOP codons (TAG, TAA, or TGA) without DSB (Billon et al., 2017; Kuscu et al., 2017). Genome-wide potential of BE3 mediated-gene silencing was

demonstrated by Ciccia *et al*., who showed that up to 3.4 million of single guide RNA can be designed to make STOP codons covering 97%–99.7% of open reading frames in the human genes (Billon et al., 2017). Notably, gene silencing by BE-Cas9 resulted in a reduced activation of apoptosis pathways compared to NHEJ-mediated knockout (Kuscu et al., 2017). Moreover, in the absence of NHEJ-mediated indel mutations which can create a mosaic population of distinct Knockout alleles in germ lines, base editing tools resulted in efficient generation of precise base edited animal embryo models (Kyoungmi Kim et al., 2017; Lee et al., 2018; P. Liang et al., 2017; Zhen Liu et al., 2018; Zhiquan Liu et al. 2018; Yang et al., 2018) Only recently, demonstration of the potential of base editing for RDEB was reported by the use of ABE in primary RDEB fibroblasts and iPSCs for two different *COL7A1* nonsense mutations (c.2005C>T/c.1573 C>T and c.553C>T+/+). Overall, direct gene-editing by CRISPR/Cas9 system holds great promise for EB. In particularly, the ability to exploit NHEJ or more accurate gene repair process such as HDR expanded the way how CRISPR/Cas9 technologies be employed for sequence-specific and patient-specific mutations within *COL7A1.* However, concerns with regards to unwanted off-target modifications should be considered in clinical applications.

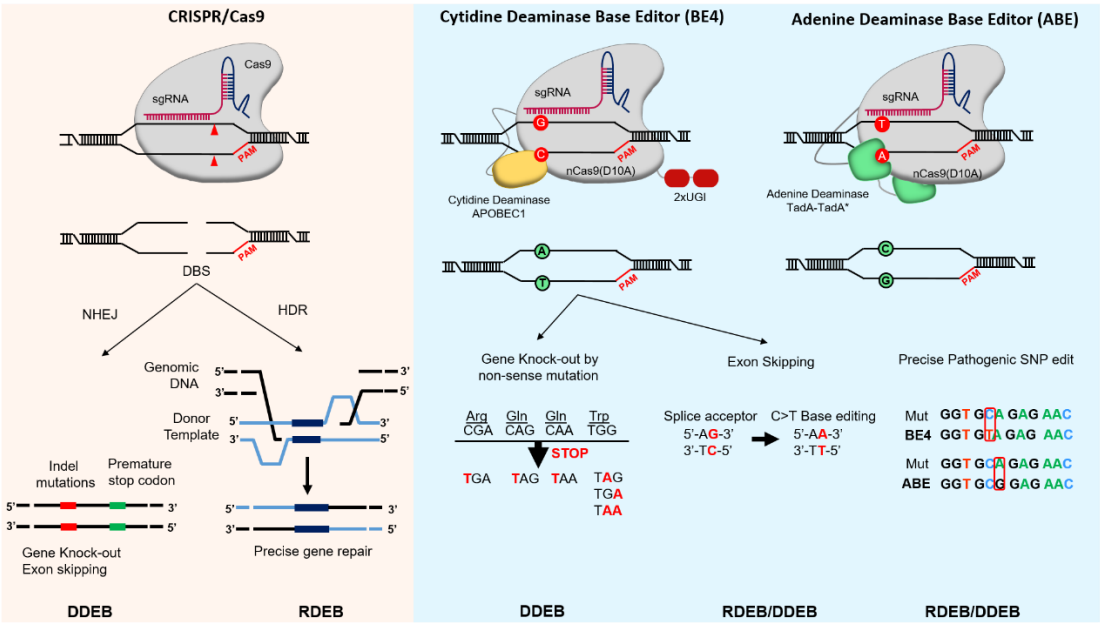

Figure 1.11 Application of CRISPR/Cas9 based technologies in dystrophic epidermolysis bullosa

Cas9 enables genome editing through NHEJ or HDR leading to either gene knock-out/exon skipping or precise gene repair. Cytidine and adenine deaminase base editors, on the other hand, can make precise base correction reverting the mutation. Cytidine deaminase base editors can also be employed for gene knockout or exon skipping without DSB. Abbreviations: DSB, double stand breaks; NHEJ, non-homologous end joining; HDR, homologous directed recombination; sgRNA, synthetic guide RNA; nCas9, nickase Cas9; UGI, Uracil glycosylase inhibitor; TadA, tRNA adenine deaminase. Picture taken from Naso and Petrova (Naso and Petrova 2019).

1.11 Project aims and objectives

Over 850 mutations including nonsense, missense, splicing or complex InDels in *COL7A1* have been reported to cause DEB (Wertheim-Tysarowska, et al., 2012). Currently, several preclinical studies and clinical trials of conventional gene therapy strategies based on the addition of a full-length copy of *COL7A1* cDNA are ongoing in RDEB keratinocytes or fibroblasts (comprehensively discussed in **section 1.6**) but their progress is hurdled by technical and biological limitations. Although novel retroviral and SIN-lentiviral vectors offer an increased safety profile, random viral integration profile of the viral backbone, epigenetic silencing, sustained transgene expression and constraints related to the effective packaging capacity of viral vectors for *COL7A1* are still an issue. Additionally, access to RDEB patient's keratinocytes is not always possible. In severe forms of RDEB, where patient's skin is under chronic inflammation as a result of persistent blistering, keratinocyte stem cells might become depleted and cannot be cultivated or expanded *in vitro* (De Rosa et al., 2019; Siprashvili et al., 2010). Furthermore, extensive manipulations of primary keratinocytes and fibroblasts and clonal selection of gene-corrected cells might also lead to their exhaustion and senescence. *In situ* gene/base editing and derivation of induced pluripotent stem cells (iPSCs) from EB patients, on the other hand, have paved the way for future cell and gene therapy approaches (Itoh et al., 2011; Tolar et al., 2011). Targeted gene editing allows for precise correction of pathogenic mutations, thus restoring the expression of the functional gene under its endogenous promoter, whereas use of iPSCs allows for indefinite self-renewal, potential for single cell expansion and *in vitro* differentiation into relevant cell types in principle providing unlimited patient cell material for subsequent personalized treatments. Therefore, application of CRISPR/Cas9 or new generation base editors in iPSCs has the potential to overcome the hurdles associated with both conventional gene therapy approaches and the use of primary skin cells.

The current project aims to establish the feasibility of state-of-the-art HDR-based gene-editing and base-editing approaches using the CRISPR/Cas9 or BE systems to correct a missense mutation hotspot (c.425A>G) within exon 3 of *COL7A1* gene.

To this end, I aimed to:

1) Develop a robust and reproducible CRISPR-Cas9-mediated HDR gene editing platform that can be applied for different cell lines with future therapeutic applications for RDEB. This was achieved by designing highly specific gene editing strategy against a distinct region of the *COL7A1* gene that permitted to achieve high frequency of Cas9-induced DSBs (NEHJ) and increase the likelihood of gene repair by HDR once the donor template is delivered (Remy et al., 2014; Duda et al., 2014; Hendel et al., 2014). By virtue of the different methods of CRISPR/Cas9 formats (DNA, mRNA, protein) and deliveries (viral and non-viral), alternative strategies were compared for guide delivery, including in combination with Cas9 protein as a ribonucleoprotein complex (RNP), or Lentiviral vector (LV) in combination with Cas9 mRNA by electroporation. Optimization of repair template designs and delivery was carried out alongside to increase levels of donor integration by HDR. The following optimizations aimed to obtain high levels of gene correction in the cell treated pool hence minimizing the need of extensive clonal analysis that could be detrimental for cell viability and expansion.

2) Validate the effiency of CRISPR/Cas9 mediated HDR in patient RDEB iPSCs harbouring a homozygous c.425A>G splice site mutation within *COL7A1*. Optimization of CRISPR/Cas9 and donor delivery in iPSCs allowed high rates of *COL7A1* correction while minimising Cas9-induced toxicity (Ihry et al. 2018). Furthermore, characterisation of potential off-target activities was analysed by next generation sequencing.

3) An alternative approach alongside HDR was the use of a cytosine base editor technology to overcome limitations associated with the random creation of InDels upon Cas9-induced DSBs. Refine of the sgRNA design helped to narrow C>T changes in the pathogenic SNP reducing the level of unwanted conversions of further cytosines within or next the base editing window. Moreover, next generation sequencing was used to characterize base editing

specificity and possible guide-RNA dependent C>T conversion in off-target loci. The same strategy will be also tested in primary fibroblasts.

4) Finally, efforts were made to differentiate gene and base-edited patient iPSCs into keratinocyte-like cells in order to assess recovery of *de novo* C7 on protein level upon gene and base editing. In parallel, expression markers of epidermal differentiation were evaluated in gene corrected iPSC-derived keratinocyte-like cells.

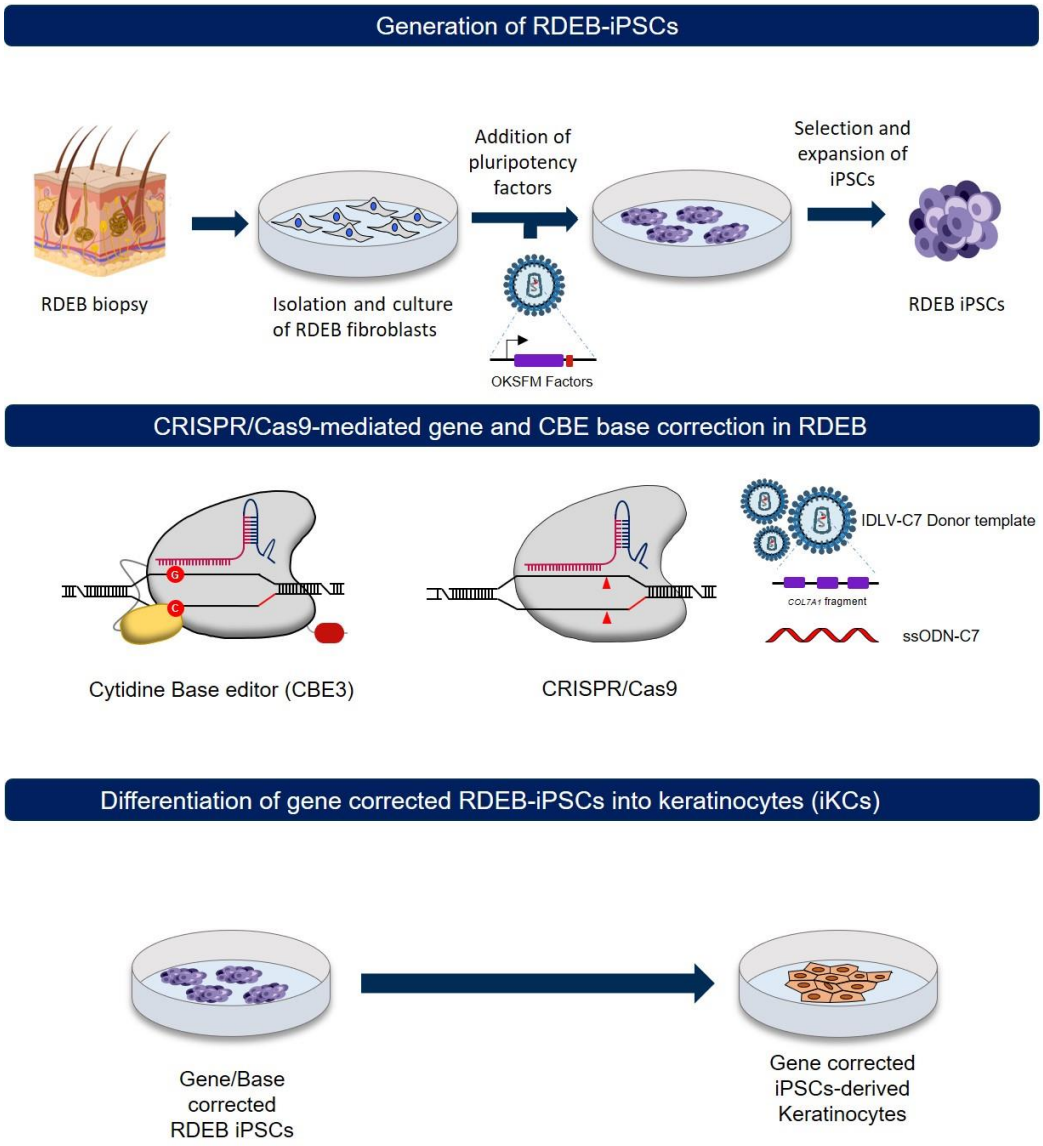

Figure 1.12 Gene modification strategy for the correction of autologous iPS cells.

Autologous RDEB patient fibroblasts were initially isolated from a punch biopsy and expanded prior to 1) reprograming into induced pluripotent stem cells (iPSCs) using Sendai vectors encoding for the Yamanaka's OKSFM factors. 2) RDEB iPSCs were then gene corrected at the *COL7A1* mutation site using site-specific CRISPR/Cas9 nuclease co-delivered with homologous donor repair templates by viral and non-viral delivery methods. 3) Corrected RDEB iPSCs were differentiated towards keratinocyte stem cells**.**

Chapter 2 Material and methods

2.1 Materials

2.1.1 Reagent used for DNA

Table 2.1 List of the reagents used for DNA and RNA

Reagent:	Manufacturer:	Catalogue number:
50X Tris-acetate-EDTA (TAE) buffer	ThermoFisher Scientific, Massachusetts, USA	B49
Nuclease-Free Water (not DEPC-Treated)	ThermoFisher Scientific, Massachusetts, USA	AM9939
1Kb plus DNA ladder	ThermoFisher Scientific, Massachusetts, USA	10787018
Q5® high-fidelity DNA polymerase	New England Biolabs, England	M0491S
Gel loading dye: Orange G 6X	ThermoFisher Scientific, Massachusetts, USA	R0631
UltraPure™ Agarose	ThermoFisher Scientific, Massachusetts, USA	16500500
SYBR™ Safe DNA Gel Stain	ThermoFisher Scientific, Massachusetts, USA	S33102
Branched Polyethylenimine (PEI)	Sigma-Aldrich, Dorset, UK	408727
T4 DNA ligase (5U/µl)	ThermoFisher Scientific, Massachusetts, USA	EL0014
T4 Polynucleotide Kinase	NEW ENGLAND BioLabs, Massachusetts, USA	M0201S
FastAP Thermosensitive Alkaline Phosphatase (1U/µl)	ThermoFisher Scientific, Massachusetts, USA	EF0651
FastDigest XhoI	ThermoFisher Scientific, Massachusetts, USA	FD0694
FastDigest EcoRI	ThermoFisher Scientific, Massachusetts, USA	FD0274
FastDigest DpnI	ThermoFisher Scientific, Massachusetts, USA	FD1704
FastDigest StyI (Eco130I)	ThermoFisher Scientific, Massachusetts, USA	FD0414
High-Capacity cDNA Reverse Transcription Kit	ThermoFisher Scientific, Massachusetts, USA	4368814

2.1.2 List of the reagents used for protein

Table 2.2 List of the reagents used for protein

Reagent:	Manufacturer:	Catalogue number:
Amersham™ ECL™ Rainbow™ Markers- Full Range	GE LifeSciences, Buckinghamshire, UK	GERPN800N
Amersham Hybond P 0.22µm PVDF blotting membrane	GE LifeSciences, Buckinghamshire, UK	10600021
Tran-Blot® Turbo™ Mini PVDF Transfer Packs (0.22µm)	Bio-Rad, California, USA	1704156
NuPAGE™ 4-12% Bis-Tris Protein Gels, 1.0 mm, 10-well	ThermoFisher Scientific, Massachusetts, USA	NP0321BOX
4-15% Mini-PROTEAN® TGX™ Precast Protein Gels, 10-well, 30µl	Bio-Rad, California, USA	456-1083
cOmplete protease Inhibitor cocktail tables	Roche, Basel, Switzerland	11697498001
Dithiothreitol (DTT)	ThermoFisher Scientific, Massachusetts, USA	R0861
Phenylmethylsulfonyl fluoride (PMSF)	Sigma-Aldrich, Dorset, UK	10837091001
Triton™ X-100	Sigma-Aldrich, Dorset, UK	X100-5ML
Sodium Dodecyl Sulphate (SDS)	Sigma-Aldrich, Dorset, UK	71725-50G
TrueCut™ Cas9 Protein v2	ThermoFisher Scientific, Massachusetts, USA	A36496
10x Tris/Tricine/SDS Running Buffer, 1L	Bio-Rad, California, USA	1610744
Glycerol	Sigma-Aldrich, Dorset, UK	G5516-100ML
β - mercaptoethanol	Sigma-Aldrich, Dorset, UK	M6250
Dried skimmed milk power	Marvel	n/a
Trizma® base	Sigma-Aldrich, Dorset, UK	T1503-25G
Bromophenol blue	Sigma-Aldrich, Dorset, UK	114391-5G
TWEEN® 20	Sigma-Aldrich, Dorset, UK	P9416-50ML
UltraPure™ 0.5M EDTA pH 8.0	ThermoFisher Scientific, Massachusetts, USA	15575-038
NaCL	Sigma-Aldrich, Dorset, UK	S9888

2.1.3 Reagents used for bacterial culture

Table 2.3 List of the reagents used for bacterial culture

Reagent:	Manufacturer:	Catalogue number:
Ampicillin Sodium salt	Sigma-Aldrich, Dorset, UK	A0166-25G
Kanamycin sulphate from Streptomyces kanamyceticus	Sigma-Aldrich, Dorset, UK	K1377-25G
LB broth	Sigma-Aldrich, Dorset, UK	L3022-250G
LB agar	Sigma-Aldrich, Dorset, UK	L3147-1KG
S.O.C. Medium	ThermoFisher Scientific, Massachusetts, USA	15544034
One Shot™ Stbl3™ Chemically Competent *E. coli*	ThermoFisher Scientific, Massachusetts, USA	C737303
Stellar™ Competent Cells	Takara Bio Europe, Saint-Germain-en-Laye, France	636766

2.1.4 Reagents used for cell culture

Table 2.4 List of the reagents used for cell culture

Cell type: HaCaT and primary fibroblasts		
Reagent:	**Manufacturer:**	**Catalogue number:**
Dimethyl sulfoxide (DMSO)	Sigma-Aldrich, Dorset, UK	276855-100ML
Dulbeco's Modified Eagle Medium (DMEM), 500ml	ThermoFisher Scientific, Massachusetts, USA	11960044
Opti-MEM™ I Reduced Serum Medium	ThermoFisher Scientific, Massachusetts, USA	31985062
Foetal Calf Serum (FCS)	ThermoFisher Scientific, Massachusetts, USA	10-082-147
Trypsin-EDTA (0.25%)	ThermoFisher Scientific, Massachusetts, USA	25200056
Penicillin-Streptomycin (Pen Strep), 10,000 U/ml, 100ml	ThermoFisher Scientific, Massachusetts, USA	15140122
Dulbecco's Phosphate-Buffered Saline (DPBS),	ThermoFisher Scientific, Massachusetts, USA	14040117
Cell type: iPSCs		
Reagent:	**Manufacturer**:	**Catalogue number:**
Essential 8	ThermoFisher Scientific, Massachusetts, USA	A1517001

mTeSR™1	STEMCELL Technologies, Vancouver, Canada	85850
TeSR™2	STEMCELL Technologies, Vancouver, Canada	05860
TeSR™E8	STEMCELL Technologies, Vancouver, Canada	05990
Y-27632 dihydrochloride	TOCRIS, Bristol, England	1254/10
Matrigel®	Corning, New York, USA	356230
Vitronectin XF™	STEMCELL Technologies, Vancouver, Canada	07180
CellAdhere™ Dilution Buffer	STEMCELL Technologies, Vancouver, Canada	07183
Vitronectin (VTN-N) Recombinant Human Protein, Truncated	ThermoFisher Scientific, Massachusetts, USA	A14700
Biolaminin™ 521 (LN 521)	BioLamina AB, Sundbyberg, Sweden	LN521-05
mFreSR™	STEMCELL Technologies, Vancouver, Canada	05855
Cell type: primary keratinocyte		
Reagent:	**Manufacturer:**	**Catalogue number:**
Keratinocyte serum –free medium (DKSFM)	ThermoFisher Scientific, Massachusetts, USA	17005042
PureCol®	Advanced BioMatrix, Inc Carlsbad, CA, USA	5006

2.1.5 Reagents used for generation of iPSCs into keratinocyte (iKer)

Table 2.5 List of the reagents used for iKer

Basal Medium		
Reagent:	**Manufacturer:**	**Catalogue number:**
MCDB 153	Sigma-Aldrich, Dorset, UK	M7403-10X1L
Water	Sigma-Aldrich, Dorset, UK	W3500-6X1L
Sodium bicarbonate	Sigma-Aldrich, Dorset, UK	S8761-500ML
Sodium hydroxide	Sigma-Aldrich, Dorset, UK	S2270-100 ML
Hydrochloric acid	Sigma-Aldrich, Dorset, UK	H9892-100ML
L-Carnitine	Sigma-Aldrich, Dorset, UK	C0283-100G
L-Histidine	Sigma-Aldrich, Dorset, UK	H8125-25G
L-Isoleucine	Sigma-Aldrich, Dorset, UK	I2752-10G
L- Methionine	Sigma-Aldrich, Dorset, UK	M9625-5G
L-Phenylalanine	Sigma-Aldrich, Dorset, UK	P2126-100G
L- Threonine	Sigma-Aldrich, Dorset, UK	T8625-10G
L-Tryptophan	Sigma-Aldrich, Dorset, UK	T0254-1G
L-Tyrosine	Sigma-Aldrich, Dorset, UK	1024130100

Calcium Chloride	Sigma-Aldrich, Dorset, UK	C1016-100G
8-Bromo-cAMP	Sigma-Aldrich, Dorset, UK	B5386-100MG
Ethanolamine	Sigma-Aldrich, Dorset, UK	411000
Phosphorylethanolamine	Sigma-Aldrich, Dorset, UK	P0503-1G
Hydrocortisone	Sigma-Aldrich, Dorset, UK	H4001-1G
Insulin	Sigma-Aldrich, Dorset, UK	I2643
Apo-Transferrin	Sigma-Aldrich, Dorset, UK	T1147-100MG
Triiodothyronine	Santa Cruz Biotechnology Dallas, USA	SC-204035
Unstable active differentiation factors for different KD media		
Reagent:	**Manufacturer:**	**Catalogue number:**
AA2P (P-Vitamin C)	Sigma-Aldrich, Dorset, UK	49752-10G
All-trans retinoic acid	Sigma-Aldrich, Dorset, UK	R2625-50MG
BMP4	R&D Systems, Minnesota, USA	314-BP-010
Cholera Toxin	Sigma-Aldrich, Dorset, UK	C8052-5MG
EGF	Sigma-Aldrich, Dorset, UK	E9644-.2MG
FGF1	Sigma-Aldrich, Dorset, UK	F5542-25UG
Niacinamide	Sigma-Aldrich, Dorset, UK	N5535-100G
SB431542	R&D Systems, Minnesota, USA	S1067

2.1.6 Flow cytometry, western blot and immunofluorescence antibodies

Table 2.6 List of primary antibodies

Pluripotency Markers				
Class:	**Target:**	**Manufacturer:**	**Cat number:**	**Dilution**
Conjugated Antibody	Anti SOX2-human-FITC	Miltenyi Biotech, Surrey, UK	130-120-790	1:50
	Anti NANOG-human APC	Miltenyi Biotech, Surrey, UK	130-120-774	1:50
	Anti TRA 1-60-human PE	Miltenyi Biotech, Surrey, UK	130-122-965	1:50
	Anti TRA 1-81-human PE	Miltenyi Biotech, Surrey, UK	130-101-427	1:11
	Anti SSEA-4-human PE	Miltenyi Biotech, Surrey, UK	130-122-958	1:50
Primary antibody	Rabbit anti SOX2	Sigma-Aldrich, Dorset, UK	48-1400	1:100

	Mouse anti OCT-3/4	Santa Cruz Biotechnology Dallas, USA	sc-5279	1:100
Germ-line differentiation markers				
Class:	**Target:**	**Manufacturer:**	**Cat number:**	**Dilution**
Endoderm	Mouse anti-AFP	Sigma-Aldrich, Dorset, UK	130-101-463	1:100
Mesoderm	Mouse anti-ACTA2	Sigma-Aldrich, Dorset, UK	A5228	1:100
Ectoderm	Mouse anti-TUBB3	Sigma-Aldrich, Dorset, UK	T5076	1:100
iPSCs-derived keratinocytes, primary and immortalized keratinocytes				
Class:	**Target:**	**Manufacturer:**	**Catalogue number:**	**Dilution**
Conjugated Antibody	CD49F-APC	Miltenyi Biotech, Surrey, UK	130-100-147	1:11
	CD104-PE	Miltenyi Biotech, Surrey, UK	130-101-440	1:11
Primary Antibody	Mouse anti-ΔNp63	Abcam, Cambridge, UK	ab172731	1:100
	Mouse anti-KRT 18	Sigma-Aldrich, Dorset, UK	C8541	1:1000
	Rabbit anti KRT14	Santa Cruz Biotechnology Dallas, USA	sc-53253	1:1000
	Mouse anti-C7 (LH7.2)	Sigma-Aldrich, Dorset, UK	C6805	1:500 (IF)
	Mouse anti-C7 (LH7.2)	Santa Cruz Biotechnology Dallas, USA	sc-53226	1:25 (Flow)
iPSCs-derived fibroblasts and primary fibroblasts				
Class:	**Target:**	**Manufacturer:**	**Cat number:**	**Dilution**
Conjugated Antibody	Anti-Vimentin-human-FITC	Miltenyi Biotech, Surrey, UK	130-116-663	1:50
	Anti-CD73-APC	Miltenyi Biotech, Surrey, UK	130-097-945	1:11
	Anti-CD90 human-FITC	Miltenyi Biotech, Surrey, UK	130-097-930	1:11
	Anti-fibroblasts-APCVio770	Miltenyi Biotech, Surrey, UK	130-100-042	1:11

	Anti-105-human-APC	Miltenyi Biotech, Surrey, UK	130-112-324	1:11
Primary Antibody	Vimentin 5G3F10	Cell signalling technology, Massachusetts, USA	3390	1:1000

Table 2.7 Secondary antibodies

Target:	Manufacturer:	Cat number:	Dilution
Goat anti-mouse Alexa Fluor 488-conjugated IgG	Sigma-Aldrich, Dorset, UK	A-11001	1:500
Goat anti-mouse Alexa Fluor 647-conjugated IgG	Sigma-Aldrich, Dorset, UK	A-21235	1:500
Rabbit anti-mouse Alexa Fluor 488-conjugated IgG	Sigma-Aldrich, Dorset, UK	A-27023	1:500
Donkey anti-mouse Rhodamine-X-conjugated IgG	Jackson Immuno-Research	715–295-150	1:100

2.1.7 Commercial kits used

Table 2.8 List of kits

Reagent:	Manufacturer:	Catalogue number:
Bio-Rad Protein assay kit II	Bio-Rad, California, USA	5000002
Clarity™ Western ECL Substrates, 200ml	Bio-Rad, California, USA	1705060
Q5® High-Fidelity DNA Polymerase	NEW ENGLAND BioLabs, Massachusetts, USA	M0491L
Monarch® Plasmid Miniprep Kit	NEW ENGLAND BioLabs, Massachusetts, USA	T1010L
Plasmid Maxi Kit	QIAGEN, Hilden, Germany	12165
Monarch® PCR & DNA Cleanup Kit (5µg)	NEW ENGLAND BioLabs, Massachusetts, USA	T1030L
Monarch® DNA Gel extraction Kit	NEW ENGLAND BioLabs, Massachusetts, USA	T1020L
DNeasy Blood & Tissue Kit (250)	QIAGEN, Hilden, Germany	69506
RNeasy Plus Mini Kit (50)	QIAGEN, Hilden, Germany	74134

In-Fusion® HD Cloning Plus	Takara Bio Europe, Saint-Germain-en-Laye, France	638910
QuikChange Lighting Multi Site-Directed Mutagenesis Kit	Agilent, California, USA	210513
Neon™ Transfection System 100 µl Kit	ThermoFisher Scientific, Massachusetts, USA	MPK10096
P3 Primary Cell 4D-Nucleofector™ X Kit L	Lonza, Basel, Switzerland	V4XP-3024
P24	ZeptoMetrix, New York, USA	0801111

2.1.8 Buffer

Lysis buffer base: 50mM Tris/HCL pH8.0, 150mM NaCL, and 5mM EDTA.

Lysis buffer: 84.5% lysis buffer base, 10% Triton-X (10 fold diluted in PBS), 5% protease inhibitor cocktail (complete), 0.5% PMSF.

Assay buffer: 98% lysis buffer base, and 2% lysis buffer.

10X Wash buffer: 0.5% Tween-20 in PBS. Stored at RT.

5X sample buffer: 10% SDS, 30% Glycerol, 10% β – mercaptoethanol, 0.001% bromophenol blue, and ~60% 0.5M Tris/HLC, pH6.8. Stored at -20tored at -20^{o}C.

Blocking solution: 5% dried skimmed milk powder in 1X Wash buffer.

Western blot primary antibody: 3% BSA in 1X wash buffer.

Western blot secondary antibody: 3% dried skimmed milk powder in 1X Wash buffer. Stored at 4^{o}C.

Flow cytometry wash and staining buffer: 2% FCS in PBS. Stored at 4^{o}C.

LB broth: 20g/L of LB broth powder in MilliQ water. Solution is autoclaved at 121^{o}C for 15min. Once at RT, kanamycin (50µg/ml) or ampicillin (100µg/ml) was added according to the bacteria antibiotic resistance. Stored RT till antibiotic was added and then moved to 4^{o}C.

LB agar: 36g LB agar powder per L of MilliQ water. Autoclaved at 121°C for 15min. Allow LB agar to cool to ~60°C before adding either kanamycin (50µg/ml) or ampicillin (100µg/ml). Once selective antibiotic was added, 18-20ml LB was added per plate. Stored at 4°C.

Bacterial glycerol stock: 100% glycerol was mixed in a 1:1 ratio with H_2O to make a 50% glycerol solution. This 50% glycerol solution was then mixed in a 1:1 ratio with overnight bacterial culture (500µl: 500µl) in a screw cap cryopreservation tube, and stored at -80°C.

Cell line freezing mix: 10% DMSO, and 90% FCS. Stored at 4°C.

2.1.9 Cell types

Table 2.9 List of Cell types

Cell ID	Tissue type	Immortalisation	Medium
HEK-293T (293T)	Human Embryonic Kidney Cell Line (Adherent)	SV40 large T antigen	Complete DMEM
HaCaTs	Human Keratinocyte (Line)	Spontaneously transformed	Complete DMEM
WT Keratinocyte	Human Keratinocyte (primary)	n/a	DKSFM
RDEB fibroblasts (Patient CK)	Human Fibroblasts (primary)	n/a	Complete DMEM
WT fibroblasts	Human Fibroblasts (primary)	n/a	Complete DMEM
WT iPSCs	Human induced pluripotent stem cells	n/a	TesR™2/mTeSR1/TesR-E8

Table 2.10 List of RDEB human patient cells

Cell ID	Mutation c.DNA level	Mutation protein level	Exon/ intron	Type of variant	Variant effect	EB type
RDEB Patient (CK)	(+/+) c.425A>G	p.K142R	Exon 3	Base substitution	missense, splicing	RDEB

2.1.10 Primers

Table 2.11 List of PCR, qPCR and SDM primers used

Primer name	Sequence 5'→ 3'	Aim
SDM-Ex3D-FWD	CACATGGAGAATTGCAGCGCCGGTT CGCGTATTGGCCCCCCTTGTAGCTAAG	Silent Directed Mutagenesis (SDM)
SDM-Ex3D-REV	CTTAGCTACAAGGGGGGCAATACGC GAACCGGCGCTGCATTCTCCATGTG	
Ex3P-PAM-Removal-FWD	GGGTAGGGATTGGGGTCC	
Ex3P-PAM-Removal-REV	CCTGGTGTCCCCAAAGTGATCCCTACCC	
Cas9-P2A removal-FWD	ATGGTGTCTAAGGGCGAAG	
Cas9-P2A removal-REV	GGTGGCAGCGCTCTAGAA	
***XhoI*-I2I7C7-FWD**	ATTACTCGAGACTCCTTCCCCAG	
***EcoRI*-I2I7C7-REV**	ACGGAATTCGAGATGGGGTCAG	
WPRE-REV	GGCATTAAAGCAGCGTATCC	PCR
Ex2-*COL7A1*-FWD(TI-5')	CAGTGCAGTACAGCGATGACC	
Ex4-SDM-ZFN-REV	CGATTTGCCATCTGTGATCAGAATACAC	
Ex4-SDM-ZFN-FWD	GTGTATTCTGATCACAGATGGCAAATCG	
Ex8-*COL7A1*-REV (TI-3')	GTCAGTTCCGGCCCTTCTAG	
EX5-*COL7A1*-REV	GGAACTCACGAGGTCGGGTC	
Intron 2 *COL7A1*-FWD	CAGTGCAGTACAGCGATGACC	
Intron2C7-StyI-FWD	GACCCCTCAAGAGAGCCTGATACC	*StyI* assay
Exon4C7-StyI-REV	CCCGTCTGTGATCAGGATGCAG	
cMYC-FWD	TTCGGGTAGTGGAAAACCAG	RT-PCR
cMYC-REV	CAGCAGCTCGAATTTCTTCC	
SOX2-FWD	ACACCAATCCCATCCACACT	
SOX2-REV	GCAAACTTCCTGCAAAGCTC	
OCT4-FWD	GTACTCCTCGGTCCCTTTCC	

OCT4-REV	CAAAAACCCTGGCACAAACT	
KLF4-FWD	CCCACACAGGTGAGAAACCT	
KLF4-REV	TTCTGGCAGTGTGGGTCATA	
NANOG-FWD	GATTTGTGGGCCTGAAGAAA	
NANOG-REV	AAGTGGGTTGTTTGCCTTTG	
GAPDH-FWD	TCATCTCTGCCCCCTCTGCT	
GAPDH-REV	CGACGCCTGCTTCACCACCT	
Exon2C7-REV	TGACCTGCACGCGCCTTTACGC	
Exon4C7-REV	CCACAGCAAATAGCTTGACCCC	
HIV packaging signal Psi reverse	TCCCCCGCTTAATACTGACG	qPCR
HIV packaging signal Psi probe	FAM-CGCACGGCAAGAGGCGAGG-TAMRA	
Human albumin forward	GCTGCTATCTCTTGTGGGCTGT	
Human albumin reverse	ACTCATGGGAGCTGCTGGTTC	
Human albumin probe	VIC-CCTGTCATGCCCACACAAATCTCTCC-TAMRA	
HIV packaging signal Psi reverse	TCCCCCGCTTAATACTGACG	
HIV packaging signal Psi probe	FAM-CGCACGGCAAGAGGCGAGG-TAMRA	
Human albumin forward	GCTGCTATCTCTTGTGGGCTGT	

Table 2.12 List of primers used for NGS

Primer name	Sequence 5'→ 3'	Aim
NGS-C7_EX3_FWD	ACACTCTTTCCCTACACGACGC TCTTCCGATCT* GTTCGGCCTGGATGCACTTG	On-target Exon 3 *COL7A1*
NGS-C7_EX3_REV	GTGACTGGAGTTCAGACGTGT GCTCTTCCGATCT* TGATCCCTGAAGTGACGACC	
Cas9 OT1 FWD	TGGACACCAAACCCACCC	Off-target for Ex3P-sgRNA
Cas9 OT1 REV	GCCCACGACCAAGACAGA	
Cas9 OT2 FWD	ATCTCTAGCCCAGCCCCT	
Cas9 OT2 REV	GCACAGAGGCCAGAGGAT	
Cas9 OT3 FWD	ACAGAGAGAGAGGCCCCA	
Cas9 OT3 REV	GAAAGGGGCTGGGATGGT	
Cas9 OT4 FWD	TGTGCCTGGTCAGAGTGG	
Cas9 OT4 REV	TGCAGACCAGGCCAAAGT	
Cas9 OT5 FWD	TTGAGCAGCTGGGGAACA	

Cas9 OT5 REV	GGCAGCAGGAAGAGCACT	
Cas9 OT6 FWD	ACTTCTCCTGGAGCTCGC	
Cas9 OT6 REV	CAAACAGCGGCCGAGAAG	
Cas9 OT7 FWD	TGCCTGTGAAGTGCCTTG	
Cas9 OT7 REV	CCCATCGTGATTGTACCAACA	
Cas9 OT8 FWD	ACCTGCCACAAGATTCCCT	
Cas9 OT8 REV	ACACAGAGACAGGCCAGC	
Cas9 OT9 FWD	AAATGGAGGCCGGAGACA	
Cas9 OT9 REV	CCCTGTCTTTCTCTGGCCA	
Cas9 OT10 FWD	GCCAAGCTCAAGAAGACAGC	
Cas9 OT10 REV	TGGTCCCTCACTCACCCT	
BE OT1 FWD	TACGCCCCAGTTCAAGCC	Off-target for x3C7-CyD-1 sgRNA
BE OT1 REV	AGGGGCTGTGGTCTCTCT	
BE OT2 FWD	AGGCATGGTCAGAGCAGG	
BE OT2 REV	CCAAGCAGCGAATCGTGT	
BE OT3 FWD	AAAGGTCTGGGCTGAGGG	
BE OT3 REV	TGGTCAGTTCTCAGCTTTCAT	
BE OT4 FWD	AATGCCCAGACCATGCCT	
BE OT4 REV	AGCCCAAGTGTGTGAGGA	
BE OT5 FWD	CCCCATGACAGCCCATCA	
BE OT5 REV	TCAGCAGCAAACCCGATG	
BE OT6 FWD	GAGTGAGGGCTGAGCAGT	
BE OT6 REV	TTGCCCACAGAGTCCCAG	
BE OT7 FWD	CAGGACTGAGGGCTGAGG	
BE OT7 REV	GTCAGTACCGAGGGCAGG	
BE OT8 FWD	GGCTCTGGGTCTTGAGGG	
BE OT8 REV	CCAGGGCAGCTTCCAAGA	
BE OT9 FWD	ACAGAGAGGCAGCCGAAG	
BE OT9 REV	CTGCTTCCCCTGCCAGAA	
BE OT10 FWD	TCCTGCCTTCTCCAAGCC	
BE OT10 REV	AGCATGAGAGAGCAGCCC	

* Blue and red bases represent overhangs on the forward and reverse NGS primers respectively

2.1.11 Parental plasmids

Table 2.13 List of parental plasmids used

Plasmid:	Description:	Source:
pMD2.G	CMV driven Vesicular Stomatitis Virus envelope glycoprotein (VSV-G) expressing plasmid	Addgene #12259
pCMV-dR8.74 D64V	2nd generation integrase mutant gag-pol-tat-rev expressing lentiviral packaging plasmid driven by CMV promoter for generation of non-integrating lentiviral vectors (NILV)	Addgene #22036
pRSV-Rev	3rd generation REV expressing lentiviral plasmid driven by RSV promoter	Addgene #12253.
pMDLg/pRRE	3rd generation gag-pol expressing lentiviral packaging plasmid driven by CMV promoter.	Addgene #12251
pHR'SIN.cPPT-SW	SIN 2nd generation lentiviral backbone including a MCS flanked by a SFFV promoter upstream and Woodchuck hepatitis virus post-transcriptional regulatory element (WPRE) downstream	(Georgiadis 2016)
COL7A1 in2-ex7 donor template	A portion of the COL7A1 cDNA sequence spanning intron 2 – exon 7 including a 5' EcoRI and 3' XhoI restriction site.	(Georgiadis 2016)
pSpCas9(BB)-2A-GFP (PX458)	CMV-driven plasmid expressing Cas9 from *S pyogenes* with 2A-EGFP tag and a U6 promoter guide RNA expression cassette.	Addgene #48138
NILV-OriginalTemp	pHR'SIN.cPPT-SW-based transfer vector designed to carry the *COL7A1 in2-ex7* donor template.	(Georgiadis 2016)
NILV-SDMTemp	The NILV-OriginalTemp was modified by site directed mutagenesis (SDM) for the introduction of 7 silent mutations in ex4 COL7A1 template	(Georgiadis 2016)
LentiCRISPRV2	3rd generation transfer vector plasmid contains two expression cassettes encoding for hSpCas9-P2A-EGFP and the chimeric guide RNA under EF-1α and U6 promoters, respectively.	Addgene #52961

2.1.12 Generated plasmids

Table 2.14 List of generated plasmids

Plasmid:	Description:
NILV-LentiV2CRISPR-Ex3D	LentiV2CRISPR-derived plasmid encoding for the Ex3D sgRNA and the hSpCas9-P2A-EGFP cassette under the EF-1α promoter.
LentiV2 noCas9	LentiV2CRISPR-derived plasmid with in frame PCR-based excision of the SpCas9-P2A cassette, leaving the expression of the EGFP cassette under the EF-1α promoter.
LentiV2-Ex3D	LentiV2 noCas9 parental plasmid encoding for the Ex3D sgRNA expressed by the U6 promoter.
LentiV2-B2M	LentiV2 noCas9 parental plasmid encoding for the B2M sgRNA expressed by the U6 promoter.

2.1.13 CRISPR/Cas9 reagents

2.1.13.1 Cas9

CleanCap® Cas9 mRNA

This off-the-shelf mRNA (Cat. No. L-7606) is manufactured from Trilink biotechnologies (San Diego, USA) and encodes for the SpCas9 endonuclease (transcript length: 4521bp). It incorporates two nuclear localisation signals, one at either terminus of the protein to increase trafficking to the nucleus. Additionally, co-transcriptional capping supported a naturally occurring Cap 1 structure which in conjunction with polyadenylation optimises mRNA expression and stability.

Custom made CleanCap® coBE3 mRNA

This mRNA (Cat. No. L-7007) is a custom-made product from TriLink, encoding a human codon optimised, third generation BE (coBE3) (transcript length: 5664bp). The plasmid DNA used for mRNA synthesis containing the coBE3 sequence was sent to TriLink for mRNA production (180µg). This involved template linearization by BtgZI restriction digest, and mRNA purification by high performance liquid chromatography (HPLC) to help remove truncated mRNA by-products, increasing product purity. Unlike the SpCas9 mRNA, the coBE3 only contains a single NLS at the C terminus.

TriLink's CleanCap technology was used to add a co-transcriptional Cap 1 structure, and this mRNA was further polyadenylated to increase expression and stability.

2.1.13.2 Single guide RNA (sgRNA)

Synthetic sgRNAs were manufactured by Synthego (California, USA) using automated solid-phase synthesis with 2'-O-methyl 3' phosphorothioate modifications in the first and last 3 nucleotides. Single guide RNA containing a 20 nucleotide protospacer with an 80 nucleotide CRISPR scaffold were produced at either a 1.5 nmol (~50µg), or 3 nmol (~100µg) production scale. These were eluted in nuclease-free Tris-EDTA buffer provide by Synthego at 2µg/µl.

Table 2.15 List of protospacer sequences designed

sgRNA	Gene Target	Sequence 5' – 3'	Nuclease	Benchling on-target (off-target) score
TAP1-PC	TAP1 Ex1	ACTGCTACTTCTCGCCGACT	SpCas9	59.3 (48.7)
Ex3C7-1	COL7A1 Ex3	AAGGGGGGCAACACTCGCAC	SpCas9	49.0 (47.4)
Ex3C7-2	COL7A1 Ex3	AGGGGGGCAACACTCGCACA	SpCas9	63.1 (46.4)
Ex3C7-3	COL7A1 Ex3	TCCGTGAGCTTAGCTACAAG	SpCas9	65.8 (46.0)
Ex3C7-4	COL7A1 Ex3	CATCCGTGAGCTTAGCTACA	SpCas9	51.8 (45.6)
x3C7-CyD-1	COL7A1 Ex3	CACCCTGGGGACACCAGGTC	BE3	C1 4.1, C3 5.6, C4 9.3, C5 20.3, (36.2)
x3C7-CyD-2	COL7A1 Ex3	TCACCCTGGGGACACCAGGT	BE3	C2 6.4, C4 11.6, C5 20.3, C6 21.4, (39.9)
B2M Ex1	B2M Ex1	GAGTAGCGCGAGCACAGCTA	SpCas9	56.3, (88.6)
B2M-CyD	B2M Ex1	ACTCACGCTGGATAGCCTCC	BE3	C2 2.5, C4 21.7, C6 13.5, C8 2.8, (85.0)

Protospacer sequences used throughout this project with either SpCas9 or BE3. All protospacer sequences are presented in the 5'-3' orientation, with cytidines within the BE3 editing window (positions 4-8 distil to the PAM) shown in Red. Benchling online tool (https://benchling.com) was used to score both on-target and off-target potential.

2.1.14 Single stranded oligonucleotide (ssODN):

The 127bp-ssODNs (Ultramer® DNA Oligo), were manufactured by Integrated DNA Technologies Inc. (Coralville, USA) by standard desalting purification with two phosphorothioate chemical modifications (2PS) at both the 5' and 3' ends (De Ravin et al. 2017). ssODNs were produced at 4nmol (~157µg) production scale. These were eluted in nuclease-free Tris-EDTA buffer provide by Synthego at 5µg/µl.

Table 2.15 List of ssODN-donor templates

ssODN name:	**NT-2PS-ssODN-AAA**
Target exon:	COL7A1 Exon 3
Sequence:	
A*T*GTCTTCCTGCCCCAGCTGGCCCGACCTGGTGTCCCCAAGTGATCCCTACCCCTAC CATGCCTCCCAAGATGACCCCAAATGAAGTGTCCAGGGGAACCGTGATTTGACCCCTGC ACCTGTCC*C*A	
ssODN name:	**T-2PS-ssODN-AAA**
Target exon:	COL7A1 Exon 3
Sequence:	
T*G*GGACAGGTGCAGGGGTCAAATCACGGTTCCCCTGGACACTTCATTTGGGGTCATC TTGGGAGGCATGGTAGGGGTAGGGATCACTTGGGGACACCAGGTCGGGCCAGCTGG GGCAGGAAGAC*A*T	
ssODN name:	**NT-2PS-ssODN-AAA**
Target exon:	COL7A1 Exon 3
Sequence:	
A*T*GTCTTCCTGCCCCAGCTGGCCCGACCTGGTGTGCCGAAGGTGATCCCTACCCCTAC CATGCCTCCCAAGATGACCCCAAATGAAGTGTCCAGGGGAACCGTGATTTGACCCCTGC ACCTGTCC*C*A	

* Red bases represent silent point mutations introduced within the donor templates. Asterisks correspond to the phosphorothioate chemical modifications inserted in the ssODN templates

2.1.15 Software

FlowJo v10: Allowed import of *FCS* files used for all flow cytometry analysis shown in this report.

Graphpad Prism v8.0.0: Arrangement of data into appropriately formatted graphs, with subsequent statistical analysis.

SnapGene® v3.1.4: Instrumental in plasmid and gene map production, as well as restriction digest design. Additionally, this software was used to design sequencing primers for plasmid DNA and In-fusion cloning primers. Furthermore, this software was used to align Sanger sequencing to a reference sequence.

ImageJ/FIJI (plugin): Java-based image processing program used for gel and immunofluorescence analysis.

2.2 Methods

2.2.1 Bacterial transformation

All transformations were performed with 50µl of One Shot™ Stbl3™ Chemically Competent *E. coli* (ThermoFisher). Competent cells were mixed with 3µl of ligation reaction and left on ice for 30 minutes, before heat shock at 42^{o}C for 45 seconds. Transformations were then put on ice for 2 minutes, before 450µl of S.O.C. (Invitrogen, California, USA) medium was added. Transformed cells were then recovered at 37^{o}C for 1 hour, shaking at 250g. Once completed, 200µl of the bacterial transformation was plated on a pre-warmed LB agar plate containing an appropriate antibiotic and incubated at 37^{o}C overnight. Individual colonies were picked and grown in 5ml of LB broth with antibiotic at 37^{o}C, shaking at 250g. Minipreps and Maxipreps were prepared using the QIAprep spin Mini kit (QIAGEN, Hilden, Germany) and QIAGEN Plasmid Maxi Kit (QIAGEN, Hilden, Germany) according to manufacturer's instructions with the appropriate antibiotic.

2.2.2 Restriction digestion

All Restriction enzymes used in this project are sourced from ThermoFisher Scientific in their FastDigest format and used according to manufacturer's protocol. Plasmids and PCR products from genomic DNA were digested to a final volume of 20µL containing 2µL of 1X fast digest buffer, up to 2µL of restriction enzyme (<10% of the final volume) and DNA (0.5-1µg). The reactions were incubated at 37°C for 1 hour followed by heat inactivation at 65°C for 10 minutes.

Digestions with *BsmBI* (*Esl3I*), required the addition of 1.25µl DTT (20mM).

2.2.3 Dephosphorylation of DNA ends

DNA plasmids were incubated with 1U of FastAP Thermosensitive Alkaline Phosphatase within the restriction enzyme digestion mix in order to release 5' and 3' phosphate groups from the cleaved DNA ends, thereby preventing re-annealing of the plasmid backbone during ligation reactions. The reaction was incubated for 30 minutes at 37°C.

2.2.4 DNA ligation reaction

Digested plasmids (50ng) or phosphorylated sgRNA oligos (100µM) were ligated to insert DNA at 1:1 molar ratio using 1µL of T4 DNA ligase and 2µL of T4 DNA Ligase Buffer (10X) to a final volume of 20µL. Where both the plasmid backbone and insert have complimentary overhangs, reactions were incubated at room temperature (RT) for 15 minutes. Blunt end ligations were allowed to incubate for 1 hour at RT or 16^{o}C overnight. The ligated product was transformed into competent cells.

2.2.5 Polymerase chain reaction

To amplify specific sequences of DNA upon cloning of plasmids and/or to assess CRISPR/Cas9/Cytidine base editing correction in cells of my study, PCR technique was used. Q5® High-Fidelity DNA Polymerase master mix (New England, BioLabs) was used for all reactions, and PCRs were setup in accordance with manufactures

instructions. A Mastercycler® nexus X2 (Eppendorf, Hamburg, Germany) thermocycler was used for these reactions. The annealing temperature of every primer was optimised by setting gradient PCRs ranging between 58-68°C. Extension time was set at 30 seconds/kilobase (kb) for the first 5kb, and 1 minute for every additional kb.

2.2.6 Primer design

For all the primers used in this thesis, the following tools have been used:

SnapGene® v3.1.4 and **Benchling** were used for primer design.

NCBI Primer-Blast: was used to assess specificity of primer pairs and to avoid background amplifications when using genomic DNA as PCR template (https://www.ncbi.nlm.nih.gov/tools/primer-blast/).

2.2.7 Site-Directed Mutagenesis

QuikChange Lightning Multi Site-Directed Mutagenesis kit (Agilent):

Commercial kit designed to make up to five different nucleotide changes at multiple sites simultaneously. Mutagenic primers were designed using the QuikChange primer design online tool (https://www.agilent.com/store/primerDesignProgram.jsp).

A PCR reaction was set up according the user manual using 100ng of template DNA and a set of complementary primers in forward and reverse orientation (primers detailed in ***Table 2.11***). Reactions were carried out in the Mastercycler® nexus X2 PCR machine, using the appropriate cycling parameters. 1µl of *DpnI* was added to digest the parental circular DNA plasmid by incubation 1 hour at 37°C prior to bacterial transformation with 50µl of chemically competent cells and 2µl of the mutant strand synthesis reaction.

Large insertion/ deletion:

In order to remove large sections of DNA, a set of primers oriented in the opposite directions were designed according to the NEB base changer online tool

(http://nebasechanger.neb.com/). Amplification of blunt ended linearized plasmid sequence was performed using Q5® high-fidelity DNA polymerase (New England Biolabs) starting with 1ng of template plasmid DNA. The linearized PCR product was run on an agarose gel with SYBR™ safe DNA stain (ThermoFisher Scientific) to confirm the size and the lack of non-specific PCR amplified products. Gel extraction of the PCR product was performed using QIAquick gel extraction kit (QIAGEN, Hilden, Germany) and further PCR purified by QIAquick PCR purification kit (QIAGEN, Hilden, Germany).

50ng of the Purified DNA was phosphorylated by T4 Polynucleotide Kinase (NEB, Massachusetts, USA)
T4 Polynucleotide Kinase reaction:

- 50ng Purified DNA
- 0.5µl T4 Polynucleotide kinase enzyme (NEW ENGLAND Biolabs)
- 1µl T4 DNA Ligase Buffer (10X, ThermoFisher Scientific)
- Up to 10µl with dH_2O

Reactions were carried out in the Mastercycler® nexus X2, at 37°C for 30 minutes, before inactivation of the enzyme at 65°C for 20 minutes. Subsequently, T4 Polynucleotide Kinase reaction was allowed to reach RT before setting up a T4 DNA Ligation reaction:

- 10µl T4 Polynucleotide Kinase reaction
- 2µl T4 DNA Ligase Buffer (10X, ThermoFisher Scientific)
- 2µl T4 DNA Ligase enzyme (ThermoFisher Scientific)
- Up to 20µl with dH_2O

These reactions were incubated for 20 minutes at RT, before transformation in chemically competent cells.

2.2.8 Genomic DNA Extraction

Individual cell pellets from $1x10^5$ -$1x10^6$ were processed using the QIAGEN DNA kit according to manufacturer's instruction. Cells were suspended in Phosphate-buffered saline (PBS) and lysed with the addition of proteinase K and buffer AL at

56°C for 10 minutes. Extracted DNA was precipitated with 100% ethanol and collected using silica resin columns according to the manufacturer's instructions and eluted in a final volume of 30µl to 60µl with DNAse-free H_2O.

2.2.9 Total RNA extraction

Total RNA extraction was performed using the RNeasy min kit (QIAGEN) according to manufacturer's protocols. Around $5x10^5$ cells per sample were lysed with 350µL activated Buffer RLT and cellular RNAses were irreversibly denatured by adding β-mercaptoethanol in the cell lysis. The homogenized cell lysate was collected pipetted into a QIAshredder spin column at ≥8000g for 2 minutes. An equal volumes of 70% ethanol were added to the homogenized lysates and samples were processed using RNeasy spin column and spin at ≥8000g for 2 minutes. Removal of any contaminating genomic DNA was performed by a 700µl wash of buffer RW1. Two additional wash steps were then performed with 500µl of RPE buffer for 30 seconds and 2 minutes, respectively at ≥8000g. Total RNA was eluted in 20µl of RNase-free water. If not used, total RNA was stored at -80°C.

2.2.10 First-strand cDNA synthesis

1µL of total RNA was used for retro-transcription of the first cDNA using High-Capacity cDNA Reverse Transcription Kit (Thermofisher) according to manufacturer's instructions:

- 10X RT Buffer: 2.0µL
- 25X dNTP Mix (100 mM) 0.8µL
- 10X RT Random Primers: 2.0µL
- MultiScribe™ Reverse Transcriptase: 1.0µL
- RNase Inhibitor: 1.0µL
- Nuclease-free H_2O: up to 20µL

Reactions were carried out in the Mastercycler® nexus X2, at 25°C for 10 minutes and 37°C for 120 minutes before inactivation of the enzyme at 85°C for 5 minutes.

2.2.11 Agarose gel electrophoresis

UltraPure agarose was dissolved at concentration of 1% - 2% with 1X TAE and allowed to cool before adding 1% SyBR safe (Thermofisher). The agarose was cast in gel trays and allowed to set. DNA/cDNA samples were loaded with the addition of a 10X loading dye and a 1kb Plus DNA ladder was run alongside as a size reference. Electrophoresis was carried out at 80–110 V and gels were visualised under ultraviolet light using a NuGenius (Syngene, Cambridge, England) gel documentation system.

2.2.12 Agarose gel purification of digested DNA fragments

PCR bands or digested DNA fragments were separated by gel electrophoresis on a 0.8-1% 1X TAE agarose gel and exposed to UV light. The desired DNA fragments were excised using a sterile scalpel and gel slices of up to 400mg and purified using the QIAquick Gel Extraction Kit according to the manufacturer's instructions and eluted in 20µl of dH2O.

2.2.13 Lentiviral vector

2.2.13.1 Vector Production

Lentiviral vectors were produced by transient transfection of 22–30x10^6 HEK-293T cells seeded in T175 cm^2 flasks with third generation transfer plasmids and packaging/accessory plasmids developed by Dr. Trono`s lab and manufactured from PlasmidFactory (Bielefeld, Germany) at 1µg/µl, in 0.1 x TE buffer (Dull et al. 1998) (see table 2.11). Second generation lentiviral vector production relied on two packaging plasmids, pCMVR8.74 (Addgene #22036) comprising the viral gag-pol, tat, and rev, as well as pMDG2 (Addgene #12259) expressing the vesicular stomatitis virus-G (VSV-G) envelope. In a third generation packing system, the nuclear exporter rev signal is expressed from a separate plasmid (pRSV-Rev, Addgene #12253). Additionally, tat expression has been removed entirely from the gag-pol expressing plasmid (pMDLg/pRRE, Addgene #12251). The same VSV-G envelope was used for both second and third generation vectors (pMDG2, Addgene #12259). Transfection of these plasmids was done using 1x10^7 mol/L of polyethylenimine (PEI) in reduced

serum Opti-MEM. DNA-PEI mix was incubated for 20 minutes at room temperature and added to the cells. Flasks were washed with Opti-MEM to remove residual serum and then incubated with the transfection mix for 6 hours at 37°C, after which the transfection mix was replaced with fresh DMEM supplemented with 10% Foetal Bovine Serum (FBS). Media containing lentiviral particles was harvested at 48 hours post transfection and passed through a 0.45µm pore sterile filter. The viral supernatant was then concentrated by ultracentrifugation in a Sorvall Discovery SE or a Beckman Coulter LE-80 for 2 hours at 100,000g. Virus was resuspended in reduced serum Opti-MEM and incubated on ice for 1 hour. Virus was aliquoted and stored at -80°C for further use.

2.2.13.2 Vector titration

HEK-293Ts were seed at $1x10^5$ in a 24-well plate in DMEM/10%FBS and allowed to attach overnight. The following day, concentrated viral stocks were serially diluted 5-fold for 5 times (10, 2, 0.4, 0.08, 0.016, and 0.0032) and used to transduce cells in a minimal culture volume of 1ml DMEM/10% FCS and incubated for 72 hours. Cells were then harvested for quantification of the viral titre by qPCR, flow cytometry or by detection of the viral p24 particle by ELISA.

2.2.13.3 Lentiviral vector titration by flow cytometry – Detection of GFP

Transduced cells were harvested 3 days post-transduction, collected in FACS tubes and washed once in PBS buffer supplemented with 2% FBS. The percentage of GFP+ cells and their relative expression were detected by flow cytometry using the CyAn™ ADP Analyzer (Beckman Coulter, High Wycombe, UK). Forward and side scatter were used to exclude debris and aggregates whereas combination of side scatter and pulse with was used to include only single cells. Once eGFP fluorescence was measured, viral titre was calculated off dilutions resulting in 1-10% of transgene expression to ensure 1 viral copy per cell. The titre was calculated using the formula:

$$TUs/\,per\,ml = [(\%\,transgene\,positive - background)\,x\,1000)]\,x\,(1000 / lentiviral\,vector\,volume).$$

2.2.13.4 Titration of non-integrating lentiviral vector by p24 - ELISA

The HIV-1 p24 antigen was analysed by ELISA to assess the physical HIV-1 titre of the NILVs. Viruses were diluted 1:1x10^5 and 1:1x10^6 fold in Opti-MEM and the ELISA was performed according to manufacturer's instructions (ZeptoMetrix, New York, USA). Analysis for each dilution was made in duplicate. A standard curve with serial dilutions of p24 antigen was made for quantification. The plate was read at 450 nm using a FLUOstar OPTIMA (BMGLabtech, Offenburg, Germany). A physical titre was derived using the following conversion factor: 1): (2x10^3molecules) x (24x10^3 Da of p24 per Physical Particle (PP)) = 48x106 2): 48x106 /Avogadro's constant = (48x106) / (6x1023) = 8x10^{-17} g of p24 per PP 3): There is approximately 1 PP per1x10^{-16} g of p24 4):1x10^4 PP per pg of p24 v. 100 Transducing Units (TU) per 1000 PP.

2.2.13.5 Titration of integrating lentiviral vector by quantitative PCR (qPCR)

Genomic DNA of lentivirally transduced cells was extracted with DNeasy Blood and Tissue Kit (QIAGEN). For each sample, 250ng of DNA, 0.1mM (0,25µl) of each Psi and Albumin forward and reverse primers (Eurofins), 0.1mM (0.25µl) fluorescently labelled probes (Applied Biosystems) and 1X of qPCR mastermix (12,5µl) in a 25µl reaction volume. The reaction was run for 1 cycle at 50°C for 2 minutes, 1 cycle at 95°C for 10 minutes, 40 cycles at 95°C for 15 seconds and 60°C for 1 minutes on CFX96 TouchTM Real Time PCR Detection system (BioRad). Integrated copy number was calculated with the aid of standard curves generated using serially diluted plasmid encoding both viral packaging Psi and endogenous housekeeping Albumin sequences by dividing the mean quantity value of the psi by the mean value of the housekeeping gene.

2.2.14 Cell culture

2.2.14.1 Isolation and culture of primary fibroblasts and keratinocytes

Primary human fibroblasts and keratinocytes were obtained from skin biopsies of the RDEB patient and healthy control subjects with authorisation from the National Research Ethics Services, Westminster (07/H0802/104) and with written informed consent from patients. The RDEB patient bears a homozygous splice-site c.425A>G

mutation in exon 3 of *COL7A1*. Fibroblasts and keratinocytes were isolated by Dr Anastasia Petrova. Fibroblasts were grown in DMEM supplemented with 10% FBS and 1% penicillin-streptomycin. Primary keratinocytes were plated on lethally irradiated 3T3 cells and cultured in DMEM and Ham's F12 medium (2:1 mixture) supplemented with irradiated fetal bovine serum (10%), insulin (5 µg/mL), adenine (0.18 mM), hydrocortisone (0.4µg/mL), cholera toxin (0.1 nM), triiodothyronine (2 nM), glutamine (4 mM), epidermal growth factor (10 ng/mL), and penicillin–streptomycin (50 IU/mL). Subculture of primary fibroblasts and keratinocytes were performed using 0.05 % and 0.25%, respectively, at 37°C, 5% CO_2. Identification of the c.425A>G point mutation was performed by PCR using primers *COL7A1*-FWD/Ex5-*COL7A1*-REV described in ***Table 2.12***.

2.2.14.2 Reprograming of primary fibroblasts to iPSCs

Patient and wild-type iPSC lines were generated using the CytoTune™-iPS 2.0 Sendai Reprogramming Kit (ThermoFisher Scientific, Massachusetts, USA) under feeder free conditions. To generate iPSCs from fibroblasts, cells were seeded at concentration of 3×10^5 into 2x6-well plates until 60% confluence prior to transduction, and grown in DMEM (Gibco) supplemented with 10% FBS and 1% penicillin-streptomycin (fibroblasts medium). On day 0, fibroblast cells were transduced with three reprogramming Sendai vectors carrying the four Yamanaka factors, Oct, Sox2, Klf4, and c-Myc, provided within the kit at the requested multiplicity of infection (MOI) (vectors composition and MOI described in **Table 2.17**). Fresh media was replaced the following day (day 1) and cells were kept in culture until day 7. On day 7, transduced cells were trypsinized with 0.05% Trypsin-EDTA, washed once with PBS, and seeded on human recombinant truncated vitronectin (VTN-N) coating dishes (5µg) and cultured in fibroblasts medium for 24 hours. The following day (day 8), media was replaced with iPSCs medium mTeSR™1 (STEMCELL Technologies, Vancouver, Canada) and refreshed every 2 days. Around day 12, small colonies were observed and cultured until maturation (3 weeks). 4 weeks post transduction, colony picking of mature iPSCs colonies was performed and cells were further cultured on vitronectin-coated plates with mTeSR™1.

Table 2.16 List of Sendai-vectors for iPSCs reprogramming

CytoTune™ Sendai vector	Factors	MOI
CytoTune™ 2.0 KOS	Human KLF4 (K) Human Oct3/4 (O) Human SOX2 (S)	5
CytoTune™ 2.0 hC-MYC	Human c-MYC	5
CytoTune™ 2.0 hKLF4	Human KLF4	3

2.2.14.3 Culture and maintenance of iPSCs

iPSCs culture was performed using either TeSR-E8 8 or TesR™2 (STEMCELL Technologies). For passaging, a split ratio 1:6 was routinely used using Gentle Cell Dissociation Buffer (GCDR). Before passaging, cells were washed once with PBS and then incubated with 1mL of GCDR for 7 minutes at room temperature followed by aspiration and addition of fresh medium. Cell scraping was done manually using a 1.9cm wide cell-lifter in 1mL of iPSCs medium and clumps were immediately seeded without the need of further pipetting. Disaggregated colonies were transferred immediately to coated plates. Two different protein matrices, laminin-511 E8 fragments (iMatrix-511) (2.4µg/mL) and human recombinant truncated vitronectin (10µg/mL) were used to seed cells. Plates coated with vitronectin were kept at RT for at least 1 hour before use. For iMatrix, laminin-511 was added directly to harvested iPSCs clumps before plating.

2.2.14.4 HaCaT cell line

HaCaT cells (ATCC® PCS-200-011™) were cultured in DMEM containing 10% FBS and 1% penicillin–streptomycin. Subculture was performed using 0.25% Trypsin-EDTA

2.2.14.5 Freezing and recovery of cells

Cell were cryopreserved in 800µL aliquots (cell lines: 2 x10^6, primary cells: 1-2x10^6) in either cell line or primary cell freezing mix.

For iPSCs, cells were resuspended upon dissociation in either TeSR-E8 medium and collected by centrifugation for 3 minutes at 130g. The cell pellets of approximately 2 x10^6 cells were resuspended in 800µL of cold freezing serum-free cryopreservation medium designed for the cryopreservation of pluripotent stem cells, mFreSR™ (STEMCELL Technologies) to individual cryovials.

For HaCaT cell line and primary keratinocytes and fibroblasts, the pellet was obtained by centrifugation at 350g for 5 minutes and resuspended in the appropriate volume of cold freezing media containing 90% FBS + 10% Dimethyl Sulfoxide ($DMSO_4$) to obtain a final concentration of $1x10^6$ cells/mL and 1 mL volumes were transferred to individual cryovials.

Cryovials were wrapped in 3 layers of paper tissue and stored for 24 hours at -80°C and then transferred to a liquid nitrogen tank for long-term storage. Cells were recovered from liquid nitrogen by thawing the cryovials in a 37°C water bath before transferring them to a 15mL falcon tube containing pre-warmed TesR™2 with 10µM of Y-27632 dihydrochloride or DMEM 10%/FBS for iPSCs and HaCaTs, respectively. The suspension was centrifuged at 130g (iPSCs) or 350g (HaCaTs) for 3 minutes and the pellet was resuspended in appropriate media. For iPSCs, 10µM of Y-27632 was added to the medium to improve cell viability upon thawing and culture dishes were pre-coated as described in section 2.2.14.3.

2.2.14.6 Single cell isolation by limiting dilution

To obtain single cell clones, bulk iPSCs were serially diluted to a concentration of 0.3-0.5 cells/100µl in medium containing 1:1 fresh and conditioned TesR™2 media supplemented with 10µM of Y-27632 and seeded in multiple 96-well plates coated with iMatrix-511 at a concentration of 2.4µg/mL.

2.2.15 In vitro trilineage differentiation of iPSCs

iPSCs were cultivated and expanded in TesR™2 and laminin-511-coated plates at a concentration of 2.4µg/mL until reaching 80% confluence. To make embryoid bodies, undifferentiated cells were dissociated as single cell (day 0) with Accutase for 8 minutes at 37°C and seeded at high density in AggreWell™800. Cells were resuspended in EB formation medium (STEMCELLS technologies) supplemented with 10µM of HA-100 (STEMCELLS technologies) for 1 week (Day 7). iPSC aggregates were then transferred on Matrigel®-coated plates with coverslips and cultured in DMEM 10% FBS for 3 weeks. After differentiation, cells were fixed in PFA 4% and analyzed by immunofluorescence for the expression of mesoderm, endoderm and ectoderm markers.

2.2.16 CRISPR single guide RNA design

All guide RNAs (sgRNAs) compatible with either SpCas9 or BE3 reported in table 2.15 were designed using the online Benchling CRISPR design tool (https://benchling.com/crispr). For each potential sgRNA designed, Benchling assigns an *in silico* on- and off-target CRISPR cutting score. The on-target evaluation is scored based on the algorithm developed by Doench, Fusi *et al.* (Doench et al., 2016) which takes into account the position of the predicted cut site within the translated gene sequence and provides a score from 0–100 (higher scores indicate better predicted on-target activity). The off-target score is evaluated according to the number of mismatches between the selected sgRNA and similar exonic off-target site (Hsu et al. 2013). The score for *in silico* off-targets is deducted from an initial score of 100 and higher scores mean lower off-target activity.

For cytidine base editing C>T predictions, the Benchling scores *in silico* on-targets base editing using a first generation base editor (Komor et al., 2016), while off-target score is based on work by Hsu and colleagues (Hsu et al., 2013).

2.2.17 Electroporation

Neon transfection system (ThermoFisher Scientific): For all electroporation in keratinocyte cell line, the Neon™ Transfection System, with the 100µl tip kit (ThermoFisher) was used. Cells were electroporated at concentration of $1x10^6$ cells/ mL in buffer R, with the following electroporation parameters: 1600v/20ms/1 pulse. The application of this device has been indicated in the results section.

4D-Nucleofector™ X Unit (Lonza): This device was primarily used for iPSCs using the 100µl cuvettes. Cells were electroporated at concentrations of $1x10^6$ cells/mL in buffer P3, using the program CA137. The applications of this device have been indicated in the results section.

After electroporation cells were placed in pre-warmed plate and incubated at 30°C, 5% CO_2 overnight. Cells were then restored to normal culture conditions (37°C, 5% CO_2), the next day.

2.2.18 Sanger sequencing detection of in situ CRISPR/Cas9-mediated HDR, and targeted Cytidine deamination events

Genomic DNA extraction was performed using DNeasy Blood and Tissue Kit (QIAGEN) and ~100ng of genomic DNA was used as template for PCR with Q5® high-fidelity DNA polymerase to amplify 400-800bp over the protospacer binding site or SpCas9 cutting site. Around 5µL of PCR amplicons were visualized by gel electrophoresis on 1% agarose prior PCR purification by QIAGEN PCR purification kit. To determine the DNA sequence, PCR amplicons were sent to Eurofins Genomics for Sanger sequencing. Resulting Sanger sequencing data was analysed using either Tide (https://tide.nki.nl/) or Synthego ICE (https://ice.synthego.com/#/) online tools, to measure the frequency of InDels, at the predicted SpCas9 scission site or donor template integration. When analysing C>T conversion rates produced by cytidine deaminase base editing technologies, EDITR software was used (https://moriaritylab.shinyapps.io/editr_v10/).

2.2.19 Next generation sequencing (NGS) of HDR and C>T events

Genomic DNA extraction was performed using DNeasy Blood and Tissue Kit and a PCR was designed to amplify the edit loci over the protospacer binding site or Cas9 cutting site the predicted donor template. Reactions used Q5® High-Fidelity DNA Polymerase. PCR products were confirmed by 1% agarose gel electrophoresis, sequenced and analysed using ICE protocols. Next generation sequencing was performed by Dr. Athina Gkazi using primers detailed in **Table 2.13**.

Sequencing libraries were generated according to the Nextera XT DNA Library Prep Kit Reference Guide (https://emea.support.illumina.com/content/dam/illumina-support/documents/documentation/chemistry_documentation/samplepreps_nextera/nextera-xt/nextera-xt-library-prep-reference-guide-15031942-05.pdf). Libraries were then pooled and 12pM of each pooled sample was loaded on MiSeq (Illumina). A bioinformatics workflow using UseGalxy tools (https://usegalaxy.org/) was developed in house to analyse the NGS data to determine HDR and base editing frequencies. Quality reads check was assessed by FastQC. Reads were then trimmed by Trim Galore to remove Nextera/NGS adapters. The remaining reads were then

aligned to a reference genome with BWA-MEM. Quality control of reads paired with the reference genome was assessed by Flagstat. For the detection of gene and base editing, the following programs were employed:

1) **Pindel** was used to evaluate homology-directed repair (HDR) efficiency and to quantify percentages of InDels within the same read. The obtained files from the alignment were visualised on IGV genome browser and any further investigation was done in Microsoft Excel (initial analysis) and R (plots) using the csv files from Pindel.

2) **Naïve variant caller (NVC)** was used to quantify the percentage of nucleotide variation at each nucleotide position within the same read upon base editing. The obtained files from the alignment were visualised on IGV genome browser and any further analysis was done in Microsoft Excel.

For haplotype-based variant detection, raw MiSeq data were analysed by a javaScript-based instant assessment tool for high-throughput sequencing data for genome edited cells CRISPResso2 (https://crispresso.pinellolab.partners.org/submission) (Clement et al., 2019).

2.2.20 Direct differentiation of iPSCs into keratinocytes (iKer)

2.2.20.1 Protocol 1

The first protocol used for generation of iPSC-derived keratinocytes (iKer) was developed by Prof. Angela M. Christiano's group (Umegaki-arao et al., 2014; Shinkuma et al.,2016; Jackόw et al., 2019). The outline of the differentiation protocol is schematically represented in **Figure 4.12**. iPSCs were subcultured as clumps of ~10-20 cells onto vitronectin-coated plates with daily media change with TesR-E8. Upon reaching 40% confluence, iPSCs colonies were incubated in TeSR-E8 medium supplemented with 1µM of retinoic acid (RA) and 10ng/mL of BMP-4, for 7 days with daily media change. At day 7, the medium was switched to Defined Keratinocyte

Serum-Free Medium (DKSFM, Thermofisher) without RA and BMP-4 supplements for about 60 days without cell passaging and with media change every 2 days.

2.2.20.2 Protocol 2

A second protocol for keratinocyte differentiation used in this study was developed in collaboration with Prof. Dusko Ilic. Schematic of the protocol is represented in **Figure 4.14**. Prior to differentiation, iPSCs were cultivated and expanded in TesR™2 and laminin-511-coated plates at a concentration of 2.4µg/mL. Cells were cultivated in TesR™2 until reaching 80% confluence. On day 0, undifferentiated cells were dissociated as single cell with accutase for 8 minutes at 37°C in order to obtain 28-33 $x10^6$ cells. To make embryoid bodies of ~3000 cells size, cells were resuspended in EB formation medium (STEMCELLS technologies) supplemented with 10µM of HA-100 (STEMCELLS technologies) and plated at a concentration of ~5.6 $x10^6$ cells/well in a 6 well plate of AggreWell™800 according to manufacturer's instructions. Plates were incubated at 37 °C, 5%CO_2 and 5%O_2 for 24 hours. After 24 hours in suspension culture (Day 1), uniform iPSC aggregates were visible under inverted phase-contrast microscope and cells were supplemented with fresh initiation medium (KDM1) with daily media change up to day 3 and incubated at 37 °C, 5%CO_2 and 5%O_2. Composition of every media used in this protocol is showed in **table 2.18**. On day 4, EBs were collected, dissociated as single cells with Accutase for 10 minutes at 37 °C, plated onto vitronectin-coated flasks (10µg/mL) at a concentration of 10,000 cells per cm^2 in KDM2 medium for 3 further days. On day 7, niacinamide at final concentration of 3000µM was added to the KDM2 medium (KDM3) and cells were left in culture for 3 days without additional media change. From day 10 of differentiation, SB431542 inhibitor (10µM) was added to the KDM3 medium to form KDM4. Epithelial-like progenitors were cultivated for 4 days in KDM4 with media change every 48 hours. Fist passage of iPSCs-derived keratinocytes on day 15 was done by incubating cells in 0.1% Trypsin for 6-10 minutes at 37 °C. Trypsinization was blocked with equal volume of defined trypsin inhibitor (DTI) and cells were spun down for 5 minutes at 400g. The cell pellets were resuspended in KDM5 medium (**Table 2.18**) and seeded onto laminin-511-coated flasks (1µl/mL) with media change every 3 days. From day 15 onwards, iPSCs-derived keratinocytes were passaged at concentration of 20,000

cells/cm^2 in KDM5 medium onto laminin-511-coated flasks (1µl/mL) with media change every 3 days until reaching 80% confluence.

Table 2.17 Keratinocyte defined media composition

Keratinocyte defined media 1 KDM1			
Reagents	**Stock Solutions (mg/mL)**	**Stock Molarity (µM)**	**Final Molarity (µM)**
Cholera Toxin (1/10 dilution)	0.5 mg in 0.5 mL of H_20	11.905 µM	0.0001 µM
AA2P (P-Vitamin C)	300 mg in 10 mL of H_2O	93168 µM	174 µM
EGF	0.2 mg in 2 mL of 0.001M CH_3COOH	15.6 µM	0.0156 µM
FGF1	0.025 mg in 250 µL of 0.1% BSA	6.33 µM	0.000316 µM
IGF1	0.2 mg in 1 mL of 0.1% BSA	26.13 µM	0.00131 µM
Niacinamide	1 g in 10 mL of H2O	819672 µM	3000 µM
Keratinocyte defined media 2 KDM2			
Reagents	**Stock Solutions (mg/mL)**	**Stock Molarity (µM)**	**Final Molarity (µM)**
Cholera Toxin (1/10 dilution)	0.5 mg in 0.5 mL of H_20	11.905 µM	0.0001 µM
AA2P (P-Vitamin C)	300 mg in 10 mL of H_2O	93168 µM	174 µM
EGF	0.2 mg in 2 mL of 0.001M CH_3COOH	15.6 µM	0.0156 µM
FGF1	0.025 mg in 250 µL of 0.1% BSA	6.33 µM	0.000316 µM
IGF1	0.2 mg in 1 mL of 0.1% BSA	26.13 µM	0.00131 µM
Keratinocyte defined media 3 KDM3			
Reagents	**Stock Solutions (mg/mL)**	**Stock Molarity (µM)**	**Final Molarity (µM)**
Cholera Toxin (1/10 dilution)	0.5 mg in 0.5 mL of H_20	11.905 µM	0.0001 µM
AA2P (P-Vitamin C)	300 mg in 10 mL of H_2O	93168 µM	174 µM
EGF	0.2 mg in 2 mL of 0.001M CH_3COOH	15.6 µM	0.0156 µM
FGF1	0.025 mg in 250 µL of 0.1% BSA	6.33 µM	0.000316 µM
IGF1	0.2 mg in 1 mL of 0.1% BSA	26.13 µM	0.00131 µM

Niacinamide	1 g in 10 mL of H2O	819672 µM	3000 µM
Keratinocyte defined media 4 KDM4			
Reagents	**Stock Solutions (mg/mL)**	**Stock Molarity (µM)**	**Final Molarity (µM)**
Cholera Toxin (1/10 dilution)	0.5 mg in 0.5 mL of H_20	11.905 µM	0.0001 µM
AA2P (P-Vitamin C)	300 mg in 10 mL of H_2O	93168 µM	174 µM
EGF	0.2 mg in 2 mL of 0.001M CH_3COOH	15.6 µM	0.0156 µM
FGF1	0.025 mg in 250 µL of 0.1% BSA	6.33 µM	0.000316 µM
IGF1	0.2 mg in 1 mL of 0.1% BSA	26.13 µM	0.00131 µM
Niacinamide	1 g in 10 mL of H2O	819672 µM	3000 µM
SB431542	3.84 mg in 1 mLof DMSO	10000 µM	10 µM
Keratinocyte defined media 5 KDM5			
Reagents	**Stock Solutions (mg/mL)**	**Stock Molarity (µM)**	**Final Molarity (µM)**
AA2P (P-Vitamin C)	300 mg in 10 mL of H_2O	93168 µM	5.8333 µM
Cholera Toxin (1/10 dilution)	0.5 mg in 0.5 mL of H_20	11.905 µM	0.0001 µM
BMP4 (1/10 dilution)	0.01 mg in 0.4 mL of 0.004 M HCl	0.735 µM	0.000015 µM
EGF	0.2 mg in 2 mL of 0.001M CH_3COOH	15.6 µM	0.00156 µM
FGF1	0.025 mg in 250 µL of 0.1% BSA	6.33 µM	0.000316 µM
IGF1	0.2 mg in 1 mL of 0.1% BSA	26.13 µM	0.00131 µM
Niacinamide	1 g in 10 mL of H2O	819672 µM	3000 µM
SB431542	3.84 mg in 1 mL of DMSO	10000 µM	10 µM

2.2.21 Protein detection

2.2.21.1 Flow cytometry

Generally between 0.1 - 1x10^6 cells were used for flow based phenotyping. All wash and staining steps occurred in FACS buffer (PBS with 2% FCS). Cell acquisition was carried out on a 2-laser CyAn™ ADP Analyzer. Conjugated antibodies listed in **Table**

2.1.7 were used for extracellular staining following incubation at 4°C form 20 minutes. For intracellular staining, cells were fixed in Fix & Perm® Medium A (ThermoFisher) for 20 minutes at room temperature in the dark. The cells were then washed with 2% FBS/PBS, spun down at 400g for 5 minutes at RT. The cell pellets were resuspended in Fix & Perm® Medium B with the antibody of interest at 4°C for 1 hour in the dark. The cells were them washed with 2% FBS/PBS and pelleted at 400g for 5 minutes. In case of non-conjugated antibody, cell pellets were resuspended in Fix & Perm® Medium B with secondary antibody and incubated at 4°C for 30 minutes in the dark. The cells were washed with 2% FBS/PBS, resuspended in 0.5ml 2% FBS/PBS for the analysis.

2.2.21.2 *In situ* immunostaining

Generally between 0.2-0.5- $1x10^6$ cells were seeded onto sterile 13mm coverslips in a 24 well plate, cultured for 48 hours then fixed in 4% paraformaldehyde for 15 minutes at RT and washed three times with 1x PBS. Cells were simultaneously blocked and permeabilized with 0.1% Triton X-100 3% BSA in PBS for 30 minutes at RT, and then incubated overnight at 4°C with the primary antibody (see table 2.2.7). After three washes with PBS, cells were incubated with secondary antibody at the concentration listed in table 2.2.7 in PBS for 1 hour at RT in the dark, washed with PBS and counterstained with DAPI (4',6-Diamidino-2-Phenylindole) for 5 minutes at RT in the dark. The coverslips were mounted on glass microscope glass with Prolong gold. Micrographs were imaged using a Zeiss observer 7 (Zeiss, Oberkochen, Germany) and processed using Image J (Wayne Rasband (NIH)).

2.2.21.3 SDS-PAGE immunoblotting

$1x10^6$ cells were harvested and cell pellets were resuspended in cell lysis buffer for total protein isolation. The lysis buffer was prepared as follows: 50mM Tris/HCL, pH 8.0, 150mM NaCl, 5mM EDTA, 1:25 dilution of stock cocktail protease inhibitor (complete cocktail tablets) and 1mM PMSF. As C7 is a secreted protein, culture media was also harvested prior 48 hours cultivation in serum-free medium with the supplementation of 50µg/mL of ascorbic acid for to promote C7 secretion (Titeux et al. 2010). The total protein concentration was determined using a Bio-Rad protein

assay kit (BIO-RAD, Hertfordshire, UK). A standard curve was formulated using 40µg/ml of BSA serially diluted 2-fold to 2.5 µg/ml. BCA reagent was added at a 1:5 concentration to all samples and 96 absorbance was at an OD 595 nm. Equal quantities (30µg) of total protein were resuspended in 5X sample buffer (10% SDS, 30% Glycerol, 10% β-mercaptoethanol, 0.001% bromophenol blue, 1M DTT) and loaded on a 6% sodium dodecyl sulphate polyacrylamide separating SDS-PAGE gel. After electrophoresis, proteins were transferred to polyvinylidene fluoride membranes (PVDF), blocked with 5% milk in 0.05% Tween-20 in 1X PBS and incubated with anti-C7 antibody (gift from Prof. M. Chen) at a 1:2500 dilution overnight at 4°C or anti-vinculin mAb (cl.V284, Sigma-Aldrich, Dorset, UK) at a 1:250,000 for 1 hour at RT with shaking, followed by incubation with secondary antibodies (anti-Rabbit RG-96 IgG, and anti-Mouse IgG, respectively) conjugated with HRP (both at 1:4000 dilution, from Sigma-Aldrich). Signal detection was performed using the ECLplus system (GE Healthcare, Hatfield, UK).

2.2.22 Statistics

All statistical analysis was performed using GraphPad Prism software version 8.0.0. Details of analysis preformed can be found in the relevant figure legends.

Chapter 3 Investigation of genome editing tools for efficient targeting of *COL7A1* mutation hotspot

3.1 Background

Application of CRISPR/Cas9 technology for *ex vivo* skin gene-editing approaches opens the possibility of site-specific correction of the mutant *COL7A1* alleles under endogenous promoter (**Section 1.9**). *In situ* integration of donor template by HDR following CRISPR/Cas9-induced DSBs can overcome various limitations associated with retroviral and lentiviral vectors used in conventional gene therapy (Naso and Petrova, 2019). To date, the majority of Cas9-mediated correction by donor template delivered via viral vectors (such as NILV and AAV) or plasmid DNA relied on an extensive clonal isolation of *COL7A1*-corrected cells due to limited HDR efficiency in primary RDEB cells (Chamorro et al., 2016; Kocher et al., 2019). Such selection increases the risk of cellular senescence and can lead to the loss of keratinocyte stem cells, which are crucial for successful long-term skin regeneration.

On the other hand, high levels of donor integration could guarantee modest recovery of C7 in the gene edited cell pool, hence avoiding the need for single clonal selection upon HDR (Bonafont et al., 2021; Izmiryan et al., 2018). To achieve this, optimizations of all the components of CRISPR/Cas9 system, including delivery (viral and non-viral) and format (DNA-encoded, mRNA or protein) are required. The choice of delivery strategy and format of the reagents often has to be tailored to cell type and experimental design.

For skin disorders, such as RDEB, non-integrating lentiviral vectors (NILV) and adeno-associated virus have previously been used to deliver gene editing tools (Meganucleases, TALENs and CRISPR/Cas9) or donor templates for HDR strategies due to their high infection efficiency, tropisms, mild immunogenicity, large packaging capacity and stable expression following integration of viral DNA into the host genome (Chamorro et al., 2016; Izmiryan et al., 2018; Izmiryan et al., 2016; Georgiadis 2016; Benati et al., 2018). Prolonged expression of the endonuclease, however, raises

concerns surrounding off-target cleavage and activation of host immunity, thereby hampering clinical translation of NILV-based strategies (Kim et al., 2014; Crudele and Chamberlain 2018; Charlesworth et al., 2019). More recently, viral-free, transient delivery of CRISPR/Cas9 components by co-electroporation of a sgRNA coupled with SpCas9 as either mRNA or RNP, has been investigated and can circumvent concerns related to viral-based delivery, offering a more clinically relevant strategy (Liu et al., 2015; Kim et al., 2014; Hendel et al., 2015).

It is also important to note that the mode of donor template delivery and design have rapidly evolved in the last few years. For example, donor template delivery via single-stranded oligo DNA was very recently shown to mediate efficient HDR repair, while also allowing for the increased precision, lower toxicity and avoidance of viral vectors requirement (Guo et al., 2018; Kwart et al., 2017; Paquet et al., 2016; Martin et al., 2019; Yang et al., 2013; Roth et al., 2018).

3.2 Hypothesis

The development for a robust and selection-free CRISPR/Cas9 mediated gene-editing approach to correct a recessive splice site mutation hotspot (c.425A>G, p.K142R) within exon 3 of *COL7A1* could be achieved towards the investigation and optimization of CRISPR/Cas9 reagents delivery and rational design of donor templates for HDR-mediated correction.

3.3 Aims

1) To investigate targeting efficiency of the *COL7A1* locus by testing CRISPR/Cas9 delivery via either ribonucleoprotein complex (RNP) or chemically modified guide RNAs (sgRNA) with SpCas9 mRNA. This will be achieved by:

    a) Design sgRNAs targeting c.425A>G mutation within *COL7A1*. Evaluate the efficiency of the designed sgRNA by comparing *COL7A1* knockout in a permissive HEK-293T cells line. Assess knockout efficiency on genomic level

by Sanger sequencing followed by computational decomposition of sequence traces using bioinformatics tools such TIDE, ICE and EDIT-R.

b) Evaluate the chosen sgRNA in HaCaT keratinocyte cell line by comparing different CRISPR/Cas9 delivery methods, such as RNP-mediated delivery and lentiviral vector transduction of the guide alongside SpCas9 mRNA electroporation.

2) To design, validate and optimize gene repair strategies by HDR testing DNA-stranded or single-stranded oligonucleotides (ssODN) repair template delivered via either viral- (NILV) or non-viral-based (electroporation) methods. This will be achieved by:

a) Design and test donor repair template sequences for delivery via NILV by transducing HaCaT cells and quantifying the intended nucleotide changes by computational decomposition of the Sanger trace data and next generation sequencing (NGS).

b) Design and evaluate ssODN donor template for a viral-free correction strategy by co-delivering Cas9 mRNA by electroporation into HaCaT cells and assessing knock-in frequency on genomic level by computational decomposition of the Sanger trace data.

3.4 Characterization and description of the c.425A>G mutation in RDEB

The *COL7A1* gene is characterized by the presence of more than 800 variants either single base insertion/deletions and complex ones spanning over its 118 exons (Kowalewski et al., 2011). Around 15% of all DEB variant mutations were described to fall within intron–exon junctions resulting in splicing defects. This class of mutations, has a double impact on mRNA and protein level and are responsible of aberrant or absent expression of type VII collagen in DEB patients. One of the most described splicing mutation for DEB is the mutation c.425A>G (p.K142R). This single A>G transition was firstly described by Christiano *et al*., as a neutral intragenic Lysin (K) to Arginine (R) polymorphism which abolishes a *StyI* restriction enzyme site mapped by direct nucleotide sequencing of the type VII collagen cDNA at the end of exon 3 (Christiano et al., 1994). Correlation of the c.425A>G genotype with the clinical manifestation of EB blistering phenotype was furtherly discovered in DEB patients (Gardella et al., 1996; Hammami-Hauasli et al., 1997). The inheritance pattern of the c.425A>G variant has been reported either autosomal dominant (less common) and autosomal recessive (more common) with an allelic frequency of 3.9% in the central European population (Csikós et al., 2005; Gardella et al., 1996; Wertheim-Tysarowska et al., 2012; Jeřábková et al., 2010). In the latter, patients were found compound heterozygous, commonly presenting a second mutation described in different sites of the *COL7A1* gene (Csikós et al., 2005). The genetic cause of the pathogenesis is related with the positon of this variant sequence. The pathogenic A>G substitution falls in position -2 of the consensus sequence of the donor splice (SD) site at the end of exon 3 albeit resulting in an impaired splicing between exons 3 and 4 (Gardella et al., 1996). On molecular level, three different aberrant transcripts leading to premature termination codons (PTCs) have been observed (**Figure 3.1**): 1) retention of intron 3 due to a PTC at its 66th nucleotide, 2) activation of a secondary cryptic GT splice site localized in within exon 3 containing a PTC around 61bp downstream the cryptic splicing donor and 3) complete skipping of the exon 3 with PTC after the 10th base of exon 4 (Gardella et al., 1996; Hammami-Hauasli et al., 1997). Overall, the presence of a PTC on transcriptional levels determines the complete absence of C7 in c.425A>G$^{+/+}$ patients whereas variable C7 protein expression have been detected in

patients' skin biopsies when compound heterozygous (Hammami-Hauasli et al., 1997).

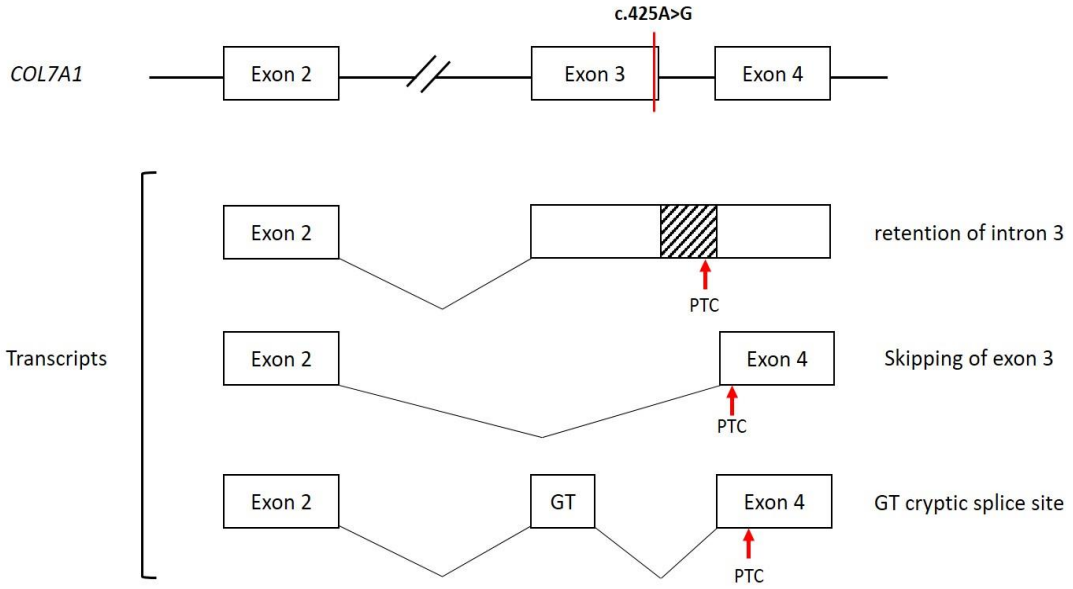

Figure 3.1 Generation of aberrant transcripts described in c.425A>G RDEB patients

Generation of the anomalous transcripts observed in the RDEB patients from different cohorts (Gardella et al., 1996; Hammami-Hauasli et al., 1997). In sequence: 1) Retention of intron 3 and creation of a premature termination codons PTC in its sequence. 2) Activation of a secondary cryptic GT splice site localized in within exon 3. 3) Complete skipping of the exon 3 with PTC on exon 4. Figure adapted from (Gardella et al., 1996)

3.5 Design concept of CRISPR/Cas9 strategy of the *COL7A1* locus

Genome editing using CRISPR/Cas9 provides an attractive opportunity for *ex vivo* cell modifications and could be used to tackle specific mutation hotspots within the *COL7A1* gene as described in **section 1.9**. The success of homologous recombination (HDR) relies on the efficiency of DNA scission through non-homologous end joining (NHEJ) and optimal reagents delivery in the first instance (Hendel et al., 2014). This section describes optimizations of CRISPR/Cas9 reagents delivery to target a hotspot mutation within exon 3 of *COL7A1* (425A>G, p.K142R). In the first instance, design of *COL7A1* specific sgRNAs was performed using the Benchling design tool (https://benchling.com/crispr). Four different sgRNA guides targeting within exon 3 of the *COL7A1* gene (**Figure 3.2A**) were selected based on their on- and off-target

scores (**Table 3.1**). A guide RNA targeting exon 1 of the *TAP1* gene was used as positive control.

Table 3.1 Guide sequences tested for *COL7A1* CRISPR/Cas9 knockout

Guide	Sequence	PAM	Strand	On-Target Score	Off-target Score
Ex3C7-1	AAGGGGGGCAACACTCGCAC	AGG	sense	49.0	47.4
Ex3C7-2	AGGGGGGCAACACTCGCACA	GGG	sense	63.1	46.4
Ex3C7-3	TCCGTGAGCTTAGCTACAAG	GGG	sense	65.8	46.0
Ex3C7-4	CATCCGTGAGCTTAGCTACA	AGG	sense	51.8	45.6
TAP1-PC	ACTGCTACTTCTCGCCGACT	GGG	sense	59.3	48.7

Guides Ex3C7-1 to Ex3C7-4 were selected to assess the NHEJ efficiency for exon 3 of *COL7A1*. *TAP1-PC* guide was used as positive control. Guide orientation is shown as sense or anti-sense and binds complementary DNA strand by Watson and Crick base pair. On-target score is the target activity evaluated by the algorithm developed by Doench, Fusi *et al.* (Doench et al., 2016) The score is from 0-100 and higher scores mean higher on-target activity. Off-target score is evaluated according to the number of mismatches between the selected guide RNA and similar exonic off-target site (Hsu et al., 2013). The score is from 0-100 and higher scores mean lower off-target activity.

Designed sgRNA were separately cloned into the PX458 parental plasmid (**Table 2.14**) encoding for a sgRNA cassette containing the RNA Pol III U6 promoter, a mini-stuffer sequence containing 2 *BbsI* restriction enzyme sites to accommodate the designed sgRNA protospacer, a guide scaffold and a chicken β-actin promoter-driven SpCas9:T2A:eGFP expression cassette. To increase the expression of the cloned sgRNAs from the human U6 promoter, a single guanine G at potion +1 of the sgRNA transcription start site (TSS) was added (Ranganathan et al., 2014). An oligo annealing protocol was then used to clone protospacer sequences within the PX548 plasmid.

Initial validation of these guide was performed in HEK-293T cell line by DNA plasmid transfection. Five days post transfection, knockout efficiency was analysed on genomic level by PCR by designing primers flanking the predicted SpCas9 cut sites within exon 3 of *COL7A1* (**Figure 3.2B**). PCR products were Sanger sequenced and knockout was quantified using TIDE (https://tide.deskgen.com/). TIDE is a bioinformatics assay which allows to precisely determine the spectrum and frequency of targeted InDels generated by genome editing tools such as CRISPR/Cas9

by the comparing Sanger sequences from edited and unedited cells (Brinkman et al., 2018).

TIDE analysis revealed a low NHEJ-mediated SpCas9 effect for guides Ex3C7-1 and Ex3C7-3 (5% and 7.4% respectively), while Ex3C7-2 and Ex3C7-4 showed higher targeted disruption at 57.5% and 30%, respectively (**Figure 3.2C**). Additionally, genomic disruption by EX3C2-2 guide was similar to that of the positive control TAP1-PC guide (~53%). Therefore, guide Ex3C7-2 (from now called "Ex3-distal"-Ex3D-sgRNA) was used for further NHEJ and HDR-strategies and the distance from the predicted Cas9-sgRNA-induced DSBs to the c.425A>G *COL7A1* mutation of this study is 71bp.

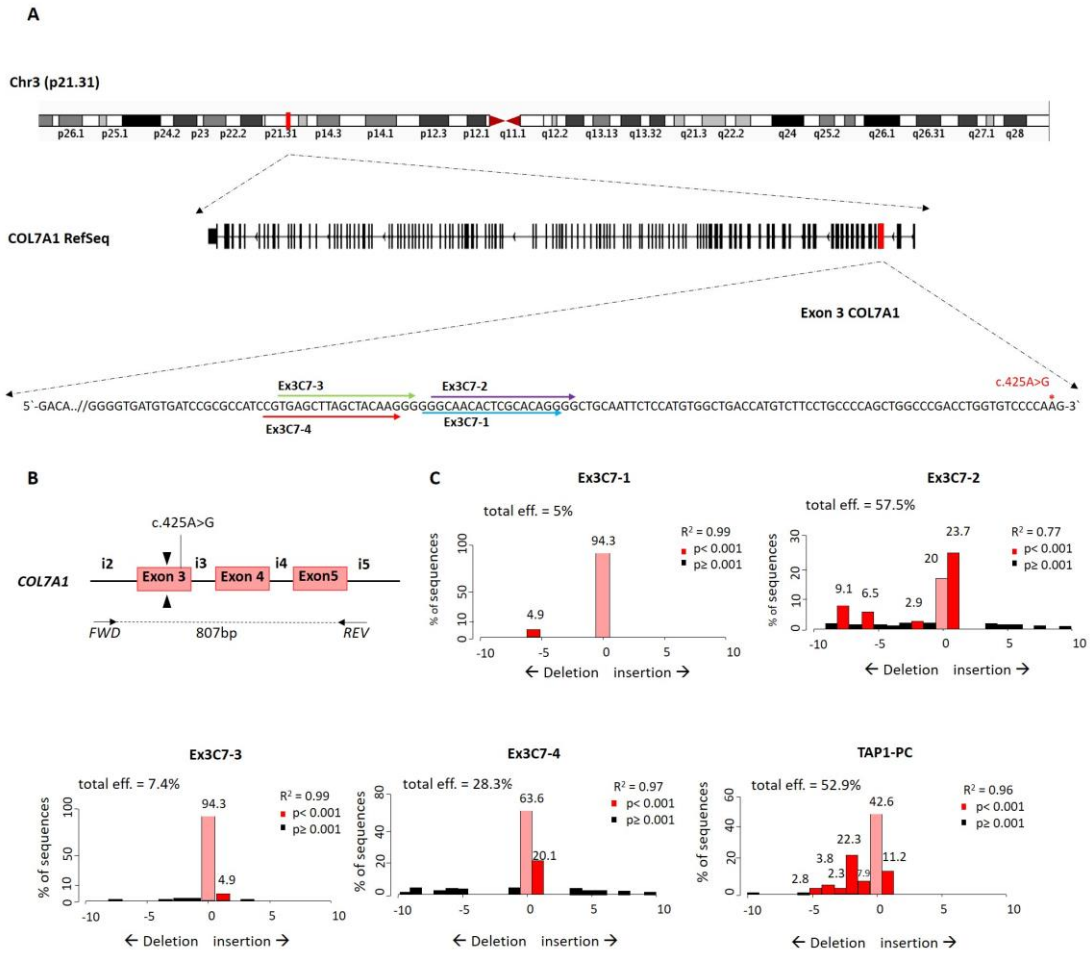

Figure 3.2 Validation of *COL7A1* knockout in HEK-293T cells

A. Schematic representation of human chromosome 3 and *COL7A1* gene. The magnified view illustrates chromosome 3 where *COL7A1* gene is mapped. The red box in the *COL7A1* RefSeq represents the position of the point mutation within exon 3. Magnified, the sequence of exon

3. The red asterisk shows the c.425A>G mutation. Arrows indicate different sgRNAs tested for *COL7A1* knockout. **B.** Schema of the PCR strategy used to quantify the percentage of NHEJ events by Sanger sequencing-based TIDE of the targeted area. Black arrows illustrate the primers used for sequencing. **C.** Evaluation of the cleavage activity of the designed sgRNAs by TIDE analysis for the detection of NHEJ events. Cell edited with Ex3C7-2 guide RNA showed the highest *COL7A1* disruption (57.5%). Lower percentages of NHEJ were observed with the other sgRNAs tested (30% for Ex3C7-4, 7.4% for Ex3C7-3, 5% for Ex3C7-1). X axis: size of deletion (left) or insertion (right): Y axis: percentage of alleles with insertion or deletions: pink bar: unedited alleles; red bar: edited alleles (p-value <0.001); black bar: edited alleles (p-value ≥0.001). The *P*-value associated with the estimated abundance of each indel is calculated by a two-tailed *t*-test of the variance–covariance matrix of the standard errors determined by default by TIDE **(https://tide.deskgen.com/)**.

3.6 Viral delivery of Ex3D-guide RNA

As detailed above in **section 1.9**, there are a number of delivery strategies that have been applied to the SpCas9 endonuclease for epidermolysis bullosa in the last few years. At the time of this project, use of non-integrating viral platforms for CRISPR/Cas9 delivery have shown to achieve up to 19% editing in the *COL7A1* locus in primary RDEB keratinocyte stem cells (Izmiryan et al., 2018). For the initial testing of the chosen guide RNA, the Ex3D-sgRNA was cloned into a conventional LV (LentiCRISPRV2) backbone (**Table 2.14**) expressing a single guide RNA scaffold and a SpCas9 cassette under the hU6 and EF1-α promoter, respectively. As previously described in **section 3.5**, to increase the expression of the guide RNA under the hU6 promoter, an initial guanine was placed in position +1 from the sgRNA TSS. On-target *COL7A1* disruption was then evaluated in wild type HaCaT keratinocyte cell line. To do so, two different viral configurations have been tested.

The first configuration, similar to that used by Izmiryan *et al*. (Izmiryan et al., 2018), comprised a non-integrating lentiviral vector stock (NILV-LentiV2CRISPR-Ex3D) encoding for both SpCas9 and Ex3D-sgRNA. Delivery of non-integrating viral vectors expressing SpCas9 was shown to be effective in preclinical applications, as they promote a temporal expression of the endonuclease (Izmiryan et al., 2018). Although suitable for proof-of-concept studies, the use of NILV expressing SpCas9, would pose a problematic risk in clinical applications firstly as extended exposure to SpCas9 has

proven immunogenic (Mehta and Merkel 2020) and furthermore as this would increase the likelihood of off-target cleavage. To help mitigate these issues, delivery of stabilised SpCas9 mRNA (capped, and polyadenylated) in combination with lentiviral delivery of sgRNA was also tested. This approach has been shown to produce effective targeted knockout of the TRAC gene for CAR cell therapies and is in clinical trials (Georgiadis et al., 2018).

Therefore, for the second configuration, a hybrid viral and non-viral CRISPR/Cas9 delivery was tested. To do this, the SpCas9-P2A expressing cassette was removed through site-directed mutagenesis from the original LentiCRISPRV2 plasmid backbone (13,136bp) leaving the eGFP cassette directly under the EF1-α promoter (**Figure 3.3A**). In detail, the SpCas9-P2A cassette was removed by PCR amplification of the viral backbone designing a couple of primers in opposite direction from the desired site of deletion. Molecular weight of the resulting vector (LentiV2-Ex3D, 8884bp) was confirmed by restriction digestion with *KpnI* (**Figure 3.3B**) followed by Sanger sequencing to verify the correct in frame orientation of the eGFP cassette under the EF1-α promoter (**Figure 3.3B**). The resulting 3rd generation integrating self-inactivating (SIN) lentiviral vector expressing only the Ex3D-sgRNA (LentiV2-Ex3D) was used alongside a capped, polyadenylated SpCas9 mRNA delivered by electroporation. Transient expression of the nuclease delivered as mRNA was previously confirmed by western blot by measuring the expression of the SpCas9 protein at different time points (Georgiadis et al., 2018). SpCas9 protein appeared to peak at 0.5 days and had mostly dissipated by day 3 post electroporation. A similar lentiviral vector expressing a sgRNA targeting exon 1 of the Beta-2-Microglobulin (*B2M*) gene designed by Dr. Roland Preece, was used as a positive control for CRISPR editing (LentiV2-B2M).

Both NILV-LentiV2CRISPR-Ex3D and LentiV2-Ex3D/B2M vector stocks were made by co-transfection in HEK-293T cells with VSV-G envelop encoding plasmid (pMDG) and 2nd generation Δ64 integration defective packaging plasmids (pMCV-dR8.74-D64V *gag/pol*) for NILV or 3rd generation (pMDLg/pRRE – *gag/pol*) and pRSV-REV plasmids for integrating lentiviruses. HIV-1 p24 levels by ELISA of the NILV-LentiV2CRISPR-Ex3D showed a range of 8.5x10^{8} TU/100-8.5x10^{9} TU/1000 p24 Physical Particle (PP) with

an average titer of $4.6x10^9$ TU/mL (**Figure 3.3C**). Titration by flow cytometry analysis of eGFP expression for LentiV2-Ex3D indicated the viral titre of $8.5x10^8$ TU/mL (**Figure 3.3C**). Both viral configurations were tested in HaCaT keratinocyte cell line. HaCaT cells were transduced with either NILV-LentiV2-Ex3D at multiplicity of infection 20 (MOI 20) or with LentiV2-Ex3D at MOI 20. LentiV2-Ex3D transduced cells were subsequently electroporated with SpCas9 mRNA (10μg) 4 days post transduction (Georgiadis et al., 2018). qPCR for the corresponding number of proviral LentiV2-Ex3D copies within the endogenous DNA (VCN) was performed using a probe complementary to the viral packaging signal sequence, Psi (Ψ), and normalized to the level of albumin in the same cells. VCN was quantified 5- and 14-days post-transduction and equated 4.8 (n=2 ±0.5) and 1.2 (n=2 ±0.5) copies/cells, respectively (**Figure 3.3C**).

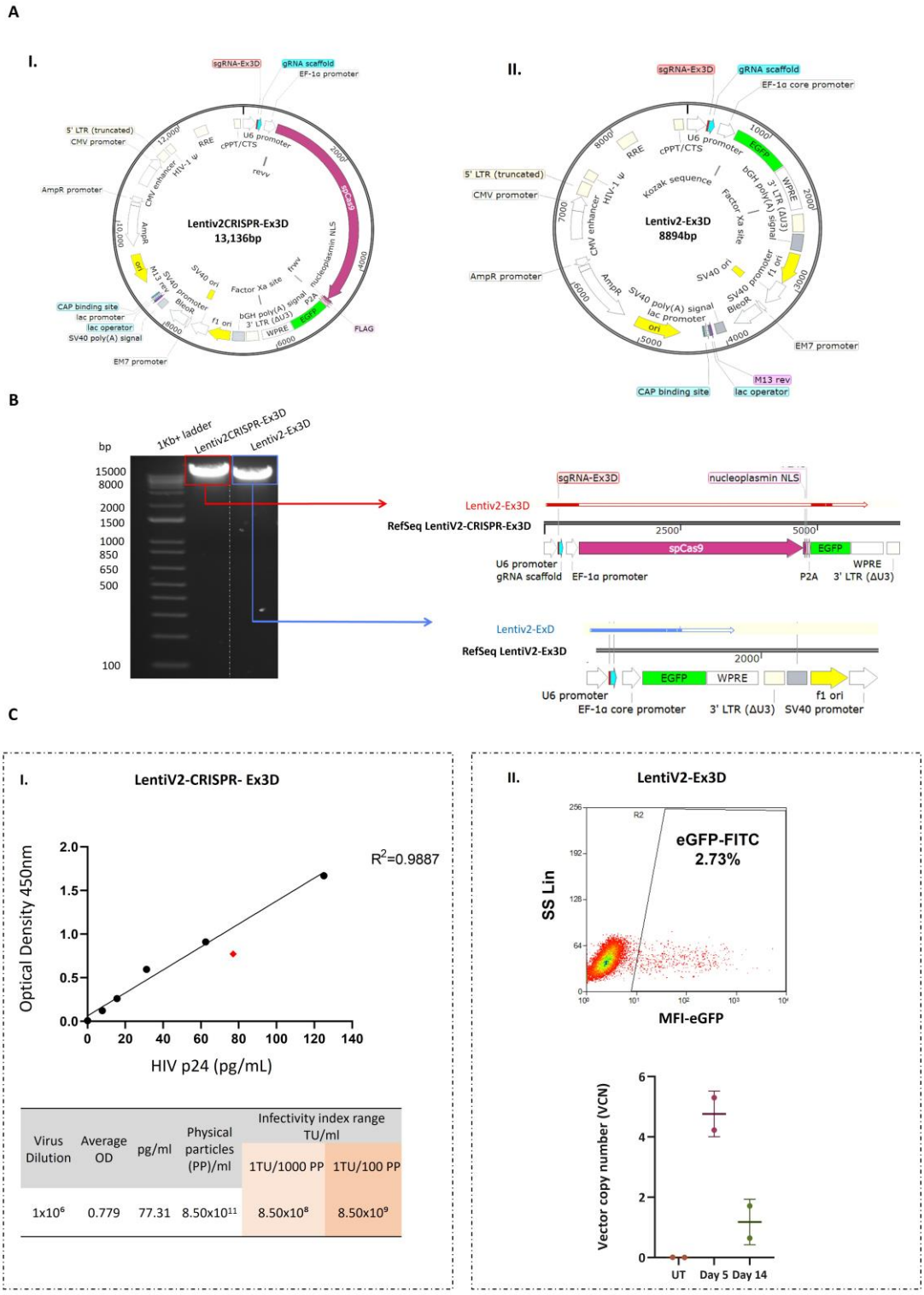

Virus Dilution	Average OD	pg/ml	Physical particles (PP)/ml	Infectivity index range TU/ml	
				1TU/1000 PP	1TU/100 PP
$1x10^{6}$	0.779	77.31	$8.50x10^{11}$	$8.50x10^{8}$	$8.50x10^{9}$

Figure 3.3 Vector Design and titration of LentiV2-based vectors

A. Plasmid map of LentiV2-CRISPR-Ex3D (**I.**) and LentiV2-Ex3D after SpCas9-P2A cassette removal (**II.**). **B**. Confirmation of the correct vector molecular size upon cloning of the Ex3D guide RNA by *KpnI* digestion. Alignment of Sanger sequenced linearized LentiV2-Ex3D (sequence in red) with the RefSeq LentiV2-CRISPR-Ex3D confirmed the SpCas9-P2A cassette removal (top) and the in-frame eGFP cassette orientation (sequence in blue) under the EF1α-

promoter (bottom). **C**. Viral titration of NILV-LentiV2-CRISPR-Ex3D and LentiV2-Ex3D. (**i.**) Physical titre of NILV-LentiV2CRISPR-Ex3D evaluated by quantitative measurement of HIV-p24 protein by ELISA in cell culture supernatant. The standard line was obtained using known concentrations of HIV-p24 protein (black dots, R^2=0.9887). From this, the concentration of NILV-LentiV2CRISPR-Ex3D (red square) was determined (table below). Abbreviations: OD, optical density; TU, transducing unit; PP, physical particle. (**ii.**) LentiV2-Ex3D titre was determined by the percentage of GFP positive cells using flow cytometry. For accurate titre calculation, the mean fluorescent intensity (MFI) of the GFP within 2%-10% were used (2.73% of eGFP+ cells for 0.0032µL of virus). Below, vector copy number (VCN) of keratinocytes transduced with LentiV2-Ex3D (MOI 20) (n=2, error bars ±0.5). The plot shows the VCN in untransduced (UT) cells and transduced cells 5 days and 14 days post viral transduction.

Five days post electroporation, cells were harvested and a PCR with primers flanking the predicted cutting site was performed. The PCR product obtained was subsequently Sanger sequenced and analysed by TIDE. Genomic disruption of *COL7A1* was 90% and 36% for NILV-LentiV2-CRISPR-Ex3D and LentiV2-Ex3D + SpCas9 mRNA, respectively (**Figure 3.4A**). Knockout of *B2M* was evaluated 5 days post SpCas9 mRNA electroporation by TIDE showing 49% allelic disruption. To optimize the hybrid strategy of LentiV2-Ex3D transduction coupled with SpCas9 mRNA electroporation, a time course experiment of SpCas9 mRNA delivery post sgRNA transduction was carried out. To do so, HaCaT cells were transduced with LentiV2-Ex3D (MOI 20) on day 0 and 10µg of SpCas9 mRNA was delivered by electroporation at days 1, 2, 3 and 4 post sgRNA transduction. Knockout of *COL7A1* was evaluated for each sample 5 days post electroporation. No significant differences in *COL7A1* disruption were observed among all samples, showing around 50% of NHEJ (n=2) (**Figure 3.4B**). Therefore, for all downstream experiments, electroporation with SpCas9 mRNA was performed 3 days post transduction. In line with the gene knockouts observed on the genomic level, flow cytometry analysis at 15 days post electroporation showed 30.1% and 46% of Beta-2-Microglobulin and C7 downregulation, respectively, using an anti-human monoclonal antibody which recognizes the N-terminal non-collagenous domain of type VII collage (mAb-C7-LH7.2) (**Figure 3.4C**).

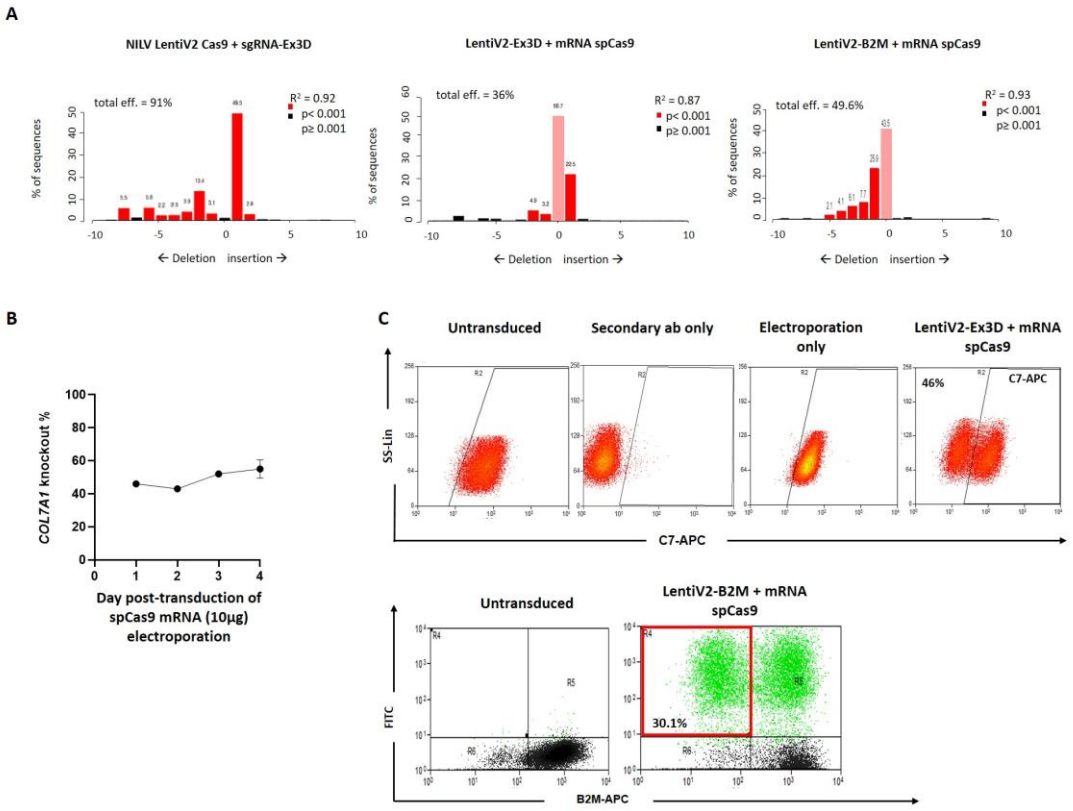

Figure 3.4 Viral delivery of guide RNA and optimization of LentiV2-Ex3D+ SpCas9 mRNA strategy

A. Evaluation of the cleavage activity of the designed Ex3D-sgRNA by TIDE analysis for the detection of NHEJ events in cells transduced with NILV-LentiV2-CRISPR-Ex3D (91%), LentiV2-Ex3D + SpCas9 mRNA (36%) and positive control LentiV2-B2M + SpCas9 mRNA (49.6%). X axis: size of deletion (left) or insertion (right): Y axis: percentage of alleles with insertion or deletions: pink bar: unedited alleles; red bar: edited alleles (p-value <0.001); black bar: edited alleles (p-value ≥0.001). **B**. Time course of SpCas9 mRNA delivery from day 1 to 4 post LentiV2-Ex3D transduction of keratinocyte cells (n=2, error bars ±1). Quantification of *COL7A1* knockout by Sanger sequencing-based TIDE displays comparable NHEJ rates even after electroporation of SpCas9 mRNA at different time points. The frequency of NHEJ was around 50% for each time point. **C.** Quantification of protein knockout by flow cytometry in keratinocytes transduced with LentiV2-Ex3D and LentiV2-B2M + SpCas9 mRNA at MOI 20. Top panel shows staining for C7: untransduced cells, cells stained with isotope control and cells electroporated only, were used as control. Approximately 46% of the total population treated with LentiV2-Ex3D + SpCas9 mRNA were negative for C7 after CRISPR/Cas9-induced knockout. Bottom panel: eGFP+ LentiV2-B2M + SpCas9 mRNA treated keratinocytes show a knockout of 30.1% in Beta-2-Microglobulin expression (red square)**.**

3.7 Non-viral delivery of the guide RNA

At the time of the development of the strategy described in section 3.2, physical non-viral method, such as electroporation delivery of individual in-vitro transcribed or synthetic sgRNA coupled with SpCas9 as mRNA or protein (as ribonucleoprotein complex or RNP) have shown to enable transient expression of the CRISPR/Cas9 system therefore minimizing potential off-target events or unwanted random integration of plasmid DNA or viral vectors (Hendel et al., 2015; Kim et al., 2014). Of these methods, electroporation is compatible with all CRISPR/Cas systems and is widely used in mammalian cells. Upon electroporation the cell membrane is temporarily made more permeable, allowing proteins or nucleic acids to enter the cytoplasm. However, electroporation protocols have to be carefully optimised for each target cell type, as this process can result in high levels of cell death.

CRISPR/Cas9 genome editing also relies on the appropriate delivery of sgRNA. Initial reports using a 2-part synthetic gRNA (tracRNA:crRNA) or synthetic sgRNA have been shown increased levels of editing over virally-expressed sgRNA. Moreover, the addition of 2'-O-methyl 3'phosphorothioate modifications to the first and last three nucleotides in the sgRNA, has significantly improved stability and editing efficiencies over non-modified sgRNAs when transiently co-delivered with Cas9 mRNA or as ribonucleoprotein (RNP) and are now being implemented in the vast majority of studies (Hendel et al., 2015; Seki et al., 2018 Schumann et al., 2015).

Initially, a 2-part synthetic sgRNA was obtained by hybridizing the customized crRNA encoding for the Ex3D protospacer sequence designed and validated in **section 3.4** with a universal tracrRNA synthesized by IDT (Integrated DNA Technologies Inc. Coralville, USA). To investigate the efficiency of the RNP complex delivery, a dye-labelled synthetic tracrRNA (transcrRNA-ATTO™ 5500, IDT) was hybridized with B2M and Ex3D crRNA and Cas9 protein. Flow cytometry analysis 48 hours post electroporation showed that nearly 100% of the electroporated cells successfully received the RNP complex (**Figure 3.5A**).

To evaluate the on-target knockout activity of the RNP complex, a 1.2:1 sgRNA/Cas9 molar ratio (corresponding to 220pmol (7µg) and 180pmol (29.4µg), respectively)

was used (for all conversions, see **Table 3.2**). The B2M-RNP complex was used as positive control of correct hybrization of the 2-part sgRNA and subsequent functional complexing with the Cas9 protein *in vitro*. Efficiency of the hybridized dual guide RNAs were evaluated by their ability to create targeted DNA DSBs followed by functional knockout of C7 and the Beta-2-Microglobulin by flow cytometry. Five days post electroporation, an average knockout of 5.1% (n=3) and 63.8% (n=3) for *COL7A1* and *B2M*, respectively, was observed (**Figure 3.5B**). Despite the low indel frequency in the target *COL7A1* sequence, the considerable knockout of *B2M* indicates that no biases in either crRNA:tracrRNA hybridization or in RNP complexing occurred.

In order to increase knockout efficiency, a synthetic single chemically modified sgRNA from Synthego (Synthego corporation, Menlo Park, California, USA) as reported by Hendel *et al*. (Hendel et al., 2015) was tested in my gene editing settings.

Table 3.2 Conversion from µg to pmol of sgRNA-Cas9 components for RNP assembly

µg sgRNA	pmol sgRNA	µg SpCas9	pmol SpCas9
1	31	4.2	25.6
2	62	8.4	51.2
3	93	12.6	76.8
4	124	16.8	102.5
5	155	21	128
6	186	25.2	153.7
7	220	29.4	180

Table conversion from µg to pmol of sgRNA and SpCas9 protein used to generate ribonucleoprotein (RNP) complex *in vitro*. Optimization of RNP concentrations is performed on molar concentrations of the CRISPR/Cas9 components which vary according to manufacturer instructions or experiment settings. The concentrations reported here are based on a 1:1.2 molar ratio between sgRNA and SpCas9 protein, respectively.

Maintaining the same molar ratio of 1.2:1 sgRNA/Cas9, comparison of *COL7A1* gene knockout between 2-part sgRNA and chemically modified sgRNA was firstly evaluated by Sanger sequencing on genomic level. Editing for Ex3D showed a significant 17-fold increase ($p<0.0001$) in knockout efficiency with up to 88.3% (n=3) of allelic disruption compared to the 2-part guide RNA (**Figure 3.5B**). For *B2M* control, only 1.3-fold

increase (p=0.0621) of NHEJ was observed with chemically modified sgRNA (81.6%, n=3) compared to hybridized crRNA:tracrRNA (**Figure 3.5B**). In line with the gene editing rates observed by Sanger sequencing, flow cytometry at 15 days post electroporation showed 4% and 78% C7 knockout when using a 2-part-Ex3D sgRNA and chemically modified Ex3D-sgRNA, respectively (**Figure 3.5C**). No difference in Beta-2-Microglobulin downregulation was observed between the two guide RNA configurations (**Figure 3.5C**).

In order to attempt to increase the percentage of *COL7A1* allelic disruption, evaluation of different sgRNA:Cas9 molar ratios was performed. Molar ratios of 1.2:1 and 3:1 for sgRNA:Cas9 were tested and delivered as RNP complexes by electroporation in HaCaT keratinocyte cell line. Knockout efficiency was evaluated 5 days post electroporation by Sanger sequencing followed by ICE analysis. Similarly to TIDE, ICE (Inference of CRISPR Edits) is a software developed by Synthego which enables analysis of CRISPR edits using Sanger data (Hsiau et al., 2018).No difference in *COL7A1* knockout was observed between the two molar ratio tested (75% and 85%, respectively), therefore a 1.2:1 sgRNA:Cas9 setting was used in the next gene editing applications (**Figure 3.5D**).

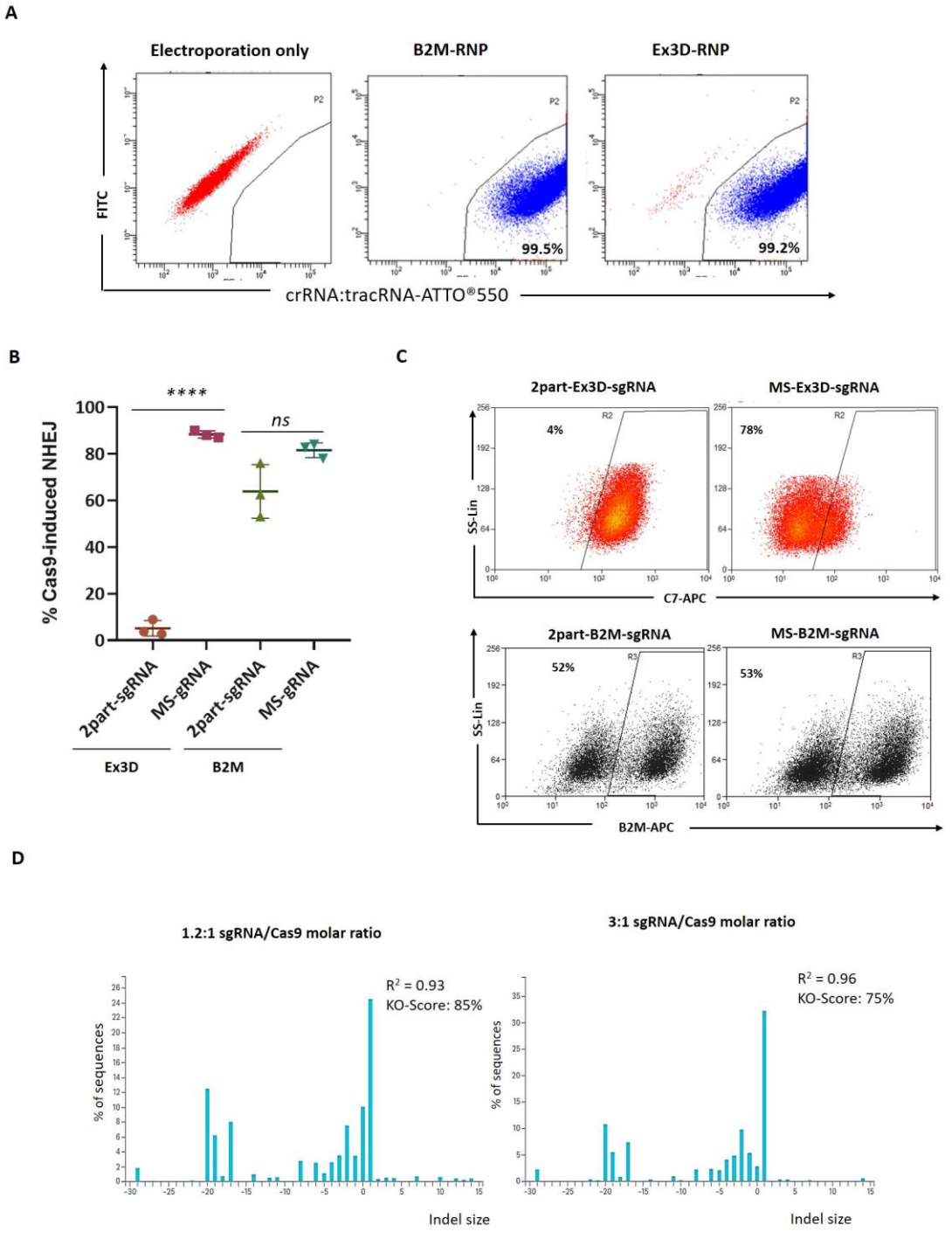

Figure 3.5 Evaluation and optimization of CRISPR/Cas9 non-viral delivery

A. Flow cytometry analysis of the intracellular incorporation of RNP complex post electroporation. From left to right: cells electroporated only, cells electroporated with B2M-RNP or Ex3D-RNP, respectively. Both B2M-RNP and Ex3D-RNP resulted in nearly 100% of sgRNA-Cas9 incorporation. **B.** Sanger sequencing based Knockout efficiency of synthetic chemically modified sgRNA (MS-sgRNA) and crRNA:tracrRNA guide RNA for Ex3D and B2M in HaCaTs. *COL7A1* knockout by crRNA:tracrRNA guide RNA is approximately 17-fold lower than with the synthetic chemically modified sgRNA (88.3% and 5.1% n=3, respectively). Data analysed by non-parametric Student t-test (****p = 0.0001). The error bars represent

standard error of n=3 biological repeats. For B2M, 81.6% and 63.8% of knockout (n=3, p=0.0621) was observed using synthetic and dual guide RNA, respectively. **C.** Quantification of C7 protein knockout by flow cytometry using synthetic chemically modified sgRNA and dual guide RNA. C7 downregulation was around 4% and 78% with 2part-sgRNA and MS-sgRNA, respectively. Comparable Beta-2-Microglobulin downregulation was observed between 2part-B2M-sgRNA (52%) and chemically modified MS-B2M-sgRNA (53%). **D.** Quantification of *COL7A1* gene disruption by Sanger sequencing based ICE analysis in cells receiving different sgRNA:Cas9 molar ratios. Allelic disruption was around 85% and 75% with 1.2:1 and 3:1 molar ratio, respectively.

3.8 Comparison between viral and non-viral delivery of the guide RNA

After optimization of both viral and non-viral based sgRNA and Cas9 deliveries separately, the two methods, namely LentiV2-Ex3D + SpCas9 mRNA and Ex3D-RNP, were compared in parallel in HaCaT keratinocyte cell line. The NHEJ InDels frequency of both delivery methods was evaluated by Sanger sequencing-based ICE analysis with either SpCas9 mRNA or RNP complex. Significant difference in NHEJ frequencies was observed. Up to 50% (n=3) of allelic disruption with LentiV2-Ex3D + SpCas9 mRNA was detected versus 86% (n=3) obtained with the RNP counterpart (p=0.0009) (**Figure 3.6A**). In line with the different percentages of knockout observed on genomic level, western blot (**Figure3.6B**) and immunofluorescent staining for C7 (**Figure3.6C**) on treated bulk populations confirmed 75% and 43% reduction in C7 expression in cells treated with the Ex3D-RNP complex and LentiV2-Ex3D + Cas9 mRNA, respectively.

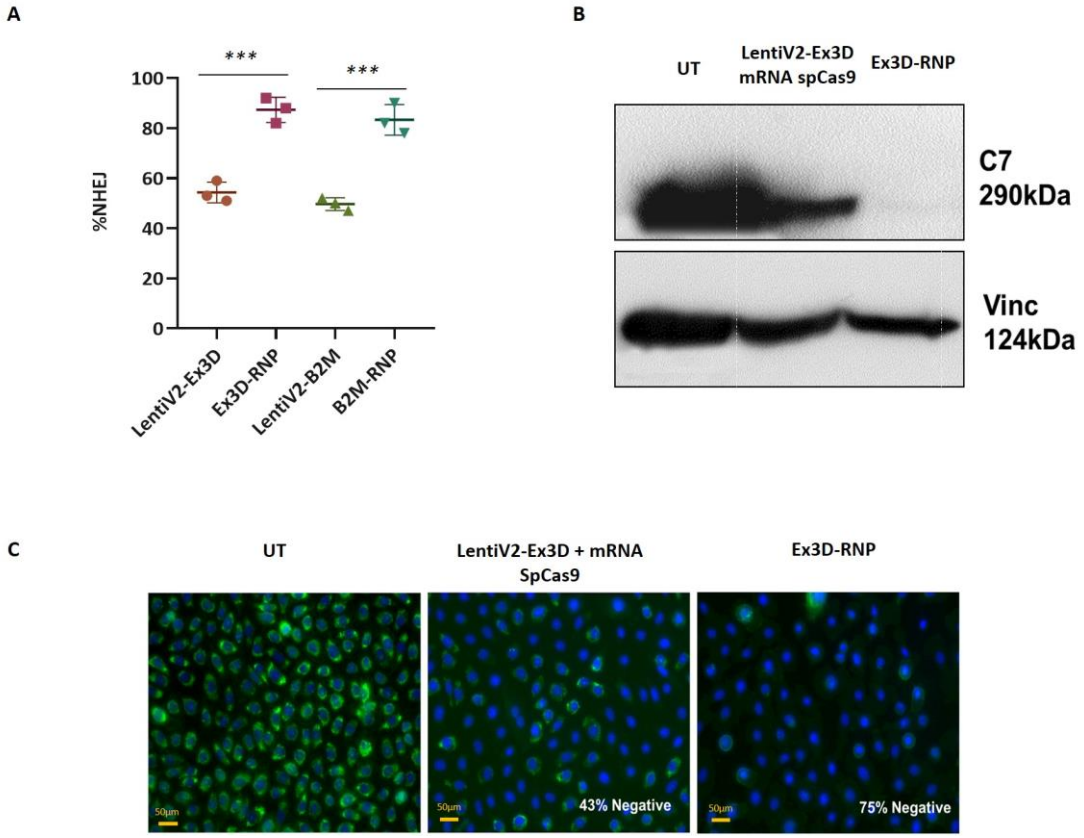

Figure 3.6: **Comparison between viral and non-viral CRISPR/Cas9 deliveries**

A. Comparison of allelic disruption between LentiV2-Ex3D + SpCas9 mRNA and Ex3D-RNP complex by TIDE analysis for the detection of NHEJ events (n=3). *COL7A1* knockout was 50% for LentiV2-Ex3D and up to 86% when using the Ex3D-RNP complex. Similar trend in terms of NHEJ efficiency was observed for *B2M* knockout strategies, 49.6% with LentiV2-B2M and 83.3% with RNP-B2M. All data sets were analyzed using a non-parametric Student t-test (***p = 0.0009, n=3). The error bars represent standard error of n=3 biological repeats. **B.** In line with the percentages of *COL7A1* knockout observed on genomic level, comparable C7 downregulation on protein level was confirmed by western blot. Vinculin was used as a loading control. **C**. Immunofluorescent quantification of protein downregulation in keratinocytes populations edited with LentiV2-Ex3D + Cas9 mRNA and Ex3D-RNP showed 42% and 75% of C7 knockout, respectively. Untreated keratinocytes (UT) were used as control (top right). Scale bar = 50µm.

3.9 Donor template design for genetic correction of COL7A1 c.425A>G mutation

To test HDR-mediated correction, a therapeutic donor template, previously designed by Dr David Almarza, bearing a portion of the wild type *COL7A1* (~1.8kb) sequence spanning from intron 2 to 7 was used (I2I7-OriginalTemplate) (**Figure 3.7A**). The designed template was subsequently modified by Dr. Christos Georgiadis for the investigation of HDR-based *COL7A1* correction by co-delivery of NILV-ZFNs and donor template (**Table 2.14**) (Georgiadis 2016). To avoid ZFN re-cutting upon donor integration, a total of 7 silent mutations within exon 4 of the donor template were introduced (NILV-SDMTemplate) (**Figure 3.7B**). Moreover, *EcoRI* and *XhoI* restriction enzyme sites were added at the 5' and 3' ends of the donor template, respectively, in order to subclone it into the pHR'SIN.cPPT-SW lentiviral transfer plasmid for NILV production (**Table 2.14**) (Georgiadis 2016). The modified donor template was synthesised by GeneArt and subsequently cloned into the pHR'SIN.cPPT-W lentiviral transfer plasmid lacking an SFFV promoter (Georgiadis 2016). For the purpose of the correction of the c.425A>G mutation, this donor template bears asymmetric homology arms with a span of 720bp and 1070bp on the left and the right, respectively.

Furthermore, the NILV-SDMTemplate was further optimized to allow it to be used for CRISPR/Cas9-based gene editing. In order to avoid Cas9-mediated cleavage of the donor template containing the Ex3D-sgRNA site, 5 missense mutations were introduced in the sgRNA recognition sequence of the template by site directed mutagenesis (SDM) through designing overlapping primers encoding for the intended mutations (**Figure 3.7B**). Specifically, 4 silent sgRNA-blocking mutations in position +1 (A>C), +4 (C>A), +7 (T>G) and +10 (C>T) and 1 additional missense PAM-blocking mutation (G>C) were introduced within the donor vector (from now called I2I7C7-SDMTemplate) (**Table 2.15**) (**Figure 3.7C**). The number, position and nucleotide change introduced within the I2I7C7SDMTemplate, was based on the likelihood of disruption to SpCas9 cleavage activity as described previously in Hsu *et al*. (Hsu et al. 2013).

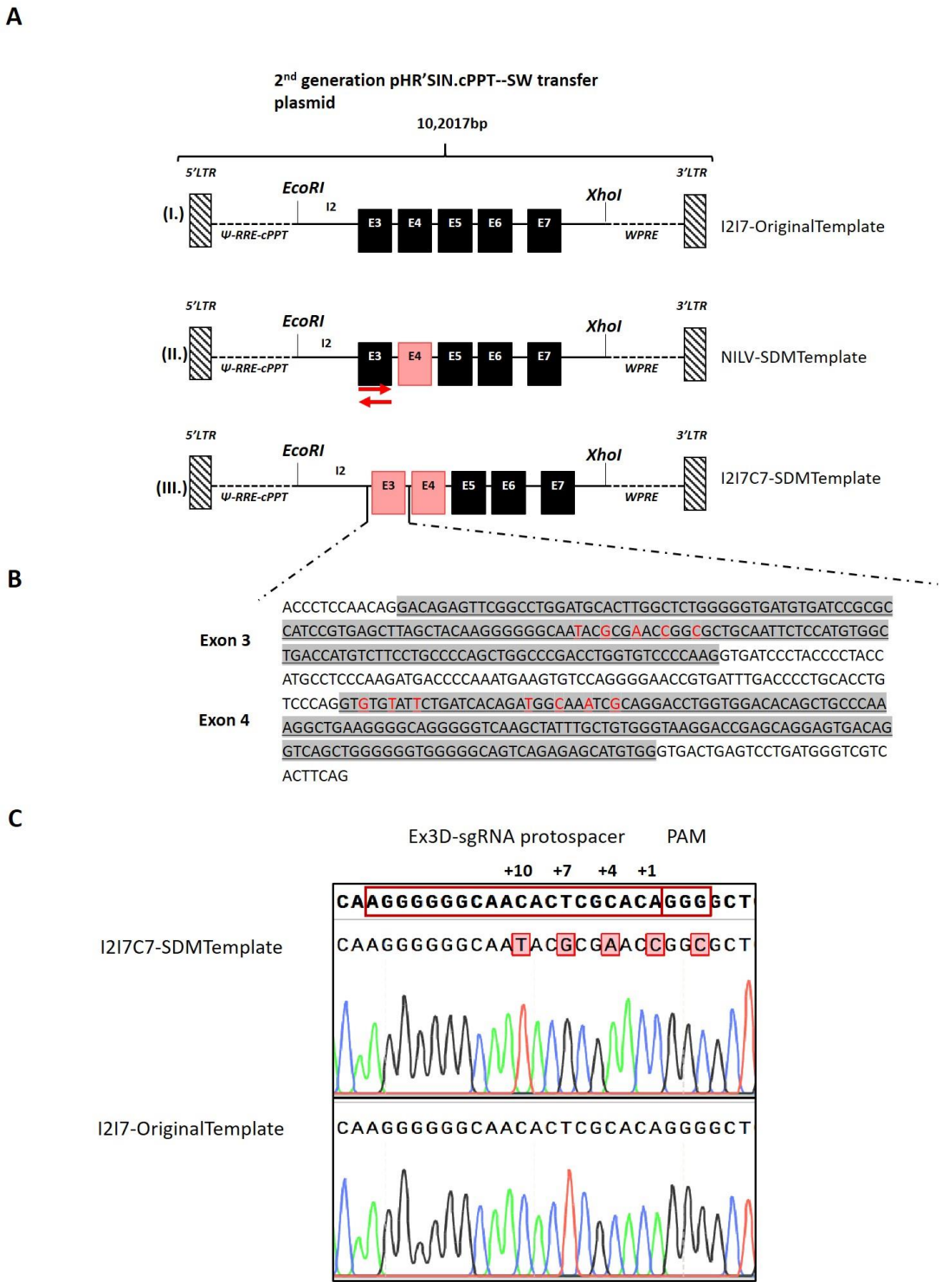

Figure 3.7 Design of *COL7A1* donor template strategy

A. (**I.**) Schematic representation of the 2nd generation pHR'SIN.cPPT transfer vector encoding for wild type *COL7A1* sequence from intron 2 to intron 7 (I2I7-original-donor template). (**II.**) The previous version of the donor template contained 7 SDMs within exon 4 (NILV-SDMTemplate). Arrows in red represent the primers used to introduce additional silent point mutations within the Ex3D-sgRNA DNA binding site to block any further Cas9-mediated cutting upon integration of the donor template. (**III.**) The final I2I7C7-SDMTemplate shows

to retain SDMs in both exon 3 and exon 4. **B.** Summary of the silent mutations introduced within I2I7C7-SDMTemplate. Magnified representation of exon 3-4 of recombinant donor template sequence indicating Cas9-blocking mutation (in red) in exon3 and previous SDMs in exon 4. Highlighted in grey, exons 3 and 4. **C.** SDMs within exon 3 were confirmed by Sanger sequencing. Alignment of I2I7-SDMTemplate with I2I7-OriginalTemplate (used as RefSeq) showed the presence of total 5 mismatches with the wild type *COL7A1* sequences. In details, 4 mismatches were introduced within the sequence recognized by the Ex3D-sgRNA and 1 within its PAM sequence.

To avoid creating cryptic splicing site in 5' long terminal repeat (LTR) which can cause expression of truncated proteins (Paleari et al., 2012; Benati et al., 2018), the I2I7C7-SDMTemplate cassette was cloned in reverse orientation into the pHR SIN.cPPT-W transfer vector (I2I7C7-SDMTemplate-F). To do so, a PCR based plasmid cloning was designed using primers complementary to the 5' and 3' ends of the I2I7C7-SDMTemplate within the *XhoI* and *EcoRI* restriction sites, respectively (**Figure 3.8A**). Confirmation of the flipped orientation of the donor template was evaluated by Sanger sequencing using a primer designed to bind the WPRE cassette in reverse orientation (**Figure 3.8B**). The resultant plasmid was packaged for the production of a non-integrating lentiviral vector (NILV-I2I7C7-SDMTemplate-F). The NILV-I2I7C7-SDMTemplate-F was made by co-transfection in HEK-293T cells with the I2I7C7-SDMTemplate-F transfer vector, VSV-G envelop encoding plasmid (pMDG) and a 2nd generation Δ64 integration defective packaging plasmids (pMCV-dR8.74-D64V *gag/pol*) (**Figure 3.8C**). HIV-1 p24 levels by ELISA of the NILV-LentiV2CRISPR-Ex3D showed a range 2.5x10^{8} TU/100 PP to 2.5x10^{9} TU/1000 PP with an average of 1.25x10^{9} TU/mL (**Figure 3.8C**).

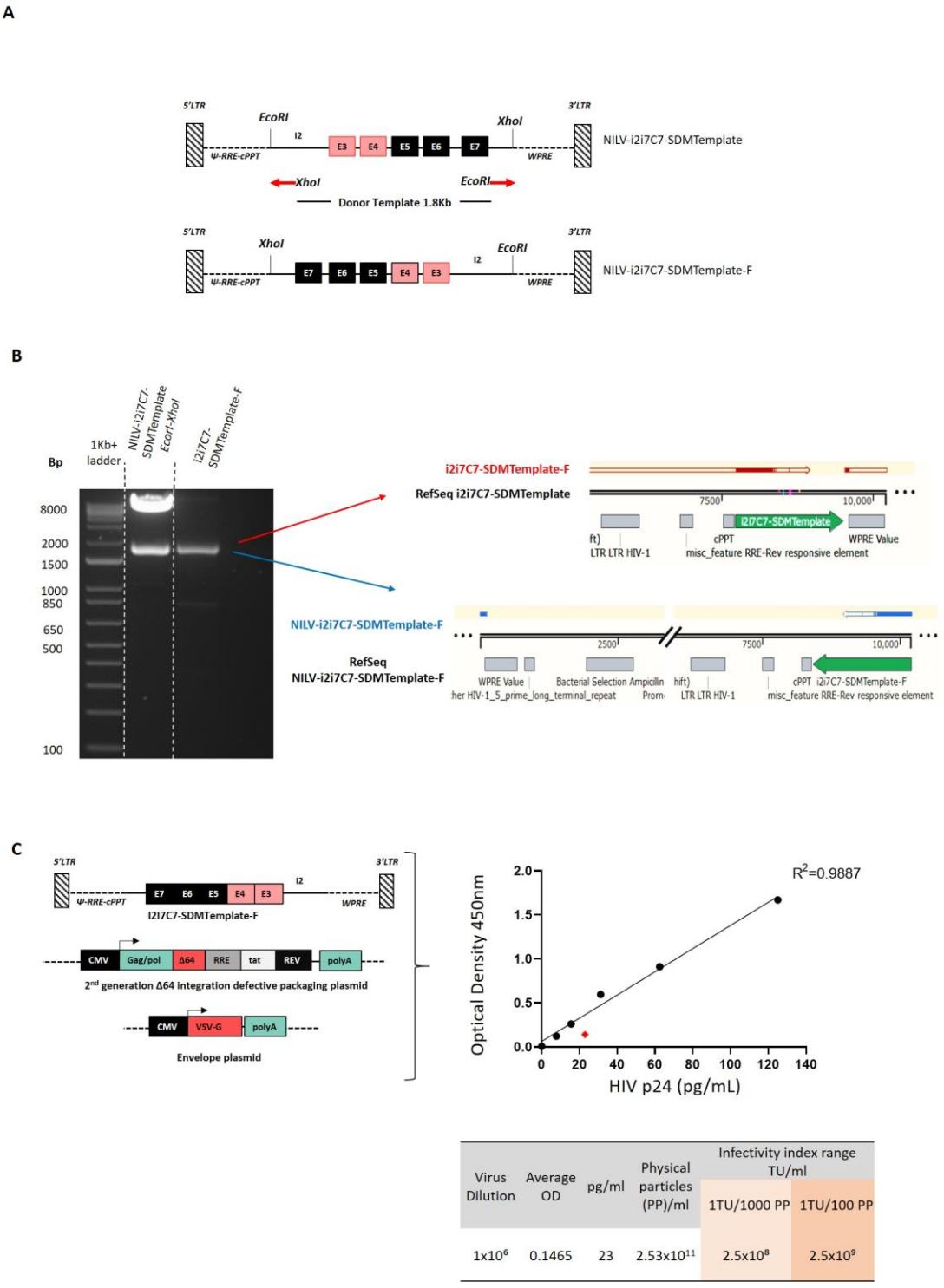

Virus Dilution	Average OD	pg/ml	Physical particles (PP)/ml	Infectivity index range TU/ml	
				1TU/1000 PP	1TU/100 PP
$1x10^{6}$	0.1465	23	$2.53x10^{11}$	$2.5x10^{8}$	$2.5x10^{9}$

Figure 3.8 Development of *COL7A1* donor template and vector titration

A. The NILV-I2I7C7SDMTemplate was used to excise the 1.8Kb I2I7C7-SDMTemplate donor from the pHR'SIN.cPPT vector backbone with a couple of primers (red arrows) containing *XhoI* and *EcoRI* restriction enzyme sites at their 5' ends. The excised *COL7A1* fragment (I2I7C7-SDMTemplate-F) was cloned in reverse orientation within the viral backbone (NILV-I2I7C7-SDMTemplate-F). **B.** Confirmation of the correct molecular size of the I2I7C7SDMTemplate-F with inverted *EcoRI* and *XhoI* enzymes restriction sites (lane 3). The

size of the new donor were compared to the linearized version of I2I7C7SDMTemplate-F following *EcoRI* and *XhoI* digestion by gel electrophoresis. Alignment of the Sanger sequenced NILV-I2I7C7-SDMTemplate-F (sequence in red) with NILV-I2I7C7-SDMTemplate. Blue arrow on the NILV-I2I7C7-SDMTemplate-F represents the primer used to confirm the flipped orientation of the donor template by Sanger sequencing. **C**. I2I7C7SDMTemplate-F transfer vector, 2nd generation packaging system and envelope plasmids were transfected into HEK-293T to make the NILV-I2I7C7SDMTemplate-F. Physical titre was evaluated by quantitative measurement of HIV-p24 protein by ELISA in cell culture supernatant. The standard line was obtained using known concentrations of HIV-p24 protein (black dots). From this, the concentration of NILV-I2I7C7SDMTemplate-F (red dot) was determined and equated to 1.25x109 TU/mL. Abbreviations: OD, optical density; TU, transducing unit; PP, Physical particle; LTR: Long terminal repeats; ψ: psi packaging signal; RRE: rev response element; cPPT: central polypurine tract; WPRE: woodchuck hepatitis posttranscriptional regulatory element; CMV: cytomegalovirus promoter; gag/pro-pol: HIV-1 structural and accessory polyproteins; Δ64: substitution of aspartic acid to valine in HIV-1 integrase; tat: HIV-1 trans-activating regulatory protein; rev: HIV-1 accessory protein; polyA: polyadenylation tail; VSV-G: vesicular stomatitis virus glycoprotein.

3.10 *In situ* integration of NILV-donor template by HDR mediated by Lentiviral delivery of guide RNA

In order to achieve the highest levels of donor template integration, an optimal time point delivery for the NILV-I2I7C7-SDMTemplate-F was conducted. As described previously, HaCaT cells were transduced with LentiV2-Ex3D (MOI 20) followed by electroporation of 10µg of SpCas9 mRNA at day 3 post transduction. In order to synchronize Cas9-mediated DNA cleavage with reverse transcription of the donor template upon infection, LentiV2-Ex3D-transduced HaCaT cells were infected with NILV-I2I7C7-SDMTemplate-F at MOI 20, either 30 minutes or 24 hours post electroporation. In parallel, co-infection of HaCaT cells with LentiV2-Ex3D and NILV-I2I7C7-SDMTemplate-F on day 0 followed by SpCas9 mRNA electroporation on day 3, was evaluated (**Figure 3.9A**). HaCaT cells transduced with LentiV2-Ex3D alone or infected with only the donor template were used as negative controls. Targeted integration was evaluated 15 days post NILV-I2I7C7-SDMTemplate-F infection to ensure complete absence of the episomal donor within the cells. To do so, a 5' (TI-5') and 3' (TI-3') donor-genome junction PCRs were established. Two sets of primers were designed to amplify from exon 2 (TI-5') and 8 (TI-3') of the endogenous *COL7A1*

to the SDMs previously introduced by Dr. Christos Georgiadis in exon 4 for TI-5' and TI-3', respectively. Keratinocyte treated with NILV donor showed positive amplicons for the 5' and 3' junctions consistent with the expected homologous recombination (973bp and 1007bp respectively) (**Figure 3.9B**). Sequence specificity of TI5'/TI3' PCRs was assayed by Sanger sequencing.

To precisely quantify the percentage of the integrated template, a second 5' donor-genome junction PCR was developed. Primers were designed to amplify from exon 2 (region outside the donor template) *COL7A1* to exon 4. The latter primer was designed to recognize both endogenous and donor template sequences in order to quantify targeted integration. HDR rates analysed by Sanger sequencing-based ICE analysis showed 9% and 11% of donor integration when NILV template was administered 30 minutes and 24 hours post SpCas9 mRNA electroporation, respectively, and 5% when keratinocyte cells were co-infected with both LentiV2-Ex3D and NILV-I2I7C7-SDMTemplate-F on day 0 (n=3) (**Figure 3.9C**).

Cells treated with NILV-I2I7C7-SDMTemplate-F 24 hours post SpCas9 mRNA electroporation were further analysed by Next Generation Sequencing (NGS) under supervision of Dr. Athina Soragia Gkazi. Quantification of the overall HDR events showed an average of 15.8% of perfect target integration and only 0.32% of imperfect HDR due to co-presence of InDels or mutations alongside the intended SDMs (**Figure 3.9D**).

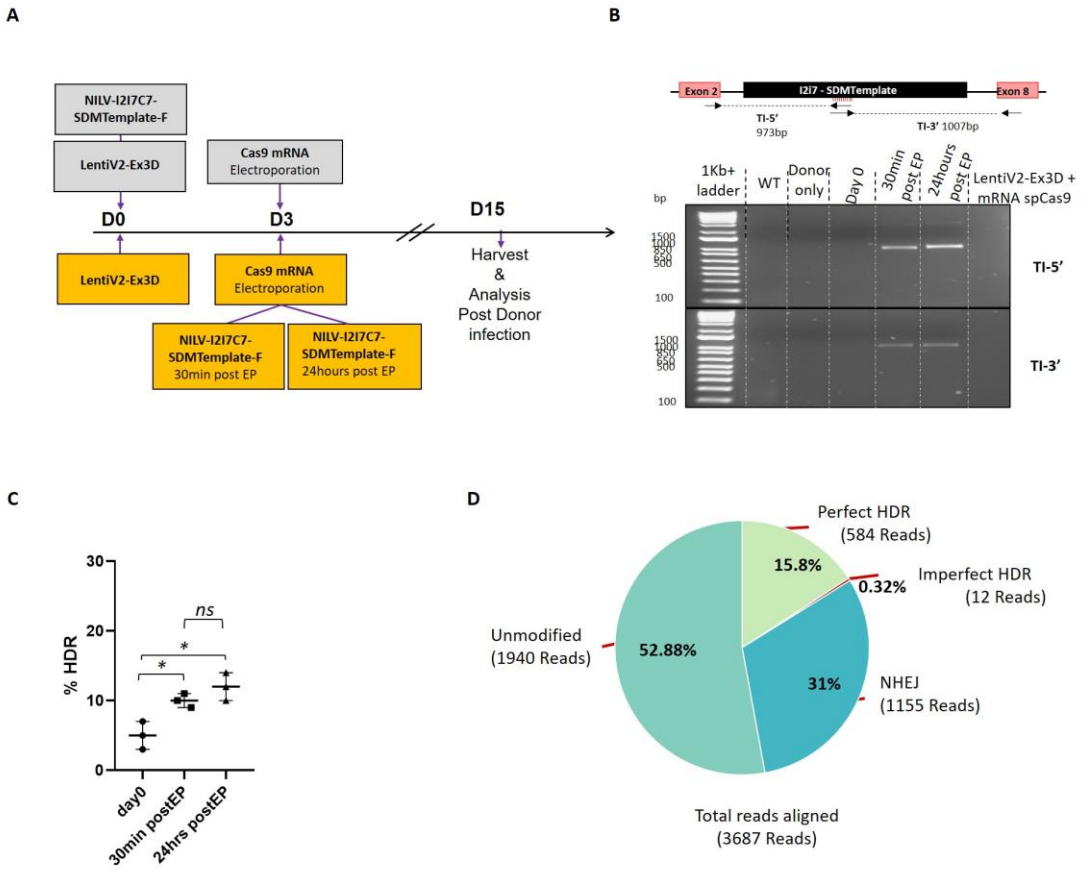

Figure 3.9 Targeted *donor template* integration using LentiV2-EX3D+ SpCas9 mRNA and NILV-I2I7C7-SDMTemplate-F

A. Schematic illustration of donor-CRISPR/Cas9 delivery strategy. Red boxes represent cells co-infected with NILV-donor and LentiV2-Ex3D on day 0 followed by SpCas9 mRNA electroporation 3 days post infection. Blue boxes represent cells treated on day 0 with LentiV2-Ex3D and electroporated with SpCas9 mRNA on day 3 followed by NILV-donor infection 30 minutes or 24 hours post electroporation. Cell were then harvested and analysed for donor template integration 15 days post NILV-donor infection. **B.** Targeted-PCR analysis of keratinocytes transduced with NILV-I2I7C7SDMTemplate-F donor with LentiV2-Ex3D+ SpCas9 mRNA on day 0, 30 minutes and 24 hours post SpCas9 mRNA electroporation, respectively. The 5' and 3' junctions (TI-5` and TI-3`) between the donor cassette and the *COL7A1* genomic locus were amplified by specific primers designed across the SDMs introduced within exon 4 of I2I7C7SDMTemplate-F (indicated by red and black arrows). The 5' and 3' junctions (TI-5` and TI-3`) amplicons showed 973bp and 1007bp bands, respectively. **C.** Quantitative evaluation of HDR-mediated donor integration delivered on day 0, 30 minutes and 24 hours post SpCas9 mRNA electroporation. Sanger sequencing-based ICE showed up to 9% and 11% of HDR when the NILV donor was administered 30 minutes and 24 hours post SpCas9 mRNA electroporation, respectively (n=3, p=0.1963)). Appreciable 5% of HDR was also detected when keratinocyte cells were co-infected with both LentiV2-Ex3D and NILV-I2I7C7SDMTemplate-F on day 0.

Comparison between groups was carried out using a one-way ANOVA test (* p <0.0143). Line represents mean of the group, with errors representing SEM. **D.** NGS analysis quantifying *COL7A1* donor integration in cells treated with LentiV2-Ex3D + NILV-donor delivered 24 hours post SpCas9 mRNA electroporation. The sample showed a total of 3687 reads aligned with the wild type *COL7A1* reference. 15.8% of perfect HDR (584 reads), 0.32% imperfect HDR (12 reads), 31% of NHEJ events (1155 reads) and 52.88% of unmodified reads (1940 reads).

3.11 Gene correction mediated by Cas9 RNP and NILV-donor

As previously described in **section 3.7**, CRISPR/Cas9 reagents delivery through Ex3D-RNP complex resulted in a significantly higher amount of InDels compared to LentiV2-Ex3D + SpCas9 mRNA delivery. Therefore, HDR correction using the Ex3D-RNP along with NILV-I2I7C7-SDMTemplate-F was evaluated. Similarly to what previously observed for coupled viral guide RNA delivery and donor template, a time point experiment for NILV-template infection was carried out. Keratinocytes were infected with NILV-I2I7C7-SDMTemplate-F (MOI 20) on day 0 followed by electroporation with Ex3D-RNP complex 1, 2 or 3 days post-infection. In parallel, HaCaT cells were electroporated with the RNP complex followed by NILV donor template infection 30 minutes post sgRNA-Cas9 delivery (**Figure 3.10A**). 21 days post infection, PCR of the TI-5' donor-genome junction for the detection of the donor was performed followed by gel electrophoresis (**Figure 3.10B**). Cells treated with the strategy described in **section 3.9** were used as a positive control. Gel bands for TI-5' showed the expected integration of the donor template for each condition tested (973bp). No bands were observed in cells treated with the donor template only. Quantification of the total editing (NHEJ+HDR) and the targeted donor template integration events were evaluated by Sanger sequencing followed by ICE analysis (**Figure 3.10C**). Up to 40% of donor template integration was detected when NILV template was delivered into the cells 30 minutes post RNP electroporation. By contrast, an average of 30%, 16% and 2% of HDR events were detected when cells were electroporated with the RNP on days 1, 2, 3 days post NILV infection, respectively. No differences in total editing amount (HDR and NHEJ events) were observed in all samples.

Quantification of the intended nucleotide changes by NGS of the bulk population showed up to 41% of perfect HDR when cells were infected with the NILV donor

template 30 minutes post RNP electroporation (**Figure 3.10D**). Only 0.52% of imperfect HDR due to co-presence of InDels or mutations was observed. However, cells receiving the RNP complex 1, 2 or 3 days post NILV infection showed a decreasing HDR efficiency of 32%, 8% and 1.6%, respectively. The gene-corrected bulk population showing the highest HDR efficiency was further cultured as single cell clones by limiting dilution.

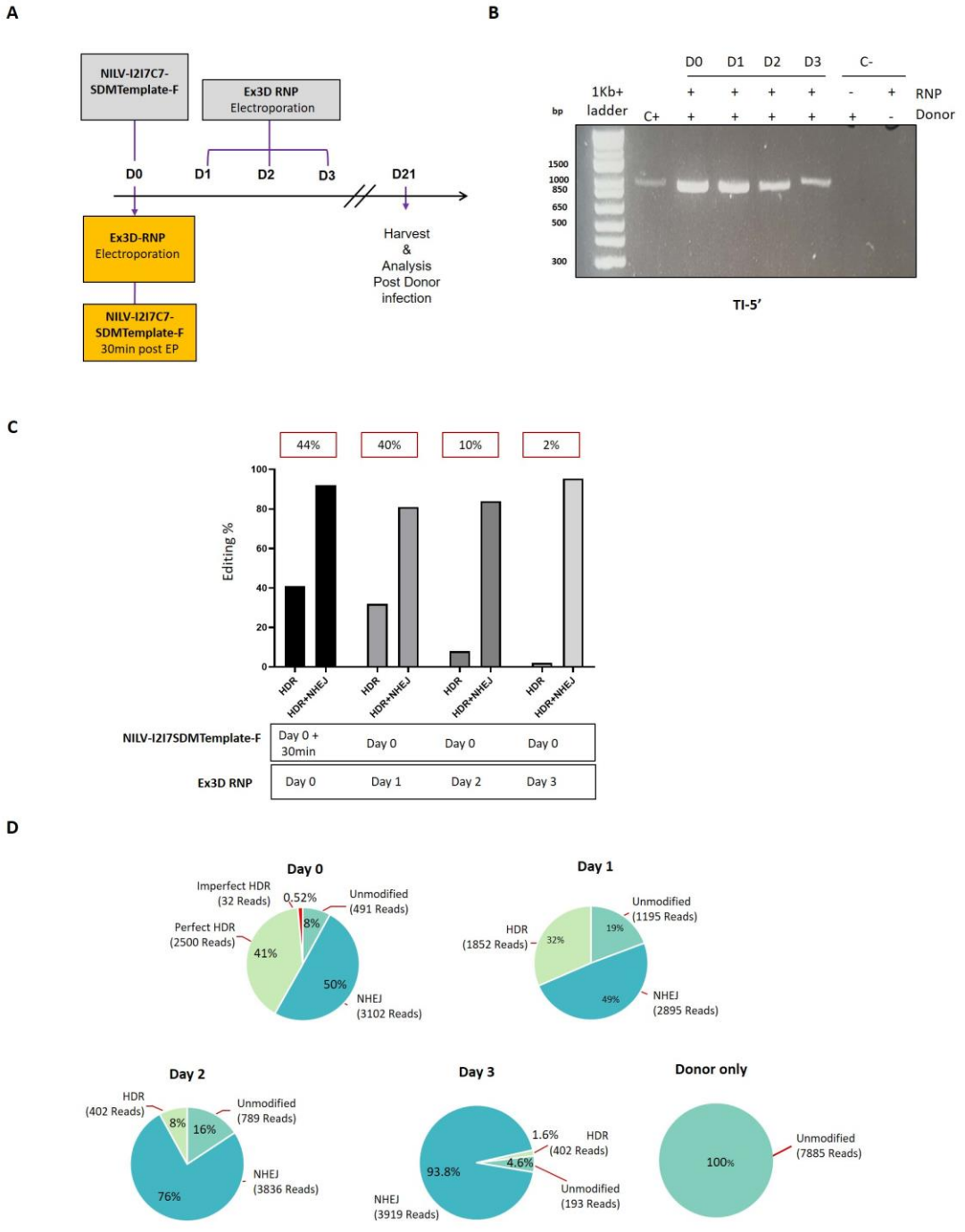

Figure 3.10 Targeted *donor template* integration using NILV-I2I7C7SDMTemplate-F and Ex3D-RNP

A. Schematic illustration of NILV-donor template and RNP-Cas9 delivery strategy. Red boxes represent the timeline of the first strategy of the study with cells receiving the Ex3D-RNP on day 0 followed by infection with NILV-donor 30 minutes post electroporation. The blue boxes represent cells treated on day 0 with NILV-donor and electroporated with Cas9 RNP 1, 2 and 3 days post infection. Cell were then harvested and analysed for donor template integration 15 days post NILV-donor infection (day 21). **B.** Targeted-PCR analysis of bulk populations transduced with NILV-I2I7C7SDMTemplate-F donor at 0, 1, 2 and 3 days post Ex3D-RNP electroporation. The 5' COL7A1–donor junction (TI-5` and TI-3`) was amplified by specific

primers designed across the SDMs introduced within exon 4 of I2I7C7SDMTemplate as previously shown in **Figure 3.8**. The 5' junction (TI-5`) amplicons showed 973bp band for each condition tested. **C.** For quantitative evaluation of donor integration, comparison of HDR rates in the gene edited populations (HDR+NHEJ) was performed on genomic level by Sanger sequencing-based ICE across the TI-5' junction. The highest HDR rate (44%) was observed in cells receiving both Ex3D RNP and NILV-donor on day 0. Lower integration frequencies were measured upon delivery of SpCas9 RNP at 1 (40%), 2 (10%) and 3 (2%) days post NILV donor infection (n=1) **D.** NGS analysis quantifying *COL7A1* donor template integration in cells treated with NILV-donor delivered on day 0 and electroporated with Ex3D-RNP on day 0 or on day 1, 2, 3 post donor delivery. NGS in cells receiving NILV-donor only was used as negative control. Each NGS sample shows percentages of perfect HDR, imperfect HDR, NHEJ events and unmodified reads. Up to 41% HDR was detected in cells receiving donor template 30 minutes after Ex3D RNP electroporation (n=1).

A total of 23 clones were expanded and sequenced for the detection of SDMs by PCR of the TI-5' donor-genome junction (**Figure 3.11A**). 15 out of 23 clones analysed by TI-5' PCR were positive for the presence of the donor template. Three different clones, clone 1 (bi-allelic for *COL7A1* knockout), clone 5 (bi-allelic HDR) and clone 14 (mono-allelic HDR) were further analysed by Sanger sequencing and NGS (**Figure 3.11B**). NGS for the quantification of the intended nucleotide changes within the exon 3 confirmed the *COL7A1* genotype observed by Sanger sequencing. Clones 1, 5 and 14 were further analysed for C7 expression *in vitro* (**Figure 3.11C**). Immunofluorescence staining for C7 showed a complete protein rescue in both bi- and mono-allelic HDR clones, whereas complete absence of C7 in clone 1 confirmed the bi-allelic knockout observed on DNA level.

A

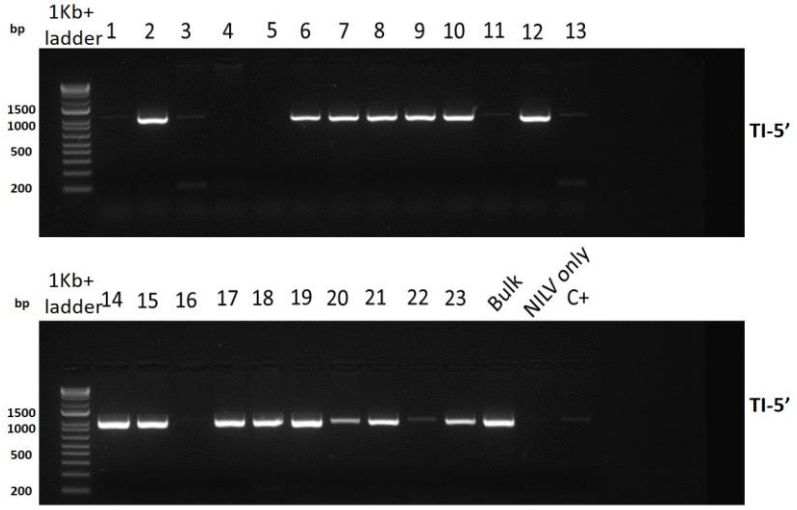

B

Allelic variation by NGS

	Reads Aligned	Indel %	HDR %
Clone 1	6546	6539 (99.9%)	2 (0.0%)
Clone 5	6440	11 (0.2%)	6417 (99.6%)
Clone 14	5983	79 (1.3%)	3261 (54.5%)

C

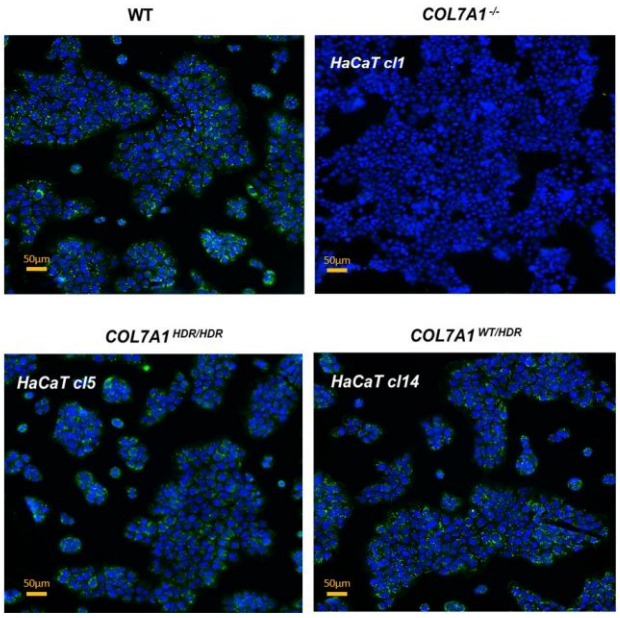

Figure 3.11 Clonal analysis of NILV-I2I7c7SDMTemplate-F corrected keratinocytes

A. From the cell population treated with EX3D-RNP and NILV-donor at day 0, 23 clones were isolated and screened for the incorporation of the donor template by TI-5' donor-junction PCR. NILV-donor only and LentiV2-Ex3D+ Cas9 mRNA + NILV (section 3.3.7) cells were used as negative and positive control, respectively. 65% of the clones screened (15 out of 23) showed the 973bp band indicating the integration of the donor template. **B.** NGS analysis of three representative clones: bi-allelic knockout (clone 1), mono-allelic (clone 14) and bi-allelic

(clone 5) for donor template integration. **C.** *In situ* Immunofluorescence staining for C7 protein expression in HaCaT clones. Top left panel indicates wild type (WT) cells expressing C7 (green). Top right panel shows absence of C7 expression representing the bi-allelic knockout. Bottom left panel shows bi-allelic corrected clone (clone 5). Bottom right panel shows mono-allelic donor template integration (clone 14). Nuclei were stained with DAPI (blue). Scale bar = 50µm.

3.12 Modelling a ssODN-based gene correction strategy to correct the *COL7A1* locus

CRISPR/Cas9-mediated HDR using double stranded DNA (dsDNA) donor templates offers the ability to generate large gene knock-ins, thereby providing an *in situ* correction of the targeted gene under its endogenous promoter. However, dsDNA donor templates are more readily incorporated by the dominant NHEJ process, resulting in duplication of homology arms or partial incorporation of the dsDNA template. Homology-independent insertion events by NHEJ can also occur at off-target DSBs or naturally occurring endogenous DSBs. To avoid these undesired consequences, single-stranded oligodeoxynucleotides (ssODNs) have been recently shown to correct a single mutation with high efficiency of small edits in primary cells and cell lines (Richardson et al., 2016; Paquet et al., 2016; Kwart et al., 2017; Martin et al., 2019). As previously described for SpCas9 mRNA and RNP, single-stranded oligo DNA became available during the project therefore development and evaluation of this approach was tested in real-time. In this second section, I describe proof-of-concept of targeted base correction of the c425A>G *COL7A1* mutation via HDR using an ssODN as donor template.

For significant levels of HDR to occur using ssODN as a donor template, it was shown that the sgRNA has to be designed in proximity of the target Cas9-mediated DSBs due to inverse correlation between ssODN size and editing efficiency (Paquet et al., 2016; Kwart et al., 2017; Yang et al., 2013b). Therefore, a new guide (Ex3-"proximal" or Ex3P) was designed to target in close proximity to c.425A>G point mutation. In detail, the A>G splice site transition falls in the "N" position of the PAM sequence (**Figure 3.12A**) with a predicted cutting site at 3bp away from the target mutation. This

particular design guarantees its use of in both wild type and RDEB cells. The designed Ex3P-sgRNA was synthesized *in silico* by Synthego (Synthego Corporation, California, USA) ensuring its high stability. The new guide design was evaluated *in silico* using the Benchling design tool (https://benchling.com/crispr) (**Table 3.3**).

Table 3.3 Guide sequence tested for ssODN-mediated c.425G>A correction

Guide	Sequence	PAM	Strand	On-Target Score	Off-target Score
Ex3P	GGCCCGACCTGGTGTCCCCA	AGG/GGG (c.425A>G)	sense	56.1	37.5

Guide Ex3P was used to assess the NHEJ efficiency for exon 3 of *COL7A1*. Guide orientation is shown as sense or anti-sense and binds complementary DNA strand by Watson and Crick base pair. In red, the PAM in wild type cells (left), in green the PAM in c.425A>G RDEB iPSCs. On-target score is the target activity evaluated by the algorithm developed by Doench, Fusi *et al*. (Doench et al., 2016) The score is from 0-100 and higher scores mean higher on-target activity. Off-target score is evaluated according to the number of mismatches between the selected guide RNA and similar exonic off-target site (Hsu et al., 2013). The score is from 0-100 and higher scores mean lower off-target activity.

Comparison of targeted NHEJ using SpCas9 protein complexed with either chemically modified Ex3D-sgRNA or Ex3P-sgRNA, at molar concentrations described in **section 3.6**, was carried out in HaCaT cells. Similar percentages of occurring InDels were observed on genomic level (91% and 92% NHEJ for Ex3D-sgRNA and Ex3P-sgRNAs, respectively n=1) (**Figure 3.12B**). In order to overcome technical volume limitations associated with co-delivery of non-viral donor templates and CRISPR/Cas9 reagents by electroporation, SpCas9 was delivered as mRNA rather than RNP complex. No impact on NHEJ efficiency was observed between the two SpCas9 delivery methods (data not shown).

Furthermore, to prevent cellular toxicity following electroporation, the volume of CRIPSR/Cas9 reagents delivered was limited to ≤10% of the total electroporation volume as suggested by the manufacturer instruction. To do so, decreasing concentrations of Ex3P-sgRNA (from 1 µg to7µg) and SpCas9 mRNA (1.25, 2.5, 5, 7.5, 10µg) were investigated in order to minimize the volume of CRISPR/Cas9 reagents delivered while achieving high levels of knockout efficiency (**Figure 3.12C**). The

reason of this volume reduction is also essential to accommodate in the same reaction mix the amount of donor template needed for HDR-based corrections. With regards to Ex3P-sgRNA titration, Sanger traces of the amplified gene edited locus subjected to ICE analysis revealed a similar trend in genomic disruption among different concentrations reaching a plateau of InDels of approximately 86% after delivering 4µg of sgRNA (**Figure 3.12C**).

Similar titration repeated on SpCas9 mRNA showed Cas9-induced *COL7A1* knockout plateauing when 5µg of the nuclease was used, with approximately 85% of NHEJ efficiency (n=1).

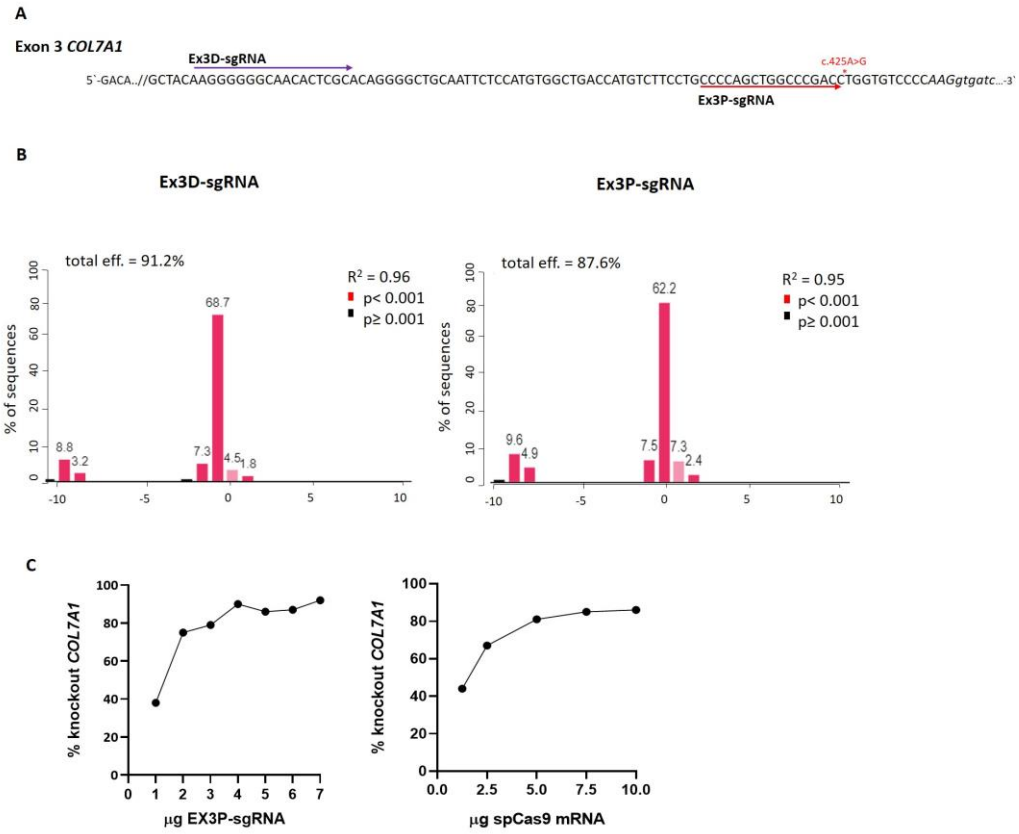

Figure 3.12 Design of a new sgRNA guide for complete non-viral COL7A1 correction

A. The magnified view illustrates the end of exon 3 of *COL7A1*. Purple arrow represents the Ex3D-sgRNA, red arrow shows the new designed sgRNA (Ex3P-sgRNA) close to the c.425A>G point mutation (red asterisks). In italics, the splicing donor sequence of exon 3. **B.** Keratinocyte cells were electroporated with 10 µg of SpCas9 mRNA in combination with Ex3D-sgRNA or Ex3P-sgRNA. Comparative analysis of NHEJ mediated by both sgRNAs showed similar editing percentages (91.2% and 87.6% respectively). **C.** Titration of Ex3P-sgRNA and SpCas9 mRNA amounts were performed in keratinocyte cells and quantification of InDels revealed stable knockout of around 86% from 4µg of Ex3P-sgRNA. Similar percentages of

NHEJ were observed in SpCas9 mRNA titration experiment reaching a plateau at 5µg of Cas9 with up 80% of InDels.

3.13 ssODN donor template design to correct the mutation hotspot c.425A>G *COL7A1*

Combinations of biophysical parameters that can influence integration of ssODN upon DNA cleavage (Richardson et al., 2016) and phosphorothioate-modifications (PS) (De Ravin et al., 2017) were taken into consideration for ssODN donor template design. In detail, a 127bp synthetic ssODN either homologous to the non-target strand (NT-2P-ssODN-AAA) or to the target strand (T-2P-ssODN-AAA) with 36bp and 91bp homology arms to the PAM-distal and PAM-proximal side from the cutting site, respectively, were designed and synthesized bearing two phosphorothioate bonds (PS bonds) flanking the last 5` and 3` ends (**Figure 3.13A**). Phosphorothioate modifications within the donor template were previously shown to protect against nuclease degradation resulting in higher level of gene correction (De Ravin et al., 2017; Renaud et al., 2016). To prevent unwanted Cas9 re-cutting upon donor template integration, G>A transition has been introduced within the NGG PAM sequence (AGG>AAA) recognized by the Ex3P-sgRNA (Paquet et al., 2016). This PAM-blocking mutations within the donor template results in a single and double mismatch/es when aligned with the wild type COL7A1 sequence (AGG>AAG) and the c.425A>G mutated allele (GGG>AAG) in patient cells, respectively. This particular donor configuration prevents further Cas9 editing after ssODN integration in both wild type and RDEB cells. In addition, the presence of the mismatch in the donor template did not interfere with the wild type amino acid sequence of exon 3 *COL7A1* (AAG>AAA>Lys) (**Figure3.13A**).

Initial comparison between the two designed ssODNs, was performed in HaCaT cell line electroporating 10µg of NT-2P-ssODN-AAA and T-2P-ssODN-AAA alongside optimized concentrations of Ex3P-sgRNA and SpCas9 described in **section 3.11**. Sanger-based quantification of the intended nucleotides changes upon donor integrations was used to assess the percentage of homologous recombination.

Insertion of donor mismatches using the donor NT-2PS-ssODN-AAA showed high percentage of integration events (93%) whereas lower HDR rate (76%) was observed using the complementary T-2PS-ssODN-AAA donor (n=1) (**Figure 3.13B**). Furthermore, titration of NT-2P-ssODN-AAA at concentrations of 1.25µg, 2.5µg, 5µg and 10µg, resulted in significant levels of HDR reaching the plateau at concentrations of 2.5µg (90% HDR, **Figure 3.13C**). In line with the amount of ssODN used in Richardson study, 5µg of the NT-2PS-ssODN-AAA donor configuration was chosen for downstream applications. Quantification of the intended nucleotide changes by NGS of the bulk population treated with 5µg of NT-2PS-ssODN-AAA showed up to 87% of perfect HDR events and 5% of imperfect HDR integration due the co-presence of unwanted point mutations alongside the intended modification. Undesired on-target repair by NHEJ was detected in around 8% of the cells (**Figure 3.13D**).

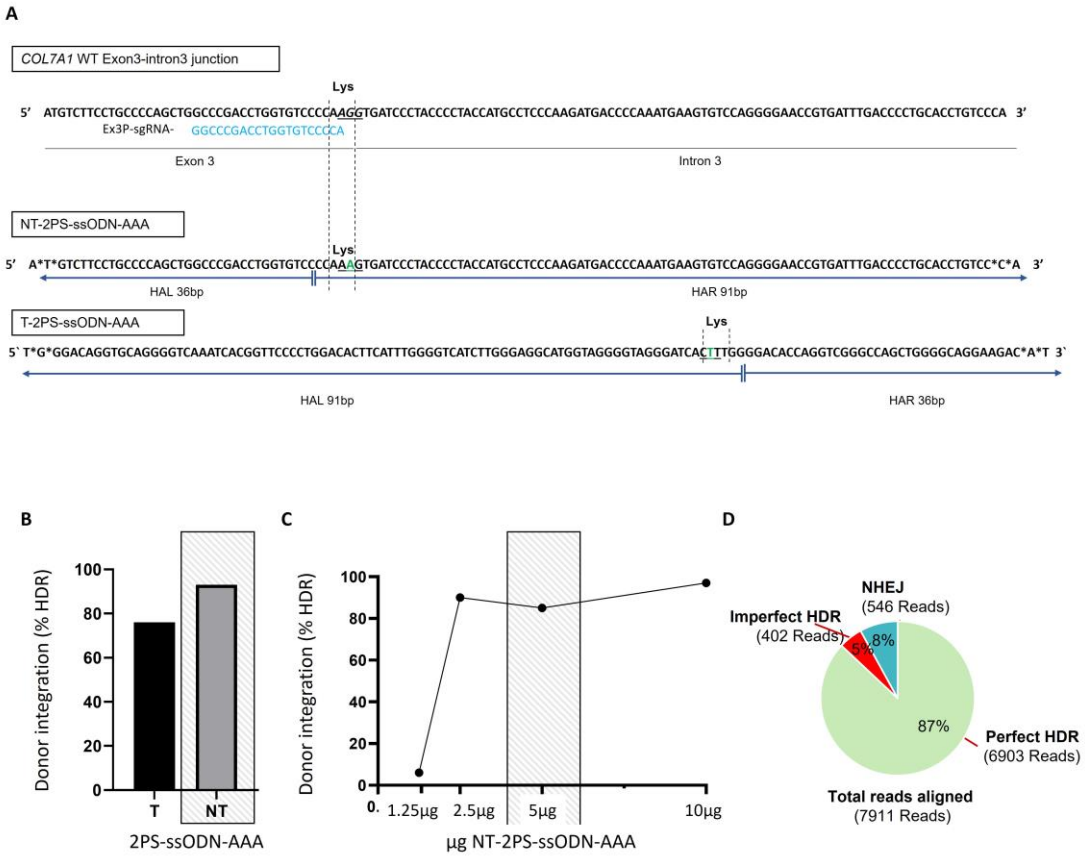

Figure 3.13 Design and gene correction using non-viral ssODN donor template

A. The magnified view illustrates the end of exon 3 of *COL7A1* in wild type cells (AAG). Underlined, the AGG PAM sequence recognized by the Ex3P-sgRNA (protospacer shown in blue). Black dot lines show the last exon 3 triplet encoding for a lysine (Lys>AAG). Below, nucleotide sequence of ssODNs complementary to target (NT-2PS-ssODN-AAA) and non-target (T-2PS-ssODN-AAA) *COL7A1* strands. Black asterisks indicate the phosphorothioate bonds (2PS) flanking the last 5` and 3` ends of each ssODN. The asymmetric homology arm left (HAL) and right (HAR) are showed by blue arrows. **B.** Evaluation of ssODN-mediated HDR by ICE analysis of cells electroporated with 10µg T-2PS-ssODN-AAA (black bar) and NT-2PS-ssODN-AAA (grey bar). Cells receiving the NT-2PS-ssODN-AAA template showed up to 93% of knock-in rate whereas 76% HDR with the complementary donor. **C.** Titration of NT-2PS-ssODN-AAA amount in HaCaT cells. Quantification of donor integration by Sanger sequencing revealed high knock-in starting at 2.5µg (90%) and plateauing thereafter. **D.** NGS analysis quantifying *COL7A1* donor integration in cells treated with 5 µg of NT-2PS-ssODN-AAA donor template. The NGS sample shows percentages of perfect HDR (87%), imperfect HDR (5%), and NHEJ events (8%).

3.14 Efficiency of HDR-mediated correction in keratinocytes treated with SpCas9 mRNA and ssODN

To confirm the expression of the gene-edited Col7 transcripts upon integration of the NT-2PS-ssODN-AAA-donor template, cells were harvested and the total RNA extracted. Isolation of *COL7A1* edited clones was not performed due to the high percentage of donor integration confirmed by NGS in the initial electroporated population. Total cDNA was obtained by RT-PCR and a PCR across exon 2 to exon 4 of *COL7A1* was performed to allow for the detection of correct exon 3 splicing in the gene edited cells. Untreated HaCaT cells were used as a positive control. Gel electrophoresis of the PCR product from gene-edited cells showed unexpected 4 different bands at 366bp, 279bp, 175bp and 119bp suggesting that splicing aberrations have occurred upon insertion of NT-2PS-ssODN-AAA (**Figure 3.14A**). All the observed amplicons were gel extracted and PCR purified and sent for Sanger sequencing. Alignment of Sanger traces from the cDNA amplicons with the wild type *COL7A1* RefSeq confirmed that the silent mutation inserted within the donor template interfered with the correct *COL7A1* splicing between exon 3 and exon 4. The impaired splicing pattern observed was similar to that reported in the amplified splice site region of c.425A>G alleles in RDEB patients using similar primers for the detection (Gardella et al., 1996). As previously observed from Gardella *et al*., analysis of the 366bp band confirmed the (89bp) retain of intron 3 within the Col7 transcript whereas partial or complete exon skipping of exon 3 was observed in band 170bp and 130bp, respectively (**Figure 3.14B**). Based on the intensity of the PCR bands, the majority of the cells within the bulk population harboured a 279bp amplicon with similar molecular weight of the amplicon in the positive untreated control (280bp). Sanger sequencing analysis of the 280bp band confirmed the presence of a 1bp Cas9-induced indel at the level of the second-last triplet of exon 3. The depleted C falls within the predicted Cas9-induced DSB site when using the Ex3P-sgRNA. The relative frequency of 1bp deletion upon Ca9-induced knockout comprise around 70% of editing outcomes observed in my data (representative InDels distribution in (**Figure 3.12B**)). *In silico* analysis of the 1bp edited sequence using the Benchling tool revealed that this recurrent deletion creates a frameshift of the *COL7A1* reading frame leading

to a stop codon within exon 4 at the amino acid 146 (p.Leu146X) (**Figure 3.14B**). Flow cytometry analysis showed marked decrease of C7 expression in the gene-edited population compared to wild-type HaCaTs. Only up to 10% of C7 protein expression was detected suggesting that only cells that did not integrate CRISPR/Cas9 in their nucleus were able to express full-length C7 (**Figure 3.14C**). The observed splicing aberration was also confirmed *in silico* using a bioinformatics tool for prediction of effects of mutations on splicing signals in human sequences (Human Splicing Finder v3.1) (http://www.umd.be/HSF/). The analysis revealed that one of the 'Cas9-blocking' G>A transitions introduced in the NT-2PS-ssODN-AAA fell in position -2 of the consensus sequence of the exon 3 splice donor site, thereby accidently recapitulating the molecular splicing impairment observed in RDEB patients bearing c.425A>G point mutations (Gardella et al., 1996).

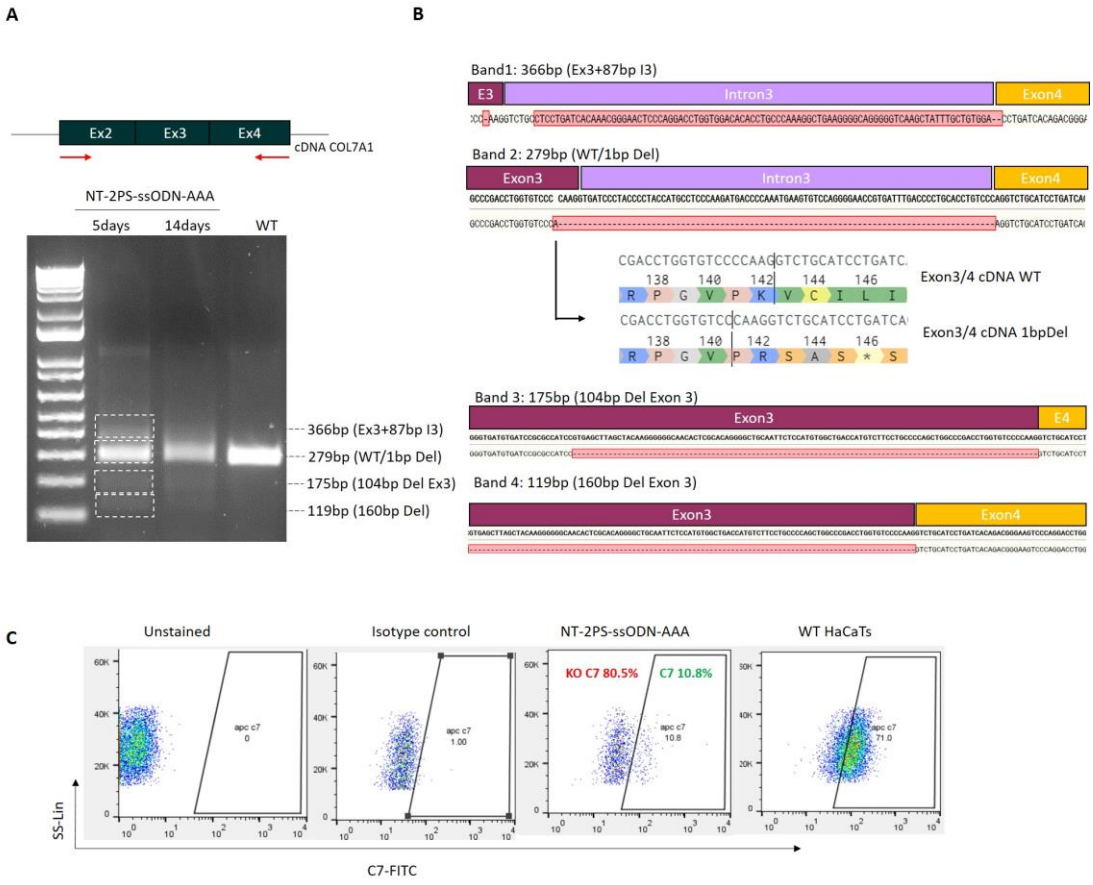

Figure 3.14 Splicing impairments after integration of NT-2PS-ssODNAAA donor template

A. PCR amplification of *COL7A1* cDNA across the NT-2PS-ssODN-AAA integration site. Cells treated with NT-2PS-ssODN-AAA and harvested on days 5 and 14 post electroporation displayed spicing aberration events across exons 3 intron-junction. Gel electrophoresis of the PCR amplicons showed 4 bands of different molecular sizes replicating the pattern observed in RDEB patients with c.425A>G mutation (Gardella et al., 1996). **B.** Alignment of Sanger sequenced gel extracted bands with wild type exons 3 and 4 of *COL7A1 cDNA* showed the following splicing and transcription impairments 1) partial retention of intron 3 (366bp), 2) 1bp deletion (279bp) leading to a frameshift in *COL7A1* coding region creating a stop codon within exon 4, 3) partial (104bp Del) (175bp) and 4) complete (160bp Del) (119bp) exon 3 skipping. **D.** Flow cytometry analysis of cells edited with NT-2PS-ssODN-AAA showed that only unedited cells were able to express C7 (10.8%).

To overcome these unexpected problems associated with the use of NT-2PS-ssODN-AAA donor template, a revised ssODN (NT-2PS-ssODN-AAG) was designed (**Figure 3.15A**). In this new configuration, mismatches designed across the Ex3P-sgRNA protospacer sequence were introduced instead of PAM-blocking mutation. It has been reported that two mismatches within a window of 10bp from the predicted DSBs are enough to impede Cas9-re-cutting upon donor integration (Paquet et al., 2016). Therefore, two single C>G silent mutations were introduced in position +2 and +5 from the PAM sequence (**Figure 3.15B**). The newly introduced mismatches did not fall within the splicing donor consensus sequence, thereby preserving the PAM sequence (AGG) and the final codon of exon 3 (AAG).

Similar to what was shown with the previous ssODN donor design, delivery of NT-2PS-ssODN-AAG in HaCaTs resulted in up to 92% of total editing of which 79% of NHEJ and a 13% of the intended C>G integration by HDR. Only 5% of the electroporated cell bulk was unedited for *COL7A1*. Despite the lower knock-in rate obtained at this round of electroporation, gene edited cells analysed by flow cytometry showed 19.5% of residual C7 expression (**Figure 3.15C**). These results are in line with what was observed on genomic level, where a total of 18% (5% unedited and 13% HDR) of cells could potentially express C7. Importantly, these results confirm that the NT-2PS-ssODN-AAG donor does not interfere with the correct expression of C7 upon HDR-mediated integration.

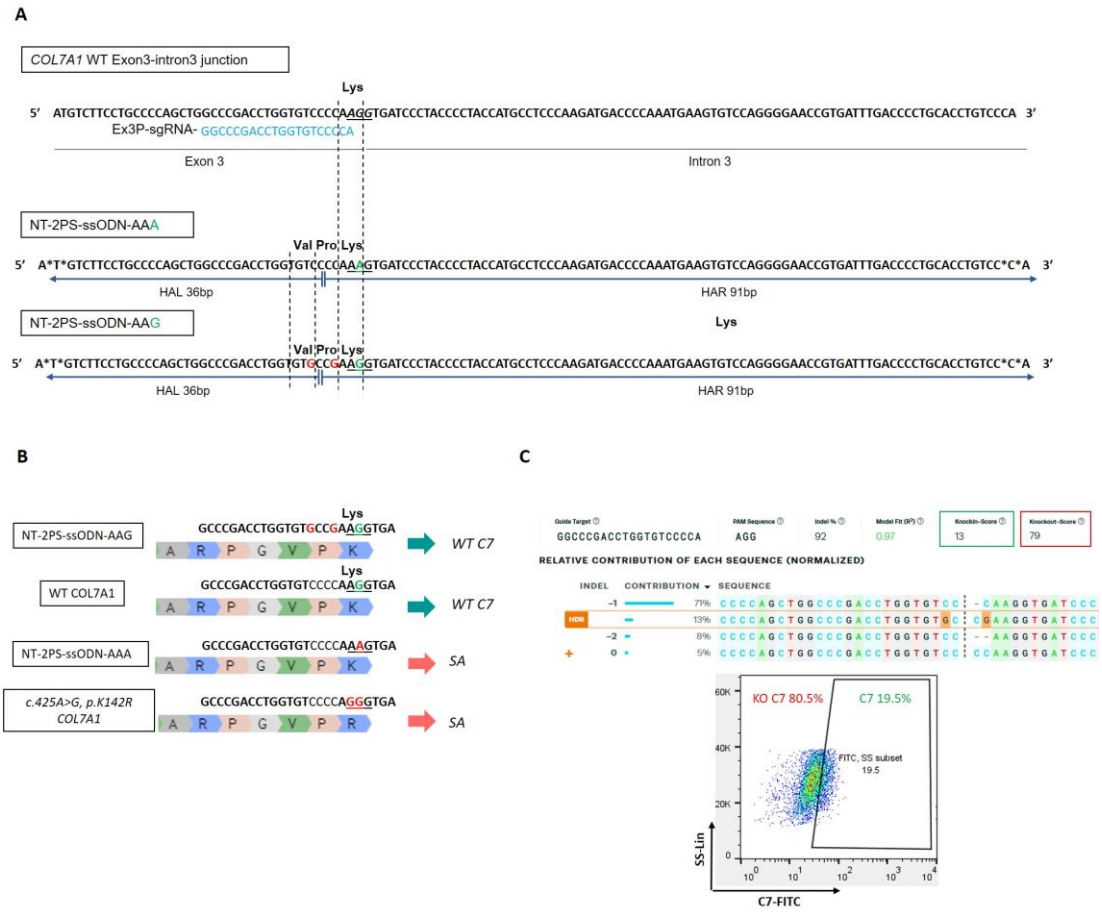

Figure 3.15 Comparative design of NT-2PS-ssODN-AAA and NT-2PS-ssODN-AAG

A. The magnified view illustrates the end of exon 3 of *COL7A1* wild type sequence (AAG). Underlined, the AGG PAM sequence recognized by the Ex3P-sgRNA (protospacer shown in blue). Black dot lines show the last exon 3 triplet encoding for a lysine (AAG). Below, comparison of donor design between NT-2PS-ssODN-AAA and NT-2PS-ssODN-AAG. The new donor was designed with the same orientation (non-target, NT) and with asymmetric homology arm left (HAL) and right (HAR). Black asterisks indicate the phosphorothioate (2PS) bonds flanking the last 5` and 3` ends of the ssODN. In contrast to the previous design, the last triplet sequence of exon 3 (AAG) remained unaltered. Instead, two C>G sgRNA blocking mutations were introduced (shown in red). **B.** Prediction of the mismatches introduced within NT-2PS-ssODN-AAA and NT-2PS-ssODN-AAG donors upon HDR and their potential effects on C7 transcription. Wild type (WT) and c.425A>G RDEB genomic and amino acid sequences are also shown. Upon integration of NT-2PS-ssODN-AAG, no perturbations in C7 transcription and translation (WT C7) are expected. Whereas similar splicing aberration (SA) are predicted in RDEB c.425A>G *COL7A1* and NT-2PS-ssODN-AAA donor sequences. **C.** Sanger based-ICE analysis and flow cytometry confirmed that cells integrating the NT-2PS-ssODN-AAG donor template are able to express C7. All values presented here in this figure are gated on the C7- (80.5%) and C7+ (19.5%) cells.

3.15 Chapter Discussion

This chapter of work describes the development of novel CRISPR/Cas9 platforms for the correction of a RDEB mutation hotspot via *in situ* Homology Directed Repair (HDR)-mediated donor integration upon Cas9-induced DSBs. For significant levels of donor integration to occur, it has been demonstrated that higher frequency of Cas9-induced DSBs (NEHJ) increase the likelihood of the target site to be repaired by HDR (Remy et al., 2014; Duda et al., 2014; Hendel et al., 2014). In this direction, preliminary guide RNA screening was performed to allow for the highest levels of DSBs in exon 3 of *COL7A1*. Using a similar strategy reported for RDEB by Izmiryan *et al.* (Izmiryan et al., 2018), high levels of editing efficiency were achieved in a keratinocyte cell line using NILV-based delivery of the SpCas9 cassette and sgRNA. However, utility of this platform is limited due to potential proviral DNA integration and long-term expression from episomal cassette, which could be detrimental for cell viability and increase the possibility of off-target events (Izmiryan et al., 2018; Kim et al., 2014; Nightingale et al., 2006).

The study by Georgiadis *et al.* demonstrated that high levels of on-target TCR disruption, with undetectable levels of off-target SpCas9 scission effects, can be achieved by co-delivery of a lentiviral vector expressing sgRNA and SpCas9 mRNA by electroporation (Georgiadis et al., 2018). Therefore, at the beginning of this project, the LentiV2-Ex3D + SpCas9 mRNA delivery strategy was tested and optimised to increase gene editing efficiency for *COL7A1,* while exploiting the advantage of transient Cas9 expression. qPCR of the proviral LentiV2-Ex3D cassette confirmed stable integration of 1.2 copy/cell of the guide RNA cassette, thereby mimicking the natural number of gene copies per cell. Furthermore, the timing and amount of SpCas9 mRNA delivery was optimised with the most effective condition being 10µg delivered at day 3 post transduction. Additionally, C7 knockout by western blot and flow cytometry confirmed similar levels of protein knockout (~50%) as the percentage of knockout observed on genomic level.

During the course of my project, the CRISPR/Cas9 technology has seen significant advancements with the development of commercial viral-free formats by which the

Cas9 (mRNA or protein) and sgRNA (2-part sgRNA, single guide RNA or chemically modified sgRNA) can be delivered, thereby augmenting targeting capabilities and avoiding toxicity associated with plasmid or viral delivery (Preece and Georgiadis 2019). The rapid development of the field has also seen the application of viral-free deliveries for RDEB where ribonucleoprotein complex was shown to achieve more efficient gene-editing compared to viral or plasmid delivery of the nuclease (Bonafont et al., 2018). With the idea of developing novel strategies, several of the reported sgRNA and Cas9 formats were tested in my project. This was initially done by comparing editing efficiencies between single chemically sgRNA vs. 2-part guide RNA in combination with SpCas9 protein (RNP). The initial comparison between 2-part sgRNA and single guide RNA for the *COL7A1* locus resulted in greater percentages of *COL7A1* disruption from the latter (88%) over the former (5.1%). It is believed that the significant difference in the editing performance is likely to be due the presence of 2'-O-methyl 3'phosphorothioate (MS) chemical modifications at both 5' and 3' termini in the ribose-phosphate backbone of the sgRNA scaffold. These modifications significantly enhance resistance to intracellular RNAses, thus increasing the sgRNA persistence and on-target editing efficiency compared to the less stable crRNA:tracrRNA guides (Hendel et al., 2015). Finally, parallel comparison of the two CRISPR/Cas9 optimized strategies showed targeted *COL7A1* knockout at frequencies of up to 50% and 86% for the hybrid LentiV2-Ex3D + SpCas9 mRNA delivery and RNP, respectively.

Next, the second part of this chapter aimed to investigate gene repair by HDR using either non-integrating lentiviral vector (NILV) or viral-free ssODNs donor templates. For both donor templates, similar modifications were introduced, such as silent point mutations to reduce the likelihood of SpCas9 re-cutting upon template integration and to assist with the evaluation of the frequency of *in situ* HDR by quantification of the nucleotide changes. Use of a NILV cargo for donor template delivery was initially chosen due to their reported ability to infect hard-to-transfect keratinocytes (Benati et al., 2018; Izmiryan et al., 2018; Izmiryan et al., 2016; Georgiadis 2016). This donor configuration was designed to span 6 exons of endogenous *COL7A1* in order to cover a wider range of mutations clustered around this portion of the gene and, therefore,

in theory could be used for site-specific correction of multiple mutation hotspots. In an effort to further improve targeting rates, time course optimization between CRISPR/Cas9 deliveries (LentiV2-Ex3D + mRNA SpCas9 and Cas9-RNP) and the NILV-donor template infection was performed. HDR efficiency by NILV-I2I7C7-SDMTemplate-F was the highest when the template was delivered 24 hours post SpCas9 mRNA electroporation in LentiV2-Ex3D transduced keratinocyte cells. By contrast, cells receiving NILV-donor 30 minutes after Cas9-RNP electroporation showed increased HDR rates of up to 41% as confirmed by NGS. In both settings, PCR amplification of the genome-donor junction demonstrated the correct integration of the NILV-donor upon Cas9-mediated DSBs.

As with CRISPR/Cas9 components, development of viral-free methods of donor template delivery, such as ssODN or linearized double stranded DNA (ldsDNA), offers an alternative HDR strategy for correction of small pathogenic variants (Guo et al., 2018; Kwart et al., 2017; Paquet et al., 2016; Martin et al., 2019; Yang et al., 2013; Roth et al., 2018; Ott et al., 2006). Therefore, a complete viral-free HDR-based gene editing strategy was developed by designing a short donor template in the form of single-stranded DNA (ssODN), able to make small edits within the range of a few nucleotides from the c.425A>G mutation. Due to the novelty of ssODN for gene correction applications, a standard donor design architecture (symmetric vs asymmetric, length of the homology arms, presence of chemical modifications) to promote higher HDR is not by far available. Therefore, the ssODN was designed according to Richardson' *et al.* studies (Richardson et al., 2016). Initial comparison of donor template complementary to the non-target and target strands (T-2P-ssODN-AAA and NT-2P-ssODN-AAA, respectively) were then carried out in a keratinocyte cell line alongside Cas9 mRNA. In this setting, higher HDR (96%) was observed when NT-2P-ssODN-AAA was used. Despite the encouraging results, several hurdles were encountered when attempting to quantify the percentage of collagen VII restoration on protein and mRNA levels in gene edited cells. The designed PAM-blocking mutation which falls within the splicing donor consensus sequence of exon 3 of *COL7A1* resulted in aberrant splicing upon integration of the donor template and hence, absence of protein expression. Therefore, a new template was designed (NT-

2PS-ssODN-AAG) by introducing two sgRNA-blocking mutations upstream the splicing donor consensus sequence, while keeping the former intact. Flow cytometry analysis confirmed the ability of cells integrating the NT-2PS-ssODN-AAG donor to express C7.

In conclusion, the first part of this study demonstrated that the *COL7A1* locus can be successfully edited using different CRISPR/Cas9 formats by viral or non-viral modes of delivery. The high rate of nuclease-induced DSBs resulted in a significant frequency of donor integration by HDR, thereby eliminating the need of clonal selection. Finally, rational engineering of NILV donor template and ssODN allowed me to assess their applicability for HDR-based gene correction strategies even in wild type keratinocytes without the requirement for patient cells at this stage. The designed gene editing platforms can be further translated for downstream applications in primary cells or patient-derived iPSCs.

Chapter 4 Generation and CRISPR/Cas9 genome correction of c.425A>G RDEB patient induced pluripotent stem cells (iPSCs)

4.1 Background

Derivation of iPSCs from somatic cells has paved the way for modelling disease and may eventually help the development of new gene and cell therapy strategies in regenerative medicine. In dermatology, iPSCs have already been investigated for *in vitro* disease modelling and for the generation of *de novo* keratinocytes when patient's cell material is limited. For RDEB, reprogramming of spontaneously-revertant keratinocytes into iPSCs has demonstrated the potential of pluripotent stem cells to create stable cell models of the disease (Umegaki-arao et al., 2014; Tolar et al., 2011). Moreover, the power of this strategy lies in the importance to derive autologous iPSCs thereby offering an inexhaustible supply of patient-derived cells for the development of targeted gene and cell therapies alongside their ability to be differentiated into keratinocytes and fibroblasts (Shinkuma et al., 2016; Umegaki-Arao et al., 2014; Jacków et al., 2019; Webber et al., 2016). Recently, combinatorial approaches using iPSCs and CRISPR/Cas9-editing strategies have opened new horizons for studying inherited skin diseases.

4.2 Hypothesis

Patient primary fibroblasts harbouring a homozygous splice site mutation hotspot (c.425A>G, p.K142R) could be successfully derived into iPSCs and adpted to grow in xeno-free conditions while still maintaining all the properties of pluripotent stem cells, such as expression of marker genes and proteins associated with iPSCs/hESCs and spontaneous differentiation through embryoid body formation. This could allow the creation of a stable cell line that can be used for HDR-based strategies, previously described in **Chapter 3**, with a therapeutic potential for the c.425A>G *COL7A1* mutation. The obtained *COL7A1*-corrected iPSCs could provide a valuable source for the generation of iPSC-derived keratinocytes in order to evaluate their ability to secrete collagen VII *in vitro*.

4.3 Aims

1. Demonstrate reprogramming patient's fibroblasts into iPSCs (RDEB-iPSCs) in order to create a stable cell model homozygous for the c.425A>G splice site mutation in *COL7A1*.
2. Confirm the expression of pluripotency-associated markers in the generated RDEB-iPSC line and its multilineage differentiation potential.
3. Optimize gene editing described in chapter 3 in RDEB iPSCs and assess the percentage of *COL7A1* correction on genomic level.
4. To evaluate the ability of gene corrected iPSCs to express *de novo* C7 by direct keratinocyte differentiation from pluripotent stem cells
5. Evaluate *in silico* predicted off-targets for gene and base editing correction strategies by NGS.

4.4 Characterization of c.425A>G patient-derived fibroblasts and reprogramming into iPSCs

Primary keratinocytes and fibroblasts from RDEB patient (c.425A>$G^{+/+}$, p.K142R) involved in this study were previously isolated from a 6-mm skin biopsy and expanded *in vitro* by Dr. Anastasia Petrova with authorisation from the National Research Ethics Services, Westminster (07/H0802/104) and with written informed consent from the patient. These cells are characterized by a homozygous *COL7A1* mutation hotspot (c.425A>G), 2bp upstream of the distal junction of exon 3. As initially discovered by Gardella *et al*, the pathogenic A>G substitution in c.425 *COL7A1* results in p.K142R substitution and impaired splicing at the exon 3 and 4 junction, leading to absent collagen protein. Lack of C7 expression in the isolated RDEB fibroblasts was previously confirmed in our group at the protein level by western blot and immunofluorescence using a mouse mAb-C7-LH7.2 antibody. Noteworthy, the RDEB keratinocytes isolated from this subject were found to express C7 by western blot and immunofluorescence and showed a bi-allelic G>A reversion in position c.425, possibly due to spontaneous revertant mosaicism, commonly observed in RDEB keratinocytes (Twaroski et al., 2019). Due to the recent descriptions of mosaicism in RDEB fibroblasts (Twaroski et al., 2019), the presence of the splice-site mutation was re-confirmed in primary fibroblasts by Sanger sequencing before their reprogramming into iPSCs and their further use for gene editing applications (**Figure 4.1**).

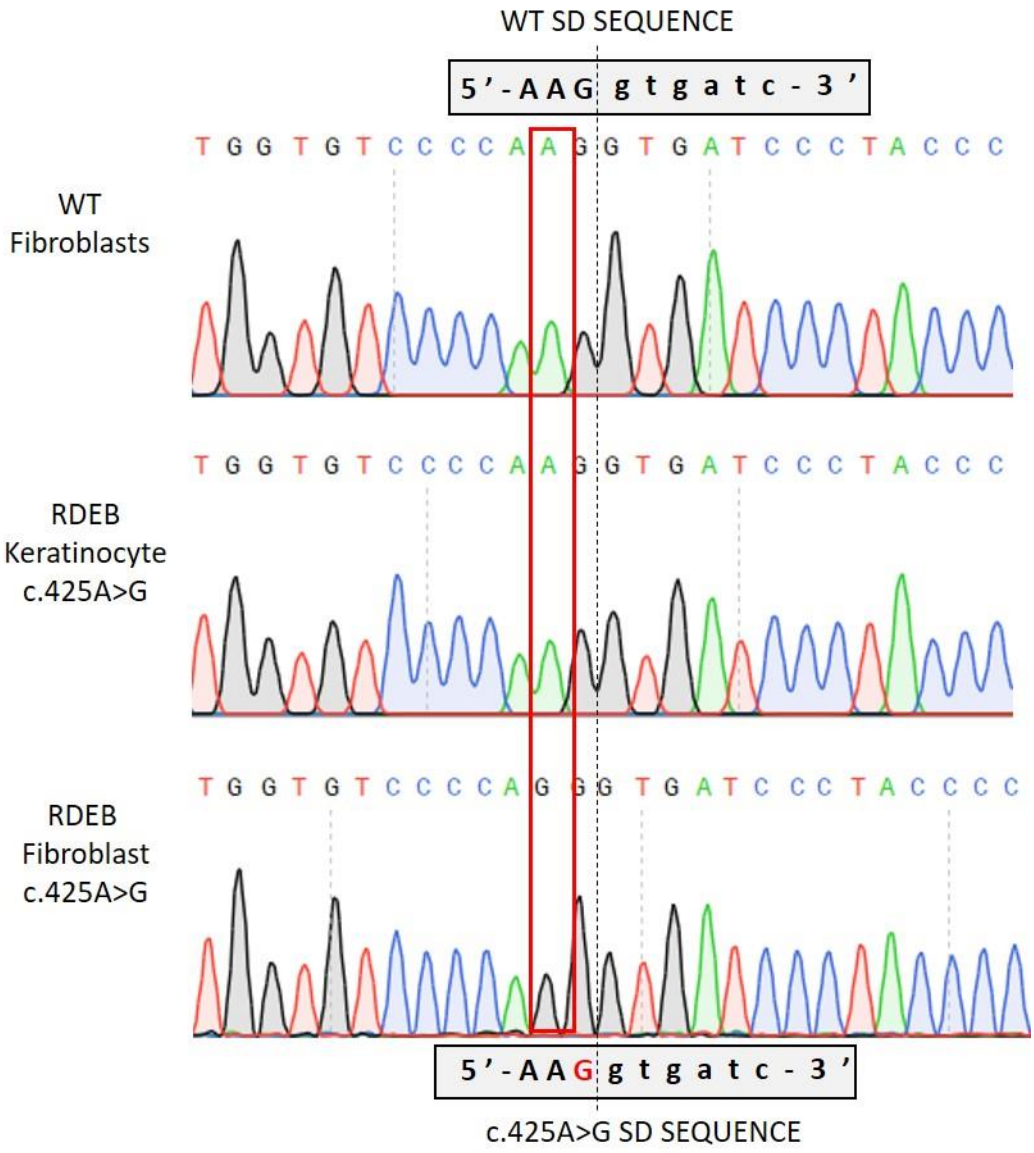

Figure 4.1 Analysis of the c.425A>G splice site mutation in RDEB keratinocytes and fibroblasts

Representative chromatogram of Sanger sequencing of *COL7A1* exon 3/intron 3 junction in wild type (WT) fibroblasts, RDEB keratinocytes and RDEB fibroblasts. Red square indicates the position of the c.425A>G mutation. Horizontal grey boxes indicate the splicing donor sequence (SD) between exon 3 (capital letters) and intron 3 (lowercase letters) in wild type (top) and RDEB cells (bottom).

In this direction, c.425A>G RDEB fibroblasts were reprogrammed into iPSCs in order to make a stable long-lasting cellular model that can be used to assess the efficiency of HDR-based gene and cytidine deaminase base corrections described in **Chapter 3** and **Chapter 5**, respectively. RDEB fibroblasts were initially expanded and transduced with integration-free Sendai (SeV) based reprogramming vectors (Fusaki et al., 2009), encoding for the four Yamanaka factors (hOCT4, hSOX2, hC-MYC, hKLF4) under feeder-free conditions (**Figure 4.2A**). Upon infection, fibroblasts were cultured in fibroblast medium until day 8 when the cells were transferred to vitronectin-coated plates and cultured in iPSCs medium. Two weeks post transduction, a significant change in cell morphology was observed in culture followed by the emergence of defined colonies indicative of the reprogramming process. Around 3 weeks post infection, the colonies with a characteristic iPSC-like morphology were large enough to be mechanically picked and sub-cloned for their characterization and gene editing purposes.

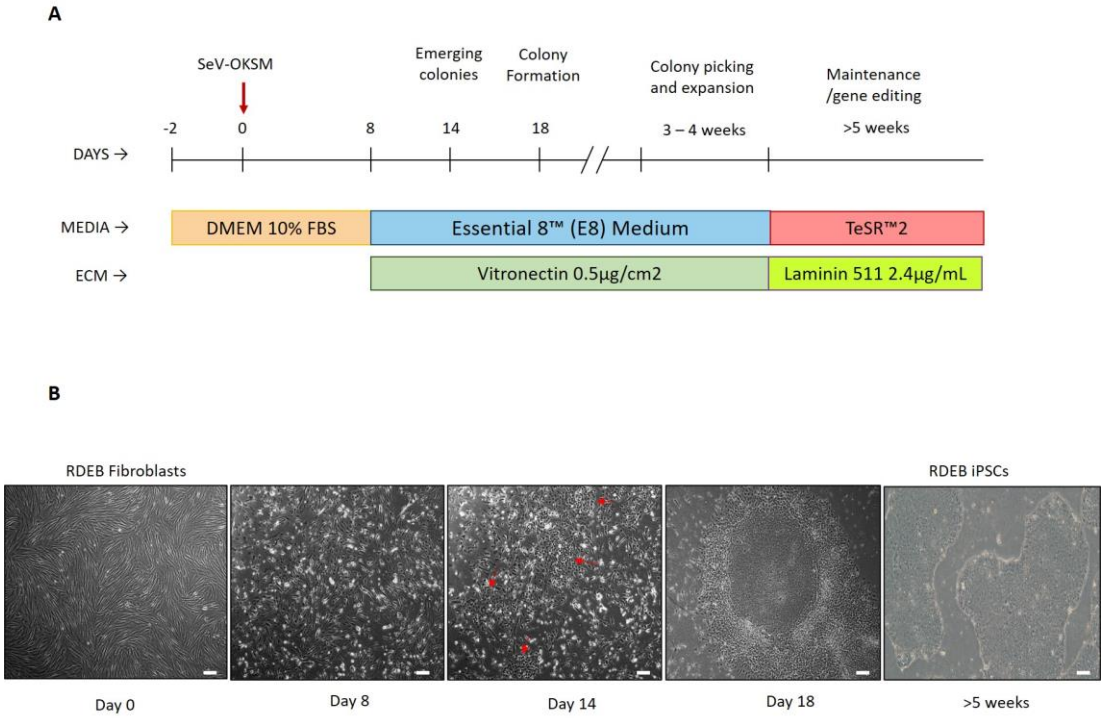

Figure 4.2 Derivation of RDEB iPSC colonies under feeder-free conditions

A. Schematic of the Sendai-based reprogramming protocol into iPSCs. The main time points, media and extracellular matrix (ECM) are shown. **B.** Morphological changes of RDEB fibroblasts into mature iPSCs. RDEB fibroblasts were transduced at day 0 with the CytoTune™-iPS 2.0 Sendai (SeV) Reprogramming Kit encoding for OKSM reprogramming factors: "O", OCT4; "K", KLF4; "S", SOX2; "M", C-MYC. Cell were allowed to proliferate in Dulbecco's medium (DMEM) containing 10% fetal bovine serum (FBS) for 8 days. On day 8, change in cellular morphology due to the reprogramming process is observable. On day 14, small cell clumps are emerging (red arrow) followed by colony formation and iPSCs maturation (day 18). After 5 weeks post reprogramming cells are tightly packed with distinct colony borders. Scale bar=100µm. The images were obtained using a 4X objective.

4.5 Morphology of the RDEB-iPSC line adapted to growth in different feeder-free conditions

Undifferentiated iPSCs display characteristic hESC-like morphology that can be evaluated under phase-contrast microscope: cells show a high nuclear/cytoplasmic ratio, prominent nucleoli and formed tight colonies with clear borders. Optimization of cell culture methods were tailored in RDEB iPSCs to prevent spontaneous differentiation. In this direction, three different conventional cell culture protocols were tested (**Figure 4.3**): (1) iPSCs were passaged onto Matrigel® substrate and cultured with mTeSR™1 (Matrigel®/mTeSR™1). (2) Cells cultured onto human recombinant vitronectin (N-VTN) in the presence of serum-free defined medium for pluripotent stem cells such as Essential 8 medium (Vitronectin/E8). (3) Cells maintained in xeno-free GMP-compatible culture conditions (TeSR™2) and laminin 511 as feeder-free matrix (laminin511/ TeSR™2) (Jeriha et al., 2020). Of note, the switch from each condition tested took required at least 2 passages for cellular adaptation to the new substrate/media combination. In order to limit spontaneous differentiation during the adaptation process, cells were passaged into small cell clumps of ~20cells with addition of rho-kinase inhibitor (Y-27632) to the growth medium prior to passaging.

For each culture condition, evaluation of iPSC colony morphology, presence of differentiated cells and adherence to the substrate were determined under phase contrast microscope. In presence of Matrigel®/mTeSR™1, RDEB iPSCs appeared flattened and colony poorly packed with indented and irregular borders indicating spontaneous differentiation. By contrast, Vitronectin/E8 or laminin511/TeSR™2 showed to support a more robust cell growth and uniformity compared to Matrigel® /mTeSR™1. For long-term maintenance and expansion, however, a more reproducible and stable culture was achieved with laminin511/TeSR™2 with no spontaneous differentiation observed after single-cell passaging required for gene editing. A healthy donor (wild type, WT) iPSC line obtained from the United Kingdom Regenerative Medicine Platform (UKRMP) was used as a positive control for culture

condition optimization experiments (data not shown). Therefore, RDEB iPSCs were cultivated in laminin511/TeSR™2 for downstream experiments.

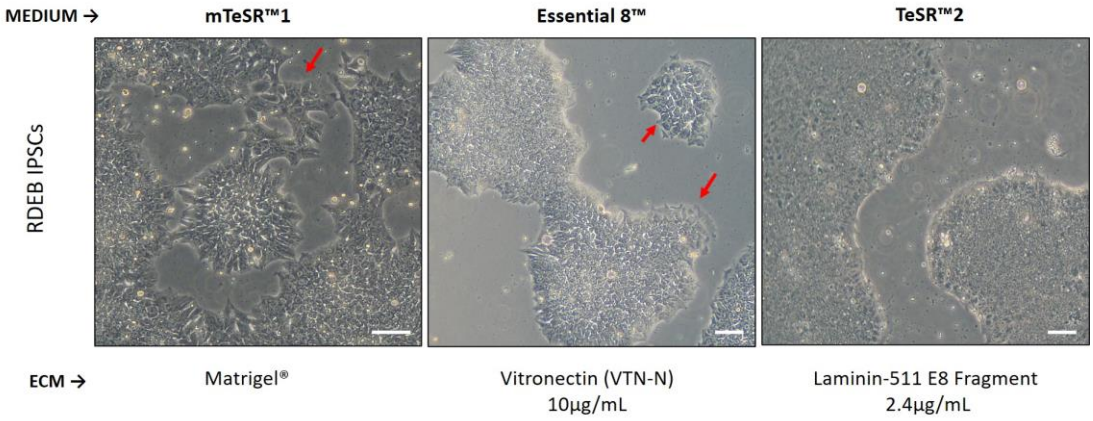

Figure 4.3 Characterization of RDEB iPSCs culture conditions

Morphology of RDEB iPSCs colonies with different substrate (ECM) and media combinations. Red arrows indicate spontaneous differentiation. Red arrows show irregular and flattened group of cells indicating spontaneous differentiation. The images were obtained using a 4X objective. Scale bar =50mm and 100 mm.

4.6 RDEB iPSCs retain the parent c.425A>G COL7A1 mutation

Upon reprogramming, Sanger sequencing of exon 3 *COL7A1* was performed to confirm the presence of the c.425A>G mutation in RDEB iPSCs. Persistence of the single base variant was evaluated at every 10 cell passages by Sanger sequencing (**Figure 4.4A**). Restriction Fragment Length Polymorphism (RFLP) to confirm the presence of the single nucleotide substitution in RDEB iPSCs was performed by enzymatic digestion of the PCR amplified exon 3 *COL7A1* using the *StyI* enzyme. RFLP exploits variations in homologous DNA sequences that can be detected by the presence of fragments of different lengths after digestion of the DNA samples in question with specific restriction endonucleases. As demonstrated by Christiano *et al.*, the c.425A>G polymorphism abolishes a *StyI* restriction enzyme site mapped at the end of exon 3 of *COL7A1* cDNA by direct nucleotide sequencing (Christiano et al., 1994). Enzymatic digestion of PCR amplicons from samples treated with the *StyI* enzyme revealed the presence of two bands of 268bp and 115bp in wild type fibroblasts and WT iPSC used as control. No evidence of enzymatic digestion was detected in RDEB fibroblasts and RDEB-iPSCs (**Figure 4.4B**).

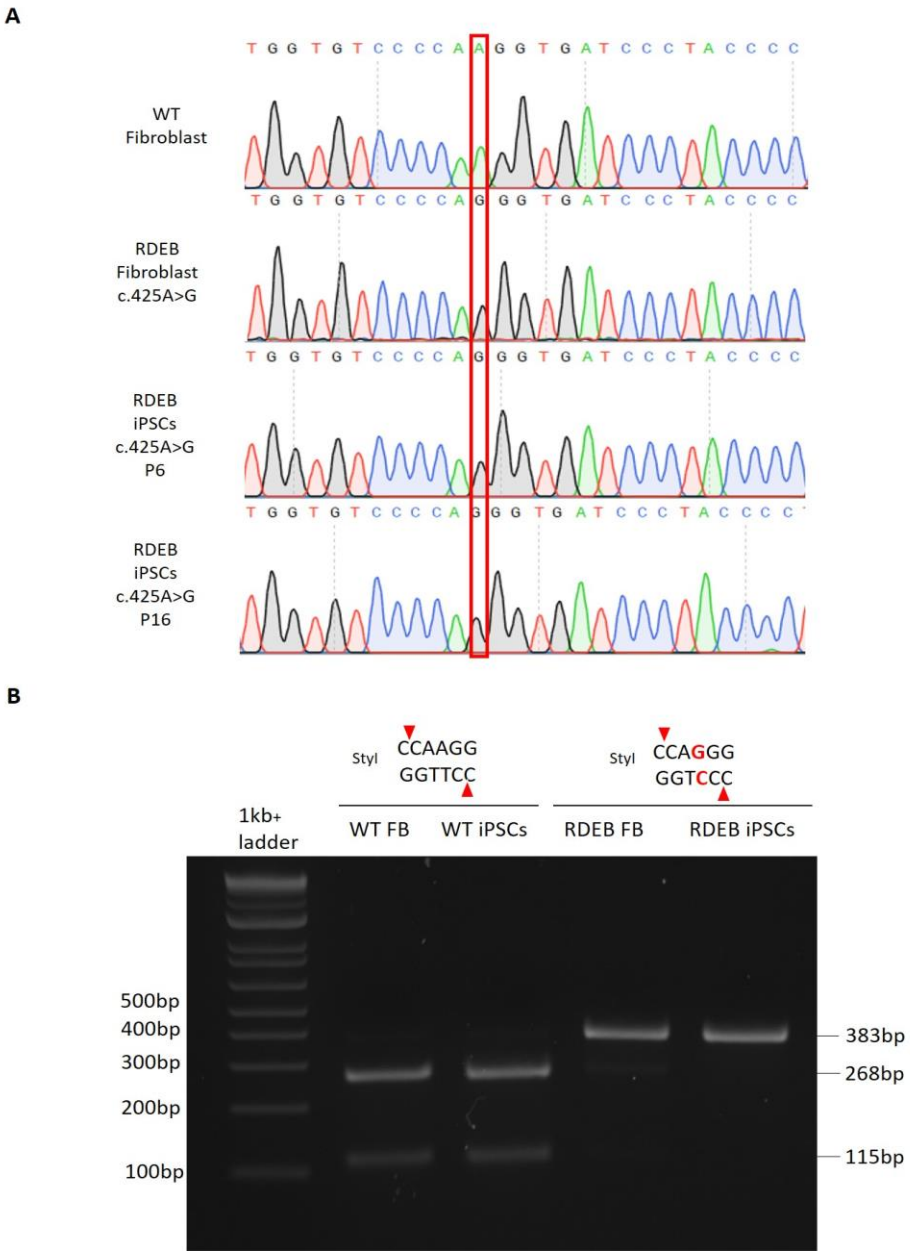

Figure 4.4 Evaluation of RDEB iPSCs genomic c.425A>G at early and late passage

A. Representative chromatogram of Sanger sequencing of exon 3 and intron 3 junction of *COL7A1* in RDEB iPSCs (bottom) at passage 6 and passage 16 confirms the presence of the A>G splice site mutation upon reprograming from RDEB fibroblasts (second chromatogram from the top). Wild type (WT) fibroblasts (top) were used as a control. The Red square indicates the position of the c.425A>G mutation in all samples. **B.** *StyI*-based enzymatic digestion of the PCR amplified exon 3 *COL7A1* in wild type and RDEB cells. On the top, the restriction digestion site sequence recognized by the *StyI* enzyme and its cutting site positions (red triangles). In red, the A>G base substitution in RDEB patients which abolishes the *StyI* endonuclease cut. Electrophoresis gel showed 2 bands of 268bp and 115bp due to the presence of the *StyI* digestion enzyme site at the end of exon 3 in WT fibroblasts and WT iPSCs. The presence of the undigested 383bp band in RDEB fibroblasts and iPSCs confirmed the presence of the c.425A>G point mutation.

4.7 Expression of pluripotency associated markers in RDEB iPSCs

To confirm the pluripotency-like state of RDEB-iPSCs upon reprograming, *in situ* immunofluorescence staining for nuclear transcription factors SOX2 and OCT3/4 and a glycosphingolipid SSEA-4 was performed. Evaluation of the cellular ground state was also evaluated in wild type WT iPSCs. Colonies of RDEB- and WT-iPSCs showed bright protein expression and correct localization of all the three markers (**Figure 4.5A**). Qualitative analysis of pluripotency marker expression was performed in three independent fields (n=3) selected at random. Further quantification was carried out by flow cytometry for nuclear (NANOG, SOX2, OCT3/4) and extracellular (SSEA4, TRA-1-81, TRA-1-60) pluripotency-associated markers expression in both cell lines (**Figure 4.5B**). Data confirmed high levels of expression of all pluripotency markers in both RDEB and WT- iPSCs with no MFI differences observed between the 2 cell lines. To confirm the maintenance of the pluripotency state, the flow analysis was consequently repeated in RDEB-iPSCs at late passage 16 for quality control (data not shown). Cellular pluripotency state was also assessed in both cell lines on cDNA level by PCR amplification of the RT-PCR products for SOX2, OCT3/4, NANOG, KLF4 and cMYC (**Figure 4.5C**). No expression of iPSCs-associated genes was seen in parental RDEB fibroblasts.

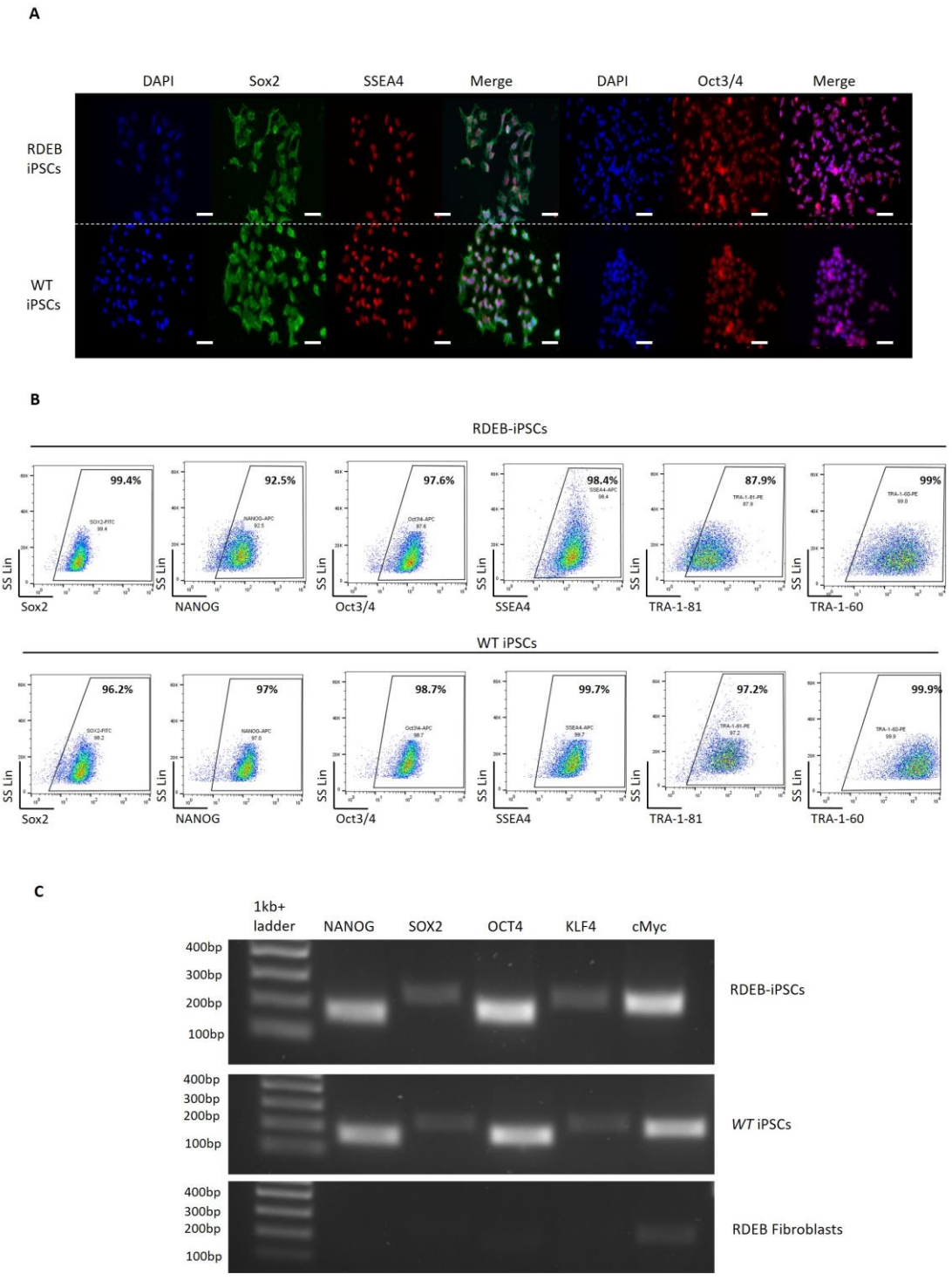

Figure 4.5 Expression of pluripotency-associated markers in RDEB- and WT iPSCs

A. *In situ* immunofluorescence staining for different pluripotency markers. From left to right: Sox2, SSEA-4 and Oct3/4. Nuclei were counterstained with DAPI (blue). All images were taken with 20x objectives. Scale bar = 50µm. **B.** Representative quantification of pluripotency-associated markers by flow cytometry for RDEB (top) and WT (bottom) iPSCs. **C.** Confirmation of expression of NANOG, Sox2, Oct4, KFL4, cMYC pluripotency markers in RDEB (top) and wild-type (WT) WTWT (middle) iPSCs by RT-PCR. RDEB fibroblasts were used as a negative control (bottom).

4.8 In vitro Trilineage differentiation assay

The capacity of RDEB iPSCs to differentiate into all three germ layers, namely ectoderm, endoderm, and mesoderm, was confirmed *in vitro* by spontaneous differentiation of RDEB iPSCs as embryoid body (EBs) as described in **section 2.2.15**. Upon differentiation cells were analysed by immunofluorescence for appropriate germ-layer markers such as alpha-fetoprotein (AFP) for endoderm, anti-α-smooth muscle actin (α-SMA) for mesoderm and tubulin-beta-3 (TUBB3) for ectoderm. *In situ* immunofluorescence staining of the EBs demonstrated that patient-derived iPSC line was capable of differentiating into all 3 germs layers *in vitro*, thereby confirming their pluripotency upon reprograming.

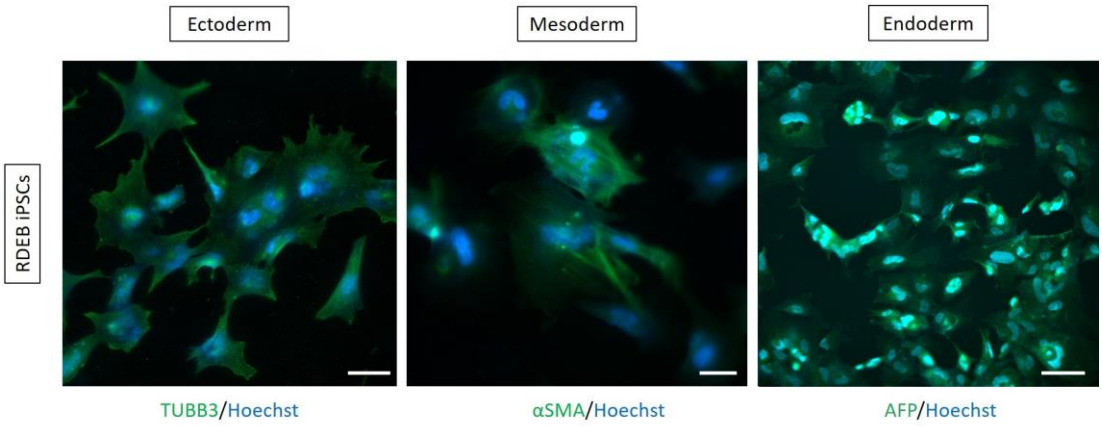

Figure 4.6 *In vitro* differentiation of RDEB iPSCs into three germ layers

The potential for trilineage differentiation of RDEB iPSC evaluated by embryoid body formation *in vitro*. TUBB3, αSMA, and AFP indicate ectodermal, mesodermal and ectodermal differentiation, respectively. All images were taken with 20x objectives.

4.9 Optimization of HDR-based COL7A1 correction in RDEB iPSCs using NILV donor template delivery

COL7A1 correction using the Ex3D-RNP CRISPR/Cas9 delivery coupled with NILV-I2I7C7-SDMTemplate-F donor template described in **section 3.10** was successfully tested in RDEB and wild type iPSCs. In order to achieve modest gene correction efficiency in iPSCs, optimizations of different parameters within the gene-editing strategy were carried out. To improve cellular viability upon electroporation, different parameters, including voltage, pulse with and duration of the pulse, were tested in RDEB iPSCs using the Neon electroporation system (ThermoFisher, USA). Six different electroporation programs described in literature as suitable for iPSCs were tested (**Figure 4.7A**). Cellular viability and electroporation efficiency upon transfection of 2µg of GFP mRNA in RDEB iPSCs were evaluated 5 days post electroporation (**Table 4.1** and **Figure 4.7A**). Cell viability was assessed by cell count of viable cells upon Trypan Blue staining and the obtained cell number was normalized by the initial amount of cells used for electroporation ($1x10^6$ cells). Similar cell viability, 5 days post electroporation, was obtained for every electroporation protocol tested.

Table 4.1 Cell viability of RDEB iPSCs post electroporation

Electroporation program (Neon electroporation system)	Cell viability after 5 days post electroporation
P-13	8.3×10^5
P-14	8.0×10^5
P-21	7.21×10^5
P-16	6.0×10^5
P-3	7.6×10^5
P-4	7.8×10^5

Cell viability of RDEB iPSCs upon transfection with 6 different electroporation protocols.

GFP expression measured by flow cytometry showed high MFI in RDEB iPSCs electroporated with programs P-14, P-21 and P-3 ($3.95x10^2$, $3.18\ x10^2$, $3.41x10^2$, respectively), whereas lower reporter expression was obtained with programs P-13, P-21 and P-4 ($2.29\ x\ 10^2$, $2.14\ x\ 10^2$, $2.56\ x\ 10^2$, respectively) (**Figure 4.7A**). Consequently, the program P-14 was used for downstream gene correction applications due to the low cellular toxicity and the higher MFI observed by flow.

To prevent Cas9-induced cell toxicity (Ihry et al., 2018; Schiroli et al., 2019) while obtaining high-frequency editing in iPSCs, several concentrations of Ex3D-RNP complex (1:1.2 of Cas9 to sgRNA) were tested in parallel (**Figure 4.7B**). Upon cell recovery, at seven days post electroporation, *COL7A1* knockout was evaluated on genomic level and cellular recovery was measured by cell count. Sequencing data upon PCR amplification of the targeted *COL7A1* region showed high percentages of NHEJ (82%) from 2µg of sgRNA. Similar knockout frequencies were observed with higher concentrations of Ex3D-RNP complex (82% 3µg sgRNA, 88% 4µg sgRNA, 88% 5µg sgRNA, 93% 6µg sgRNA, 91% 7µg sgRNA) whereas lower NEHJ rate (30%) was obtained with 1µg of guide RNA. The titration curve obtained showed that NHEJ events reached plateau at 2µg of sgRNA, therefore 2µg of EX3D guide RNA hybridized with 8.4µg of SpCas9 RNP (1:1.2 of Cas9 to sgRNA) were further used to evaluate the percentages of gene correction using the NILV-donor template.

A

Electroporation programs (Neon Electroporation System)	Program parameters
P-13	1100V-20ms-2p
P-14	1200V-20ms-2p
P-21	1300V-10ms-3p
P-16	1400V-20ms-1p
P-3	1500V-20ms-1p
P-4	1600V-20ms-1p

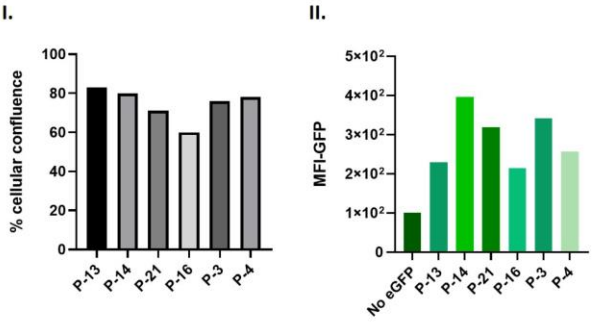

B

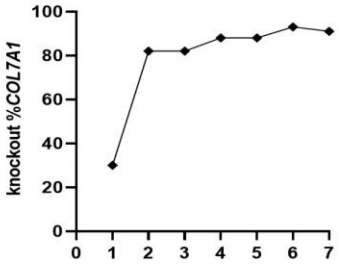

sgRNA		spCas9	
µg	pmol	µg	pmol
1	31	4.2	25.6
2	62	8.4	51.2
3	93	12.6	76.8
4	124	16.8	102.5
5	155	21	128
6	186	25.2	153.7
7	220	29.4	180

Figure 4.7 Optimization of electroporation conditions in RDEB iPSCs

A. Table reporting different electroporation programs for iPSCs transfection using the Neon device. For each program, voltage (V), width (ms) and number of pluses (p) are shown. (**I.**) Cell count of RDEB iPSCs after electroporation of GFP mRNA using different electroporation protocols. Each bar shows the percentage of cellular viability obtained for each electroporation condition. (**II.**) Flow cytometry for the quantification of GFP expression in RDEB iPSCs transfected with different electroporation protocols showed different MFI. The highest MFI was observed with program P-14 ($3.95x10^2$). **B.** Titration of guide Ex3P and SpCas9 protein at 1:1.2 Cas9:sgRNA molar ratio was performed in RDEB iPSCs and quantification of InDels showed that significant knockout (82%) was achieved with 2µg of Ex3P-sgRNA and 8.4 µg SpCas9 protein, reaching a plateau thereafter. The table below, shows µg>pmol conversions of different concentrations of sgRNA and spCas9 protein used to make RNP complex *in vitro* before electroporation.

In order to achieve the highest rate of HDR upon delivery of NILV-donor, a similar strategy for RNP and donor template delivery used for keratinocyte cell line described in **section 3.10** was employed. Around $1x10^6$ RDEB iPSCs and WT iPSCs, used as control, were electroporated with 2µg of Ex3D-sgRNA complexed with 8.4µg of Cas9 RNP followed by NILV-donor template infection (MOI 20) 30 minutes post electroporation. To exclude the presence of episomal state of the donor template, integration of I2I7C7-SDMTemplate-F was evaluated 15 days post infection by PCR of the TI-5' donor-genome junction in treated cell bulk population and cells infected with NILV donor only. Quantification of on-target donor integration events was performed by Sanger sequencing (**Figure 4.8A**). Percentage of total gene editing (NHEJ+HDR) in RDEB iPSCs was lower 36% (n=2) than the rate observed in WT cells 63% (n=2). Noteworthy, an average of 75% (RDEB-iPSCs) and 82% (WT) of the edited cell population showed integration of the donor template by HDR. Furthermore, EDIT-R analysis for the quantification of the corrected nucleotide in position c.425 *COL7A1* showed an average of 41% (n=2) upon donor integration in RDEB iPSCs whereas no detectable donor integration was observed in cells receiving the donor template only.

Furthermore, NGS analysis was carried out for the detection of the SDM modifications within the donor template. Quantification of the intended nucleotide changes in the bulk populations equated to 70% in wild type iPSCs and ~32% in RDEB-iPSCs for all the 5 Cas9-blocking mutations (**Figure 4.8B**). Single base correction at position c.425 was detected in around 28% of RDEB-iPSCs.

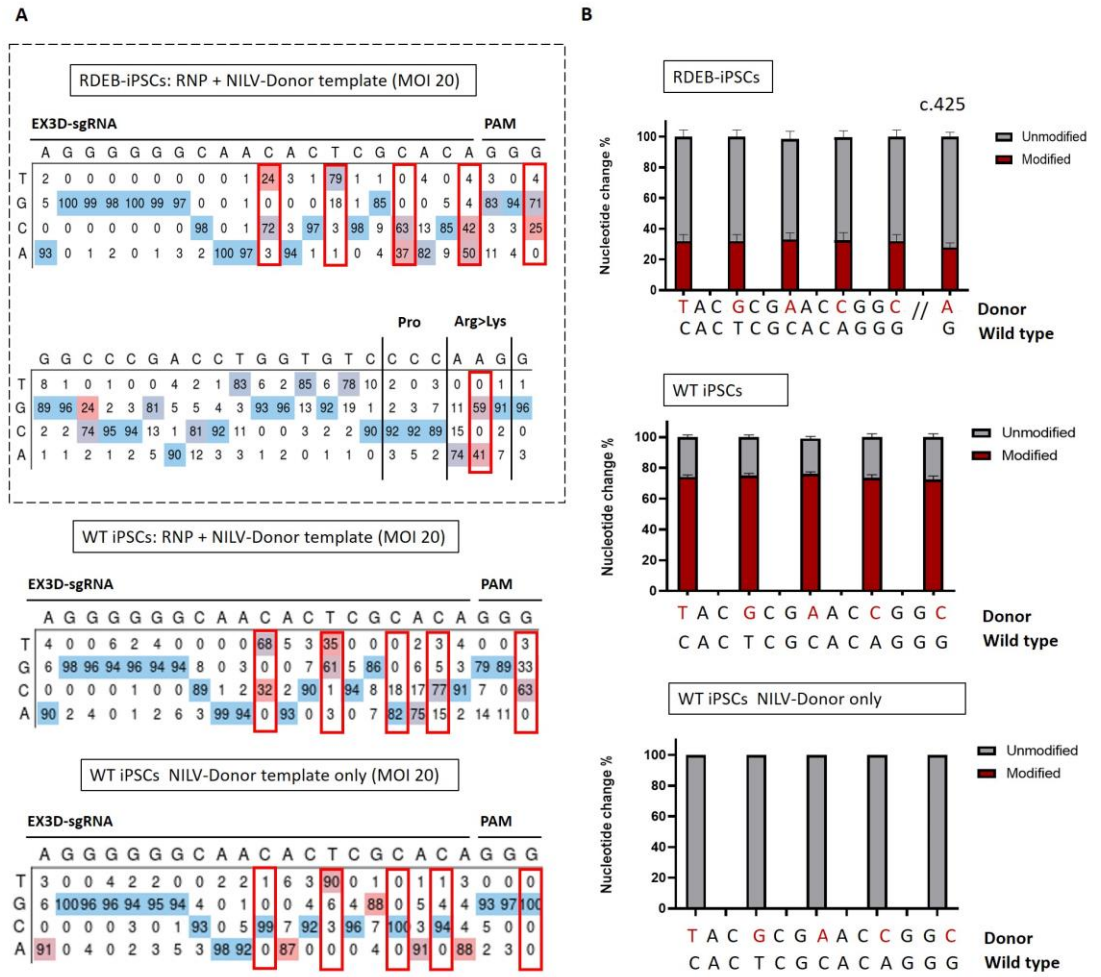

Figure 4.8 Evaluation of *COL7A1* correction by HDR using NILV-donor template in WT IPSCs

A. Sanger sequencing-based EDIT-R analysis of the *COL7A1* locus. NILV-donor integration was assessed by the presence of sgRNA and PAM-blocking mutations designed across the DNA sequence recognized by the Ex3D-sgRNA and G>A single base correction at position c.425 of *COL7A1* in RDEB-iPSCs (black square). Correction at c.425 is shown in a red box (G>A 41%). Below, representative EDIT-R output in WT iPSCs treated with RNP + NILV-donor template (MOI 20) and RDEB cells receiving NILV-donor template only. **B.** NGS analysis quantifying *COL7A1* donor integration as percentage of nucleotide changes in cells treated with NILV-donor in RDEB iPSCs and WT cells. Grey bars show the percentage of uncorrected alleles, red bars represent the percentages of nucleotide changes upon HDR. Overall integration was 32% and 70% for each mismatch designed within the donor. The error bars are representative of 2 biological repeats (n=2). For RDEB iPSCs, *COL7A1* correction at position c.425 (indicated by the asterisk) was 28% (n=2).

4.10 Evaluation of electroporation conditions for RDEB iPSCs using the Lonza 4-D system

As previously reported in **section 3.11**, a virus-free HDR-based gene editing approach using ssODN offers the ability to generate precise gene correction of a few nucleotides avoiding the introduction of large (>1kb) donor templates for homologous recombination strategies (Martin et al., 2019). In this study, the designed NT-2PS-ssODN-AAG described in **Chapter 3,** was subsequently tested in conjunction with Ex3P-sgRNA and SpCas9 mRNA in RDEB and WT iPSCs. For the delivery of these tools, the Amaxa 4D-Nucleofector X Unit (Lonza), was employed to improve transfection reproducibility and due its translational use in preclinical and GMP-grade applications for iPSCs.

Three different electroporation protocols (CA-137, CA-167 and CB-150) reported in literature for gene editing of iPSCs were investigated. Similarly to what was shown in **section 4.9**, for each program tested, $1x10^6$ cells were electroporated with 2µg of GFP mRNA and fluorescence expression was analysed by flow cytometry 48 hours post transfection (**Figure 4.9A**). Results showed that up to 90% of the electroporated cells were GFP+ (90.3% CA-137, 86.8% CB-150, 90.4% CA-167) (**Figure 4.9B**) and no observable differences in MFI were observed (~ $4x10^2$) (**Figure 4.9C**). Furthermore, appreciable cellular viability (76% CA-137, 86% CB-150, 80% CA-167) was observed upon electroporation with all the three programs tested with no significant toxicity compared to non-electroporated cells (87%) (**Figure 4.9D**). To determine whether RDEB iPSCs continued to express pluripotent markers after electroporation, the expression of Oct3/4 and NANOG, was quantified by flow cytometry. 48 hours post electroporation, up to 99% of the electroporated cells were positive for both markers thus demonstrating that the electroporation programs did not interfere with pluripotency (**Figure 4.9E**).

Furthermore, to verify whether different electroporation programs can affect gene editing frequency (Martin et al., 2019), 2µg of B2M-sgRNA combined with 5µg of SpCas9 mRNA were co-electroporated using different electroporation programs in RDEB iPSCs. Evaluation of the efficiency of *B2M* knockout for the purpose of

determining the best electroporation program was chosen as it offered a faster readout by flow cytometry. No observable differences in knockout efficiencies of beta-2-Microglobulin were observed (67.9% for CA-137 and CA-167, 71% with the CB-150 program) (**Figure 4.9F**). Although, all the conditions tested have shown to achieve similar editing results, the CA-137 protocol was chosen as the most widely used electroporation condition for pluripotent stem cells reported in numerous the literature (Kondrashov et al., 2018; Ishida et al., 2018; Dastidar et al., 2018; Yang et al., 2013).

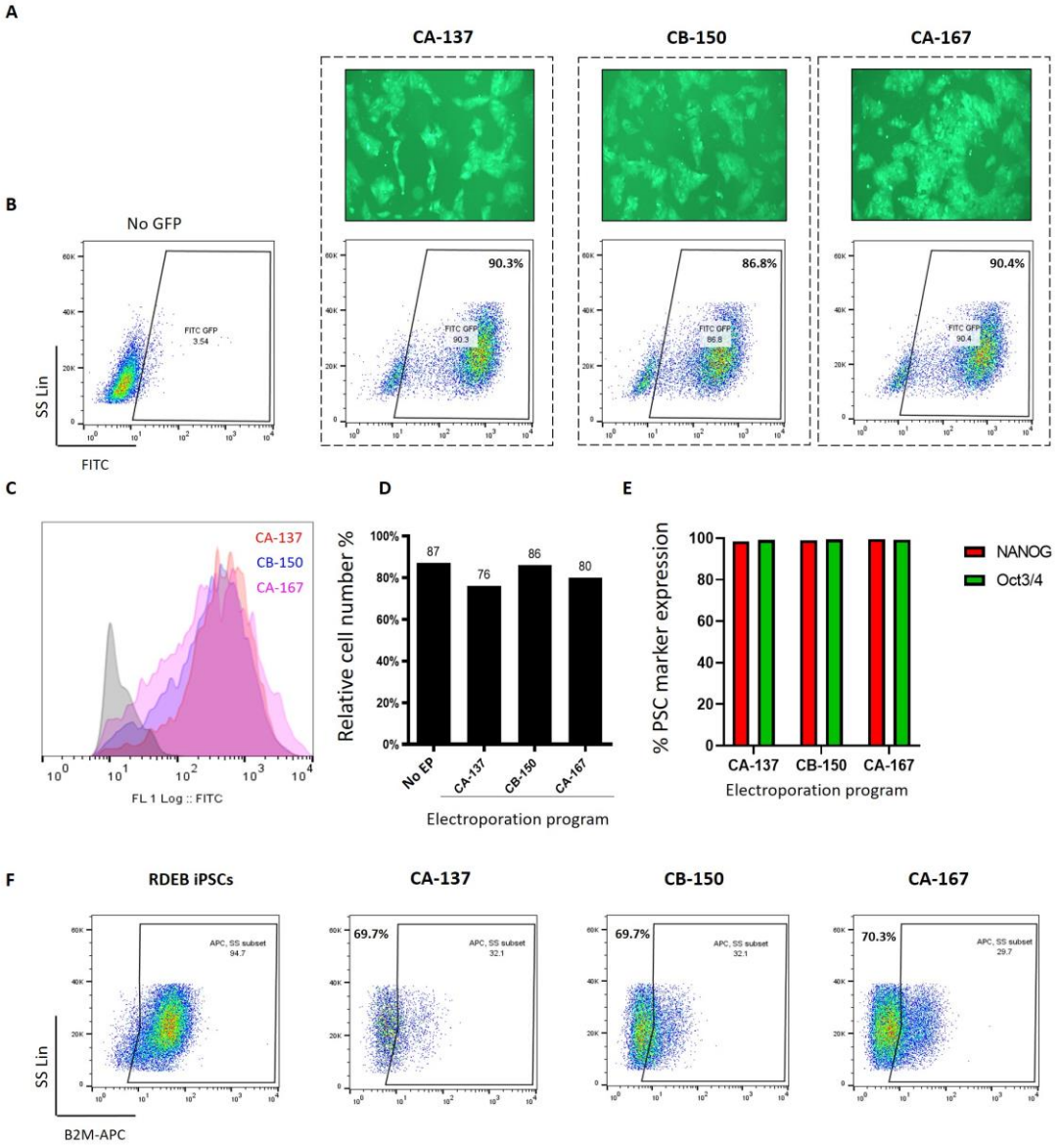

Figure 4.9 Optimization of the Lonza-4D electroporation system in RDEB iPSCs

A. Representative images of RDEB iPSCs expressing GFP mRNA 2 days post electroporation using three different electroporation programs: CA-137, CB-150 and CA-167. **B.** Relative quantification of GFP expression by flow-cytometry from RDEB iPSCs electroporated with different electroporation programs show similar percentages of GFP+ cells (90.3% CA-137, 86.8% CB-150, 90.4% CA-167) **C**. Comparison of the GFP expression intensity (MFI) showed no significant differences with all three programs tested. **D.** Cell count of RDEB iPSCs after electroporation. Cell viability percentages calculated 48 hours post electroporation:76% CA-137, 86% CB-150, 80% CA-167 and 87% non-electroporated cells (No EP). **E.** Pluripotency associated markers NANOG and Oct3/4 remained unaffected in electroporated RDEB iPSCs indicating that none of the electroporation conditions interferes with iPSCs ground state **F**. Quantification of Beta-2-Microglobulin knockout by flow cytometry upon electroporation. B2M downregulation was 69.7% (using the CA-137 and CB-150 program) and 70.3% with CA-167.

4.11 Gene correction of RDEB iPSCs using ssODN as a donor template

To reduce cell toxicity upon gene editing at the *COL7A1* locus, titration of SpCas9 mRNA using 1.25, 2.5, 5, 7.5 and 10µg was performed using 2µg of Ex3P-sgRNA (n=1) (**Figure 4.10A**). Sanger sequencing of the *COL7A1* locus showed that higher amounts of SpCas9 mRNA resulted in increased knockout frequencies in a dose-dependent manner (75% for 2.5µg, 79% for 5µg, 87% for 7.5µg and 94% for 10µg). Noteworthy, increasing amounts of Cas9 also led to higher cell toxicity (data not shown). Low viability and slow cell recovery was observed with 10µg of Cas9 whereas lower amounts of SpCas9 mRNA, showed faster cell recovery. Taken this data into account, 5µg of SpCas9 mRNA was used for gene correction via HDR. The optimized conditions were verified to not affect the expression of pluripotency markers such as Oct3/4 and NANOG (**Figure 4.10B**).

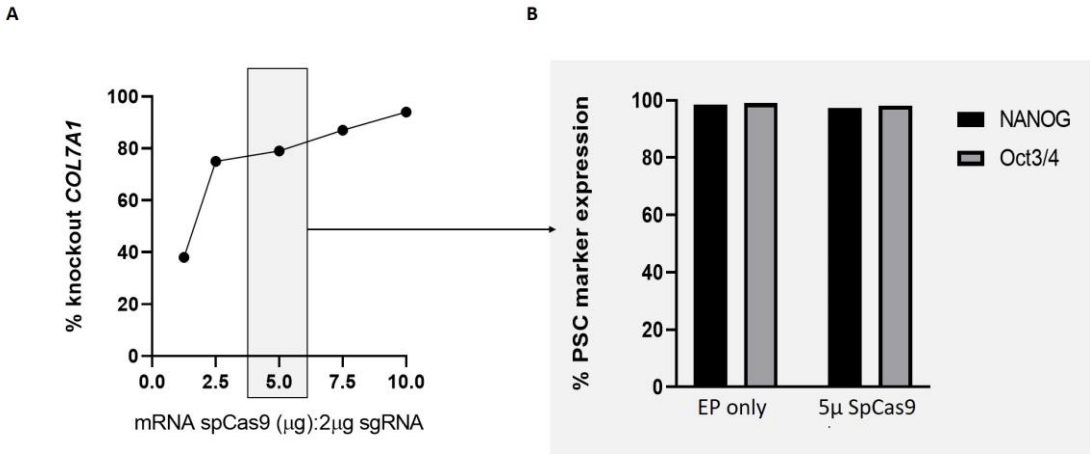

Figure 4.10 Titration of SpCas9 mRNA in RDEB iPSCs and evaluation of gene edited pluripotency post electroporation

A. Percentage of *COL7A1* knockout in RDEB iPSCs using different amounts of SpCas9 mRNA. Knockout of the *COL7A1* locus was determined by sequencing-based quantification of InDels: 94% at 10µg, 87% at 7.5, 79% at 5µg, 72% at 2.5µg and 38% at 1.25µg. The grey rectangle represents the amount of SpCas9 mRNA subsequently used for gene editing in RDEB iPSCs. **B.** Pluripotency associated markers NANOG and Oct3/4 remained unaffected in electroporated RDEB iPSCs indicating that electroporation did not interfere with iPSCs ground state.

Alongside SpCas9 mRNA titration, targeted integration frequencies with increasing amounts of NT-2PS-ssODN-AAG (1.25µg, 2.5µg, 5µg and 10µg) were analysed in RDEB iPSCs (**Figure 4.11A**). In accordance with previous results shown in **section 3.13**, Sanger sequencing-based ICE analysis for the quantification of the HDR events in the gene edited populations showed 90% of HDR when 10µg of NT-2PS-ssODN-AAG was used. Additionally, lower amounts of donor template were able to support high levels of gene correction reaching 81%, 72% and 60%, at 5µg, 2.5µg and 1.25µg of ssODN, respectively. Despite high levels of HDR rates, noticeable toxicity was observed in all conditions tested (**Figure 4.11A**). Only $1.1x10^5$ viable cells were counted when treated with 10µg of donor template whereas higher cell viability ($3.3x10^5$, $4.5x10^5$, and $5.9x10^5$) was observed when lower amounts of NT-2PS-ssODN-AGG were used (5µg, 2.5µg and 1.25µg, respectively). Therefore, 5µg of NT-2PS-ssODN-AAG was used for downstream experiments. Quantification of the donor template integration and A>G correction at c.425 position of *COL7A1* was analysed by Sanger sequencing followed by EDIT-R analysis (**Figure 4.11B**). Up to 68% of single A>G base correction was observed in RDEB iPSCs 7 days post electroporation. Furthermore, C>G silent point mutations ranged from 71% and 59% at positions 2 and 5 of the Ex3P-sgRNA binding site. RDEB and WT iPSCs electroporated with NT-2PS-ssODN-AAA and NT-2PS-ssODN-AAG, respectively, were used as positive control for gene correction. The rationale of using patient cells treated with the previous ssODN design (NT-2PS-ssODN-AAA, **section 3.11**) was due its high HDR efficiency observed post electroporation. Moreover, to assess whether the new ssODN design is able to achieve high correction rates independently from the cell type used, NT-2PS-ssODN-AAG was tested in WT iPSCs. Both controls showed similar percentages of donor template integration by EDIT-R single-base quantification analysis. Additionally, presence of both silent and corrective point mutations in WT iPSCs treated with NT-2PS-ssODN-AAG was verified at 15 and 30 days post electroporation confirming similar percentages of the gene-corrected cells in the treated population (data not shown), suggesting the stability of HDR-mediated gene correction.

The percentage of HDR upon donor integration was further corroborated by NGS analysis across the predicted editing site (**Figure 4.11C**). Donor integration was shown

by the presence of both C>G 'Cas9-blocking' mutations (75% and 61% at position +2 and -2 from the targeted Ex3P-induced DSBs) and up to 60% of G>A c.425 *COL7A1* correction, confirming the results obtained by Sanger sequencing. No integration was detected when RDEB iPSCs were treated with NT-2PS-ssODN-AAG donor template only.

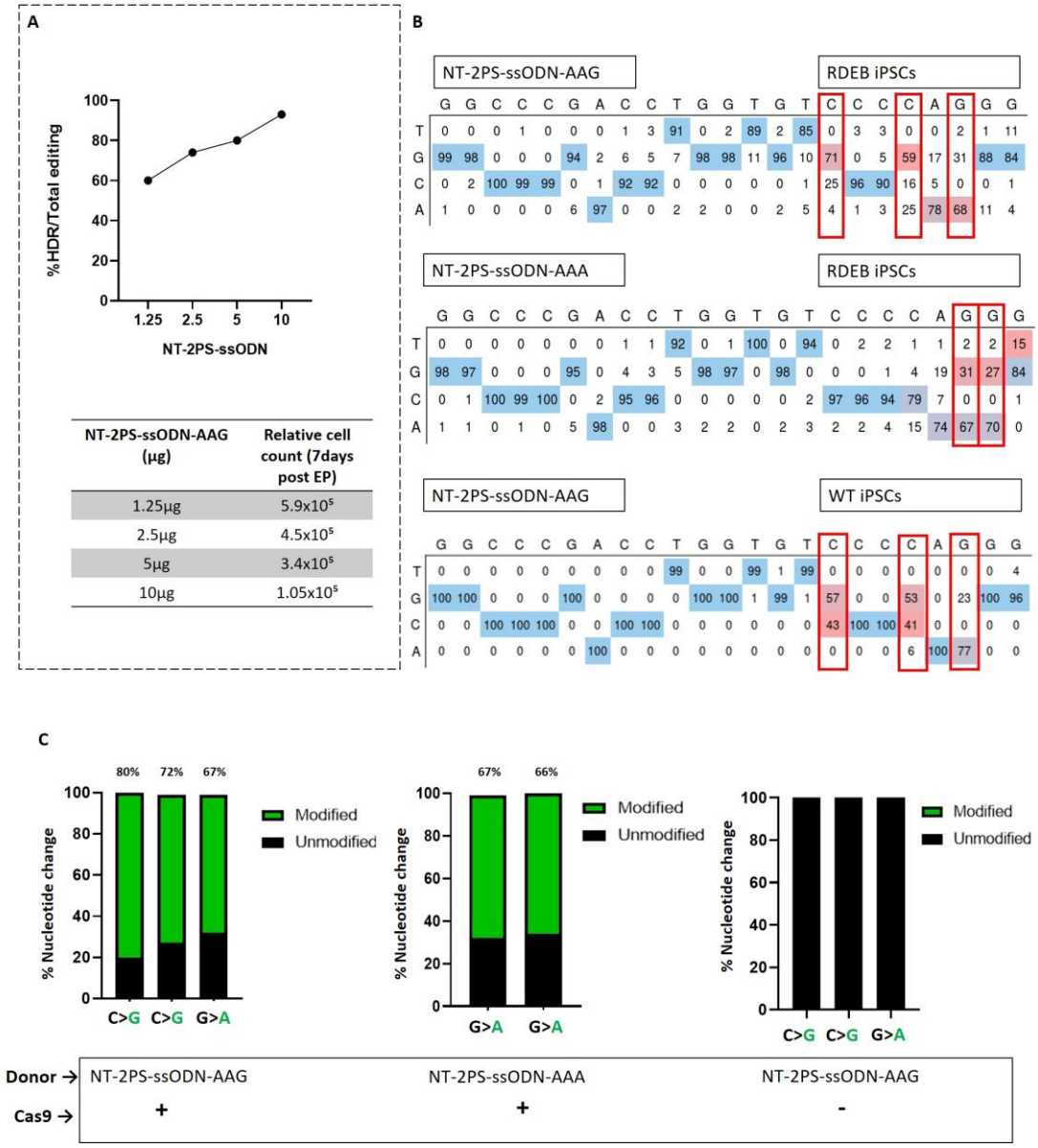

NT-2PS-ssODN-AAG (µg)	Relative cell count (7days post EP)
1.25µg	$5.9x10^5$
2.5µg	$4.5x10^5$
5µg	$3.4x10^5$
10µg	$1.05x10^5$

Figure 4.11 Optimization of targeted *COL7A1* correction by ssODN

A. RDEB iPSCs electroporated with Ex3P-sgRNA and spCas9 mRNA alongside different amounts (1.25µg, 2.5µg, 5µg, 10µg) of ssODN donor template (NT-2PS-ssODN-AAG). Numbers shown here corresponds to the percentages of G>A correction at position c.425 of *COL7A1* as detected by EDIT-R analysis following Sanger sequencing. For each sample, cell viability was measured 5 days post electroporation (table below) **B**. Representative EDIT-R output for RDEB iPSCS with 5µg of NT-2PS-ssODN-AGG, RDEB iPSCs with 5µg of NT-2PS-ssODN-AAA and WT iPSCs treated with NT-2PS-ssODN-AGG. Red boxes indicate the percentage of donor integration by insertion of Cas9-missense blocking mutations and *COL7A1* correction in treated cells. **C.** Confirmation of HDR frequencies by NGS in RDEB iPSCs treated with NT-2PS-ssODN-AAG and NT-2PS-ssODN-AAA donor templates. From left to right: RDEB iPSCs treated with NT-2PS-ssODN-AGG, RDEB iPSCs treated with NT-2PS-ssODN-AAA and cells electroporated with NT-2PS-ssODN-AAG only. Each bar shows the percentage of nucleotide changes due to integration of the donor template in exon 3 of *COL7A1* (green

bar) and the percentage of uncorrected alleles (black bar). Percentages of Cas9 blocking mutations and c.425 G>A gene correction in RDEB iPSCs are shown in black.

4.12 Directed Differentiation of iPSCs to induced keratinocytes (iKer) under Feeder-Free Conditions

For functional evaluation of restored C7 correction in RDEB iPSCs, initial studies have explored the potential of generating keratinocytes from iPSCs by mimicking the process of epidermogenesis in a 2D culture system *in vitro* (**section 1.5.5.2**) as pluripotent stem cells do not express collagen VII (Sebastiano et al., 2014). Although several research groups have reported generating keratinocytes from iPSCs (iKer) during the past several years, the approach chosen for my work is based on xeno-free and feeder-free keratinocyte differentiation studies using RDEB patient iPSCs described previously by Professor Angela Christiano and co-workers (**Figure 4.12A**) (Shinkuma et al.,2016; Jacków et al., 2019; Itoh et al., 2013). The following protocol was initially tested using untreated RDEB iPSCs with WT iPSCs used as a positive control during the differentiation. Prior to differentiation, iPSC lines were further tested for NANOG and OCT4 expression to confirm complete cell pluripotency before the initiation stage (**Figure 4.12B**). A homogenous NANOG+/OCT4+ population was required to avoid non-specific differentiation during keratinocytes differentiation. Flow cytometric analysis confirmed high percentage of NANOG+ (RDEB iPSCs: 83.5%; WT iPSCs: 82.9%) and OCT4+ (RDEB iPSCs: 91.5%; WT iPSCs: 89.5%) RDEB and WT iPSCs.

In the initiation stage (Days 0-7), cells (from now referred as RDEB iKer and WT iker) were stimulated with 1µM retinoic acid (RA) to promote commitment towards ectodermal lineage and 25ng/µL of bone morphogenetic protein 4 (BMP-4) to block neural progression over epidermal commitment (Shinkuma et al.,2016; Jacków et al., 2019; Itoh et al., 2013). On day 8 of differentiation, many cells that migrated away from the outgrown iPSC colonies exhibited a keratinocyte-like phenotype (**Figure 4.12C**). Next, marker progression towards the keratinocyte lineage was investigated to determine the identity of the differentiating cells. First confirmation of the correct ectodermal commitment was assessed at day 8 by immunofluorescence for the

expression of cytokeratin 18 (K18), an early-stage marker of simple epithelial cells (Lingyu Li et al., 2013; Metallo et al., 2008; Aberdam et al., 2008; Selekman et al., 2013). Immunostaining on differentiating cells showed correct cytoplasmatic fibrillar K18 expression therefore suggesting that the ectodermal progenitors obtained at this stage have started to acquire a more defined epidermal fate (**Figure 4.12C**).

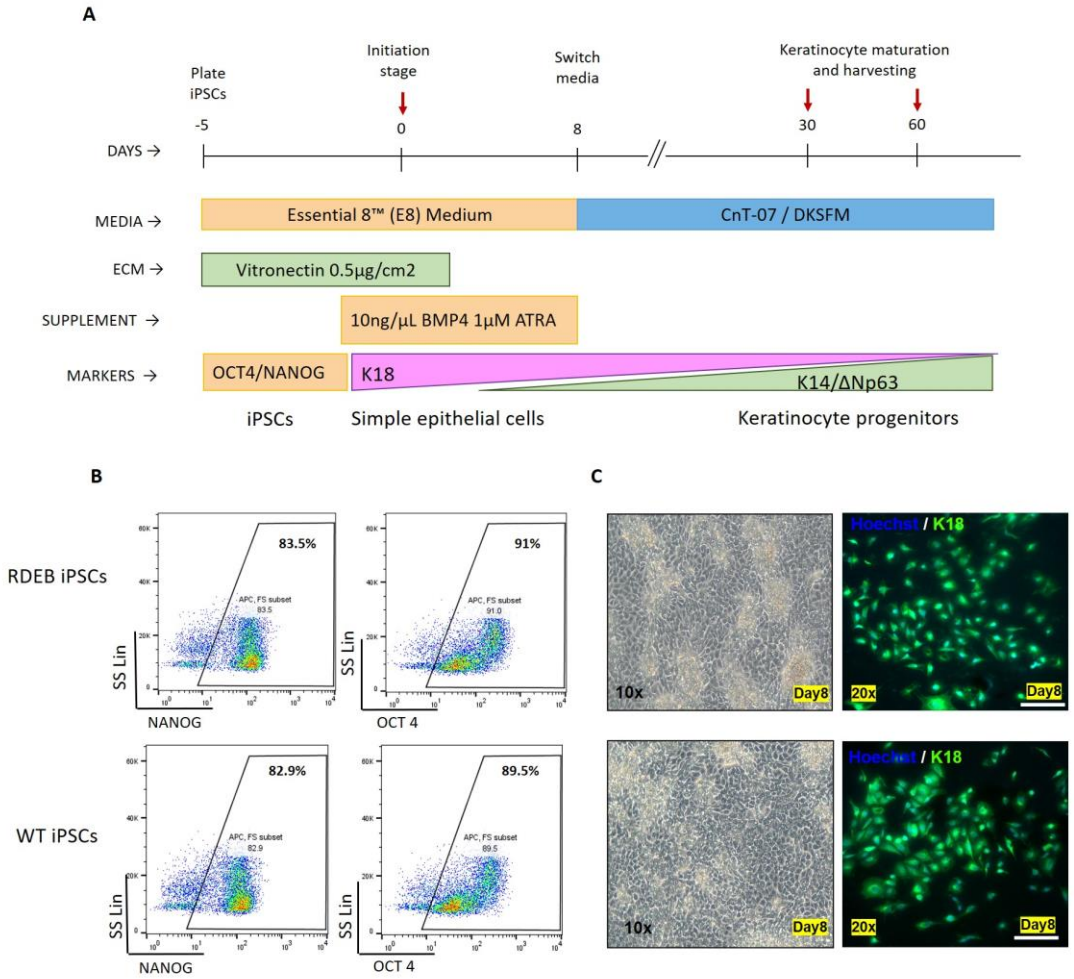

Figure 4.12 Directed differentiation of iPSCs into keratinocytes under feeder-free conditions.

A. Schematic representation of the differentiation strategy for generating keratinocytes from iPSCs described in Christiano *et al.* (Shinkuma et al.,2016; Jacków et al., 2019; Itoh et al., 2013). Different media, extracellular matrix (ECM) and supplements are indicated under each time point. At each stage of differentiation, different markers specific for pluripotent stem cells (OCT4, NANOG), epithelial commitment (K18) and keratinocyte maturation (K14 and ΔNp63) were used to verify the correct development of iPSCs towards epidermogenesis. Abbreviations: BMP-4: bone morphogenic protein; ATRA: all-trans retinoic acid; D-KSFM:

Serum-free defined keratinocyte medium; ColI: collagen type I; ColIV: collagen type IV; Cytokeratin 18: K18; Cytokeratin 14: K14. **B**. Flow cytometry analysis for pluripotent stem cell markers, NANOG and OCT4, was performed to confirm cellular pluripotency prior to initiation stage (Day 0). NANOG+ cells: RDEB iPSCs: 83.5%; WT iPSCs: 82.9%. OCT4+ cells: RDEB iPSCs: 91.5%; WT iPSCs: 89.5%. **C.** Phase-contrast images of RDEB and WT iPSCs taken at day 8. At the same day, expression of keratin 18 was assessed by immunofluorescence. Immunofluorescence confirmed the commitment of the differentiating iPSCs to epithelial progenitors.

After day 8, the cell culture was switched to Defined Keratinocyte Serum-Free Medium (D-KSFM) to promote efficient differentiation towards K14+ keratinocyte progenitors (Shinkuma et al.,2016; Jacków et al., 2019; Itoh et al., 2013). In line with the original protocol, cells were maintained in culture without passaging for 60 days to allow for complete maturation of keratinocyte progenitors. Lack of cell passage, however, resulted in a significant multi-layered cell outgrowth followed by cell death and senescence (data not shown). In contrast to the original protocol, cells were passaged at the end of the initiation stage and once confluent. Therefore, to promote keratinocyte differentiation upon passaging, cells were seeded onto collagen type IV (ColIV) and type I (ColI) coated dishes to mimic the environment of the basal epidermal layer and improve the efficiency of differentiation and maturation into K14+ keratinocyte progenitors (Itoh et al., 2011; Bilousova et al., 2011; Kogut et al., 2013). To explore the ability of K14 positive cells to rapidly adhere to collagen-coated surfaces, rapid attachment onto ColI/ColIV-coated plates was applied at every cell passaging during maturation to enrich for K14 positive keratinocytes (Itoh et al., 2013; Bilousova et al., 2011; Kogut et al., 2013). In addition to K14, △Np63-expressing pluripotent stem cells derived-epidermal progenitors have shown to regulate the commitment of ectodermal cells to keratinocyte fate and mediate K14 expression in keratinocyte-specific manner (Li et al., 2019; Pattison et al., 2018). Before the second rapid attachment (Day 14), keratinocyte-like cells were analysed by immunofluorescence for co-expression of △Np63 and K14 (**Figure 4.13A**). Primary keratinocytes from healthy donor were used as a positive control of protein expression. Qualitative analysis in two independent fields (n=2) showed that >80% of the differentiated cells expressed △Np63, although the intensity of expression was lower compared to primary cells. Immunofluorescence analysis confirmed that the

majority of △Np63+ cells also expressed K14 although in an immature (granular) form. By contrast, mature cytoplasmic K14 filaments were observed in the positive control (**Figure 4.13A**).

Despite encouraging preliminary results, only a small number of keratinocyte-like cells was observed in culture after >2 cycles of rapid attachment (**Figure 4.13B**). Significant reduction in cell proliferation was noticed followed by a high number of cells with altered structures and accumulation of autophagic vacuoles within cytoplasm indicating early cellular senescence. Therefore, cells could not be further expanded and characterized. Similar cell loss upon cell passage, limited proliferative growth and spontaneous senescence was also observed on multiple repeats of the protocol (n=3).

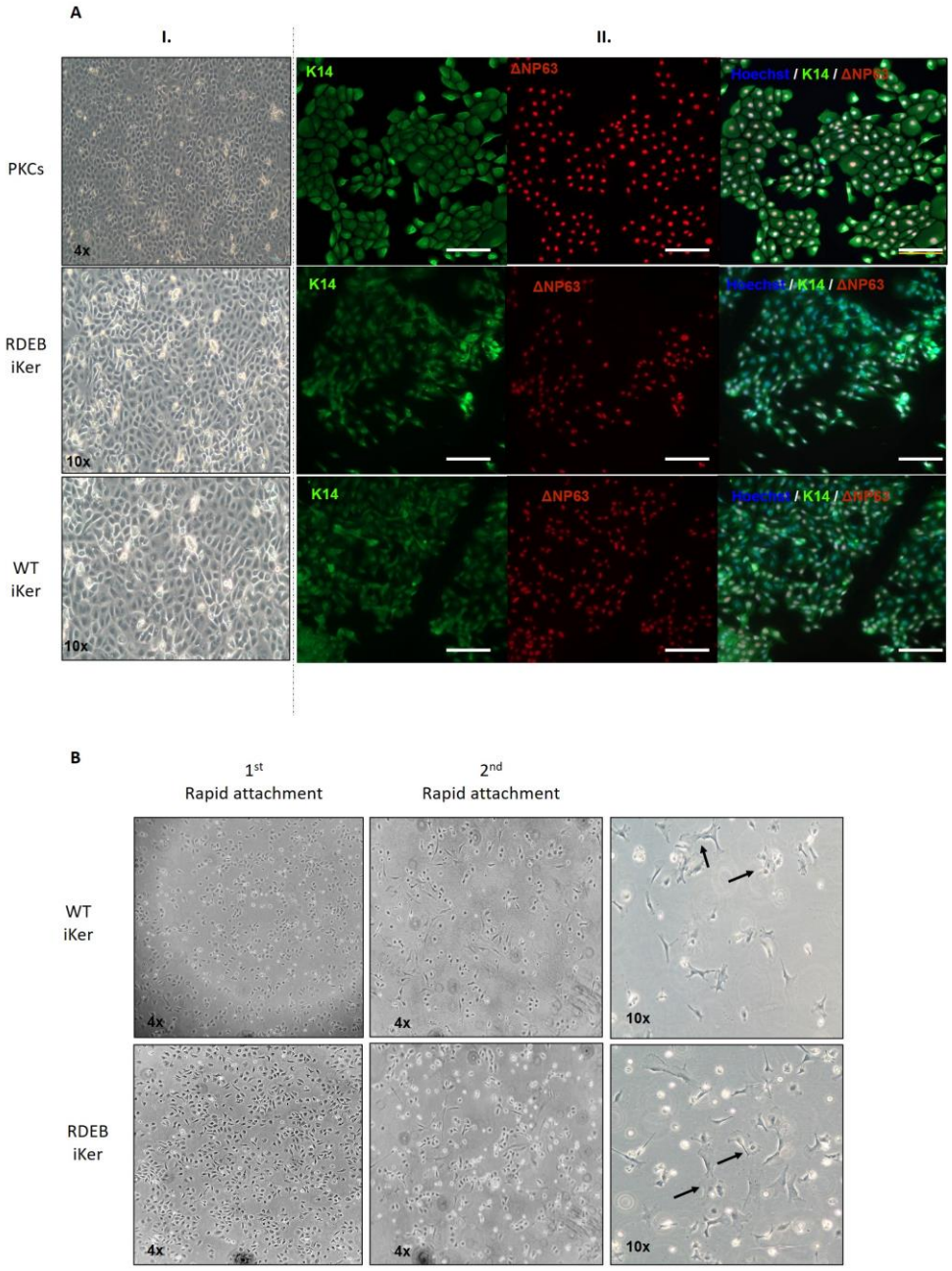

Figure 4.13 Morphology and expression of epidermal differentiation markers in iPSC-derived keratinocytes

A. (**I**) Phase-contrast images of iPSC-derived keratinocytes showed cells of similar size and shape. (**II**) Immunofluorescence of RDEB and WT iKer shows that most cells stain positive for △Np63 (red) at day 14 of differentiation. Initial expression of K14 (green) can be detected in >99% of cells although the nuclear expression pattern suggests non-mature cytokeratin formation. Primary human keratinocytes (PKCs) used as a positive control, showed correct cytoplasmatic K14 expression. All images were taken with 20x objectives. Scale bar = 50µm. **B.** Phase-contrast images of RDEB and WT iKer following the rapid attachment enrichment procedure. Only rapidly adhering cells remain attached. Lower number of cells was obtained after the second rapid attachment with reduced cell growth and appearance of cells with severely altered morphology, indicative of cellular senescence (black arrows).

Therefore, a different differentiation protocol was developed and optimized in collaboration with Professor Dusko Ilic (King's college, London) (**Figure 4.14**). All media used were made in-house and composition is detailed in material and methods (**section 2.2.20.2**). In the first step of keratinocyte differentiation, termed "initiation phase (Day 0-4)", untreated RDEB iPSCs (RDEB iKer) and RDEB iPSCs treated with NT-2PS-ssODN-AAG (NT-2PS-ssODN-AAG iKer) described in **section 4.11,** were cultured in suspension as embryoid bodies (EBs) in hypoxic atmosphere (5% O_2) and treated with 25ng/ml BMP-4 and 1µM of ATRA (**Figure 4.14**). The choice of embryoid bodies over cell clumps relies on technical and biological reasons. EBs harbour many of the hallmarks of early embryonic development and they are commonly used to initiate spontaneous differentiation which can then be manipulated and directed towards a specific cell lineage. For keratinocyte commitment, authors have shown that significant increase in K18+ and ΔNp63+ keratinocyte differentiation occurred only upon induction of pluripotent cells in form of as EBs with ATRA and BMP-4 at the early stages of differentiation (Metallo et al., 2008; Bilousova et al., 2011). Moreover, use of EBs avoids the rapid overgrowing of the committed cells in the early stages of the differentiation. Cell passaging during the initiation step is detrimental for the correct progress towards epithelial commitment.

As a positive control of differentiation, the RDEB parental cell line (heterozygous for the c.425A>G mutation (RDEB iPSCs $c.425^{-/+}$/ $c.425^{-/+}$ iKer) was used. This line was chosen due to a well-known fact that different iPSC lines have different propensity to differentiate towards a certain lineage (Rheinwald 2013; Allegrucci and Young 2007; Skottman et al., 2005). Therefore, it was hypothesised that a parental cell line with the genotype closest to the line of interest can potentially reduce this variability.

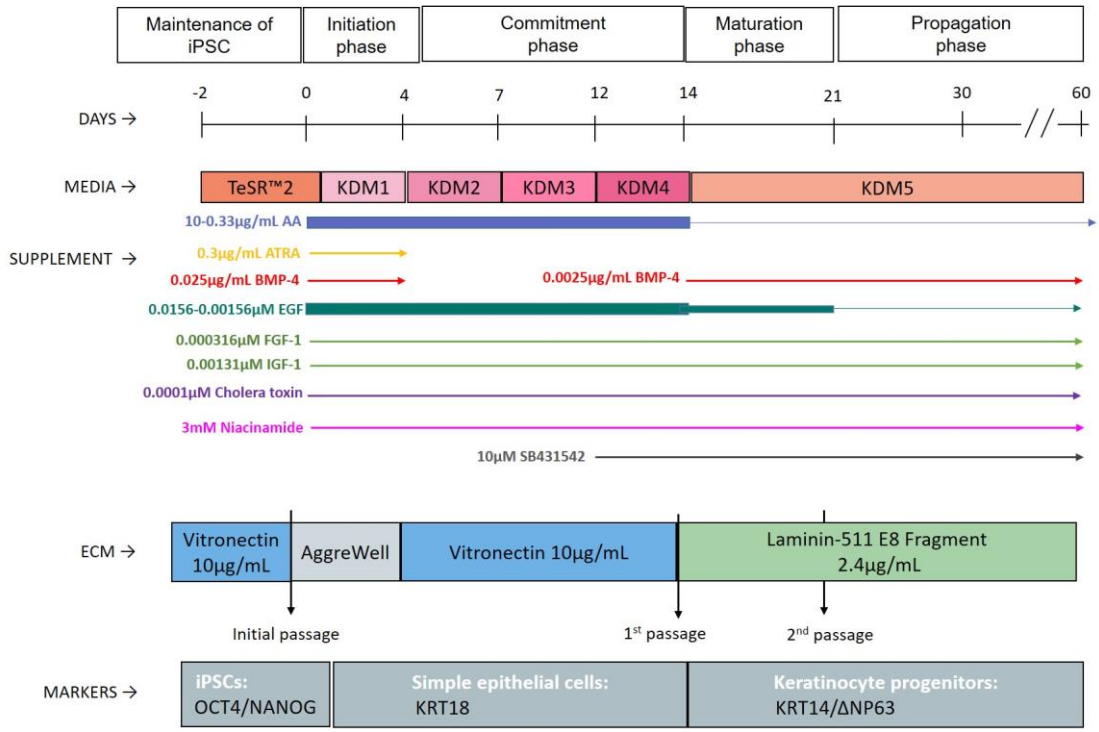

Figure 4.14 Schematic of differentiation protocol and changes in cellular morphology of iKer.

Schematic of the differentiation protocol. The differentiation of iPSC-derived keratinocytes using different in-house made keratinocyte defined media (KDM) and extracellular matrices (ECM) at the indicated time points. Concentrations of growth factors at each critical step of differentiation are listed; Abbreviations: ATRA, All-trans retinoic acid; BMP-4, Bone morphogenetic protein 4; EGF, Epidermal growth factor; TGFβR1Ki, Transforming growth factor beta receptor type I kinase inhibitor. The cells were passaged at Days 0, 14 and 21 time points. At every stage of differentiation, different markers specific for pluripotent stem cells (OCT4, NANOG), epithelial commitment (K18) and keratinocyte maturation (KRT14, ΔNp63) were used to verify the correct development of iPSCs towards epidermogenesis.

Progression towards the keratinocyte lineage was evident by phase contrast of cellular morphology throughout the different stages of the protocol (**Figure 4.15**). During the initiation stage, all the cell lines readily formed embryoid bodies which continued to grow under basal keratinocyte defined medium (KDM1) upon single cell dissociation (initial passage) at day 4. From day 4 to 14 (commitment phase), initiated iPSC lines cultured in KDM2 (day 4-6), KDM3 (day 7-9) and KDM4 (day 10-14) and plated onto vitronectin-coated plates, started to express keratin 18 indicating

commitment to simple epithelial cell lineage (data not showed). The addition of niacinamide (3mM) in KDM3 and KDM4 was found to be a key component to direct the morphology of the initiated cells towards keratinocyte-like stem cells. In additions, niacinamide provided a further boost in proliferative potential and increased life span and colony formation when co-supplemented with transforming growth factor beta receptor type I kinase inhibitor (TGFβR1Ki, SB431542) in KDM4 medium. Activation of keratinocyte markers such as ΔNp63 was assessed at the end of the "maturation stage" (Day 14-21) and "propagation stage" (from day 21 onwards). To guarantee the lifespan and stemness of iPSC-derived keratinocytes in culture, cells were passaged onto laminin-511 E8-fragments coated plates and supplemented with BMP-4 (KDM5) during the maturation and propagation stage.

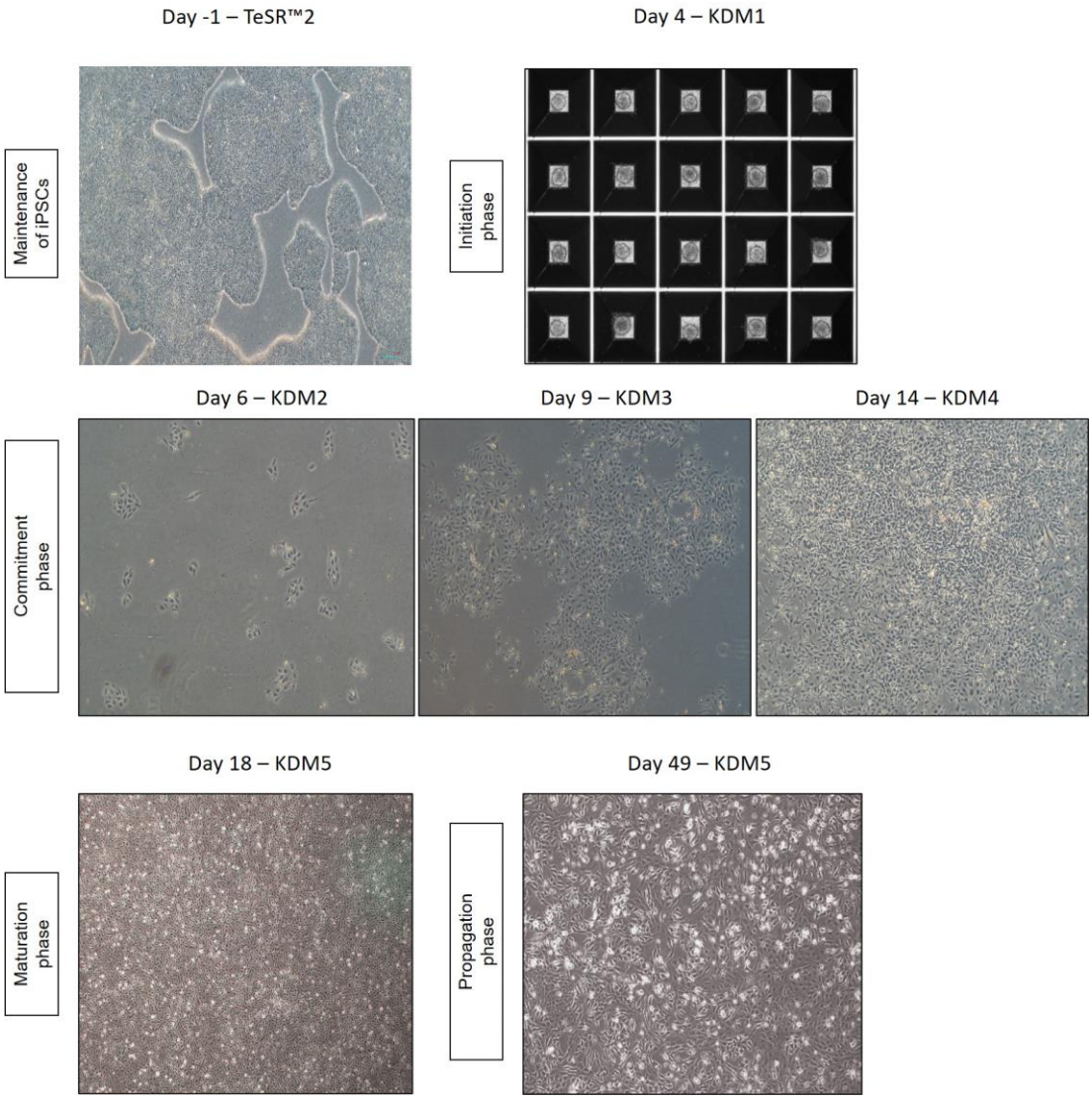

Figure 4.15 Morphology of iPSC-derived keratinocytes at different time point of differentiation

RDEB cells were taken as a representative cell line of keratinocyte differentiation. Maintenance of iPSC phase: iPSCs were cultivated in TeSR™2 until 70% confluent prior to embryoid body formation. Initiation phase: Day 4: iPSCs as embryoid bodies in keratinocyte defined media 1 (KDM1); Commitment phase: Day 6: small cell colonies, upon single cell dissociation of embryoid bodies at day 4, can be observed in culture in KDM2 medium on vitronectin; Day 9: rapidly-dividing cells with morphology resembling committed simple epithelial precursor following niacinamide supplementation (KDM3); Day 14: visible increased cell proliferation given by the synergic effect of niacinamide and transforming growth factor beta receptor type I kinase inhibitor in KDM4. Maturation phase: Day 18: Morphology of the keratinocyte progenitors and emergence of epithelial like island indicated by black arrows. All images were taken from RDEB iPSC line. Propagation phase: Day 49: formation of epithelial-like island in culture and maintenance of keratinocyte-like morphology after several cycles of cell passaging.

Immunofluorescence analysis performed at day 36 in RDEB iKer revealed that >99% of cells were co-expressing ΔNP63+ and K14+, although the latter was expressed in its immature granular form inside the nuclei (**Figure 4.16**). After a subsequent cell passage at days 45, all the cell lines started to express a mature fibrillar form of K14 with cytoplasmatic localization, indicating successful progression towards keratinocyte maturation (**Figure 4.16**). Although consistent expression of ΔNp63 was observed in the majority of the differentiated cells in culture, only approximately a fourth of the cells co-expressed both ΔNp63 and K14 (RDEB c.425$^{-/-}$: 28.3%, RDEB c.425$^{-/+}$: 27%, NT-2PS-ssODN-AAG: 23%). The main reason of a modest fraction of mature K14-expressing cells was hypothesized to be related to the different response of different cell lines to media, supplements and extracellular-matrix during the differentiation process (Rheinwald 2013). This hypothesis is supported by the empirical observation that a similar amount of K14+ cells was overserved in cell line that share the same genotype (untreated RDEB iKer and treated with NT-2P-ssODN-AAG) or a similar one (c.425$^{-/+}$ iKer).

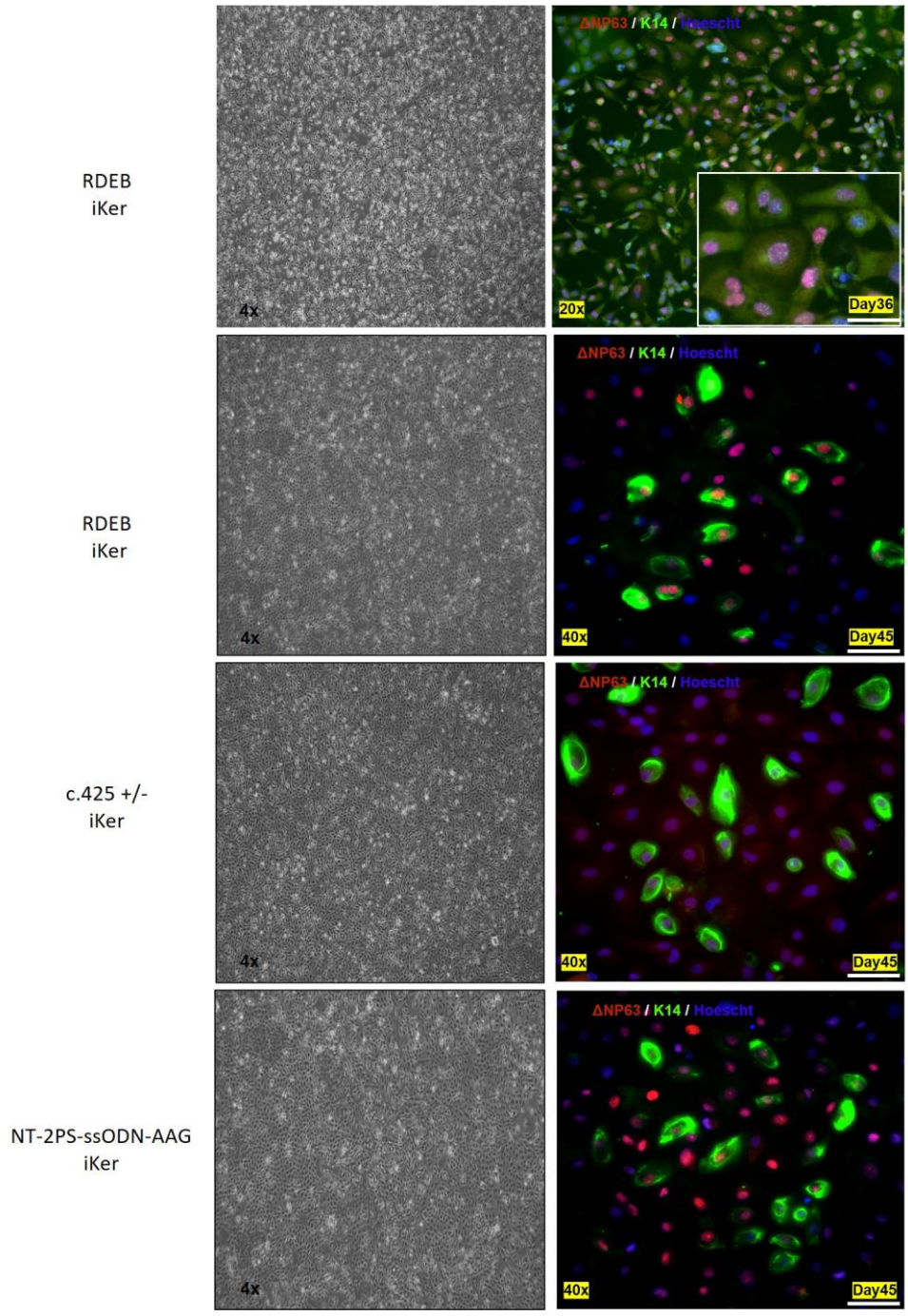

Figure 4.16 Expression of epidermal markers keratins 14 and ΔNp63 at day 45 of Differentiation.

Left column: Phase contrast images of iPSC-derived keratinocytes at day 45 resemble a keratinocyte-like morphology. Right column: Immunofluorescence analysis of co-expression of △Np63 (red) and K14 (green) markers at different time points of differentiation. Hoechst (blue) was used for nuclear staining. From the top to the bottom: RDEB iPSCs at day 36 (immature K14 indicated in the picture magnification) and day 42 (with mature K14); c.425$^{-/+}$ iKer and NT-2PS-ssODN-AAG iKer. The majority of cells were positive for △Np63, whereas approximately 25% of cells were K14+ (28.3%, 27% and 23% in RDEB iKer, c.425$^{-/+}$ iKer and NT-2PS-ssODN-AAG iKer, respectively).

iPSCs-derived keratinocytes were next characterized for C7 expression by immunofluorescent analysis. No residual C7 was observed in untreated RDEB iKer, whereas C7+ cells were detected in the parental cell line (**Figure 4.17A**). Importantly, expression of *de novo* C7 was detected in gene corrected NT-2PS-ssODN-AAG iKer at day at day 45 of differentiation. Quantitative analysis of C7 expression in four independent fields (n=4), revealed 40% of the cells were positive for C7, of which 100% co-expressed ΔNp63.

In accordance with the flow cytometry data previously described in **section 3.13**, these initial results confirmed the capability of the designed NT-2PS-ssODN-AAG template to rescue collagen VII in iPSCs-derived RDEB keratinocyte-like cells. Therefore, to assess the quality and composition of collagen type VII in the treated RDEB iKer population, a WT iPSCs-derived keratinocyte line (WT iKer) at day 52 of maturation at a separate round of differentiation was used as a second positive control (**Figure 4.17B**). Immunofluorescence staining confirmed no difference in C7 expression pattern between WT and patients cell lines.

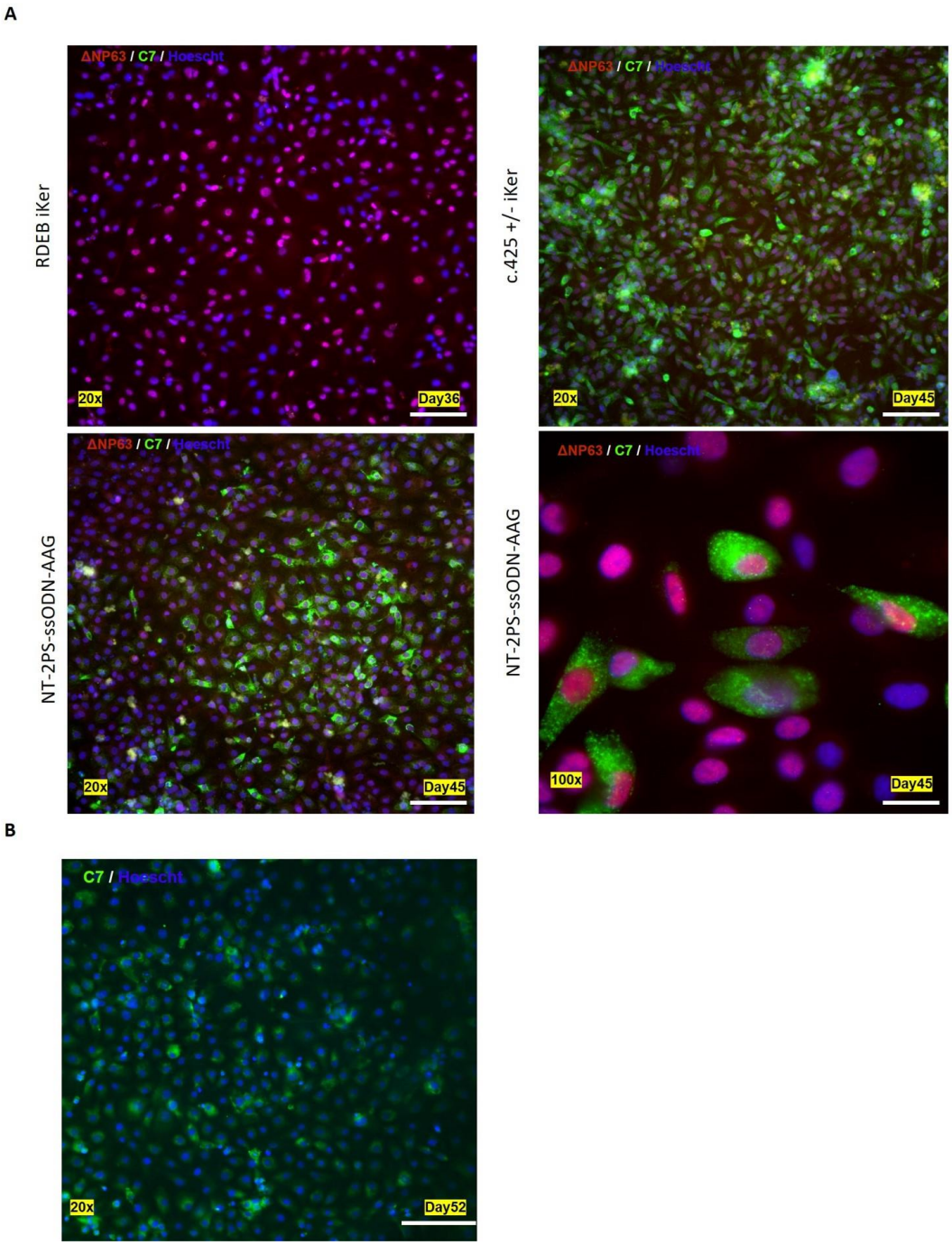

Figure 4.17 keratinocyte-derived cells and gene corrected iKer restore *de novo* C7 expression and express keratinocyte stem cell-like markers

A. Immunofluorescence analysis of co-expression of △Np63 (red) and C7 (green) in iKer. Hoechst (blue) was used for nuclear staining. Top lane: RDEB iKer confirmed to express △Np63 only while C7 is expressed in the parental c.425$^{-/+}$ line. Bottom lane: RDEB iKer treated with NT-2PS-ssODN-AAG stained at day 45 express de novo C7 and co-express △Np63. Higher resolution (100x) of treated cells at day 60 showed correct expression and localization of *de novo* C7. **B.** Staining for collagen type VII in a WT iPSC-derived keratinocyte line confirmed correct protein expression when compared to NT-2PS-ssODN-AAG. All images were taken with the magnification as indicated in the pictures.

4.13 Analysis of Ex3P-sgRNA potential Off-targets in RDEB IPSCs

One of the major challenges for safe application of CRISPR/Cas9 system is the ability to achieve efficient on-target activity (high sensitivity) and minimize the off-targets effects (high specificity) (Doenchet al., 2016; Nelson and Guyer, 2012; Xu et al., 2015). The distribution of such off-target cleavage effects is genome-wide and could be detrimental to cell survival or could potentially be oncogenic. Initial evaluation of Ex3P-sgRNA off-targets was investigated *in silico* using the Benchling tool followed by NGS of the PCR amplified predicted off-target loci from gene edited RDEB iPSCs. NGS analysis using Pindel for the detection of DNA breakpoints revealed that 9 out of 10 off-target sites harboured InDels frequencies between 0.12% and 0.66% (**Figure 4.12**). Only one off-target site, OT8, showed up to 1% DNA cleavage. Importantly, mapping of the predicted off-target site by the human genome browser (https://genome-euro.ucsc.edu/index.html) confirmed that the predicted OT8 sequence falls within an intergenic region of chromosome 16.

Target	gRNA sequence	Gene	InDels %
COL7A1	GGCCCGACCTGGTGTCCCCA	Exon 3, *COL7A1*	73%
OT1	TGCCCGGCCTGGTGTCCCCA	Exon 2, *VWA2*	*0.43%*
OT2	GTCCCGGCCTGGTGTCCCCG	Intergenic, Chr9	*0.60%*
OT3	GGCCTGGCCTGGTGTCCCCC	Intergenic, Chr16	0.18%
OT4	GGCCCAGCCTGGTGTCCCCC	Exon 31, *MUC5B*	*0.56%*
OT5	GGCCCCACCTGGTGACCCCT	Intergenic, Chr10	0.10%
OT6	GGCCCCACCTGGTTTCCCAA	Intergenic, Chr6	0.19%
OT7	GGCATGACCTGGTGTCACCA	Intergenic, Chr10	*0.12%*
OT8	GGGCTGACCTGGTGGCCCCA	Intergenic, Chr16	1.04%
OT9	GGCACGCCCTGGTGTGCCCA	Intergenic, Chr18	0.42%
OT10	GGCCCTACCTGGTCTCTCCA	Intergenic, ChrX	0.66%

Figure 4.18 Off-target analysis for Ex3P-sgRNA in RDEB iPSCs

Off-target sites for *COL7A1* editing in RDEB iPSCs with Ex3P-sgRNA were predicted with the Benchling tool and relative mismatches are showed in red (column 2). For each predicted off-target, gene name and relative location within coding or noncoding sites is indicated in column 3. NGS data from Illumina MiSeq sequencing plotted to quantify off-target Cas9-mediated InDels are showed in column 4. The percentage of reads reported are representative of 1 experiment.

4.14 Chapter discussion

As detailed in **section 1.5.5**, iPSCs have a potential to provide an alternative cell type for future gene and cell therapy applications for RDEB. In this direction, this chapter describes the derivation of iPSCs from RDEB fibroblasts bearing a homozygous c.425A>G mutation hotspot in exon 3 of the *COL7A1* gene. In accordance with previous works (Itoh et al., 2013; Shinkuma et al., 2016; Jacków et al., 2019; Webber et al., 2016; Tolar et al., 2013), the results of this chapter confirmed that derivation of a pluripotent cell line from RDEB patient material is feasible and successful acquisition of pluripotency-associated markers could be achieved as demonstrated on mRNA and protein levels. RDEB iPSCs were also capable of trilineage differentiation *in vitro* through embryoid bodies formation and outgrowth of primitive germ layers, further confirming their pluripotency. Notably, patient-derived RDEB iPSCs were shown to retain the c.425A>G mutation on genomic level, thereby creating a stable cell line that could be employed to assess efficiency of HDR-based *COL7A1* correction strategies previously described in **Chapter 3**.

Optimizing delivery and efficiency of the CRISPR/Cas9 complex for genome editing of iPSCs is still subject of intense investigation due to the well-known propensity of iPSCs to undergo apoptosis or spontaneous differentiation upon gene editing. Work performed by other researchers indicate that Cas9-mediated toxicity creates an obstacle to the high-throughput use of CRISPR/Cas9 for genome engineering in iPSCs due to the significant cell death upon editing (Xu et al., 2018; Li et al., 2014; Ihry et al., 2019). Therefore, development of minimally toxic and efficient delivery methods of the CRISPR/Cas9 machinery and donor template and optimization of iPSCs manipulation protocols were required to achieve significant frequencies of HDR, whilst mitigating cell toxicity upon gene editing.

I have shown that co-delivery of SpCas9 RNP and NILV-donor described in **Chapter 3** for human keratinocyte cell line can be replicated in iPSCs. The reason for the different percentage of donor integration between the two cell lines has been hypothesized to be due to the different cellular response to genetic manipulation, the speed of cell recovery and spontaneous differentiation rate post electroporation.

Additionally, this chapter presents compelling evidence that gene correction by ssODN donor template is able to generate high rates of HDR in the gene edited population, thereby avoiding extended manipulation, such as clonal selection, of gene edited cells. This further suggested that the bulk population of gene-corrected RDEB iPSCs could be used for directed differentiation into keratinocyte-like cells to evaluate the synthesis of *de novo* C7 *in vitro.*

Therefore, the first goal of my differentiation experiments focused on adapting and replicating previously published protocols in RDEB and WT iPSC lines (Itoh et al., 2013; Shinkuma et al., 2016; Jacków et al., 2019). To do so, I evaluated the efficiency of epidermal commitment by analysing cell morphology and expression of K18, as well as co-expression of K14 and ΔNp63 as markers of keratinocyte maturation. Co-stimulation by ATRA and BMP-4 confirmed the ability of iPSCs to change morphology towards keratinocyte-like cells. In support of the observed changes in cell morphology, expression of keratinocyte stem cell markers ΔNp63 and immature form of K14 were detected. In agreement with previous reports on the enrichment of K14+ cells during keratinocyte maturation, rapid-attachment on ColI/ColIV-coated plates resulted in a more homogenous population of keratinocyte-like cells. Despite the promising results, this protocol presented with critical drawbacks in my experimental settings. Keratinocyte-like cells could only be maintained for up to 2-3 rapid attachment passages, followed by growth arrest and early senescence. Therefore, assessment of C7 expression was not possible in these cells.

Subsequent, a second differentiation protocol was developed and optimized, resulting in epidermal differentiation of untreated and gene corrected iPSCs with a longer proliferative capacity *in vitro*. Under these differentiation conditions, the majority of the cells expressed ΔNp63 with approximately 25% of K14+ cells at day 45 of the protocol. This suggests that the longer cultivation or optimization of the protocol for this cell line might need to be carried out in the future in order to enrich for ΔNp63+/K14+ epidermal cells. Importantly though, immunocytochemistry for C7 in iPSC-derived keratinocyte-like cells confirmed the restoration of protein expressing to the levels similar to though detected on molecular level, thereby verifying the efficiency of the gene addition strategy.

Finally, to initially validate the safety profile of this gene editing strategy, NGS analysis of the top 10 computationally predicted off-target for Ex3P-sgRNA showed no evidence of Cas9-induced InDels in the predicted loci. In conclusion, ssODN-mediated HDR permits to achieve significant levels of gene correction for a mutation hotspot (c.425A>G) in patient-derived iPSCs that can be consequently used to generate keratinocyte-like cells. The efficient gene editing strategy described in Chapter 4 emphasises the importance of diligent and rational design of donor template sequence, optimization of electroporation protocols and choice of format and amount of SpCas9 and sgRNA components. Similar optimizations will be evaluated for targeted base editing discussed in the next chapter.

Chapter 5 Base editor correction of c.425A>G COL7A1 in patient-derived fibroblasts and iPSCs

5.1 Background

Current CRISPR/Cas9 editing strategies for the generation of gene knockout, exon skipping or gene knock-in have contributed to the pursuit of precise and efficient editing of DNA by NHEJ and HDR upon double stranded breaks (DSB) *in situ*. However, DNA repair processes upon Cas9-induced DSBs may result in a random introduction of insertions/deletions or other unwanted and potential harmful DNA rearrangements at the site of the breaks. This has been particularly demonstrated in hESCs and iPSCs due to activation of p53-dependent DNA damage response and apoptosis upon Cas9-induced DSBs (Ihry et al., 2018; Haapaniemi et al., 2018). Different approaches involving temporal P53 inhibition by chemicals (Pifithrin-α) or delivery of a dominant negative P53DD transgene have so far shown controversial results in alleviating Cas9-related toxicity (Li et al., 2018). In contrast, CRISPR/Cas9-derived base editors such as cytidine base editors (BE) and adenosine base editors (ABE) have recently offered the possibility for scarless C → T or A → G conversions without Cas9-induced double stranded DNA cleavage. These tools hold a significant potential for the correction of more than 60% of human pathogenic SNPs in the Clinvar database (Komor et al., 2016a; Rees and Liu 2018). Additionally, due to their mechanism of action (**section 1.10**), this technology presents a safer option for single or multiplexed genome editing reducing the risk of large chromosomal translocation events between the edited loci.

5.2 Hypothesis

Primary RDEB fibrobalsts and iPSCs described in **Chapter 4**, could restore endogenous C7 expression upon seamless nucleotide-specific correction by cytosine base editor (CBE) technology. The use of BE3 obviates the need for a repair template and avoids the introduction of InDels or off-target SpCas9-induced DSBs.

5.3 Aims

1. Investigate base editing technology by designing guide RNAs targeting the c.425A>G mutation hotspot by modelling BE editing in RDEB iPSCs
2. To evaluate the ability of base corrected iPSCs to recover C7 expression by direct keratinocyte differentiation from pluripotent stem cells
3. Investigate c.425A>G mutation correction in RDEB fibroblasts and assess C7 production *in vitro*.
4. Evaluate the ability of BE-corrected fibroblasts to restore functional C7.

5.4 Modelling coBE3 editing in RDEB iPSCs

Briefly the structure of the BE3 protein used in this study consisted of a cytidine deaminase (rAPOBEC1) joined via a 16AA linker to a D10A nCas9, fused to an uracil DNA glycosylase inhibitor (UGI) molecule via a 4AA linker, followed by an SV40 NLS separated via another 4AA linker (**Figure 5.1A**). All the components mentioned above play a key role in the function of this gene editing tool. Deactivated cas9 is directed by PAM dependent guide RNA to a specific gene locus, where rAPOBEC1 operates within a defined window to deaminate cytosine to uracil (C>U). D10A nCas9 simultaneously nicks the unedited DNA strand promoting correction from the uncut edited strand. Upon base conversion, a third element, a UGI enzyme, prevents excision repair of U bases by endogenous Uracil-DNA glycosylase (UDG). Once situated at its target site, BE3 is able to perform these C>T changes most effectively within a 5bp editing window (4-8 nucleotides distal to the PAM). Prior to its use in my

experiments, the BE3 DNA sequence was codon optimised (coBE3) by Dr. Roland Preece (GeneArt, ThermoFisher Scientific) as this has been shown to increase mRNA stability and protein production within mammalian cells (Wu et al., 2019; Zafra et al., 2018). The plasmid DNA was then used for mRNA synthesis (TriLink BioTechnologies, California, USA) for mRNA production. Moreover, a co-transcriptional 5' capping structure and a further polyadenylated site were added to increase expression and stability.

To test coBE3, 2 specific sgRNAs (named x3C7-CyD-1 and x3C7-CyD-2) were designed and verified by the Benchling tool (**Table 5.1**) to ensure that the c.425A>G mutation falls within the 5bp editing window from the 3' end of the designed protospacers (Komor et al., 2017). In detail, the c.425A>G mutation sits in position C5 and C6 from the 3' terminus of x3C7-CyD-1 and x3C7-CyD-2 sgRNAs, respectively (**Figure 5.1B**). Both guides were designed to be compatible with SpCas9 as well as BE3. Initial validation of guide RNA efficacy for x3C7-CyD-1 and x3C7-CyD-2 was therefore tested in combination with SpCas9 mRNA in RDEB iPSCs using the electroporation conditions described in **section 4.10** for gene disruption by NHEJ. Cells electroporated with Ex3P-sgRNA were used as positive control of gene disruption by NHEJ. Knockout frequency evaluated on genomic level equated to 77% and 64% for x3C7-CyD-1 and x3C7-CyD-2, respectively (n=1). Comparable percentages of NHEJ were observed with Ex3P-sgRNA (83%) (**Figure 5.1C**).

Table 5.1 Guide sequences tested for *COL7A1* Base editing

Guide No	Sequence	PAM	S	On-Target Score	Off Target Score	BE-score
x3C7-CyD-1	CACCCCGGGGACACCAGGTC	GGG	-	45.9	66.4	**21.4, 20.3, 9.3, 5.6, 4.1**
x3C7-CyD-2	TCACCCCGGGGACACCAGGT	CGG	-	52.1	70.2	**22.4, 21.4, 20.3, 11.6, 6.4**
B2M-CyD	ACTCACGCTGGATAGCCTCC	AGG	-	65.3	85.0	**2.8, 13.5, 21.7, 2.5**

Guides x3C7-CyD-1 and -2 were used to assess the G>A base conversion efficiency in exon 3 of *COL7A1*. B2M-CyD guide was used as positive control. Guide orientation is shown as sense or anti-sense and binds complementary DNA strand by Watson and Crick base pair. On-target score is the target activity evaluated by the algorithm developed by Doench, Fusi *et al*. (Doenchet al., 2016). The score is from 0-100 and higher scores mean higher on-target activity. Off-target score is evaluated according to the number of mismatches between the

selected guide RNA and similar exonic off-target site. The score is from 0-100 and higher scores mean lower off-target activity. Base editing prediction score for all the bases in red was determined by the efficiency of BE1 activity *in vitro* using a NGG PAM site.

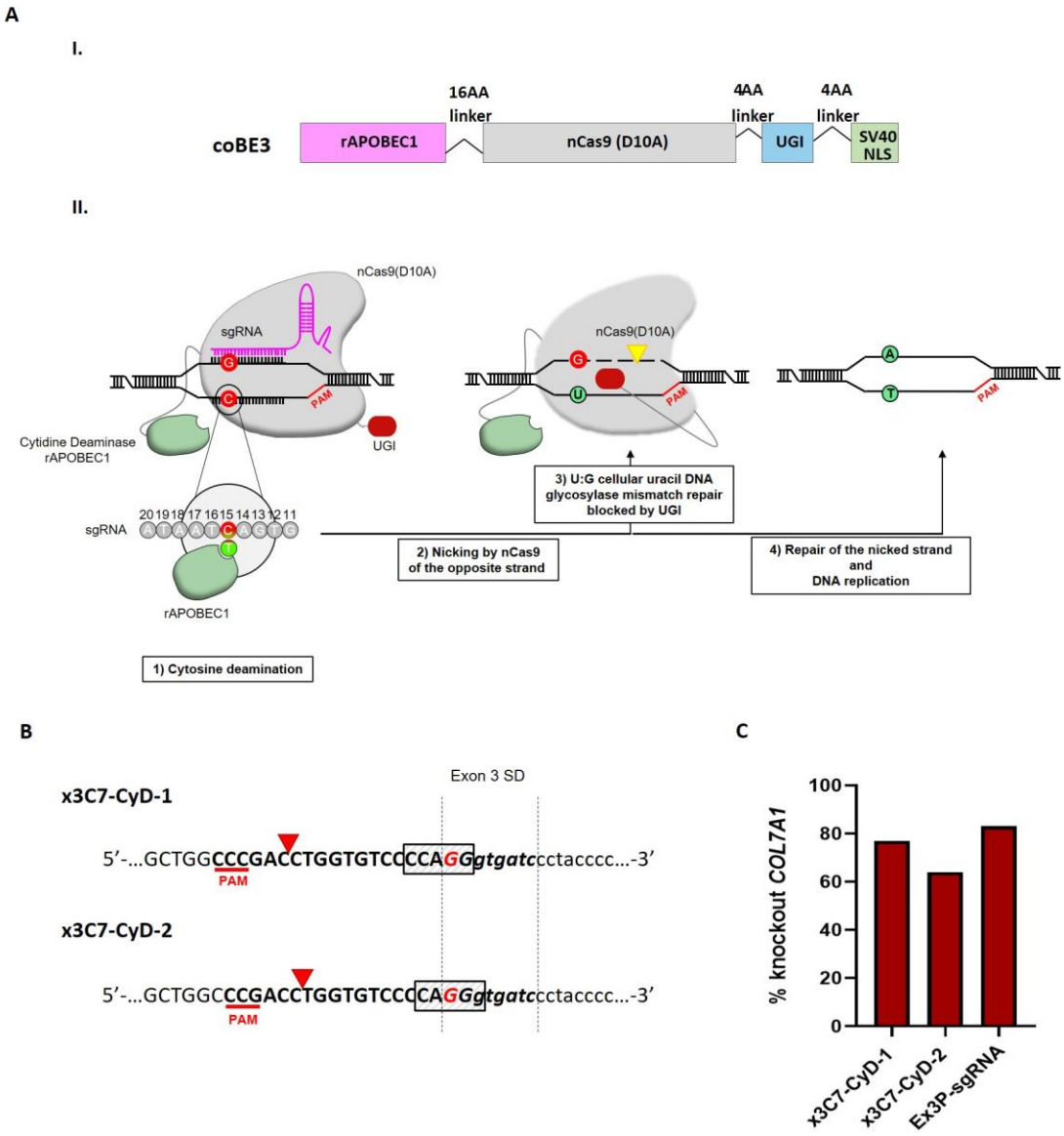

Figure 5.1 Guide RNA design for BE in c.425A>G were initially tested using SpCas9

A. (**I.**) Schematic of coBE3 protein layout and (**II.**) Mechanism of action. Abbreviations: rAPOBEC, rat APOBEC; nCa9, nickase Cas9, UGI, uracil DNA glycosylase; SV40 NLS, nuclear localization signal from SV40 T antigen; AA linker, amino acid linker. **B.** Schematic representation of x3C7-CyD-1 and x3C7-CyD-2 guide RNAs designed to target exon3/intron3 junction of *COL7A1* and their PAM sequences (underlined in red). The guanine G in red represents the c.425A>G RDEB point mutation. Grey boxes represent the base editing window of coBE3 which corresponds to the 4th and 8th nucleotides of each sgRNA counting from the 3'end of the protospacer sequence. Highlighted with vertical line the exon 3 splicing donor (SD) **C.** Validation of the designed x3C7-CyD-1 and x3C7-CyD-2 was performed by

electroporation of guide RNAs alongside spCas9 mRNA in RDEB iPSCs. Each bar represents the percentage of *COL7A1* gene knockout for x3C7-CyD-1 (74%), x3C7-CyD-2 (63%) and Ex3P-sgRNA (83%) used as positive control (n=1).

In order to confirm coBE3 ability to generate on-target C>T changes, x3C7-CyD-1 and x3C7-CyD-2 guides were then delivered in RDEB iPSCs alongside 5µg of coBE3 mRNA. Guide RNA targeting exon 1 of *B2M* gene, B2M-CyD, was used as positive control. The B2M-CyD sgRNA, designed by Dr. Roland Preece, generates a pre-mature stop codon through C>T changes within the exon 1 splice donor site resulting in early termination of translation, thereby leading to a truncated non-functional Beta-2-microglobulin protein. coBE3 edited cells were harvested on day 7 post electroporation and C>T base changes were assessed on genomic DNA. Sanger sequencing-based EDIT-R showed targeted G>A conversion at position c.425 at 45% and 32% for x3C7-CyD-1 and x3C7-CyD-2 sgRNAs, respectively (n=1) (**Figure 5.2A**). Successful base editing was also observed for *B2M* by Sanger sequencing reaching high levels of C>T conversion in both predicted position C4 (55%) and C6 (66%), whereas relatively low editing was observed at C8 (8%) (**Figure 5.2B**). In agreement with data obtained on genomic levels, flow cytometry confirmed B2M knockout of 78.8% in the control assessments (**Figure 5.2B**).

Liu and co-workers demonstrated that for target sites with multiple editable Cs within or nearby the activity window, can also be subject to base conversion in addition to the target base. It is commonly used the term “bystander editing” to describe editing in the protospacer at a different nucleotide from the target one. Due to the 5bp-wide editing window recognized by coBE3, quantification of bystander C>T base conversion was analysed in cells treated with x3C7-CyD-1 and x3C7-CyD-2 sgRNAs. On-target, in-window, coBE3 bystander activity resulted in detectable C>T conversion at position c.426 with a frequency of 4% for x3C7-CyD-1 and 21% for x3C7-CyD-2 guide RNA (n=1). As iPSCs do not express C7 (Sebastiano et al., 2014), the effects of these undesired C>T changes on mRNA and protein levels could not be verified in the first instance. However, predictive tools were used to assess coBE3-bystander effects on C7. Benchling predicted that C>T conversion at position c.426 alone resulted in a missense mutation falling on the 3rd base the last codon in exon 3 of *COL7A1* (AGG-

>AGA, Lys->Arg) in RDEB iPSCs (**Figure 5.2A**). The presence of this mutation should change in the conservative splicing donor site mimicking splicing impairments as described in RDEB patient cells (Gardella et al., 1996). Splice site disruption was also confirmed using the Human Splicing Finder v3.1 (http://www.umd.be/HSF/) online tool. On the other hand, C>T conversion at both positions c.425 and c.426 upon coBE3 base editing creates a disruption of the splicing donor consensus sequence, as previously demonstrated in keratinocyte cell lines using the NT-2PS-ssODN-AAA in chapter 3, despite restoring the wild type amino acid sequence.

To additionally confirm on target correction between x3C7-CyD-1 sgRNA and x3C7-CyD-2 sgRNA, a *StyI*-RLFP assay, described in **section 4.4**, was performed in RDEB iPSCs treated with both guide RNAs (**Figure 5.2A**). Enzymatic digestion of PCR amplicons of exon3/intron3 junction from samples treated with the *StyI* enzyme is only observable when the C>T conversion is achieved at position c.425. In the presence of in-window bystander C>T editing, the *StyI* digestion cannot be observed due to the disruption of the enzymatic DNA site and consequently of the exon3 splicing acceptor. Enzymatic digestion revealed that both cells edited with x3C7-CyD-1 and x3C7-CyD-2 sgRNAs showed positive bands at 268bp and 115bp, similar to those observed in WT iPSCs. However, densitometric analysis of the *StyI* digested fragments quantified by the ImageJ software confirmed increased level of correction with x3C7-CyD-1 guide compared to the x3C7-CyD-2 sgRNAs (22.5% and 10.3%, respectively).

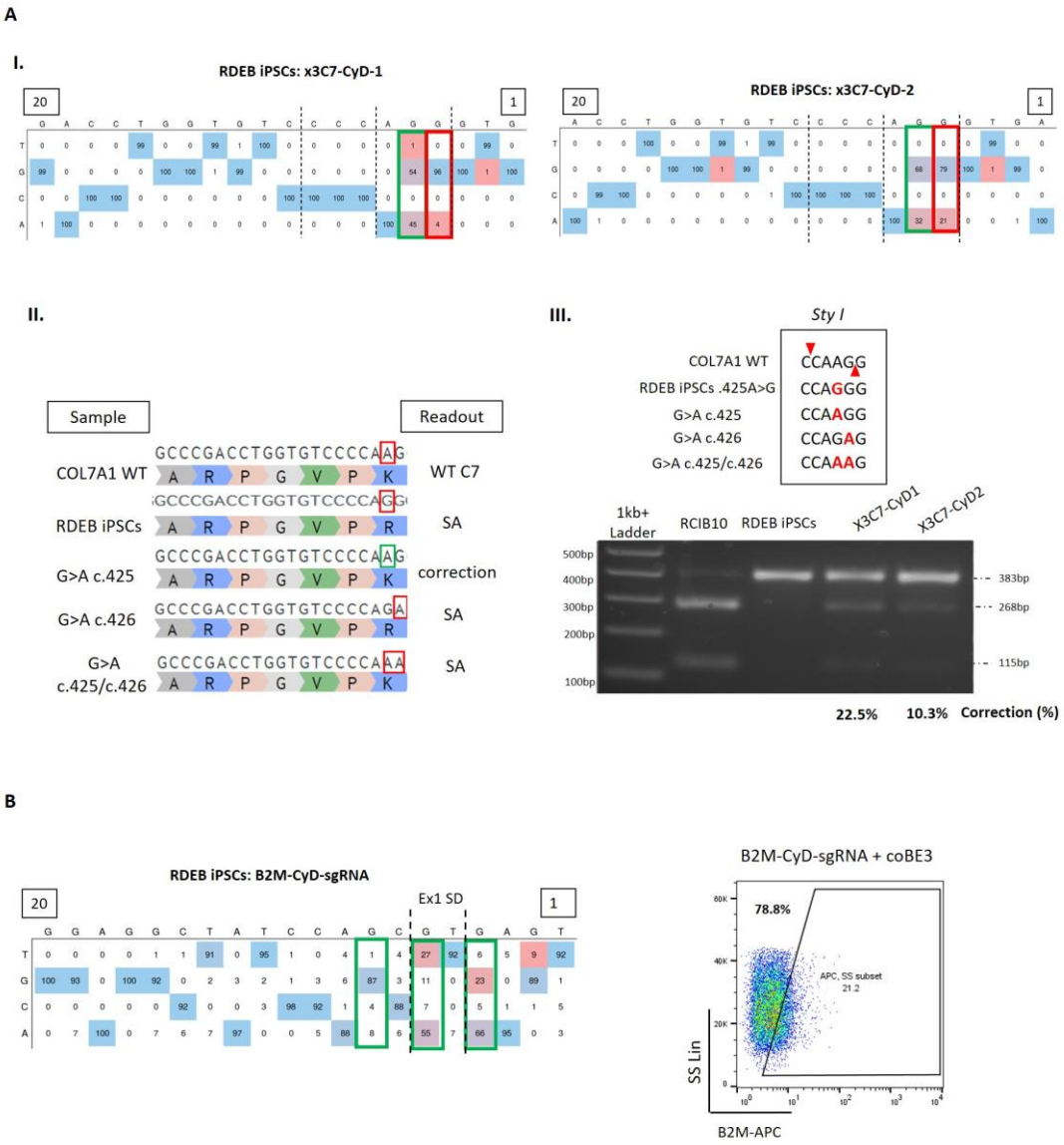

Figure 5.2 Testing of coBE3 strategy for c.425 A>G mutation hotspot in *COL7A1*

A. (I.) Representative EDIT-R output for RDEB iPSCs treated with 5µg of coBE3 mRNA and either x3C7-CyD-1 or x3C7-CyD-2 guide RNAs. Green boxes indicate the on-target G>A correction (54% for x3C7-CyD-1, 32% for x3C7-CyD-2) at position c.425 of *COL7A1*. Red boxes indicate the occurrence of C>T bystander edits within coBE3 activity window (4% for x3C7-CyD-1, 27% for x3C7-CyD-2). (**II.**) Prediction of the possible outcomes of on- and off-target C>T editing on *COL7A1* translation using the Benchling tool. For each possible outcome, DNA sequence of exon 3 of *COL7A1* and corresponding amino acid sequence are shown. From the top, the wild type (A) and RDEB (A>G) nucleotide sequences at position c.425 are boxed in green and red, respectively. Single nucleotide correction at position c.425 (c.425 G>A) in RDEB iPSCS corresponds to the restoration of the correct C7 amino acid sequence (R>K) and the splicing donor site. Single nucleotide correction at position c.426 (G>A c.426) corresponds to the introduction of a missense mutation (AGG>AGA) in the RDEB *COL7A1* sequence where both the amino acid sequence and the splicing donor are altered. This editing leads to splicing aberration (SA) upon transcription of the base edited gene. Co-presence of C>T changes (G>A

at both the positions c.425 and c.426) leads to the restoration of the wild type C7 amino acid sequence but alters the consensus sequence of the exon 3 *COL7A1* splicing donor site resulting in splicing aberration (SA). (**III.**) *StyI*-based enzymatic digestion of the PCR amplified exon 3 of *COL7A1* in RDEB treated with coBE3 and either x3C7-CyD-1 or x3C7-CyD-2. Untreated WT and RDEB iPSCs were used as control. The restriction digestion site sequence recognized by the *StyI* enzyme is shown by the red triangles. The possible combinations of coBE3-mediated nucleotide changes are shown in red. Restoration of the StyI digestion site was detected by gel electrophoresis in cells treated with either x3C7-CyD-1 or x3C7-CyD-2. The percentages of corrective C>T base change numbers at the bottom of the gel (22.5% for x3C7-CyD-1, 10.3% for x3C7-CyD-2) were quantified by ImageJ`s gel analysis function. **B.** EDIT-R analysis of C>T conversion at Ex1 sgRNA protospacer positions C8 (8%), C6 (55%) and C4 (66%) within *B2M* locus targeted as a positive control. C>T base editing in Ex1 splicing donor site resulted in 78% B2M knockout detected by flow cytometry in RDEB iPSCS.

Authentication of the on-target coBE3 editing profile within the editing window of x3C7-CyD-1 protospacer was verified by Dr. Athina Gkazi using NGS data run on a MiSeq, followed by analysis using naïve calling variant (NVC) which counts the number of base variations at each nucleotide position within the protospacer (**Figure 5.3A**). In accordance with Sanger sequence results, NGS confirmed up to 44% (59% of the total C>T changes) of on-target coBE3 editing activity at position c.425. In-window and out-of-widow bystander C>T conversions were also observed at significant frequencies at different nucleotides within the x3C7-CyD-1 protospacer. For the former, 19.4% of C>T conversion was detected at position c.426.while significant percentages of C>T conversion were also found outside the predicted editing area at positions C3 (3.8%) and C1 (7.4%) of the x3C7-CyD-1 protospacer. Other out-of-window coBE3-dependent conversion was <1% above background across the sequencing window. Noteworthy, as described in Komor *et al*. studies (Komor et al. 2016), non C>T changes (C>A and C>G conversions) were also observed within and near the coBE3 editing window for the x3C7-CyD-1 guide, thereby disrupting the wild type C7 amino acid sequence (**Figure 5.3A**).

Despite the confirmation of base editing efficacy in RDEB iPSCs by NGS, the main limitation of the analysis described above is the lack of a haplotype-based variant detection of the corrective coBE3 editing activity without the presence of bystander events within the same sequenced read. Raw NGS data was also analysed by

CRISPResso2 bioinformatical tool to quantify haplotype variants due to different C>T combinations inside and outside the coBE3 editing window and within the exon 3 splicing donor. Of the 44% of C>T conversion at position c.425 detected by single nucleotide base calling, 23.5% of the NGS reads (1144 of 4444 total reads) were found to be able to restore the wild type *COL7A1* sequence without the presence of unwanted C>T changes (**Figure 5.3B**). Importantly, the obtained percentage of corrective haplotype by deep sequencing confirms what previously observed by densitometric assay on DNA level. The analysis also showed the presence of different haplotype combinations harbouring undesired C>T coBE3-mediated substitutions and C>A or C>G changes within the exon 3 of *COL7A1* splicing donor. Collectively, all the haplotypes bearing unwanted combinations in splicing donor would be expected to interfere with the generation of correct Col7 transcripts upon splicing as observed in **section 3.13**.

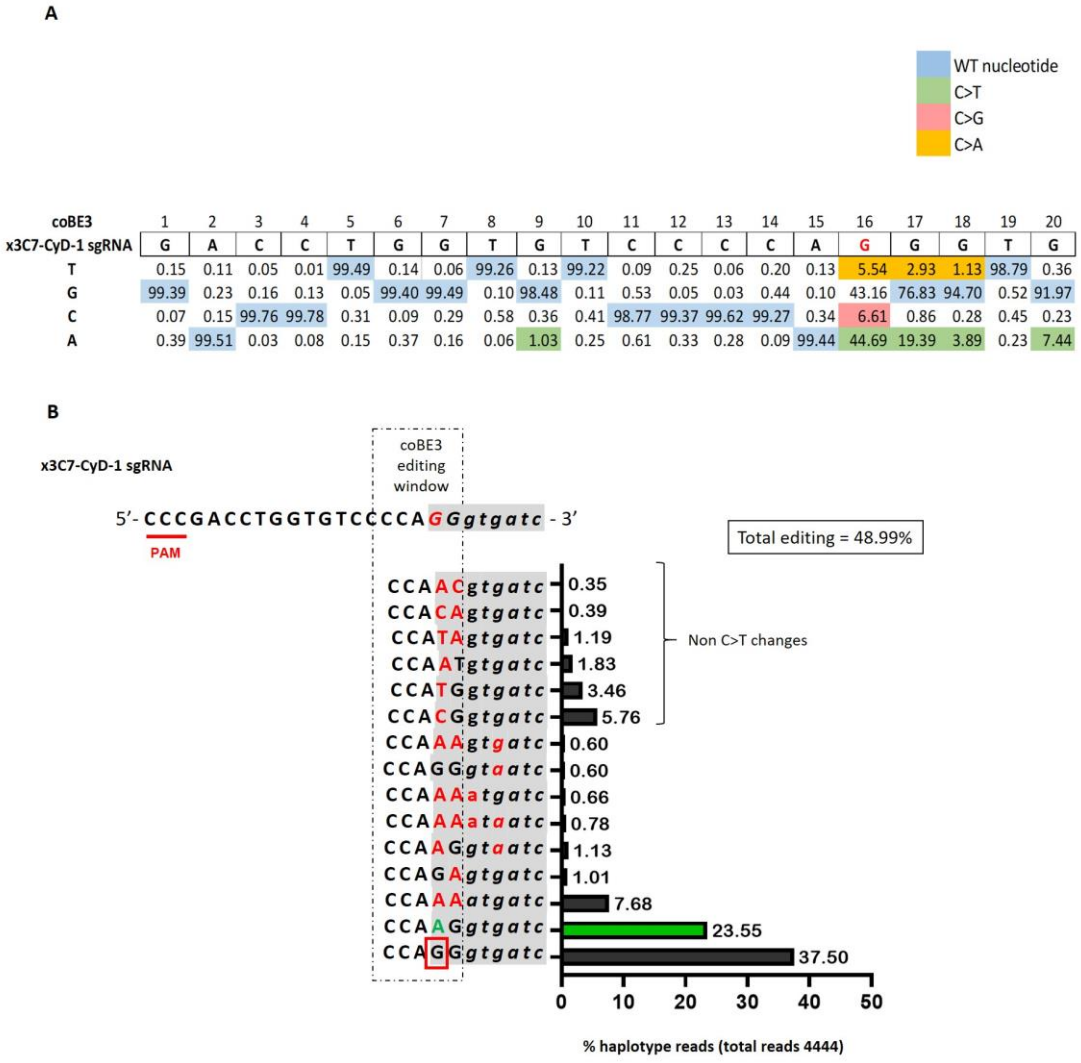

coBE3	1	2	3	4	5	6	7	8	9	10	11	12	13	14	15	16	17	18	19	20
x3C7-CyD-1 sgRNA	G	A	C	C	T	G	G	T	G	T	C	C	C	C	A	G	G	G	T	G
T	0.15	0.11	0.05	0.01	99.49	0.14	0.06	99.26	0.13	99.22	0.09	0.25	0.06	0.20	0.13	5.54	2.93	1.13	98.79	0.36
G	99.39	0.23	0.16	0.13	0.05	99.40	99.49	0.10	98.48	0.11	0.53	0.05	0.03	0.44	0.10	43.16	76.83	94.70	0.52	91.97
C	0.07	0.15	99.76	99.78	0.31	0.09	0.29	0.58	0.36	0.41	98.77	99.37	99.62	99.27	0.34	6.61	0.86	0.28	0.45	0.23
A	0.39	99.51	0.03	0.08	0.15	0.37	0.16	0.06	1.03	0.25	0.61	0.33	0.28	0.09	99.44	44.69	19.39	3.89	0.23	7.44

Figure 5.3 Characterization of coBE3 changes in RDEB iPSCs by NGS

A. Base variant calling of C>T changes across the *COL7A1* locus in RDEB iPSCs electroporated with coBE3 mRNA and x3C7-CyD-1 sgRNA by NGS. Substitution rate at each position of the x3C7-CyD-1 protospacer is displayed in the table. The c.425A>G target base is highlighted in red. The green blocks represent coBE3-mediated C>T conversion across the protospacer. The c.425A>G mutation is corrected by coBE3 in 44.7% of total reads. Percentages of bystander C>T conversions are reported in the table. Non-conventional C>T conversions were reported within and near the editing window and percentages are shown in the table with the following colors: Red: C>G and yellow: C>A. Blue box represent unedited nucleotides. **B.** CRISPResso2-based haplotype quantification of corrective C>T edits (green letters) in based edited cells. The percentage of reads with a single correction at position c.425 is represented by the green bar (23.55%). Bystander C>T edits and non C>T base changes in the 5bp coBE3 deamination activity window (dotted box) and within the exon 3 *COL7A1* splicing donor (highlighted in grey: uppercase, exon 3 DNA sequence, italics intron 3 sequence) are represented by red letters in different haplotype combinations. Percentage of each haplotype is reported in the graph. Boxed in red, the c.425A>G pathogenic hotspot mutation in unedited reads (37.5%).

5.5 Base edited RDEB iPSCs express C7 in vitro after direct differentiation into keratinocytes

To confirm restoration of C7 in coBE3-edieted cells, x3C7-CyD-1 RDEB iPSCs were differentiated into keratinocyte-like cells using the previously described differentiation protocol (performed by Professor Dusko Ilic) shown in **Figure 4.14**. The differentiation of x3C7-CyD-1 RDEB iPSCs (from now called x3C7-CyD-1 iKer) was performed in parallel with all cell lines described in **section 4.12**. x3C7-CyD-1 iKer showed similar cellular morphology changes towards keratinocytes commitment at each stage of the differentiation. Correct localization of the ΔNP63+ and K14+ keratinocyte stem cell markers was assessed at day 45 of the differentiation by immunofluorescence (**Figure 5.4**). In line with the results observed in **Figure 4.16** quantification of the immunofluorescent data showed that the majority of x3C7-CyD-1 iKer displayed bright ΔNp63 positivity with around 20% of K14+ co-expressing cells in a fibrillar fashion. Next, in accordance with the percentage of corrective C>T haplotype observed by NGS, immunofluorescence for C7 confirmed rescued protein expression at 29.4% in base-edited x3C7-CyD-1 iKer, of which 100% co-expressed ΔNp63 (**Figure 5.4**). The similar correction levels on genomic and protein levels suggest that only precise C>T correction in position c.425 is able to rescue patient's collagen type VII. In window and out-of-window bystander effects, on the contrary, hinder the correct C7 synthesis due to splicing aberration.

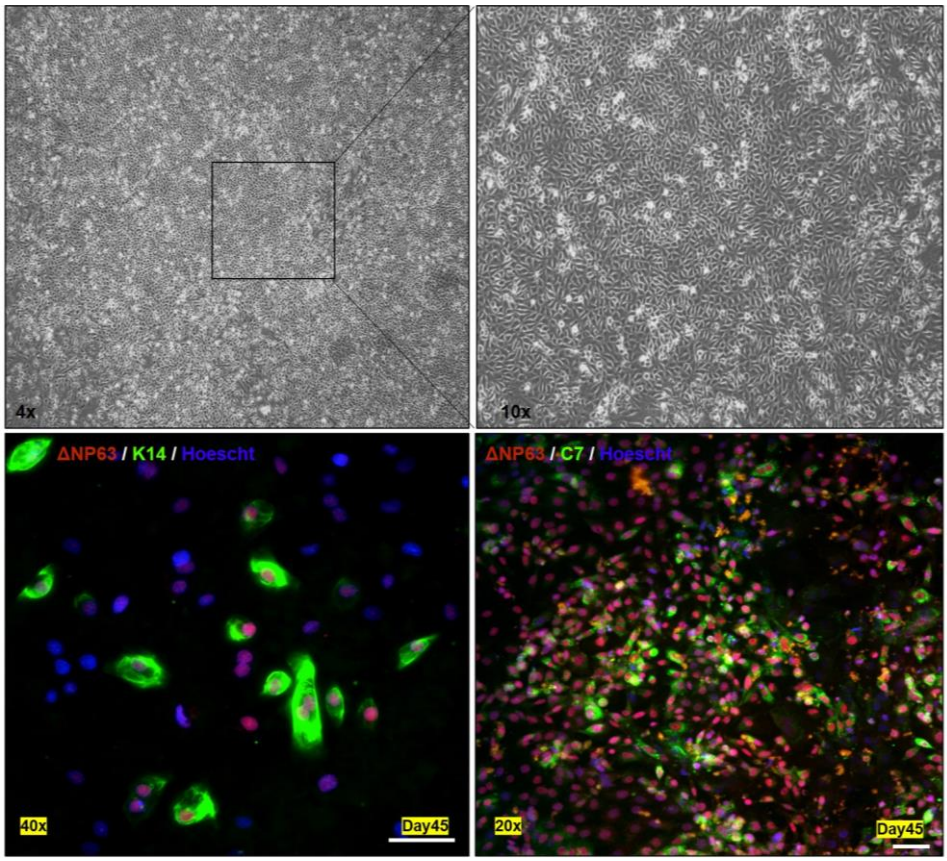

Figure 5.4 Characterization of keratinocyte stem cell markers and rescue of C7 in base edited x3C7-CyD-1 iKer

Top panel: phase contrast image of x3C7-CyD-1 iKer at day 45 of keratinocyte differentiation showed correct keratinocyte-like morphology *in vitro*. Bottom panel (left): Immunofluorescence analysis of x3C7-CyD-1 iKer co-expressing △Np63 (red) and K14 (green) at the same time point showed on the top panel. Hoechst (blue) was used for nuclear staining. The majority of cells were positive for △Np63, whereas approximately 20% of cells were K14+. Bottom panel (right): Immunofluorescence analysis confirmed *de novo* C7 and co-expression △Np63.

5.6 Base editing signatures at predicted off-target sites

Although BE3 have proved robust on-target DNA base editing efficiency for a variety of different disorders in human cells, recent studies have demonstrated that base editors can lead to low, but detectable cytosine deamination on both DNA and cellular RNA levels in a guide-dependent and guide-dependent fashion (Yu et al. 2020; Jin et al., 2019; Grünewald et al., 2019; Doman et al., 2020; Zuo et al., 2019). To assess the likelihood of coBE3 to create off-target C>T editing, the Benchling *in silico* predictive algorithm was used to identify the off-target regions that can potentially be targeted by the x3C7-CyD-1 sgRNA protospacer (**Figure 5.5**). The top 10 identified off-target genomic loci were initially PCR amplified in base edited and untreated RDEB iPSCs and amplicons were run by illumina MiSeq sequencing to assess the frequency of C>T off-target editing. Collectively, guide-dependent off-target edits were detected at frequencies below the 0.1% in 9 out of 10 off-target sites. However, a 4% C>T coBE3-mediated conversion was detected at 1 out of 10 evaluated sites (OT3). Statistical comparison by two-tailed independent student t-test of the following off-target site with the untreated sample revelated no difference between the two samples (p=0.25). Mapping of the predicted off-target site by the human genome browser showed that the OT3 sequence falls within the intron 2 of the Small glutamine-rich tetratricopeptide repeat-containing protein beta (SGTB) gene highly expressed in brain and implicated in neuronal synaptic transmission (Vuong et al. 2019). Despite the no significant reported C>T change observed by NGS, the following base correction does not seem to fall in splicing donor or splicing acceptor consensus sequences.

Due to the reported nicking activity of coBE3 by the nCas9(D10A) at the non-edited stranded (Komor et al., 2016) other changes at positions of possible residual Cas9 nuclease activity was evaluated. NGS data was then analysed to quantify the percentage of InDels in the on–target and the predicted off-target loci. Data showed a 5.64% of InDels (3.15% deletions + 2.5% insertion) within the *COL7A1* sequence recognized by the x3C7-CyD-1 sgRNA. Importantly, as confirmation of non-significant

base editing in OT3, <0.5% of residual Cas9-mediated InDels were detected at the predicted off-target site.

Target	gRNA sequence	Gene	C>T %	InDels %
COL7A1	CACCTTGGGGACACCAGGTC	*COL7A1*	44% C5, 19% C4, 3.8% C3, 7.4% C1	5.64%
OT1	TACCCTGGGGGCACCAGGTC	Exon 3, *CDH23*	*<0.1%*	*0.37%*
OT2	CACCCTGGAGACACCAGGAC	Intron 10, *GMIP*	*<0.1%*	*0%*
OT3	GACCCTGGGTACACCAGGTC	Intron 2, SGTB	4.09% C5	0.86%
OT4	CACCCTGGGGACAGCAGGTA	Exon 24, *MAP3K4*	*<0.1%*	*0.19%*
OT5	CACCCTGGGGACAGCATGTC	Intron 1, *CBFA2T3*	*<0.1%*	2.4%
OT6	GAGCCTGGGGACACCAGGTG	Intron 3, *ANO2*	*<0.1%*	0%
OT7	GACCCTGGGGCCACCAGGCC	Exon 14, *KRBA1*	*<0.1%*	*0.36%*
OT8	AACCCTGGGAACACCAGGCC	Intron 3, *RAB11FIP4*	*<0.1%*	0.31%
OT9	CTCCCTGGGGTCACCAGGCC	Intergenic, Chr17	*<0.1%*	0.16%
OT10	CTCCCTGGGGACATCAGGGC	Intron 3, *ACOT7*	*<0.1%*	0%

Figure 5.5 NGS for off- and on-target analysis of coBE3-edited iPSCs

The top 10 off-target sites for x3C7-CyD-1 sgRNA were predicted by the Benchling tool and are shown in column 1. Highlighted in red, bases representing mismatches between the off-target site and the *COL7A1* x3C7-CyD-1 sgRNA target (column 2). For each predicted off-target, gene name and relative location within coding or noncoding sites is indicated in column 3. NGS data from Illumina MiSeq sequencing plotted to quantify off-target C>T base editing is shown in column 4. Individual C>T percentages following base editing are shown in red. Percentage of insertions and deletions (InDels) for *COL7A1* and off-target sites are shown in column 5. The percentage of reads from both off-target coBE editing and nCas9-induced DSBs are representative of 1 experiment.

5.7 Base editing-mediated *COL7A1* restoration in RDEB fibroblasts

The base editing strategy described in the previous section was also tested directly in primary RDEB fibroblasts. The choice of using base editors over an HDR-based strategy in primary RDEB fibroblast was given by the fact that base editing does not rely on cell division (Rees and Liu 2018; Yeh et al., 2018). Approximately $1x10^6$ cells were electroporated with coBE3 using the same amounts of mRNA (5µg) and chemically modified x3C7-CyD-1 sgRNA (2µg) as described for iPSCs. Electroporation was performed with the Amaxa Lonza-4D using EN-150 program. B2M-CyD guide RNA was used as positive control. To verify the efficiency of the mRNA delivery with the electroporation program used, RDEB fibroblasts were also electroporated with 2µg of GFP mRNA and GFP expression evaluated 2 days post-delivery.

Almost 100% of fibroblasts were positive for GFP with no observable cell toxicity in *COL7A1* and *B2M* edited cells under phase contrast microscope at 48 hours and 4 days post electroporation (**Figure 5.6A**). In line with what was observed in iPSCs, EDIT-R analysis of RDEB fibroblasts electroporated with x3C7-CyD-1 confirmed high C>T conversion (67%) at the desired c.425 position. Additionally, a similar pattern of bystander C>T conversion observed in RDEB iPSCs was also corroborated in base edited fibroblasts. Sanger sequencing revealed bystander C>T changes were within the editing window at position c.426 (20%) and outside the predicted editing area at positions C3 (2%) and C1 (17%) of the x3C7-CyD-1 protospacer. As confirmation of coBE3 activity, 99% and 100% of editing was detected at positions C6 and C4 of *B2M* locus, respectively (**Figure 5.6B**).

StyI-RLFP assay was successfully performed in base edited RDEB fibroblasts to verify the presence of corrective on-target base editing (**Figure 5.6C**). Evidence of the correct C>T change was confirmed by gel electrophoresis with the presence of two digested bands at 268bp and 115bp, indicating the restoration of the wild type *COL7A1* sequence. As in **section 5.5**, densiometric quantification of the *StyI* digested bands showed that of the 67% of C>T conversion at position c.425 detected by EDIT-R, around 35% of base edited cells showed the on-target C>T conversion without the presence of bystander events.

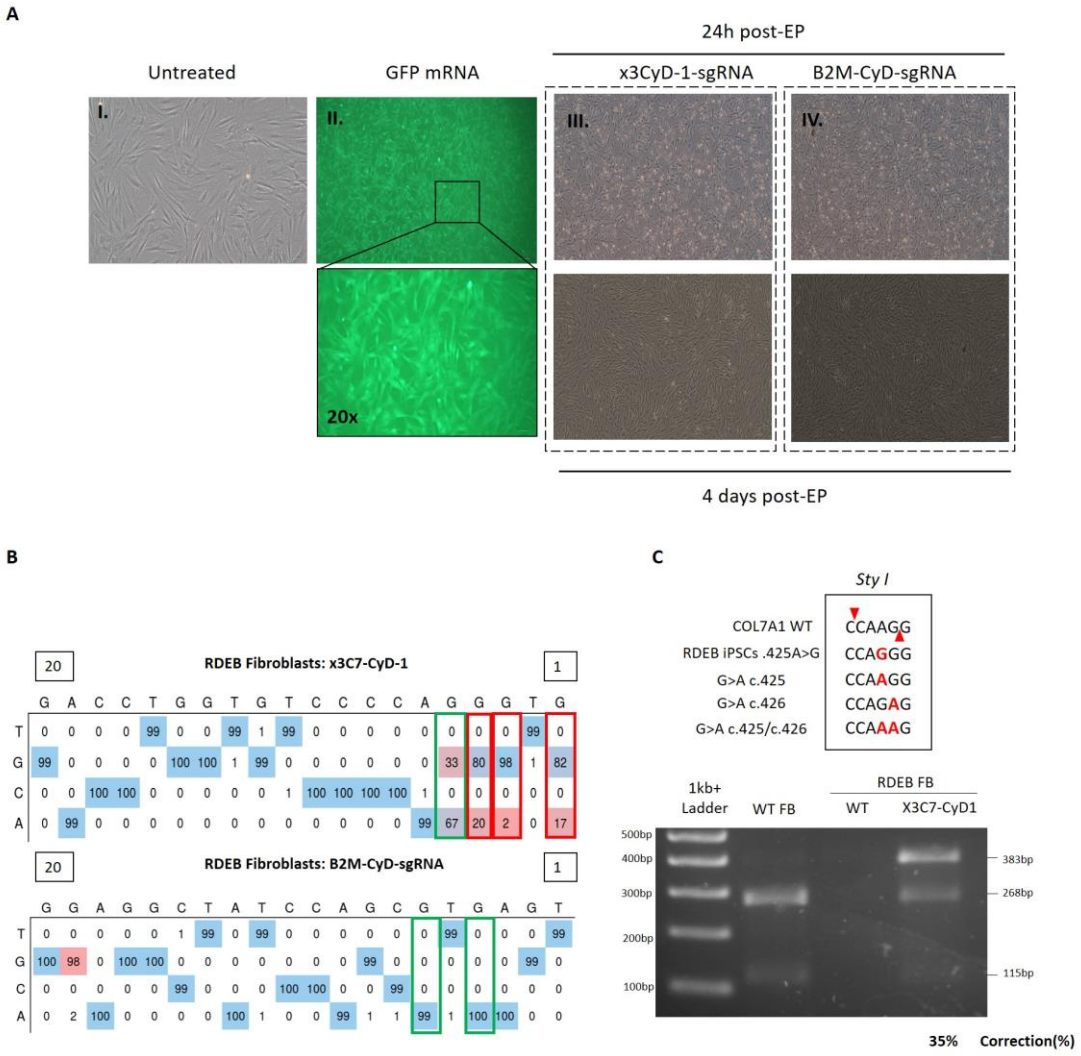

Figure 5.6 *COL7A1* base editing correction in primary RDEB fibroblasts

A. Morphology and transfection efficiency in RDEB fibroblasts before (**I.**) and after (**II.**) electroporation with GFP mRNA. Almost all cells were GFP positive. Cell viability of base edited RDEB fibroblasts with x3C7-CyD-1 (**III.**) and B2M-CyD (**IV.**) at 2 and 4 days post electroporation (post-EP) (n=1) was evaluated under phase contrast microscope. **B.** EDIT-R output for RDEB fibroblasts treated with coBE3 mRNA and x3C7-CyD-1 and B2M-CyD guide RNAs. Green boxes indicate the desired on-target G>A correction (67%) and bystander base conversion at position c.426 (20%) in *COLA71* locus. Untreated RDEB fibroblasts (below) were used as negative control. C>T base editing at positions C6 (99%) and C4 (100%) was detected in *B2M* locus. **C.** *StyI*-based enzymatic digestion of the PCR amplified exon 3 *COL7A1* in RDEB fibroblasts treated with coBE3 and x3C7-CyD-1 and untreated patient and wild type cells used as negative and positive controls, respectively. The percentage at the bottom of the gel indicates the frequency of corrective c.425G>A conversion in base edited fibroblasts (FB) calculated by ImageJ`s gel analysis function.

Characterisation of the coBE3 editing profile on the genomic level by NGS in base edited fibroblasts showed greater purity of C>T conversion (54% C>T, 89% of the total C>T changes) in the predicted c.425 position (**Figure 5.7A**). This data also confirmed the ability of coBE3 to execute the desired substitution and in turn generate high levels of *COL7A1* correction. Noteworthily, lower bystander C>T changes (C4: 4.8%, C3: 1%) and non-canonical C>T conversions (c.425C>A: 2.2%, c.425C>G: 2.70%) were also observed by NGS compared to base edited iPSCs. Subsequent haplotype-based analysis using raw NGS data by CRISPResso2 revealed up to 46% of corrective reads with C>T changes in position c.425 only (**Figure 5.7B**). This analysis further confirmed that base edited fibroblasts showed greater purity of C>T conversion at the target site than base edited RDEB iPSCs

As previously shown for base edited iPSCs, quantification of the residual Cas9 activity using Pindel to detect NEHJ events revealed InDels in only a total of 3.62% reads (2.53% deletions + 1.09% insertion) within the amplified *COL7A1* region (Data not shown).

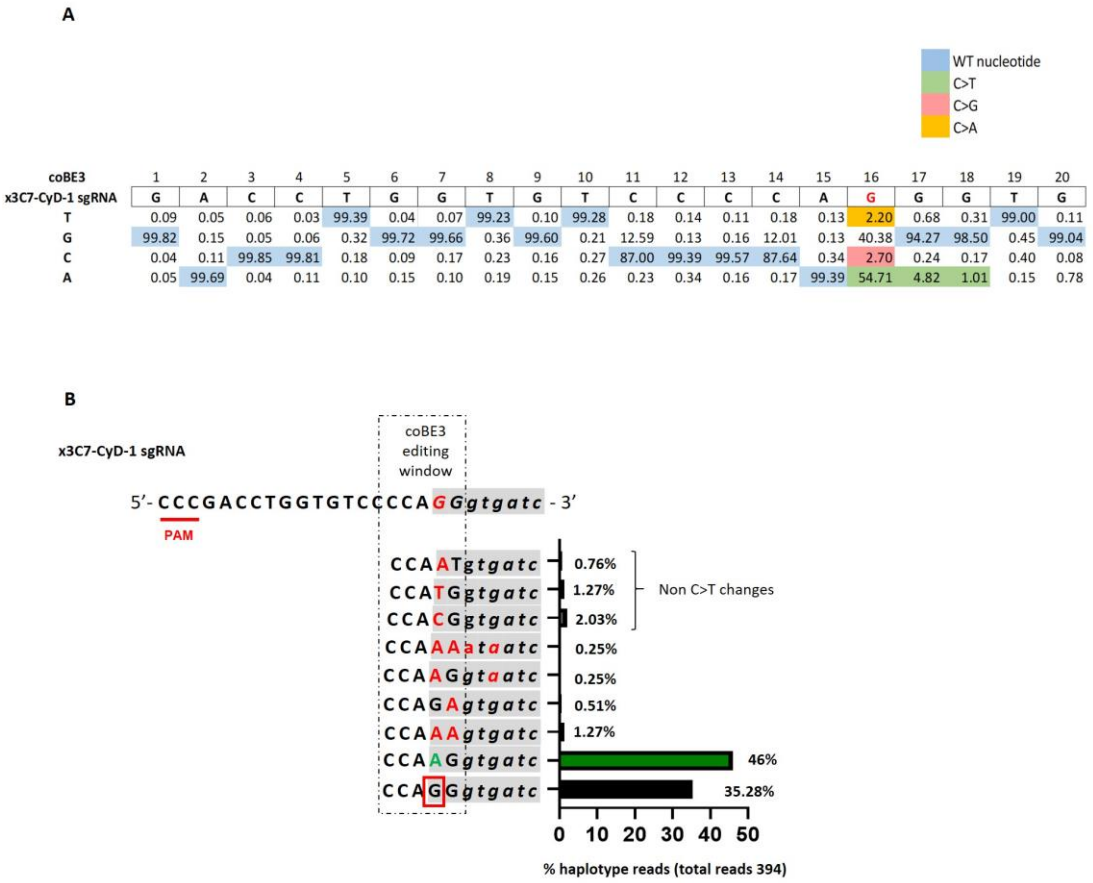

coBE3	1	2	3	4	5	6	7	8	9	10	11	12	13	14	15	16	17	18	19	20
x3C7-CyD-1 sgRNA	G	A	C	C	T	G	G	T	G	T	C	C	C	C	A	G	G	G	T	G
T	0.09	0.05	0.06	0.03	99.39	0.04	0.07	99.23	0.10	99.28	0.18	0.14	0.11	0.18	0.13	2.20	0.68	0.31	99.00	0.11
G	99.82	0.15	0.05	0.06	0.32	99.72	99.66	0.36	99.60	0.21	12.59	0.13	0.16	12.01	0.13	40.38	94.27	98.50	0.45	99.04
C	0.04	0.11	99.85	99.81	0.18	0.09	0.17	0.23	0.16	0.27	87.00	99.39	99.57	87.64	0.34	2.70	0.24	0.17	0.40	0.08
A	0.05	99.69	0.04	0.11	0.10	0.15	0.10	0.19	0.15	0.26	0.23	0.34	0.16	0.17	99.39	54.71	4.82	1.01	0.15	0.78

Figure 5.7 Deep sequencing analysis confirmed high levels of the predicted C>T in base-edited primary fibroblasts

A. Base variant calling of C>T changes across the *COL7A1* locus in RDEB primary fibroblasts electroporated with coBE3 mRNA and x3C7-CyD-1 sgRNA by NGS. Substitution rate at each position of the x3C7-CyD-1 protospacer is displayed in the table. The c.425A>G target base is highlighted in red. The green blocks represent coBE3-mediated C>T conversion across the protospacer. The c.425A>G mutation is corrected by coBE3 in 54.71% of total reads. Percentages of bystander C>T conversions are reported in the table. Non-conventional C>T conversions were reported within and near the editing window and percentages are shown in the table with the following colors: Red: C>G and yellow: C>A. Blue box represent unedited nucleotides. **B.** CRISPResso2 haplotype-based quantification of corrective C>T edits (green letter) in based edited cells. The percentage of reads harbouring a single correction at position c.425 is represented by the green bar (46%). Bystander C>T edits and non C>T base changes in the 5bp coBE3 deamination activity window (dotted box) and within the exon 3 *COL7A1* splicing donor (highlighted in grey: uppercase, exon 3 DNA sequence, italics intron 3 sequence) are represented by red letters in different haplotype combinations. Percentage of each haplotype is reported in the graph. Boxed in red, the c.425A>G pathogenic hotspot mutation in unedited reads (35.28%).

Immunofluorescence of base edited RDEB fibroblasts using a mouse mAb-C7-LH7.2 antibody confirmed restoration of C7, whilst protein expression was absent in untreated patient cells (**Figure 5.8A**). Wild type fibroblasts were used as a positive control and the percentage of C7 obtained by staining was used to normalize the rescued collagen in base edited RDEB fibroblasts. In agreement with what observed on molecular data, an average of 29.8% C7 positive cells were detected by counting the fluorescent signal of 4 independent fields**.** For further confirmation of C7 expression, western blot of total protein isolated from cell lysates was performed and revealed the presence of 290kDa band in base edited fibroblasts corresponding to full-length C7 protein (**Figure 5.8B**). Untreated patient cells and wild type fibroblasts were used as negative and positive controls of C7 expression, respectively. As additional control, RDEB fibroblasts previously engineered to express C7 by lentiviral transduction of the full-length codon optimized COL7A1 cDNA were used (Georgiadis et al., 2016). After stripping the membrane, vinculin staining was performed to ensure equal total protein loading. As C7 is a secreted protein, culture media was also harvested from each condition tested, protein precipitated and used for western blot analysis (**Figure 5.8C**). Cell lysates from the base edited cell population showed a strong full-length C7 expression comparable to that in wild type fibroblasts.

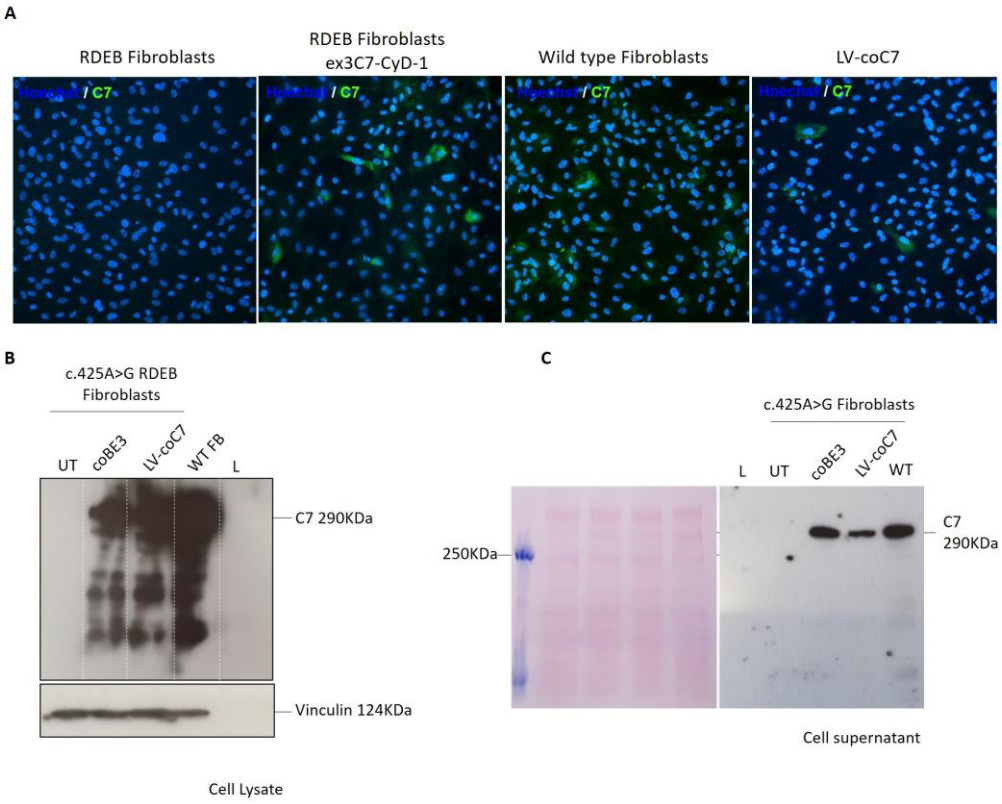

Figure 5.8 Restoration of full-length C7 in coBE3-edited RDEB fibroblasts

A. Immunofluorescence staining for C7 expression (green) and nuclear Hoechst (blue) of untreated RDEB fibroblasts and coBE3-edited RDEB fibroblasts, as well as wild type fibroblasts and keratinocytes used as positive controls. Restored C7 expression is observable in base edited cells. Scale bar = 50 µm. **B.** C7 western blotting from cell lysate and culture supernatant in untreated RDEB fibroblasts and coBE3-edited, as well as LV-C7 transduced fibroblasts and wild type fibroblasts used as positive controls. No C7 expression was observed in untransduced cells where as coBE3-edited RDEB fibroblasts showed restoration of full-length C7 (~290kDa) in both cell lysate and supernatant. Vinculin and Ponceau S staining were used as a loading control for cell lysate and supernatant blotting, respectively.

5.8 Chapter discussion

This chapter aimed to determine the potential of cytidine base editing technology for seamless correction of *COL7A1* mutation hotspot (c.425A>G) in RDEB iPSCs and primary fibroblasts. The main advantages of base editors for gene correction over HDR are: 1) the ability of introducing nucleotide specific changes with minimal InDels (NHEJ) which are the main by-product of canonical SpCas9 editing, 2) the editing activity of base editors does not rely on cell division and thus 3) no delivery of exogenous donor templates is required for gene correction. For this purpose, a codon optimized version of cytidine base editor (coBE3) was delivered as mRNA in RDEB iPSCs alongside two different guide RNAs, x3C7-CyD-1 and x3C7-CyD-2, designed to accommodate the c.425A>G mutation within their base editing window. Appreciable coBE3-mediated on-target C>T correction at position c.425 was detected and equated to 45% and 32% with x3C7-CyD-1 and x3C7-CyD-2 sgRNA, respectively. In line with other research group studies (Yu et al., 2020; Jin et al., 2019; Grünewald et al., 2019; Doman et al., 2020; Zuo et al., 2019), bystander on-target C>T changes were observed with both guide RNAs, thereby highlighting the main limitation of base editing when other potential cytosines sit within or near the coBE3 editing window. Computational prediction of unwanted C>T changes suggested that bystander edits alone or in combination with the corrective C>T change in c.425 alter the consensus splicing donor sequence in exon 3. This hypothesis was supported by splicing aberrations in the Col7 transcript reported in c.425A>G patients (Gardella et al., 1996) and due to the absence of C7 in keratinocytes with a silent G>A conversion within the NT-2PS-ssODN-AAA- donor at position c.426 described in **Chapter 3**. Additionally, deep sequencing data confirmed the C>T distribution observed by Sanger sequencing with a preference for edits to fall at position 5 of the x3C7-CyD-1 sgRNA. However, haplotype analysis and densitometric quantification of the amplified exon3/intron 3 junction by the *StyI* assay estimated that only half of the C>T edits in c.425 occurs without bystander effects, thereby restoring *COL7A1* sequence, while preserving the splicing donor site.

Differentiation of the base edited RDEB iPSCs into keratinocytes confirmed the ability of these cells to restore C7 expression. In line with the percentages of C>T changes by NGS, the amount of *de novo* synthetized C7 detected by immunofluorescence demonstrated that only cells with corrective C>T changes at position c.425 were able to express the protein.

Evaluation of potential guide-dependent C>T changes in the top 10 *in silico* predicted off-target sites showed no significant rAPOBEC1-mediated deamination activity in these loci. Furthermore, detection of the residual Cas9 nickase activity of coBE3 revealed only a minimal percentage of NHEJ events in the *COL7A1* site, whereas percentages of InDels in the predicted off-target loci was <1% above background across the sequencing window.

Next, coBE3 correction strategy was translated into RDEB fibroblasts and up to 67% of C>T correction at position c.425 was observed. Despite bystander on-target effects detected on genomic level by Sanger sequencing, restoration of C7 protein was confirmed in base edited RDEB fibroblasts by immunofluorescence. Importantly, full-length C7 was detected by western blotting using protein extracted from both the cell lysate and culture media, the latter indicating effective secretion of the protein by base edited RDEB fibroblasts.

Collectively, this chapter showed the feasibility of autologous base editing by cytidine base editor in RDEB iPSCs and primary fibroblasts. Base edited cells showed modest targeted C>T conversion and rescued C7 expression and function without the need for further clonal selection. These findings provide a proof-of-concept evidence that base editing can offer a promising seamless strategy for autologous gene and cell therapy for RDEB.

Chapter 6 Discussion

The overall aim of this project was the design and optimization of CRISPR/Cas9 gene- and cytidine deaminase-base editing platforms for the efficient correction of a RDEB mutation hotspot (c.425A>G, p.K142R) in exon 3 of the *COL7A1* gene. Particular focus has been given to the development of *COL7A1* correction through CRISPR/Cas9-associated homology-directed repair (HDR) using different donor templates such as double-stranded DNA via integrase defective lentiviral vector or single-stranded oligodeoxynucleotides (ssODNs). As first step of the project, validation of both HDR-mediated platforms was performed in a wild type keratinocyte cell line (**Chapter 3**). Next, RDEB patient iPSCs bearing a homozygous c.425A>G mutation were generated to be used as a stable cellular model to validate *COL7A1*-correction efficiency. Data presented in **Chapter 4** demonstrated that the CRISPR/Cas9-mediated HDR can introduce a corrected homologous sequence in the targeted locus and restore the normal gene sequence. In parallel, to obviate the creation of potentially deleterious DSBs and need of a repair template, seamless C>T cytidine deaminase base editor (coBE3) was validated in RDEB iPSCs and modest targeted correction at position c.425 was achieved (**Chapter 5**). Finally, efficient coBE3-mediated *COL7A1* correction was demonstrated in primary RDEB fibroblasts, leading to restoration of the endogenous full-length C7 expression *in vitro*.

6.1 NILV-based gene correction following CRISPR/Cas9-induced DSBs as proof-of-concept for HDR-based strategies for RDEB.

CRISPR/Cas9-based gene editing has provided a novel and customizable option for efficient manipulation of any genomic sequence of interest by site-specific double-strand breaks (DSBs) followed by resolution of DNA integrity by nonhomologous end-joining (NHEJ) and homology directed repair (HDR). The results presented in this report confirmed that CRISPR/Cas9-mediated correction of the c.425A>G mutation can be only achieved when a donor template is provided in patient cells (Izmiryan et al., 2016; Kocher et al., 2019). Only modest *COL7A1* correction by HDR which relied on drug selection or clonal isolation of the gene corrected cells has been reported in the literature (Osborn et al., 2013; Hainzl et al., 2017; Izmiryan et al., 2018; Izmiryan et al., 2016; Chamorro et al., 2016; Sebastiano et al., 2014; Bonafont et al., 2021). Up until now, viral platforms such as NILV and AAV (AAV6) have shown to mediate high HDR-mediated CRISPR/Cas9 correction in primary RDEB keratinocyte stem cells (Izmiryan et al., 2018; Bonafont et al., 2021). In this body of work, proof-of-concept for feasible c.425A>G *COL7A1* correction was demonstrated in wild type keratinocyte cell line and RDEB iPSCs using a therapeutic donor template bearing a portion of the wild type *COL7A1* (~1.8kb) sequence spanning from intron 2 to intron 7 and delivered by NILV.

For significant levels of donor integration to occur, higher frequency of Cas9-induced DSBs was shown to increase the likelihood of the target site to be repaired by HDR (Remy et al., 2014; Duda et al., 2014; Hendel et al., 2014). In this direction, optimization of CRISPR/Cas9 reagents transfection efficiency and guide RNA design were initially investigated and frequency of Cas9-induced DSBs by NHEJ in the *COL7A1* locus was assessed. Identifying the guide RNA with the best targeting efficiency was crucial for subsequent evaluation of HDR-based strategies. In terms of overall transfection efficiency, several configurations for genome editing reagents delivery were investigated. In recent years, the CRISPR/Cas9 technology has seen significant advancements with the development of a number of new platforms and formats by which the Cas9 and sgRNA can be delivered augmenting targeting

capabilities and maximising accessibility (Preece and Georgiadis 2019). Use of transient or complete non-viral delivery of sgRNA and SpCas9 supplied as mRNA or protein (RNP) have shown increased targeting efficiency without the toxicity associated with plasmid or integrating virus delivery (kim et al., 2014). In this regards, Chapter 3 describes the comparison between different strategies for CRISPR/Cas9 delivery, namely either as a ribonucleoprotein complex (RNP) containing both sgRNA and Cas9 protein or as sgRNA delivered via a Lentiviral vector in combination with Cas9 mRNA. Both methods ensured only transient expression of Cas9 nuclease, thereby safeguarding off-target activity and minimizing potential immunogenicity. The main rationale for testing a viral hybrid CRISPR/Cas9 delivery platform in the first instance was due to the previously reported preclinical application from my research group for the creation of universal CAR T cell therapies to mediate anti-leukemic effects in patients (Georgiadis et al., 2018). In this study, a lentiviral "terminal" vector platform was rationally engineered to incorporate of a sgRNA cassette into the ΔU3 3' long terminal repeat (LTR) coupled by delivery of Cas9 mRNA by electroporation resulting in around 50% knockout in T cells. The main limitation of this hybrid platform for *COL7A1* editing was its significant lower capacity of generating DSBs suitable for HDR correction compared to Cas9 RNP delivery. Although the significant differences in editing efficiency between the 2 platforms were observed, it is worth noting that a direct comparison cannot be carried out. Due to the different formats of Cas9 and sgRNA used in these delivery systems, ensuring that equal amounts of these reagents are delivered into the cells is not technically possible. In addition, technical limitations prohibit from accurate evaluation of intracellular functional RNP complexes formation between the two delivery systems. It is important to note that we aimed to limit the expression of guide RNA from lentiviral vector by controlling the vector copy number per cell to meet the requirement for preclinical or clinical applications. Subsequently, the higher editing rate achieved by RNP delivery of the gene editing reagents, led me to investigate it further for gene correction in patient-derived RDEB iPSCs. For proof-of-concept of HDR-mediated gene correction, a non-integrating lentiviral (NILV) platform was initially chosen as it has previously been shown to mediate modest correction rates without perturbing the proliferative capacity of JEB and RDEB primary keratinocytes (Coluccio et al., 2013; Izmiryan et al.,

2018; Benati et al., 2018; Izmiryan et al., 2016). As a rationale for using NILV-mediated HDR for RDEB, a study by Izmiryan *et al*. demonstrated that skin grafts made form primary fibroblasts and keratinocytes which were gene edited using NILV donor template for CRISPR/Cas9-mediated HDR presented with up to 26% of C7 rescue at the DEJ, which was sufficient for *de novo* AF formation with no dermal-epidermal separation.

The NILV platform described in this thesis was initially developed in my research group for ZFN-mediated *COL7A1* correction (Georgiadis 2016). The use of a promotorless donor template has an advantage of reducing the probability of activating neighbouring oncogenes upon integration. The NILV-I2I7C7-SDMTemplate-F was rationally designed to span 6 exons of endogenous *COL7A1* in order to cover a wide range of mutations clustered around this portion of the gene and, therefore, in theory could be used for site-specific correction of multiple mutation hotspots.

In addition, the rational design of the corrective template included optimized lengths of the donor and its homology arms lengths, inclusion of both intronic and exonic sequences and introduction of silent mismatches, as previously described (Izmiryan et al., 2016; Izmiryan et al., 2018; Georgiadis 2016). Although it has been shown that the distance of the corrective mismatches from the cut site is directly correlated with the efficiency of HDR-mediated donor integration (Elliott et al., 1998; Chu et al., 2015), NGS results from NILV-corrected RDEB iPSCs showed similar integration rates of silent Cas9 blocking mutations and the introduced corrective G>A mismatch at position c.425, despite the differences in the distance from the cut site (1-10bp and 71bp, respectively). Moreover, PCR analysis for targeted integration of both 5' and 3' ends of the donor template confirmed that all integrations were HDR-dependent due to the presence of the predicted PCR band size with no evidence of HDR-independent integrations previously reported for NILV-based correction strategy in JEB keratinocytes (Benati et al., 2018). Upon clonal analysis, immunofluorescence analysis of HDR-edited keratinocytes confirmed that the co-presence of silent point mutations within the donor template did not interfere with C7 expression.

Several studies have shown that efficient reproducible HDR-mediated correction can be achieved by coordinated/sequential delivery of the genome editing tools and donor template depending on their format, delivery cargo and cell-cycle progression (Bak and Porteus 2017; Knipping et al., 2017; Genovese et al., 2014). In my study, simultaneous co-delivery of CRISPR/Cas9 RNP and NILV-donor resulted in higher levels of HDR compared to sequential delivery of the reagents, with the RNP complex being delivered post NILV infection. The high percentage of homologous recombination observed supports the hypothesis that a synchronous timing of Cas9-RNP induced DSBs and template availability upon retrotranscription can promote efficient HDR. Importantly, this system was not only highly efficient in human keratinocyte cell lines, but modest HDR rates were also observed in wild type and RDEB iPSCs. The key aspect of the system is that delivery of gene-editing components can be performed in a single step. This is particularly important when working with stem cells like iPSCs that do not tolerate repeated genetic manipulations. A previous time course study by Genovese *et al*., demonstrated that modest gene correction of the *IL2RG* gene, responsible for SCID-X1, when the donor template was delivered by NILV one day prior to ZFNs mRNA (Genovese et al., 2014). In my studies, however, electroporation of the RNP complex 24 hours post NILV-donor infection resulted in slightly lower template integration. Kinetic studies of Cas9 half-life by western blotting has shown that on average the protein expression peaked between 12-24 hours post electroporation of either Cas9 mRNA or RNP, resulting in the highest rate of DSBs within 24 hours post nuclease delivery (Kim et al. 2014., Georgiadis et al., 2018). Similarly, a recent paper by Uchida *et al*. has demonstrated that a comparable peak time of retrotranscription of lentiviral donor template by reverse transcriptase, which is then followed by 10-fold decrease within 3 days post infection (Uchida et al., 2016). Furthermore, evidence of high HDR events in the total gene edited population (NHEJ+HDR) supports the hypothesis that nuclease-mediated HDR is more effective in iPSCs than in primary skin cells (Cherry and Daley 2013; Inoue et al., 2014; van Sluis and McStay 2015).

Although, preliminary results are indicative of the feasibility of NILV-based template delivery in patient-derived iPSCs, several drawbacks may impede the use of this

vector format for HDR-based strategies for clinical translation. Large scale manufacturing of NILV is expensive and quantification of the HIV-p24 provides an inaccurate titre as levels of this antigen provide a measure of physical titre rather than functional. Use of different formats for donor delivery such as ssODNs for correction of small pathogenic variants, can overcome manufacturing and cost-related issues and have shown to be highly efficient in mediating HDR in iPSCs (Guo et al., 2018; Kwart et al., 2017; Paquet et al. 2016; Martin et al., 2019; Yang et al., 2013).

6.2 Evaluation of complete viral free *COL7A1* correction by HDR using ssODN donor templates

In addition to allowing higher *COL7A1* correction, single stranded oligo donor configuration can provide an ideal platform to explore the efficiency of a viral-free template delivery for HDR-based strategies. Use of viral-free donor templates, such as plasmid DNA, for HDR-based gene correction in primary keratinocytes so far only resulted in low correction rates, hindering the application of this platform for preclinical and clinical settings. It is well established that primary keratinocytes are notoriously resistant to plasmid transfections, subsequently resulting in low HDR (Hainzl et al., 2017). To increase the rate of HDR, several strategies, including addition of antibiotic resistance cassette with or without a Cre/Lox excisionable system (Kocher et al., 2019), reporter genes for cell sorting, or clonal isolation of the gene-edited cells (Chamorro et al., 2016; Benati et al., 2018; Jackόw et al., 2019), are currently being investigated. A limiting factor to be considered is the short lifespan of primary fibroblasts and keratinocytes. Extended culture and manipulations, such as gene editing and clonal selection, can rapidly lead to growth arrest, terminal differentiation and senescence of both cell types *in vitro*. Although iPSCs have been shown to be more amenable to extensive manipulations, recent reports have also demonstrated significant low cell viability upon plasmid transfection (Jackόw et al., 2019; Shinkuma et al., 2016) or p53-depended cell death upon Cas9-induced DSBs (Ihry et al. 2018). In addition, clonal selection of Cas9 edited iPSCs might select for

cells more resistant to DNA damage with p53 dominant negative mutations making them unsuitable for any potential cell therapy approach (Merkle et al., 2017).

More recently, alternative strategies using single stranded oligonucleotides (ssODN) or linearized-double stranded DNA (ldsDNA) were investigated to correct monogenic disorders in primary cells and iPSCs (Guo et al., 2018; Kwart et al., 2017; Paquet et al., 2016; Martin et al., 2019; Yang et al., 2013; Roth et al., 2018). Donor delivery via ldsDNA in combination with CRISPR/Cas9 reagents has been shown to be effective for correction of pathogenic mutations in cells from patients with monogenic autoimmune disorders and genetic reprograming of the endogenous T cell receptor (*TCR*) locus against cancer antigens (Roth et al., 2018). Co-electroporation of Cas9 RNP and >1kb ldsDNA templates showed significantly high integration rates with only modest impact on T cells viability. In my work I investigated ldsDNA donor template designed for the correction of the c.425G>A mutation in wild type HaCaTs by testing varying concentrations of the donor template co-electroporated with the Ex3D RNP complex. However, overall low percentage of donor integration (approximately 6%) was detected by PCR based methods of the gene-edited population. In order to potentially improve the HDR rates, several improvements can be employed, such as optimizing homology arm lengths or use of electroporation protocols more permissive for the access of ldsDNA to the nucleus. However, the major barriers to effective ldsDNA-based genome targeting are significant cell toxicity in response to large naked DNA templates (Hornung and Latz 2010; Zhao et al.,2006) and unwanted 'footprints' caused by random integration of ldsDNA at CRISPR/Cas9 induced and naturally occurring endogenous DSBs loci (Roth et al., 2018), which occurs in ~1% and ~0.01% cases, respectively.

By contrast, single-stranded oligo DNA nucleotide (ssODN) donor have advantages over double-stranded DNA molecules, such are lower cell toxicity, no random integration and easier delivery and access into cells. Single-stranded DNA does not require integration of large gene cassettes due its short length (~100bp), thus making it suitable for base-to-base gene correction and guarantees physiological expression of the corrected gene under its endogenous promoter (Martin et al., 2018; Paquet et al., 2016; Kwart et al., 2017; Yang et al., 2013). Moreover, HDR-based gene editing

approaches using ssODN templates have been widely used to make iPS cell disease models or for potential gene correction strategies in patient-derived iPSCs (Guo et al., 2018; Kwart et al., 2017; Paquet et al., 2016; Martin et al., 2019; Yang et al., 2013). Feasibility of ssODN-based gene correction for RDEB has recently been demonstrated for two different *COL7A1* mutations (c.2470insG in exon 19 and c.3948insT in exon 32), reporting high percentages of mono- and bi-allelic HDR events in iPSCs (Jacków et al., 2019).

As discussed for NILV donor-mediated HDR, introduction of intended Cas9-blocking mutations within the template is crucial in order to prevent re-editing upon ssODN integration. Kwart *et al*. showed that most of the HDR events after incorporation of ssODN without Cas9-blocking mutations presented with unwanted InDels/recombinations due to concomitant NHEJ repair (Kwart et al., 2017). However, due to the small size of ssODNs, rational design of the intended mismatches has been demonstrated to affect HDR rates. It was shown in fact, a clear inverted correlation between the increasing distance of the intended single mismatches from the Cas9-induced DSB and the exponential decrease in ssODN integration by HDR (Yang et al., 2013; Paquet et al., 2016). Therefore, in order to increase the efficiency of ssODN-based gene editing, a new guide RNA (Ex3P-sgRNA) binding immediately downstream from the c.425A>G site was designed. Furthermore, insertion of PAM-blocking mutations (NT-2PS-ssODN-AAA) or silent mutations across the sgRNA sequence (NT-2PS-ssODN-AAG) led to high levels of HDR in keratinocyte cell line and in RDEB iPSCs. The significant levels of homologous recombination suggest that a substantial fraction of the gene corrected cells may be bi-allelic for donor template integration. This hypothesis is supported by the findings of Paquet *et al.,* where cut-to-mutation distance can be optimized to introduce heterozygous or homozygous mutation incorporation in iPSCs (Paquet et al., 2016). Bi-allelic integration was shown to occur at high rates when the intended mutation sits within 5bp from the Cas9 cut and decrease exponentially thereafter.

ssODN architecture and template complementarity have also shown to affect HDR rates, although there have been some discrepancies between the findings of different research groups. Lin *et al.* found that homology arms length play a more important

role in determining HDR rates compared to strand complementarity (Lin et al., 2014). By contrast, a more detailed investigation into how the structure of donor oligos affects HDR demonstrated that ssODNs complementary to the non-target strand were more effective in promoting HDR than donors complementary to the target strand recognized by the sgRNA (Richardson et al., 2016). However, I have not observed any significant HDR differences between ssODN complementary to non-target or target DNA strands for NT-2PS-ssODN-AAA and T-2PS-ssODN-AAA. Of note, Jackow *et al.,* showed to efficiently achieve up to 50% of HDR in RDEB iPSCs by symmetric ssODN (Jacków et al., 2019). Although many potential designs have been envisioned by several research groups (homology arm lengths, donor strand complementarity and homology arm symmetry), it is important to highlight that by far, a standard donor design to promote higher HDR is not feasible. Nevertheless, the optimized ssODN described in this manuscript successfully introduced desired genetic correction at high efficiency, future studies should be directed towards a systematic evaluation (symmetric vs asymmetric) of ssODN design for gene correction applications.

As part of donor template design, chemical modifications were introduced in both 5` and 3` of the ssODN termini to improve ssODN stability upon electroporation (De Ravin et al., 2017; Renaud et al., 2016). Integration of phosphorothioate bonds within ssODN backbone was shown to increase HDR in myeloid CD34+ cells for X-linked chronic granulomatous disease compared to the donor without chemical modifications. Additionally, exposure of iPSCs to a 24 and 48 hours “cold-shock” of 32°C has been shown to increase the amount of HDR by two-to-ten-fold (Guo et al., 2018). Although similar results were observed in HSPCs (Lattanzi et al. 2019), the biological mechanism by which hypothermia can increase HDR events is still under investigation. Current hypothesis suggests that transient exposure to “cold-shock” potentially decreases mRNA and protein turnover, thereby resulting in the increased activity of nucleases, including Cas9, delivered as mRNA (Doyon et al., 2010; DiGiusto et al., 2016).

Although high HDR efficiency was observed in RDEB cells treated with ssODNs, assessment of protein restoration was not possible in these cells due to the inability

of these cells to produce C7 (Sebastiano et al., 2014). Therefore, the ability of the cells with HDR-mediated integration of ssODN templates to produce C7 was evaluated in HaCaTs in the first instance. Of particular relevance, C7 expression was absent in HaCaTs harbouring NT-2P-ssODN-AAA template. Molecular analysis of the amplified exon 3-4 Col7 cDNA junction confirmed similar splicing impairments as clinically observed in c.425A>G patient cells (Gardella et al., 1996; Hammami-Hauasli et al., 1997). Although the intended G>A PAM-blocking mutation introduced within NT-2P-ssODN-AAA restored the wild type C7 amino acid sequence, the mismatch fell at position -3 of the consensus sequence of the exon 3 donor splice site (SD), hence resulting in the an impaired splicing between exons 3 and 4 (Gardella et al., 1996). Sanger sequencing of incorrectly spliced *COL7A1* transcripts confirmed the presence of different anomalous transcripts observed in RDEB patients in Gardella *et al.* study: 1) retention of intron 3 due to a PTC at its 66th nucleotide, 2) activation of a secondary cryptic GT splice site within exon 3 and leading to a PTC 61bp downstream the cryptic splicing donor and 3) complete skipping of exon 3 with a PTC after the 10th base of exon 4 (Gardella et al., 1996; Hammami-Hauasli et al., 1997). By contrast, the new donor configuration confirmed that the introduced silent mutations within the protospacer did not interfere with C7 expression. Comparable HDR rates were observed by NGS with both the two donors in RDEB iPSCs, hence confirming that the absence of a PAM blocking mutation did not lower the frequency of HDR events. Importantly, high levels of *COL7A1* correction achieved in RDEB iPSCs suggest that this strategy can potentially provide a selection-free, one-step editing protocol able to generate gene corrected cells without clonal isolation. Importantly, optimization of Cas9/ssODN concentrations and electroporation conditions were also confirmed to be essential factors for high HDR rates, as it has been shown previously (Xu et al., 2018; Li et al., 2014; Lattanzi et al., 2019).

Despite the encouraging results achieved, several technical issues related to relatively low cellular viability and high cellular debris in gene edited cells culture. Of note, faster cellular recovery measured over time in iPSCs electroporated without CRISPR/Cas9 reagents confirmed that mechanisms of cell transfection did not impact on cellular viability. By contrast, gene edited cells showed slower recovery and high

toxicity, although it is worth noting that minimal amount of spontaneous differentiation was observed. High toxicity and colony detachment of RDEB iPSCs was frequently observed within 72 hours post electroporation or upon the first passage of gene edited iPSCs, despite optimized cell culture conditions. Importantly, similar toxicity and cellular behaviour was observed not only in RDEB iPSCs clone, but also in wild type iPSCs. Reduced cell viability upon CRISPR/Cas9 editing has previously been reported by several groups in different disorders, including EB (Shinkuma et al., 2016; Jacków et al., 2019). Only a small number of gene edited iPSCs can survive upon editing, indicating that Cas9 toxicity could create an obstacle to the high-throughput use of this technology for genome engineering (Ihry et al., 2018). One reason for high cellular toxicity is related to the activation of p53-depended cell death upon Cas9-induced DSBs in on-target sites (Ihry et al., 2018). In the context of PSCs, the extreme sensitivity of these cells to DNA DSBs was initially postulated to be a natural mechanisms that ESCs use to prevent the development of aberrant cells in the early embryo stages (Dumitru et al., 2012). In our lab, a semi-quantitative measurement of p53 phosphorylation at serine 15 (pS15-p53) confirmed an increase in the amount of pS15-p53 in response to Cas9-induced DSBs 24 to 48 hours post electroporation. These observations support the hypothesis that p53 can be activated immediately after SpCas9-induced DSBs. To avoid p53 activation, transient inhibition through dominant negative forms of p53 transgene was shown to be well tolerated in hPSCs, facilitating the generation of significant numbers of engineered hPSCs by increasing efficiency and reducing yields' variability (Ihry et al., 2018; Geisinger and Stearns 2020). In this regard, it would have been beneficial to fully evaluate the capacity of transient p53 inhibition in my work.

As described in **section 1.7.5**, one of the major limitation of the CRISPR/Cas9 system is the creation of unpredicted InDels resulting in genetic damage, and also to off-target DNA breaks. Due to the high reported toxicity of CRISPR/Cas9 in iPSCs or hESCs, it has been hypothesized that a second reason of low viability can be linked to the presence of chromosomal abnormalities in most of the edited cells in culture (Assou et al., 2018). By contrast, chromosomal or genomic aberrations can also positively favourite cell competition among the cell clones. To avoid possible selection of

chromosomally impaired cells, genomic integrity of gene edited or gene corrected iPSCs must be verified (Jacków et al., 2019). Due to unprecedented circumstances happened during the course of my study, assessment of normal karyotype in the NT-2PS-ssODN-AAG RDEB iPSCs pool and in-depth molecular studies of these cells on clonal level has not been possible.

In conclusion, ssODN-mediated HDR permits to achieve significant levels of gene correction for a mutation hotspot (c.425A>G) in patient-derived iPSCs. The efficient gene editing strategy described in Chapter 4 emphasises the importance of diligent and rational design of donor template sequence, optimization of electroporation protocols and choice of format and amount of SpCas9 and sgRNA components.

6.3 Base editor correction of c.425A>G *COL7A1* in patient-derived fibroblasts and iPSCs

Cytidine and adenine base editors present a novel and versatile technology to correct pathogenic SNPs without the need of Cas9-induced DSBs followed or exogenous donor DNA template (Gaudelli et al., 2017; Komor et al., 2016). In this report, a third-generation codon optimized cytidine base editor was used to evaluate frequency of on-target C>T conversion in patient-derived iPSCs and RDEB fibroblasts for the correction of c.425A>G *COL7A1* mutation. At the time of writing, to our knowledge, this study represents the first attempted approach of cytidine base editor for seamless DSBs-free C>T single nucleotide correction for RDEB. By far, only one example of base editing application in RDEB was reported by Osborn *et al*. using adenosine deaminase base editors to correct RDEB fibroblasts and iPSCs for two C>T point mutations in exons 5 (c.553C>T, R185X) and 12 (c.1573C>T, R525X) (Osborn et al., 2020). As described for HDR-based gene correction using ssODNs, a completely non-viral delivery of sgRNA and coBE3 mRNA was chosen using optimized electroporation conditions. Due to the restricted C>T deamination window activity of coBE3, optimization of guide RNA design was also taken into account to increase the efficiency of targeting the c.425A>G mutation and decrease the likelihood of

converting other cytosine within the coBE3 activity window (Komor et al., 2017; Gaudelli et al., 2017). Data obtained from Sanger sequencing indicated that coBE3 can produce appreciable levels of on-target C>T conversion (35% (n=3) in RDEB iPSCs and RDEB fibroblasts 67% (n=1)). In contrast with data obtained at genomic level, densitometric analysis of base edited iPSCs and fibroblasts, upon target-specific *StyI* digestion, highlighted that only half of the c.425C>T edited cells do not present any associated C>T edits. Characterization of the coBE3 editing profile by NGS demonstrated the ability of base editor to execute C>T and no C>T changes inside and outside the editing window of x3C7-CyD-1 sgRNA. Haplotype analysis confirmed percentages of gene correction observed by *StyI* assay but also showed that different unwanted C>T combinations can occur alongside the predicted site. Each of the bystander edits leads to changes in the splicing donor sequence which can have a negative impact in the C7 protein expression as observed in untreated c.425A>G keratinocytes. This is supported by the effects of splicing aberrations observed in RDEB patients and my experimental settings with the NT-2PS-ssODN-AAA donor. Frequency of coBE3 bystander edits and their impact on C7 splicing aberration needs to be corroborated by other additional NGS analyses. Preference of coBE3 to mediate on-target c.425 C>T conversion was also confirmed in RDEB fibroblasts, although bystander edits within the editing window were detected at a higher frequency than RDEB iPSCs. Nevertheless, consistent with the *StyI*-RFLP assay, significant C7 restoration (~30%) was confirmed by western blot and immunofluorescence for base edited RDEB fibroblasts. This percentage would be critical to evaluate the capacity of fibroblasts to sustain epidermal function *in vivo* without the need of clonal analysis. The ability of base edited C7 to create *de novo* AFs and functional restoration of skin integrity are currently underway *in vivo*. In hypomorphic RDEB mouse models it has been demonstrated that mouse keratinocytes expressing 10% of wild type C7 levels are able to incorporate the protein and generate AFs at the DEJ, significantly improving the RDEB phenotype (Nyström et al., 2013). However, this data is currently missing from human studies, although we would speculate that this number might be similar. For example, in a recent study by Izmiryan *et al.*, grafting of skin equivalents composed of 11% and 15% CRISPR/Cas9-gene corrected keratinocytes

and fibroblasts, respectively, resulted in 26% C7 re-expression as well as AF formation at the DEJ.

Although the development of base editors has broadened the range of pathogenic SNP that can be targeted for patient specific therapies, further characterisation of both desirable and unwanted effects is required. For example, initial studies on base editors employing rAPOBEC1 (including coBE3 of my studies) reported the presence of C-to-non-T edits which hinder base editing purity (Komor et al., 2016). This was also observed in my settings with equal rates of C>G and C>A conversion within the coBE3 editing window. While this targeted random mutagenesis could be problematic for precise base editing application, newer generation of rAPOBEC1-based cytidine base editors (BE4, (Komor et al., 2017)) and new variants (targeted activation-induced deaminase (AID)-mediated mutagenesis (Ma et al., 2016), CRISPR-X (Kim et al., 2017)) with higher base editing specificity have been developed. Importantly, DNA base editors demonstrated to produce a detectable level of InDels at the target site due to the constitutive activity of Cas9 nickase on the non-edited strand (Gaudelli et al., 2017; Komor et al., 2016). Nicking of the opposite strand was shown to result in DSBs which are likely to be resolved by indel-prone end joining processes. Although BE4 was shown to have a reduced number of the indel formation events, cytidine deaminases typically lead to higher indel frequencies than adenosine base editors (Komor et al., 2017). However, even with the improved adenine base editor, ABEmax, an average of 1.5% and 1.9% InDels were previously detected for RDEB c.553C>T and c.1573C>T RDEB mutations, respectively (Osborn et al., 2020). Consistent with previous reports, on-target indel activity (~2.5%) was detected by by NGS. Base editors were also shown to mediate transcriptome-wide off-target DNA and RNA edits due to their constitutive deamination activity which can be independent of Cas9 target DNA binding site (Grünewald et al., 2019; Zhou et al., 2019; Xin et al., 2019; McGrath et al., 2019).

Despite expansion of available tools widens the potential applications of base editing technology and increases their safety profile, the on- and off-target data from several studies highlight the benefits of choosing a base editor and protospacer combination with only a single editable nucleotide in the target window. This approach has the

advantage to lead to a more uniform mutation correction but also decreases the likelihood of introducing unwanted changes at off-target loci.

Collectively, results of base editing in RDEB iPSCs and primary fibroblasts supports the ability of coBE3 to execute the desired substitution without clonal selection. Despite editing outside the predicted editing window and no C>T changes were observerd, base edited fibroblasts have shown significant protein restoration *in vitro*. *In vivo* results will be also of crucial importance to confirm the degree of correction and the ability of base edited cells to support epidermal grafts by generation of functional AFs (Izmiryan et al., 2018).

6.4 The promise of autologous pluripotent stem cells therapy for RDEB

The potential of iPSCs derivation from RDEB primary cells has given an opportunity for the development of unlimited patient-specific cell types for cell therapies and disease modelling. *Ex vivo* gene transfer in primary RDEB keratinocytes and fibroblasts has demonstrated modest outcomes in preclinical and clinical trials and highlighted the importance of targeting resident skin stem cells to achieve a meaningful long-term effect. The main prerequisite for cell therapy approaches for EB and other genodermatoses is sufficient amount of keratinocyte stem cells, known as holoclones, in order to attain therapeutic longevity of the transgenic cell product (Hirsch et al., 2017). In severe forms of RDEB, this may be challenging as multiple skin biopsies required are painful and invasive. In addition, extensive manipulation and clonal selection of RDEB keratinocytes can rapidly lead to growth arrest, terminal differentiation and senescence. Development of iPSC-based approaches for RDEB provided proof-of-principle evidence of their potential to bypass these limitations in future cell therapy applications. Due to their indefinite proliferating capacity, iPSCs can in theory provide an unlimited reservoir of autologous cells. Significant effort has been directed into the development and validation of differentiation protocols for obtaining keratinocytes and fibroblasts from iPSCs as a potential cell therapy for

RDEB (Itoh et al., 2011; Umegaki-arao et al., 2014; Bilousova et al., 2011; Jacków et al., 2019; Rami et al., 2021).

For EB, initial studies have explored the use of iPSCs for large-scale generation of spontaneously corrected keratinocytes from the patients with revertant mosaicisms in order to obtain an unlimited source of cells for potential autologous cell therapy application (Umegaki-arao et al., 2014; Tolaret al., 2014). As described by Georgiadis *et al.,* (Georgiadis et al., 2016), genetic instability of c.425A>G RDEB keratinocytes and their ability to naturally revert towards a wild type *COL7A1* sequence *in vitro* hinders their *ex vivo* use as a reliable cellular model for gene editing applications. Nevertheless the possibility of making iPSCs from the revertant keratinocytes, the main purpose of this work was to establish novel gene editing strategies for the correction of the c.425A>G mutation. Therefore, c.425A>G fibroblasts were chosen for iPSCs generation due to their ability to retain the mutation of the study. The generated RDEB iPSCs described in **Chapter 4** retained the c.425A>G mutation, hence providing a stable cellular platform that was used for the development of HDR-mediated gene correction and base editing approaches. RDEB iPSCs derived for this study were shown to have the correct morphological characteristics of PSCs alongside their ability to express pluripotency associated markers and multipotential differentiation into the 3 germ layers. Moreover, data presented in **Chapters 4** and **Chapter 5** demonstrated that significant level of gene correction using gene or base editing strategies can be achieved without perturbing cellular pluripotency. In line with the observation from other studies, the feasibility of CRISPR-Cas9 genome editing of *COL7A1* in RDEB iPSCs, can potentially open new horizons for future personalized tissue replacement therapies. In this context, several groups have been working on establishing protocols of iPSCs differentiation into epidermal and dermal skin cells. In this regard, differentiation of HDR- or base-edited patient-derived iPSCs generated in this study into keratinocytes is a critical step for evaluation of their capacity to express relevant keratinocyte stem cells markers, such as K14 and ΔNp63, and to reconstitute functional C7 *in vitro* and *in vivo.*

Application of different differentiation protocols for *COL7A1* corrected iPSCs into keratinocyte described in **Chapter 4** confirmed the capacity of iPSCs to undergo

epidermal commitment during the early stages of differentiation. In both the approaches tested, a somatic ectodermal cell population positive for ΔNp63 was obtained. However, a homogenous expression of mature K14+ cells was not detected, limiting the potential application of these cells for further downstream experiments, such as generation of 3D human skin equivalent (HSE). It is also important to highlight that although several groups have reported different protocols for generating iPSCs-derived keratinocytes, none of the reported studies demonstrated the generation of a completely homogenous p63+/K14+ cell population (Rheinwald 2013). Generally, a cell culture with >80% ΔNp63 and K14 positive keratinocytes can be used for HSE (Professor Dusko's personal communication). Several studies have addressed the low percentage of p63+/K14+ cells by enriching for keratinocyte progenitors by rapid attachment method or cell sorting for integrin alpha 6 (ITGA6, CD49F), another marker highly expressed in basal keratinocyte stem cells (Torkelson et al., 2019; Petrova et al., 2014; Itoh et al., 2013). As hypothesized in **section 4.12** a possible explanation of the incomplete maturation of iPSCs-derived keratinocyte can be related to the well-known variability between different iPSC lines, which suggests that differentiation protocols might need to be optimized for every cell line in order to obtain a pure population of mature keratinocytes (Rheinwald 2013). In this regard, optimizations of the culture conditions are currently underway.,

A second major problem encountered during the investigation of the first differentiation protocol (**Figure 4.12**) was the low expansion potential and early senescence of the cells. These observations are in line with several previous differentiation studies that reported limited proliferation potential of hESC and iPSCs-derived keratinocytes with less than 10 population doublings (Aberdam et al., 2008; Green et., 2003; Metallo et al., 2008). This low proliferation capacity was suggested to be a consequence of early activation of cell cycle inhibitor, such as p16INK4A, in PSC-derived keratinocytes (Dabelsteen et al., 2009).

Despite advances in iPSCs generation and their subsequent differentiation into keratinocytes, both technologies have several limitations in terms of potential clinical translation. With regards to iPSCs derivation, one major roadblock is the risk of iPSCs-

tumorigenicity related to the method of delivery of the reprogramming factors (Griscelli et al., 2019). Several studies have demonstrated that human iPSCs generated by “footprint-free” methods based on certain viral vectors, such as adenoviral and Sendai virus-based vectors, or non-viral vectors, such as piggyBac system, mRNA, minicircle and episomal vectors, are more suitable to circumvent the risk of tumorigenicity compared to lentiviral or retroviral based reprogramming (Griscelli et al., 2019). Furthermore, concerns about iPSC safety such as genomic instability, potential introduction of somatic mutations and retention of epigenetic memory pose challenges to the integrity of iPSCs derivates and their applications in disease modelling and regenerative medicine (Tapia and Schöler 2016; Wasik et al., 2014; Nashun et al., 2015). In addition, stem cell culture and differentiation systems relying on animal-derived components make them unsuitable for therapeutic applications. In this regard, use of xeno-free culture systems described in Chapter 4 can have a better potential for the development of GMP-compliant reagents and protocols for clinical translation, reduce risks of spontaneous differentiation during cell propagation and support undifferentiated growth upon gene correction.

Furthermore, for *ex vivo* engineering, Cas9 toxicity combined with single cell clonal expansion of iPSCs can potentially select for p53 mutant cells, which are more tolerant of DNA damage (Merkle et al., 2017). Noteworthy, according to RNA-SEQ databases, basal rate of 4% and 29% of p53 mutations were found in commonly used iPSC and hESC lines (Merkle et al., 2017). Therefore, after iPSCs derivation and/or gene engineering of patient cells, ensuring the absence of aberrant p53 expression would be critical.

In addition, further efforts should be directed toward establishing efficient and reproducible protocols for iPSCs differentiation into keratinocytes and fibroblasts. Although some progress has been made in identifying consistent methods for deriving and characterizing cells with skin cells properties, protocols reproducibility and proliferation potential of the differentiated progeny are still limited. Moreover, a more extensive characterization of molecular markers of keratinocytes and fibroblasts should be established since similar molecular signatures were shown to be shared with non-skin epithelial and mesenchymal cell types (Shamis et al., 2012;

Hewitt et al., 2011; Kim et al., 2018; Dabelsteen et al., 2009) Overall, although iPSC technology offers an enormous potential for the development of autologous cell-based therapies for RDEB, it is not yet suitable for immediate therapeutic application. Manufacturing of a single iPSC-based cell therapy product would require a lengthy multistep process (reprogramming of patient cells towards iPSCs, gene targeting, derivation of gene edited iPSCs and keratinocyte differentiation), with potential inconsistencies at every step. To address the latter, several studies demonstrated the feasibility of a one-step reprogramming and gene correction manufacturing protocol for the generation of gene edited iPSCs (Torkelson et al., 2019; Howden et al.,2018; Howden et al., 2015). Specifically for RDEB, a recent study conducted by the EB iPS Cell Consortium (USA) described the development of a large scale and robust manufacturing protocol to produce CRISPR-corrected, CD49f-enriched autologous keratinocyte progenitors suitable for skin grafting (Torkelson et al. 2019).

6.5 Future directions

Despite the established importance of genome editing technologies for discovery research and clinical studies, significant advancements with the improvement of the existing Cas9-based platforms and the emergence of new targeting systems, including prime editors, are currently under evaluation (Anzalone et al., 2019). Currently in its 3rd generation, the prime editor complex (PE3) consist of a guide RNA, known as prime editing gRNA (pegRNA), and a Cas9 nickase (Cas9 H840A) fused to an engineered reverse transcriptase (RT). The peculiarity of the pegRNA is related to its longer-than-usual RNA sequence and its ability to interact with the reverse transcriptase using a primer binding site (PBS) on its 3' end followed by a spacer sequence with the desired genetic sequence. Following recognition of the PAM sequence, the PE3-pegRNA complex is able to induce a nick to the PAM-containing strand followed by hybridization of the 3' nicked end with the PBS within the pegRNA. The resulting guide RNA-DNA complex primes reverse transcription of the desired DNA edit using pegRNA as a template. The generated single-stranded cDNA flap with the intended edits is then resolved and incorporated by cellular DNA repair machineries. Prime editors, therefore, eliminate the need for co-delivery of a

corrective DNA template for HDR strategies for small pathogenic InDels and, similarly to base editors, can perform C>T and G>T substitutions without the requirement of base editing window. The potential of this technology has already been demonstrated in a number of proof-of-concept experiments in human cells (Anzalone et al., 2019). Due to its increased editing flexibility, prime editing might provide a suitable alternative for the correction of *COL7A1* mutations. In the light of this, pegRNA targeting the c.425A>G point mutation has already been designed using the prime editing design tool (https://primeedit.nygenome.org/) (Morris et al., 2020).

6.6 Implications of the present study and concluding remarks

Progress in conventional gene therapy has paved the way for the development of *ex vivo* cellular therapy approaches for RDEB. Several trials using gene corrected keratinocyte grafts, fibroblasts or skin equivalents have shown some potential for the treatment of this devastating disorder. Although a cure for RDEB is yet to be found, the most important lesson learnt from preclinical and clinical trials completed so far is that enrichment in keratinocyte stem cells is crucial for longevity of transgenic grafts in patients. Unfortunately, enrichment may not always be possible for patients with RDEB, where extensive wounding makes the isolation of epidermal progenitors challenging.

In addition, despite the recent improvements in knock-out and HDR efficiency in primary keratinocytes (Bonafont et al., 2021; Bonafont et al., 2018), limited lifespan of epithelial stem cells *in vitro* presents a further issue. Extended *ex vivo* manipulation, such as gene editing and clonal selection, of both RDEB keratinocytes and fibroblasts can rapidly lead to growth arrest, terminal differentiation and senescence. The use of iPSC technology for RDEB in the last 10 years has seen a significant leap in providing new patient-specific cellular platforms for targeted gene and cell therapy applications and disease modelling. Therefore, combinatorial approaches using iPSCs and gene editing tools provide a platform for the development of gene correction strategies for targeting recurrent mutations in specific patient cohorts.

In this direction, the relevance of the study described here is its extensive focus on the development of an iPSC model for precise genetic correction of a recurrent splice-site mutation (c.425A>G, p.K142R) in the exon 3 of the *COL7A1* gene using state-of-the art genome editing tools. To our knowledge, the optimized viral-free HDR-mediated correction strategy described in this work is the first proof-of-concept study showing that high level correction of RDEB causative mutation can be achieved without the need of selection markers selection or extensive clonal screening. Additionally, at the time of writing, this study reports the first successful application of cytidine base editors in RDEB iPSCs and offers an important comparative study between novel seamless base correction and HDR-mediated gene correction by ssODN for *COL7A1*

With regards to clinical applications of the following CRISPR/Cas9-based strategies gene editing for gene knockout approaches have already been tested in several phase I/II clinical trials (for a comprehensive review refer to Hirakawa et al., 2020). Recently CRISPR Therapeutics reported its first clinical trial (NCT04035434) evaluating universal CD19-directed CAR T cells developed through HDR-based strategies to insert CAR into the TRAC locus, resulting in endogenous TCR disruption for Refractory/Relapsed B cell malignancies.

In particular for EB, proof-of concept for Cas9 mediated NHEJ gene editing has already showed promising results in preclinical studies in primary keratinocytes. Novel emerging base editor tools also hold promise to pinpoint base and gene correction without creating DSBs that could be detrimental for clinical applications. In this direction, the study presented here confirms that application of non-viral CRISPR/Cas9-based approaches are feasible for RDEB, both iPSC and gene editing technologies and provides foundations for further gene therapy research.

Chapter 7 References

AKIKO SEKI 1, SASCHA RUTZ. 2018. 'Optimized RNP Transfection for Highly Efficient CRISPR/Cas9-Mediated Gene Knockout in Primary T Cells'. *The Journal of Experimental Medicine* 215 (3):985–97.

AASEN TROND, ANGEL RAYA, MARIA J. BARRERO, ELENA GARRETA, ANTONELLA CONSIGLIO, FEDERICO GONZALEZ, RITA VASSENA, et al. 2008. 'Efficient and Rapid Generation of Induced Pluripotent Stem Cells from Human Keratinocytes'. *Nature Biotechnology 26 (11): 1276–84.*

ABADI SHIRAN, WINSTON X. YAN, DAVID AMAR, AND ITAY MAYROSE. 2017. 'A Machine Learning Approach for Predicting CRISPR-Cas9 Cleavage Efficiencies and Patterns Underlying Its Mechanism of Action'. *PLoS Computational Biology 13 (10):e1005807*.

ABERDAM EDITH, EFRAT BARAK, MATTHIEU ROULEAU, STEPHANIE DE LAFOREST, SONIA BERRIH-AKNIN, DAVID M. SUTER, KARL-HEINZ KRAUSE, MICHAL AMIT, JOSEPH ITSKOVITZ-ELDOR, AND DANIEL ABERDAM. 2008. 'A Pure Population of Ectodermal Cells Derived from Human Embryonic Stem Cells'. *Stem Cells 26 (2): 440–44*.

AGARWAL SUNEET, YUIN HAN LOH, ERIN M. MCLOUGHLIN, JUNJIU HUANG, IN HYUN PARK, JUSTINE D. MILLER, HONGGUANG HUO, et al. 2010. 'Telomere Elongation in Induced Pluripotent Stem Cells from Dyskeratosis Congenita Patients'. *Nature 464 (7286): 292–96*.

AGARWALA VINEETA, YINQING LI, ELI J FINE, XUEBING WU, JOHN G DOENCH, NICOLO FUSI, MEAGAN SULLENDER, et al. 2016. 'DNA Targeting Specificity of RNA-Guided Cas9 Nucleases'. *Genome Research 1 (2): 827–32*.

ALAM HUNAIN, LALIT SEHGAL, SAMRAT T. KUNDU, SORAB N. DALAL, AND MILIND M. VAIDYA. 2011. 'Novel Function of Keratins 5 and 14 in Proliferation and Differentiation of Stratified Epithelial Cells'. *Molecular Biology of the Cell 22 (21):*

4068–78.

ALLEGRUCCI C., AND LORRAINE E. YOUNG. 2007. 'Differences between Human Embryonic Stem Cell Lines'. *Human Reproduction Update. 13(2):103-20*.

ALLEN FELICITY, LUCA CREPALDI, CLARA ALSINET, ALEXANDER J STRONG, VITALII KLESHCHEVNIKOV, PIETRO DE ANGELI, PETRA PALENIKOVA, et al. 2018. 'Mutations Generated by Repair of Cas9-Induced Double Strand Breaks Are Predictable from Surrounding Sequence'. *BioRxiv, 27;10.1038/nbt.4317*.

ANDERS CAROLIN, OLE NIEWOEHNER, ALESSIA DUERST, AND MARTIN JINEK. 2014. 'Structural Basis of PAM-Dependent Target DNA Recognition by the Cas9 Endonuclease'. *Nature 513 (7519): 569–73*.

ANGELIS ARIS, PANOS KANAVOS, JULIO LÓPEZ-BASTIDA, RENATA LINERTOVÁ, JUAN OLIVA-MORENO, PEDRO SERRANO-AGUILAR, MANUEL POSADA-DE-LA-PAZ, et al. 2016. 'Social/Economic Costs and Health-Related Quality of Life in Patients with Epidermolysis Bullosa in Europe'. *European Journal of Health Economics* 17: 31–42.

ANZALONE ANDREW V., PEYTON B. RANDOLPH, JESSIE R. DAVIS, ALEXANDER A. SOUSA, LUKE W. KOBLAN, JONATHAN M. LEVY, PETER J. CHEN, et al. 2019. 'Search-and-Replace Genome Editing without Double-Strand Breaks or Donor DNA'. *Nature 576 (7785): 149–57*.

AOI TAKASHI, KOJIRO YAE, MASATO NAKAGAWA, TOMOKO ICHISAKA, KEISUKE OKITA, KAZUTOSHI TAKAHASHI, TSUTOMU CHIBA, AND SHINYA YAMANAKA. 2008. 'Generation of Pluripotent Stem Cells from Adult Mouse Liver and Stomach Cells'. *Science 321 (5889): 699–702*.

ASSOU SAID, JULIEN BOUCKENHEIMER, AND JOHN DE VOS. 2018. 'Concise Review: Assessing the Genome Integrity of Human Induced Pluripotent Stem Cells: What Quality Control Metrics?' *Stem Cells 36 (6): 814–21*.

AUMAILLEY MONIQUE, NEIL SMYTH. 1998. 'The Role of Laminins in Basement Membrane Function'. *Journal of Anatomy* 193 (1): 1–21.

BÄCHINGER H P, N P MORRIS, G P LUNSTRUM, D R KEENE, L M ROSENBAUM, L A COMPTON, AND R E BURGESON. 1990. 'The Relationship of the Biophysical and Biochemical Characteristics of Type VII Collagen to the Function of Anchoring Fibrils.' *The Journal of Biological Chemistry 265 (17): 10095–101*.

BADIAVAS EVANGELOS V., MEHRDAD ABEDI, JANET BUTMARC, VINCENT FALANGA, AND PETER QUESENBERRY. 2003. 'Participation of Bone Marrow Derived Cells in Cutaneous Wound Healing'. *Journal of Cellular Physiology 196 (2): 245–50*.

BAGUTTI CLAUDIA, CAROLINE HUTTER, RUTH CHIQUET-EHRISMANN, REINHARD FÄSSLER, AND FIONA M. WATT. 2001. 'Dermal Fibroblast-Derived Growth Factors Restore the Ability of B1 Integrin-Deficient Embryonal Stem Cells to Differentiate into Keratinocytes'. *Developmental Biology 231 (2): 321–33*.

BAGUTTI CLAUDIA, ANNA M. WOBUS, REINHARD FÄSSLER, AND FIONA M. WATT. 1996. 'Differentiation of Embryonal Stem Cells into Keratinocytes: Comparison of Wild-Type and B1 Integrin-Deficient Cells'. *Developmental Biology 179 (1): 184–96.*

BAK RASMUS O., AND MATTHEW H. PORTEUS. 2017. 'CRISPR-Mediated Integration of Large Gene Cassettes Using AAV Donor Vectors'. *Cell Reports 20 (3): 750–56.*

BAKER JULIE C., ROSA S.P. BEDDINGTON, AND RICHARD M. HARLAND. 1999. 'Wnt Signaling in Xenopus Embryos Inhibits Bmp4 Expression and Activates Neural Development'. *Genes and Development 13 (23): 3149–59*.

BALDESCHI C., Y. GACHE, A. RATTENHOLL, P. BOUILLE, O. DANOS, J.-P. ORTONNE, L. BRUCKNER-TUDERMAN, AND G. MENEGUZZI. 2003. 'Genetic Correction of Canine Dystrophic Epidermolysis Bullosa Mediated by Retroviral Vectors'. *Human Molecular Genetics 12 (15): 1897–1905*.

BAMBERGER CASIMIR, HARTWIG SCHMALE, AND DIETER POLLET. 2002. 'Retinoic Acid Inhibits Downregulation of ΔNp63α Expression during Terminal Differentiation of Human Primary Keratinocytes'. *Journal of Investigative Dermatology 118 (1): 133–38*.

BARRANDON Y, AND H GREEN. 1987. 'Three Clonal Types of Keratinocyte with Different Capacities for Multiplication.' *Proceedings of the National Academy of Sciences of the United States of America 84 (8): 2302–6.*

BARRANGOU RODOLPHE, AND LUCIANO A. MARRAFFINI. 2014. 'CRISPR-Cas Systems: Prokaryotes Upgrade to Adaptive Immunity'. *Molecular Cell 54 (2): 234–44*.

BATISTA LUIS F.Z., MATTHEW F. PECH, FRANKLIN L. ZHONG, HA NAM NGUYEN, KATHLEEN T. XIE, ARTHUR J. ZAUG, SHARON M. CRARY, et al. 2011. 'Telomere Shortening and Loss of Self-Renewal in Dyskeratosis Congenita Induced Pluripotent Stem Cells'. *Nature 474 (7351): 399–404.*

BENATI DANIELA, FRANCESCA MISELLI, FABIENNE COCCHIARELLA, CLARISSA PATRIZI, MARTA CARRETERO, SAMANTHA BALDASSARRI, VIRGINIA AMMENDOLA, et al. 2018. 'CRISPR/Cas9-Mediated In Situ Correction of LAMB3 Gene in Keratinocytes Derived from a Junctional Epidermolysis Bullosa Patient'. *Molecular Therapy 26 (11): 2592–2603.*

BENITAH SALVADOR AZNAR, MICHAELA FRYE, MICHAEL GLOGAUER, AND FIONA M. WATT. 2005. 'Developmental Biology: Stem Cell Depletion through Epidermal Deletion of Rac1'. *Science* 309 (5736): 933–35. https://doi.org/10.1126/science.1113579.

BENTZ H., N. P. MORRIS, L. W. MURRAY, L. Y. SAKAI, D. W. HOLLISTER, AND R. E. BURGESON. 1983. 'Isolation and Partial Characterization of a New Human Collagen with an Extended Triple-Helical Structural Domain'. *Proceedings of the National Academy of Sciences of the United States of America 80 (11): 3168–72.*

BICKENBACH J. R. 1981. ‘Identification and Behavior of Label-Retaining Cells in Oral Mucosa and Skin.’ *Journal of Dental Research* C:1611–20.

BILLON PIERRE, ERIC E. BRYANT, SARAH A. JOSEPH, TARUN S. NAMBIAR, SAMUEL B. HAYWARD, RODNEY ROTHSTEIN, AND ALBERTO CICCIA. 2017. ‘CRISPR-Mediated Base Editing Enables Efficient Disruption of Eukaryotic Genes through Induction of STOP Codons’. *Molecular Cell 67 (6): 1068–1079.*

BILOUSOVA GANNA, JIANG CHEN, AND DENNIS R. ROOP. 2011. ‘Differentiation of Mouse Induced Pluripotent Stem Cells into a Multipotent Keratinocyte Lineage’. *Journal of Investigative Dermatology 131 (4): 857–64*.

BILOUSOVA GANNA, AND DENNIS R. ROOP. 2014. ‘Induced Pluripotent Stem Cells in Dermatology: Potentials, Advances, and Limitations’. *Cold Spring Harbor Perspectives in Medicine 4 (11) : a015164*.

BOCH JENS, HEIDI SCHOLZE, SEBASTIAN SCHORNACK, ANGELIKA LANDGRAF, SIMONE HAHN, SABINE KAY, THOMAS LAHAYE, ANJA NICKSTADT, AND ULLA BONAS. 2009. ‘Breaking the Code of DNA Binding Specificity of TAL-Type III Effectors.’ *Science 326 (5959): 1509–12.*

BOLLING M.C., H.H. LEMMINK, G.H.L. JANSEN, AND M.F. JONKMAN. 2011. ‘Mutations in KRT5 and KRT14 Cause Epidermolysis Bullosa Simplex in 75% of the Patients’. *British Journal of Dermatology 164(3):637-44*.

BOEHNKE KARSTEN, BERIT FALKOWSKA-HANSEN, HANS-JÜRGEN STARK, AND PETRA BOUKAMP. 2012. ‘Stem Cells of the Human Epidermis and Their Niche: Composition and Function in Epidermal Regeneration and Carcinogenesis’. *Carcinogenesis* 33(7): 1247–58.

BOLOTIN ALEXANDER, BENOIT QUINQUIS, ALEXEI SOROKIN, AND S DUSKO EHRLICH. 2005. ‘Clustered Regularly Interspaced Short Palindrome Repeats (CRISPRs) Have Spacers of Extrachromosomal Origin’. *Microbiology 151 (8): 2551–61*.

BONAFONT J., A. MENCIA, M. DEL RIO, M. ESCAMEZ, R. TORRES, I. HAUSER-SILLER, R. MURILLAS, AND F. LARCHER. 2018. 'Highly Efficient, Permanent Ex Vivo Correction of RDEB via Non-Viral CRISPR/Cas9 Excision of COL7A1 Exon 80 Bearing a Prevalent Mutation'. *Journal of Investigative Dermatology 138 (9): B13.*

BONAFONT JOSE, ANGELES MENCÍA, ESTEBAN CHACÓN-SOLANO, WAI SRIFA, SRIRAM VAIDYANATHAN, ROSA ROMANO, MARTA GARCIA, et al. 2021. 'Correction of Recessive Dystrophic Epidermolysis Bullosa by Homology-Directed Repair-Mediated Genome Editing'. *Molecular Therapy 18;S1525-0016(21)00086.*

BOYER LAURIE A., IHN LEE TONG, MEGAN F. COLE, SARAH E. JOHNSTONE, STUART S. LEVINE, JACOB P. ZUCKER, MATTHEW G. GUENTHER, et al. 2005. 'Core Transcriptional Regulatory Circuitry in Human Embryonic Stem Cells'. *Cell* 1*22 (6): 947–56*.

BRAMBRINK TOBIAS, RUTH FOREMAN, G. GRANT WELSTEAD, CHRISTOPHER J. LENGNER, MARIUS WERNIG, HEIKYUNG SUH, AND RUDOLF JAENISCH. 2008. 'Sequential Expression of Pluripotency Markers during Direct Reprogramming of Mouse Somatic Cells'. *Cell Stem Cell 2 (2): 151–59*.

BREMER JEROEN, OLIVIER BORNERT, ALEXANDER NYSTRÖM, ANTONI GOSTYNSKI, MARCEL F. JONKMAN, ANNEMIEKE AARTSMA-RUS, PETER C. VAN DEN AKKER, AND ANNA MG PASMOOIJ. 2016. 'Antisense Oligonucleotide-Mediated Exon Skipping as a Systemic Therapeutic Approach for Recessive Dystrophic Epidermolysis Bullosa'. *Molecular Therapy - Nucleic Acids 18(5):e379.*

BRINKMAN EVA K., ARNE N. KOUSHOLT, TIM HARMSEN, CHRIST LEEMANS, TAO CHEN, JOS JONKERS, AND BAS VAN STEENSEL. 2018. 'Easy Quantification of Template-Directed CRISPR/Cas9 Editing'. *Nucleic Acids Research 46 (10): e58*.

CAI YUJIA, RASMUS O. BAK, ANDERS LAUSTSEN, YAN ZHOU, CHENGLONG SUN, YONGLUN LUO, MARTIN R. JAKOBSEN, AND JACOB G. MIKKELSEN. 2016. 'Lentiviral Protein Transduction for Tailored Genome Editing and Site-Directed Gene Insertion'. *Molecular Therapy* 24 (3): S52.

CAMERON PETER, CHRIS K FULLER, PAUL D DONOHOUE, BRITTNEE N JONES, MATTHEW S THOMPSON, MATTHEW M CARTER, SCOTT GRADIA, et al. 2017. 'Mapping the Genomic Landscape of CRISPR–Cas9 Cleavage'. *Nature Methods 14 (6): 600–606*.

CAPECCHI M R. 1989. 'Altering the Genome by Homologous Recombination.' *Science 244 (4910): 1288–92*.

CARROLL DANA. 2011. 'Genome Engineering with Zinc-Finger Nucleases.' *Genetics 188 (4): 773–82*.

CARTWRIGHT PETER, CAMERON MCLEAN, ALLAN SHEPPARD, DUANE RIVETT, KAREN JONES, AND STEPHEN DALTON. 2005. 'LIF/STAT3 Controls ES Cell Self-Renewal and Pluripotency by a Myc-Dependent Mechanism'. *Development 132 (5): 885–96*.

CHAMORRO CRISTINA, ANGELES MENCÍA, DAVID ALMARZA, BLANCA DUARTE, HILDEGARD BÜNING, JESSICA SALLACH, INGRID HAUSSER, MARCELA DEL RÍO, FERNANDO LARCHER, AND RODOLFO MURILLAS. 2016. 'Gene Editing for the Efficient Correction of a Recurrent COL7A1 Mutation in Recessive Dystrophic Epidermolysis Bullosa Keratinocytes'. *Molecular Therapy - Nucleic Acids 5;5(4):e307*

CHARLESWORTH CARSTEN T., PRIYANKA S. DESHPANDE, DANIEL P. DEVER, JOAB CAMARENA, VIKTOR T. LEMGART, M. KYLE CROMER, CHRISTOPHER A. VAKULSKAS, et al. 2019. 'Identification of Preexisting Adaptive Immunity to Cas9 Proteins in Humans'. *Nature Medicine 25 (2): 249–54*.

CHEN BAOHUI, LUKE A GILBERT, BETH A CIMINI, JOERG SCHNITZBAUER, WEI ZHANG, GENE-WEI LI, JASON PARK, et al. 2013. 'Dynamic Imaging of Genomic Loci in Living Human Cells by an Optimized CRISPR/Cas System'. *Cell 19;155(7):1479-91.*

CHEN HSIN FU, CHING YU CHUANG, YU KAI SHIEH, HAO WEI CHANG, HONG NERNG HO, AND HUNG CHIH KUO. 2009. 'Novel Autogenic Feeders Derived from Human Embryonic Stem Cells (HESCs) Support an Undifferentiated Status of HESCs in Xeno-Free Culture Conditions'. *Human Reproduction 24 (5): 1114–25.*

CHEN JANICE S., AND JENNIFER A. DOUDNA. 2017. 'The Chemistry of Cas9 and Its CRISPR Colleagues'. *Nature Reviews Chemistry 1 (10): 0078.*

CHEN M., E. A. O'TOOLE, M. MUELLENHOFF, E. MEDINA, N. KASAHARA, AND D. T. WOODLEY. 2000. 'Development and Characterization of a Recombinant Truncated Type VII Collagen "Minigene". Implication for Gene Therapy of Dystrophic Epidermolysis Bullosa'. *Journal of Biological Chemistry 275 (32): 24429–35.*

CHEN MEI, NORIYUKI KASAHARA, DOUGLAS R. KEENE, LAWRENCE CHAN, WARREN K. HOEFFLER, DEBORAH FINLAY, MARIA BARCOVA, PAULA M. CANNON, CONSTANCE MAZUREK, AND DAVID T. WOODLEY. 2002. 'Restoration of Type VII Collagen Expression and Function in Dystrophic Epidermolysis Bullosa'. *Nature Genetics 32 (4): 670–75*.

CHERRY ANNE B.C., AND GEORGE Q. DALEY. 2013. 'Reprogrammed Cells for Disease Modeling and Regenerative Medicine'. *Annual Review of Medicine 64: 277–90.*

CHO SEUNG WOO, SOJUNG KIM, JONG MIN KIM, AND JIN-SOO KIM. 2013. 'Targeted Genome Engineering in Human Cells with the Cas9 RNA-Guided Endonuclease.' *Nature Biotechnology 31 (3): 230–32*.

CHRISTIANO A. M., D. S. GREENSPAN, S. LEE, AND J. UITTO. 1994b. 'Cloning of Human Type VII Collagen.' *Journal of Biological Chemistry 269 (32): 20256–62.*

CHRISTIANO A M, AND J UITTO. 1996. 'Molecular Diagnosis of Inherited Skin Diseases: The Paradigm of Dystrophic Epidermolysis Bullosa.' *Advances in Dermatology* 11: 199–213.

CHRISTIANO A M., GUY G. HOFFMAN, LINDA C. CHUNG-HONET, SEUNGBOK LEE, WEN CHENG, JOUNI UITTO, AND DANIEL S. GREENSPAN. 1994a. 'Structural Organization of the Human Type Vii Collagen Gene (COL7A1), Composed of More Exons than Any Previously Characterized Gene'. *Genomics 21 (1): 169–79*.

CHRISTIANO A M, LOUISE M ROSENBAUM, LINDA C CHUNG-HONET, M GABRIELA PARENTE, DAVID T WOODLEY, TE-CHENG PAN, RUI ZHU ZHANG, MON-LI CHU, ROBERT E BURGESON, AND JOUNI UITTO. 1992. 'The Large Non-Collagenous Domain (NC-1) of Type VII Collagen Is Amino-Terminal and Chimeric. Homology to Cartilage Matrix Protein, the Type III Domains of Fibronectin and the A Domains of von Willebrand Factor'. *Human Molecular Genetics 1(7):475-81*.

CHU VAN TRUNG, TIMM WEBER, BENEDIKT WEFERS, WOLFGANG WURST, SANDRINE SANDER, KLAUS RAJEWSKY, AND RALF KÜHN. 2015. 'Increasing the Efficiency of Homology-Directed Repair for CRISPR-Cas9-Induced Precise Gene Editing in Mammalian Cells'. *Nature Biotechnology 33 (5): 543–48*.

CHUAI GUOHUI, HANHUI MA, JIFANG YAN, MING CHEN, NANFANG HONG, DONGYU XUE, AND CHI ZHOU. 2018. 'DeepCRISPR : Optimized CRISPR Guide RNA Design by Deep Learning'. *Genome Biol. 26;19(1):80.*

CHUNG HYE JIN, AND JOUNI UITTO. 2010. 'Type VII Collagen: The Anchoring Fibril Protein at Fault in Dystrophic Epidermolysis Bullosa'. *Dermatologic Clinics*. *28(1):93-105.*

CHYLINSKI KRZYSZTOF, ANAÏS LE RHUN, AND EMMANUELLE CHARPENTIER. 2013. 'The TracrRNA and Cas9 Families of Type II CRISPR-Cas Immunity Systems.' *RNA Biology 10 (5): 726–37.*

CLEMENT KENDELL, HOLLY REES, MATTHEW C. CANVER, JASON M. GEHRKE, RICK FAROUNI, JONATHAN Y. HSU, MITCHEL A. COLE, et al. 2019. 'CRISPResso2 Provides Accurate and Rapid Genome Editing Sequence Analysis'. *Nature Biotechnology 37(3):224-226*

COLUCCIO ANDREA, FRANCESCA MISELLI, ANGELO LOMBARDO, ALESSANDRA MARCONI, GUIDANTONIO MALAGOLI TAGLIAZUCCHI, MANUEL A GONÇALVES, CARLO PINCELLI, et al. 2013. 'Targeted Gene Addition in Human Epithelial Stem Cells by Zinc-Finger Nuclease-Mediated Homologous Recombination.' *Molecular Therapy : The Journal of the American Society of Gene Therapy 21 (9): 1695–1704.*

CONDORELLI ANGELO GIUSEPPE, ELENA DELLAMBRA, ELENA LOGLI, GIOVANNA ZAMBRUNO, AND DANIELE CASTIGLIA. 2019. 'Epidermolysis Bullosa-Associated Squamous Cell Carcinoma: From Pathogenesis to Therapeutic Perspectives'. *International Journal of Molecular Sciences* 14;20(22):5707.

CONG LE, F ANN RAN, DAVID COX, SHUAILIANG LIN, ROBERT BARRETTO, NAOMI HABIB, PATRICK D HSU, et al. 2013. 'Multiplex Genome Engineering Using CRISPR/Cas Systems.' *Science* 339 (6121): 819–23.

CONGET PAULETTE, FERNANDO RODRIGUEZ, SUSANNE KRAMER, CAROLINA ALLERS, VALESKA SIMON, FRANCIS PALISSON, SERGIO GONZALEZ, AND MARIA J YUBERO. 2010. 'Replenishment of Type VII Collagen and Re-Epithelialization of Chronically Ulcerated Skin after Intradermal Administration of Allogeneic Mesenchymal Stromal Cells in Two Patients with Recessive Dystrophic Epidermolysis Bullosa'. *Cytotherapy 12 (3): 429–31.*

CORAUX CHRISTELLE, CAROLINE HILMI, MATTHIEU ROULEAU, ANNE SPADAFORA, JOCELYNE HINNRASKY, JEAN-PAUL ORTONNE, CHRISTIAN DANI, AND DANIEL ABERDAM. 2003. 'Reconstituted Skin from Murine Embryonic Stem Cells.' *Current Biology 13 (10): 849–53.*

COTSARELIS GEORGE, TUNG TIEN SUN, AND ROBERT M. LAVKER. 1990. 'Label-Retaining Cells Reside in the Bulge Area of Pilosebaceous Unit: Implications for Follicular Stem Cells, Hair Cycle, and Skin Carcinogenesis'. *Cell 61 (7): 1329–37*.

COULOMBE PIERRE A., MICHELLE L. KERNS, AND ELAINE FUCHS. 2009. 'Epidermolysis Bullosa Simplex: A Paradigm for Disorders of Tissue Fragility'. *Journal of Clinical Investigation 119 (7):1784-93*

CURTIS R PICKERING, JANE H ZHOU , J JACK LEE, JENNIFER A DRUMMOND, S ANDREW PENG, RAMI E SAADE et al. 2014. 'Mutational Landscape of Aggressive Cutaneous Squamous Cell Carcinoma'. *Clinical Cancer Research: An Official Journal of the American Association for Cancer Research* 20(24):6582–92.

CROSETTO NICOLA, ABHISHEK MITRA, MARIA JOAO SILVA, MAGDA BIENKO, NORBERT DOJER, QI WANG, ELIF KARACA, et al. 2013. 'Nucleotide-Resolution DNA Double-Strand Break Mapping by next-Generation Sequencing'. *Nat Methods 10 (4):361-5*.

CRUDELE JULIE M., AND JEFFREY S. CHAMBERLAIN. 2018. 'Cas9 Immunity Creates Challenges for CRISPR Gene Editing Therapies'. *Nature Communications 29;9(1):3497.*

DABELSTEEN SALLY, PAULA HERCULE, PATRICIA BARRON, MEGHAN RICE, GREGORY DORSAINVILLE, AND JAMES G. RHEINWALD. 2009. 'Epithelial Cells Derived from Human Embryonic Stem Cells Display P16 INK4A Senescence, Hypermotility, and Differentiation Properties Shared by Many P63+ Somatic Cell Types'. *Stem Cells 27 (6): 1388–99.*

DANG NINGNING, AND DÉDÉE F. MURRELL. 2008. 'Mutation Analysis and Characterization of COL7A1 Mutations in Dystrophic Epidermolysis Bullosa'. *Experimental Dermatology 17 (7): 553–68.*

DANG YING, GENGXIANG JIA, JENNIE CHOI, HONGMING MA, EDGAR ANAYA, CHUNTING YE, PREMLATA SHANKAR, AND HAOQUAN WU. 2015. 'Optimizing SgRNA Structure to Improve CRISPR-Cas9 Knockout Efficiency'. *Genome Biol 15;16:280.*

DASTIDAR SUMITAVA, SIMON ARDUI, KSHITIZ SINGH, DEBANJANA MAJUMDAR, NISHA NAIR, YANFANG FU, DEEPAK REYON, et al. 2018. 'Efficient CRISPR/Cas9-Mediated Editing of Trinucleotide Repeat Expansion in Myotonic Dystrophy Patient-Derived IPS and Myogenic Cells'. *Nucleic Acids Research 46 (16): 8275–98.*

DAVIS LUTHER, AND NANCY MAIZELS. 2014. 'Homology-Directed Repair of DNA Nicks via Pathways Distinct from Canonical Double-Strand Break Repair.' *Proceedings of the National Academy of Sciences of the United States of America 111 (10): E924-32.*

DAVIS SHANNON, SHIGETO MIURA, CHRISTIN HILL, YUJI MISHINA, AND JOHN KLINGENSMITH. 2004. 'BMP Receptor IA Is Required in the Mammalian Embryo for Endodermal Morphogenesis and Ectodermal Patterning'. *Developmental Biology 270 (1): 47–63.*

DEINSBERGER JULIA, DAVID REISINGER, AND BENEDIKT WEBER. 2020. 'Global Trends in Clinical Trials Involving Pluripotent Stem Cells: A Systematic Multi-Database Analysis'. *Npj Regenerative Medicine 2020* 5(1): 1–13.

DE ROSA LAURA, MARIA CARMELA LATELLA, ALESSIA SECONE SECONETTI, CECILIA CATTELANI, JOHANN W. BAUER, SERGIO BONDANZA, AND MICHELE DE LUCA. 2019. 'Toward Combined Cell and Gene Therapy for Genodermatoses'. *Cold Spring Harbor Perspectives in Biology* 12 *(5): a035667.*

DE ROSA LAURA, ALESSIA SECONE SECONETTI, GIORGIO DE SANTIS, GIOVANNI PELLACANI, TOBIAS HIRSCH, TOBIAS ROTHOEFT, NORBERT TEIG, GRAZIELLA PELLEGRINI, JOHANN W. BAUER, AND MICHELE DE LUCA. 2019. 'Laminin 332-Dependent YAP Dysregulation Depletes Epidermal Stem Cells in Junctional

Epidermolysis Bullosa'. *Cell Reports 27 (7): 2036–2049.*

DIGIUSTO DAVID L., PAULA M. CANNON, MICHAEL C. HOLMES, LIJING LI, ANITHA RAO, JIANBIN WANG, GARY LEE, et al. 2016. 'Preclinical Development and Qualification of ZFN-Mediated CCR5 Disruption in Human Hematopoietic Stem/Progenitor Cells'. *Molecular Therapy 9;3:16067.*

DOENCH JOHN G, NICOLO FUSI, MEAGAN SULLENDER, MUDRA HEGDE, W EMMA, HERBERT W VIRGIN, JENNIFER LISTGARTEN, et al. 2016. 'Optimized SgRNA Design to Maximize Activity and Minimize Off-Target Effects of CRISPR-Cas9'. *Nat Biotechnol 34 (2): 184–91*.

DOETSCHMAN T. C., H. EISTETTER, AND M. KATZ. 1985. 'The in Vitro Development of Blastocyst-Derived Embryonic Stem Cell Lines: Formation of Visceral Yolk Sac, Blood Islands and Myocardium'. *Journal of Embryology and Experimental Morphology 87: 27–45*.

DOMAN JORDAN L., ADITYA RAGURAM, GREGORY A. NEWBY, AND DAVID R. LIU. 2020. 'Evaluation and Minimization of Cas9-Independent off-Target DNA Editing by Cytosine Base Editors'. *Nature Biotechnology 38 (5): 620–28*.

DOUDNA J. A., AND E. CHARPENTIER. 2014. 'The New Frontier of Genome Engineering with CRISPR-Cas9'. *Science 346 (6213): 1258096–1258096*.

DOYON YANNICK, VIVIAN M CHOI, DANNY F XIA, THUY D VO, PHILIP D GREGORY, AND MICHAEL C HOLMES. 2010. 'Transient Cold Shock Enhances Zinc-Finger Nuclease–mediated Gene Disruption'. *Nat Methods 2010 7(6):459-60.*

DUDA KATARZYNA, LINDSEY A. LONOWSKI, MICHAEL KOFOED-NIELSEN, ADRIANA IBARRA, CATHERINE M. DELAY, QIAOHUA KANG, ZHANG YANG, et al. 2014. 'High-Efficiency Genome Editing via 2A-Coupled Co-Expression of Fluorescent Proteins and Zinc Finger Nucleases or CRISPR/Cas9 Nickase Pairs'. *Nucleic Acids Research 42 (10):e84*.

DULL TOM, ROMAIN ZUFFEREY, MICHAEL KELLY, R. J. MANDEL, MINH NGUYEN, DIDIER TRONO, AND LUIGI NALDINI. 1998. 'A Third-Generation Lentivirus Vector with a Conditional Packaging System'. *Journal of Virology 72 (11): 8463–71.*

DUMITRU RALUCA, VIVIAN GAMA, B. MATTHEW FAGAN, JACQUELYN J. BOWER, VIJAY SWAHARI, LARYSA H. PEVNY, AND MOHANISH DESHMUKH. 2012. 'Human Embryonic Stem Cells Have Constitutively Active Bax at the Golgi and Are Primed to Undergo Rapid Apoptosis'. *Molecular Cell 46 (5): 573–83.*

EICHSTADT SHAUNDRA, MELISSA BARRIGA, ANUSHA PONAKALA, CLAUDIA TENG, NGON T. NGUYEN, ZURAB SIPRASHVILI, JARON NAZAROFF, et al. 2019. 'Phase 1/2a Clinical Trial of Gene-Corrected Autologous Cell Therapy for Recessive Dystrophic Epidermolysis Bullosa'. *JCI Insight 3;4(19):e130554.*

EL-DAROUTI MOHAMMAD, MARWA FAWZY, IMAN AMIN, RANIA ABDEL HAY, REHAB HEGAZY, HALA GABR, AND ZEINAB EL MAADAWI. 2016. 'Treatment of Dystrophic Epidermolysis Bullosa with Bone Marrow Non-Hematopoeitic Stem Cells: A Randomized Controlled Trial'. *Dermatologic Therapy 29 (2): 96–100.*

ELLIOTT BETH, CHRISTINE RICHARDSON, JAMIE WINDERBAUM, JAC A. NICKOLOFF, AND MARIA JASIN. 1998. 'Gene Conversion Tracts from Double-Strand Break Repair in Mammalian Cells'. *Molecular and Cellular Biology 18 (1): 93–101.*

EMINLI SARAH, ADLEN FOUDI, MATTHIAS STADTFELD, NIMET MAHERALI, TIM AHFELDT, GUSTAVO MOSTOSLAVSKY, HANNO HOCK, AND KONRAD HOCHEDLINGER. 2009. 'Differentiation Stage Determines Potential of Hematopoietic Cells for Reprogramming into Induced Pluripotent Stem Cells'. *Nature Genetics 41 (9): 968–76.*

EMINLI SARAH, JOCHEN UTIKAL, KATRIN ARNOLD, RUDOLF JAENISCH, AND KONRAD HOCHEDLINGER. 2008. 'Reprogramming of Neural Progenitor Cells into Induced Pluripotent Stem Cells in the Absence of Exogenous Sox2 Expression'. *Stem Cells 26 (10): 2467–74.*

ENZO ELENA, ALESSIA SECONE SECONETTI, MATTIA FORCATO, ELENA TENEDINI, MARIA PIA POLITO, IRENE SALA, SONIA CARULLI et al. 2021. 'Single-Keratinocyte Transcriptomic Analyses Identify Different Clonal Types and Proliferative Potential Mediated by FOXM1 in Human Epidermal Stem Cells'. *Nature Communications* 12 (1): 1–15.

FATHKE C., LYNNE WILSON, JONATHAN HUTTER, VISHAL KAPOOR, ANDRIA SMITH, ANNE HOCKING, AND FRANK ISIK. 2004. 'Contribution of Bone Marrow-Derived Cells to Skin: Collagen Deposition and Wound Repair'. Stem Cells 22 (5): 812–22.

FINE JO DAVID, LEENA BRUCKNER-TUDERMAN, ROBIN A.J. EADY, EUGENE A. BAUER, JOHANN W. BAUER, CRISTINA HAS, ADRIAN HEAGERTY, et al. 2014. 'Inherited Epidermolysis Bullosa: Updated Recommendations on Diagnosis and Classification'. Journal of the American Academy of Dermatology 70 (6): 1103–26.

FINE JO DAVID, LORRAINE B. JOHNSON, MADELINE WEINER, KUO PING LI, AND CHIRAYATH SUCHINDRAN. 2009. 'Epidermolysis Bullosa and the Risk of Life-Threatening Cancers: The National EB Registry Experience, 1986-2006'. Journal of the American Academy of Dermatology 60 (2): 203–11.

FISHER G J, AND J J VOORHEES. 1996. 'Molecular Mechanisms of Retinoid Actions in Skin.' *The FASEB Journal 10 (9): 1002–13*.

FRANCESCHI RENNY T. 2009. 'The Role of Ascorbic Acid in Mesenchymal Differentiation'. *Nutrition Reviews 50 (3): 65–70*.

FRIEDLAND ARI E., RESHICA BARAL, PANKHURI SINGHAL, KATHERINE LOVELUCK, SHEN SHEN, MINERVA SANCHEZ, EUGENIO MARCO, et al. 2015 'Characterization of Staphylococcus Aureus Cas9: A Smaller Cas9 for All-in-One Adeno-Associated Virus Delivery and Paired Nickase Applications'. *Genome Biology 16 (1): 257.*

FU YANFANG, JEFFRY D SANDER, DEEPAK REYON, VINCENT M CASCIO, J KEITH JOUNG, 2014. 'Improving CRISPR-Cas Nuclease Specificity Using Truncated Guide RNAs'. *Nat Biotechnol. 32 (3): 279–84.*

FUCHS ELAINE. 1995. 'Keratins and the Skin'. *Annual Review of Cell and Developmental Biology 11 (1): 123–54.*

FUJITA Y, H SHIMIZU. 2010. 'Bone Marrow Transplantation Restores Epidermal Basement Membrane Protein Expression and Rescues Epidermolysis Bullosa Model Mice'. *Proceedings of the National Academy of Sciences 107 (32): 14514–14514.*

FUSAKI NOEMI, HIROSHI BAN, AKIYO NISHIYAMA, KOICHI SAEKI, AND MAMORU HASEGAWA. 2009. 'Efficient Induction of Transgene-Free Human Pluripotent Stem Cells Using a Vector Based on Sendai Virus, an RNA Virus That Does Not Integrate into the Host Genome'. *Proceedings of the Japan Academy Series B: Physical and Biological Sciences 85 (8): 348–62*.

GACHE YANNICK, CHRISTINE BALDESCHI, MARCELA DEL RIO, LAURENT GAGNOUX-PALACIOS, FERNANDO LARCHER, JEAN-PHILIPPE LACOUR, AND GUERRINO MENEGUZZI. 2004. 'Construction of Skin Equivalents for Gene Therapy of Recessive Dystrophic Epidermolysis Bullosa'. *Human Gene Therapy 15 (10): 921–33.*

GAJ THOMAS. 2014. 'ZFN, TALEN and CRISPR/Cas Based Methods for Genome Engineering'. *Trends Biotechnol 31 (7): 397–405.*

GALLICO G. GREGORY, NICHOLAS E. O'CONNOR, CAROLYN C. COMPTON, OLANIYI KEHINDE, AND HOWARD GREEN. 1984. 'Permanent Coverage of Large Burn Wounds with Autologous Cultured Human Epithelium'. *New England Journal of Medicine 311 (7): 448–51.*

GARDELLA RITA, LAURA BELLETTI, NICOLETTA ZOPPI, DARIO MARINI, SERGIO BARLATI, AND MARINA COLOMBI1. 1996. 'Identification of Two Splicing Mutations in the Collagen Type VII Gene (COL7A1) of a Patient Affected by the Localisata Variant of Recessive Dystrophic Epidermolysis Bullosa'. *Am. J. Hum. Genet. 59(2): 292–300*.

GAUCHER S., S.M. LWIN, M. TITEUX, A. ABDUL-WAHAB, N. PIRONON, A. IZMIRYAN, S. MISKINYTE, et al. 2020. 'EBGene Trial: Patient Preselection Outcomes for the European GENEGRAFT *Ex Vivo* Phase I/II Gene Therapy Trial for Recessive Dystrophic Epidermolysis Bullosa'. *British Journal of Dermatology 182 (3): 794–97.*

GAUDELLI NICOLE M., ALEXIS C. KOMOR, HOLLY A. REES, MICHAEL S. PACKER, AHMED H. BADRAN, DAVID I. BRYSON, AND DAVID R. LIU. 2017. 'Programmable Base Editing of T to G C in Genomic DNA without DNA Cleavage'. *Nature 551 (7681): 464–71.*

GEISINGER JONATHAN M., AND TIM STEARNS. 2020. 'CRISPR/Cas9 Treatment Causes Extended TP53-Dependent Cell Cycle Arrest in Human Cells'. *Nucleic Acids Research 48 (16): 9067–81.*

GENOVESE PIETRO, GIULIA SCHIROLI, GIULIA ESCOBAR, TIZIANO DI TOMASO, CLAUDIA FIRRITO, ANDREA CALABRIA, DAVIDE MOI, et al. 2014. 'Targeted Genome Editing in Human Repopulating Haematopoietic Stem Cells'. *Nature 510 (7504): 235–40.*

GEORGIADIS CHRISTOS. 2016. 'Development of Gene Therapy for Recessive Dystrophic Epidermolysis Bullosa'. *Doctoral Thesis, UCL (University College London).*

GEORGIADIS CHRISTOS, ROLAND PREECE, LAUREN NICKOLAY, ANIEKAN ETUK, ANASTASIA PETROVA, DARIUSZ LADON, ALEXANDRA DANYI, et al. 2018. 'Long Terminal Repeat CRISPR-CAR-Coupled "Universal" T Cells Mediate Potent Anti-Leukemic Effects'. *Molecular Therapy 26 (5): 1215–27*.

GEORGIADIS CHRISTOS, FARHATULLAH SYED, ANASTASIA PETROVA, ALYA ABDUL-WAHAB, SU M. LWIN, FARZIN FARZANEH, LUCAS CHAN, et al. 2016. 'Lentiviral Engineered Fibroblasts Expressing Codon-Optimized COL7A1 Restore Anchoring Fibrils in RDEB'. *Journal of Investigative Dermatology 136 (1): 284–92.*

GILCHREST BARBARA A., RITA L. KARASSIK, LEON M. WILKINS, MICHAEL A. VRABEL, AND THOMAS MACIAG. 1983. 'Autocrine and Paracrine Growth Stimulation of Cells Derived from Human Skin'. *Journal of Cellular Physiology 117 (2): 235–40.*

GIULIA SCHIROLI, AUTHORS, ANASTASIA CONTI, SAMUELE FERRARI, PIETRO GENOVESE, LUIGI NALDINI, RAFFAELLA DI MICCO, GIULIA SCHIROLI, et al. 2019. 'Precise Gene Editing Preserves Hematopoietic Stem Cell Function Following Transient P53-Mediated DNA Damage Response In Brief Cell Stem Cell Precise Gene Editing Preserves Hematopoietic Stem Cell Function Following Transient P53-Mediated DNA Damage Response'. *Stem Cell 24: 551–565.*

GOLDBERG GREGORY I., ARTHUR Z. EISEN, AND EUGENE A. BAUER. 1988. 'Tissue Stress and Tumor Promotion: Possible Relevance to Epidermolysis Bullosa'. *Archives of Dermatology 124 (5): 737–41*.

GOSTYŃSKI ANTONI, SARA LLAMES, MARTA GARCÍA, MARÍA J. ESCAMEZ, LUCÍA MARTINEZ-SANTAMARIA, MIRANDA NIJENHUIS, ALVARO MEANA, et al. 2014. 'Long-Term Survival of Type XVII Collagen Revertant Cells in an Animal Model of Revertant Cell Therapy'. *Journal of Investigative Dermatology 134(2):571-574.*

GOSTYŃSKI ANTONI, ANNA M.G. PASMOOIJ, AND MARCEL F. JONKMAN. 2014. 'Successful Therapeutic Transplantation of Revertant Skin in Epidermolysis Bullosa'. *Journal of the American Academy of Dermatology 70 (1): 98–101*.

GOTO MAKI, DAISUKE SAWAMURA, WATARU NISHIE, KAORI SAKAI, JAMES R. MCMILLAN, MASASHI AKIYAMA, AND HIROSHI SHIMIZU. 2006. 'Targeted Skipping of a Single Exon Harboring a Premature Termination Codon Mutation: Implications and Potential for Gene Correction Therapy for Selective Dystrophic Epidermolysis Bullosa Patients'. *Journal of Investigative Dermatology 126 (12): 2614–20*.

GREEN, H. 1991. 'Cultured Cells for the Treatment of Disease'. *Scientific American* 265 (5): 96–102.

GREEN H., O. KEHINDE, AND J. THOMAS. 1979. 'Growth of Cultured Human Epidermal Cells into Multiple Epithelia Suitable for Grafting.' *Proceedings of the National Academy of Sciences 76 (11): 5665–68.*

GREEN HOWARD, KAREN EASLEY, AND SHIRO IUCHI. 2003. 'Marker Succession during the Development of Keratinocytes from Cultured Human Embryonic Stem Cells'. *Proceedings of the National Academy of Sciences of the United States of America 100 (26): 15625–30.*

GRISCELLI FRANK, CHRISTOPHE DESTERKE, OLIVIER FERAUD, DOMINIQUE DIVERS, NOUFISSA OUDRHIRI, LUCIE TOSCA, ALI G. TURHAN, AND ANNELISE BENNACEUR-GRISCELLI. 2019. 'Genomic Landscape Analyses of Reprogrammed Cells Using Integrative and Non-Integrative Methods Reveal Variable Cancer-Associated Alterations'. *Oncotarget 10 (28): 2693–2708.*

GRIZOT SYLVESTRE, JEAN-CHARLES EPINAT, SÉVERINE THOMAS, AYMERIC DUCLERT, SANDRA ROLLAND, FRÉDÉRIC PÂQUES, AND PHILIPPE DUCHATEAU. 2010. 'Generation of Redesigned Homing Endonucleases Comprising DNA-Binding Domains Derived from Two Different Scaffolds.' *Nucleic Acids Research 38 (6): 2006–18.*

GRUBER CHRISTINA, ULRICH KOLLER, EVA M. MURAUER, STEFAN HAINZL, CLEMENS HÜTTNER, THOMAS KOCHER, ANDREW P. SOUTH, HELMUT HINTNER, AND JOHANN W. BAUER. 2013. 'The Design and Optimization of RNA Trans-Splicing Molecules for Skin Cancer Therapy'. *Molecular Oncology 7 (6): 1056–68.*

GRÜNEWALD JULIAN, RONGHAO ZHOU, SARA P. GARCIA, SOWMYA IYER, CALEB A. LAREAU, MARTIN J. ARYEE, AND J. KEITH JOUNG. 2019. 'Transcriptome-Wide off-Target RNA Editing Induced by CRISPR-Guided DNA Base Editors'. *Nature 569 (7756): 433–37*.

GRÜNEWALD JULIAN, RONGHAO ZHOU, SOWMYA IYER, CALEB A. LAREAU, SARA P. GARCIA, MARTIN J. ARYEE, AND J. KEITH JOUNG. 2019. 'CRISPR DNA Base Editors with Reduced RNA Off-Target and Self-Editing Activities'. *Nature Biotechnology 37 (9): 1041–48*.

GUDAS LORRAINE J, AND JOHN A WAGNER. 2011. 'Retinoids Regulate Stem Cell Differentiation'. *J Cell Physiol. 226(2): 322–330.*

GUENOU HIND, XAVIER NISSAN, FERNANDO LARCHER, JESSICA FETEIRA, GILLES LEMAITRE, MANOUBIA SAIDANI, MARCELA DEL RIO, et al. 2009. 'Human Embryonic Stem-Cell Derivatives for Full Reconstruction of the Pluristratified Epidermis: A Preclinical Study'. *The Lancet 374 (9703): 1745–53*.

GUENTHER MATTHEW G., GARRETT M. FRAMPTON, FRANK SOLDNER, DIRK HOCKEMEYER, MAYA MITALIPOVA, RUDOLF JAENISCH, AND RICHARD A. YOUNG. 2010. 'Chromatin Structure and Gene Expression Programs of Human Embryonic and Induced Pluripotent Stem Cells'. *Cell Stem Cell 7 (2): 249–57*.

GUMBINER BARRY M. 1996. 'Cell Adhesion: The Molecular Basis of Tissue Architecture and Morphogenesis'. *Cell 84(3):345-57.*

GUO Q, G MINTIER, M MA-EDMONDS, D STORTON, X WANG, X XIAO, B KIENZLE, D ZHAO, AND JOHN N FEDER. 2018. '"Cold Shock" Increases the Frequency of Homology Directed Repair Gene Editing in Induced Pluripotent Stem Cells'. *Scientific Reports 8(1):2080.*

HAAPANIEMI EMMA, SANDEEP BOTLA, JENNA PERSSON, BERNHARD SCHMIERER, AND JUSSI TAIPALE. 2018. 'CRISPR-Cas9 Genome Editing Induces a P53-Mediated DNA Damage Response'. *Nature Medicine 24 (7): 927–30*.

HAASE INGO, RENATE KNAUP, MARIA WARTENBERG, HEINRICH SAUER, JÜRGEN HESCHELER, AND GUSTAV MAHRLE. 2007. 'In Vitro Differentiation of Murine Embryonic Stem Cells into Keratinocyte-like Cells'. *European Journal of Cell Biology 86 (11–12): 801–5.*

HACEIN-BEY-ABINA SALIMA, ALEXANDRINE GARRIGUE, GARY P WANG, JEAN SOULIER, ANNICK LIM, ESTELLE MORILLON, EMMANUELLE CLAPPIER, et al. 2008. 'Insertional Oncogenesis in 4 Patients after Retrovirus-Mediated Gene Therapy of SCID-X1' *J Clin Invest 118(9):3132-42*.

HAINZL STEFAN, PATRICIA PEKING, THOMAS KOCHER, EVA M. MURAUER, FERNANDO LARCHER, MARCELA DEL RIO, BLANCA DUARTE, et al. 2017. 'COL7A1 Editing via CRISPR/Cas9 in Recessive Dystrophic Epidermolysis Bullosa'. *Molecular Therapy 25 (11): 2573–84*.

HAMMAMI-HAUASLI NADJA, D. ULRIKE KALINKE, HAUKE SCHUMANN, ULRICH KALINKE, BERTRAM F. PONTZ, INGRUN ANTON-LAMPRECHT, LEENA PULKKINEN, MIRJAM ZIMMERMANN, JOUNI UITTO, AND LEENA BRUCKNER-TUDERMAN. 1997. 'A Combination of a Common Splice Site Mutation and a Frameshift Mutation in the COL7A1 Gene: Absence of Functional Collagen VII in Keratinocytes and Skin'. *Journal of Investigative Dermatology 109 (3): 384–89*.

HAS C., L. LIU, M.C. BOLLING, A.V. CHARLESWORTH, M. EL HACHEM, M.J. ESCÁMEZ, I. FUENTES, et al. 2020. 'Clinical Practice Guidelines for Laboratory Diagnosis of Epidermolysis Bullosa'. *British Journal of Dermatology 182 (3): 574–92*.

HEMMATI-BRIVANLOU ALI, DOUGLAS MELTONT. 1997. 'Vertebrate Embryonic Cells Will Become Nerve Cells Unless Told Otherwise'. *Cell 10;88(1):13-7*.

HENDEL AYAL, RASMUS O BAK, JOSEPH T CLARK, ANDREW B KENNEDY, DANIEL E RYAN, SUBHADEEP ROY, ISRAEL STEINFELD, et al. 2015. 'Chemically Modified Guide RNAs Enhance CRISPR-Cas Genome Editing in Human Primary Cells'. *Nat Biotechnol 33(9):985-989*.

HENDEL AYAL, ERIC J. KILDEBECK, ELI J. FINE, JOSEPH T. CLARK, NIRAJ PUNJYA, VITTORIO SEBASTIANO, GANG BAO, AND MATTHEW H. PORTEUS. 2014. 'Quantifying Genome-Editing Outcomes at Endogenous Loci with SMRT Sequencing'. *Cell Reports 7 (1): 293–305*.

HEWITT KYLE J., YULIA SHAMIS, MARK W. CARLSON, EDITH ABERDAM, DANIEL ABERDAM, AND JONATHAN A. GARLICK. 2009. 'Three-Dimensional Epithelial Tissues Generated from Human Embryonic Stem Cells'. *Tissue Engineering - Part A 15 (11): 3417–26.*

HEWITT KYLE J., YULIA SHAMIS, RYAN B. HAYMAN, MARIAM MARGVELASHVILI, SHUMIN DONG, MARK W. CARLSON, AND JONATHAN A. GARLICK. 2011. 'Epigenetic and Phenotypic Profile of Fibroblasts Derived from Induced Pluripotent Stem Cells'. *PLoS ONE 28;6(2):e17128*.

HIRAKAWA MATTHEW P., RAGA KRISHNAKUMAR, JERILYN A. TIMLIN, JAMES P. CARNEY, AND KIMBERLY S. BUTLER. 2020. 'Gene Editing and CRISPR in the Clinic: Current and Future Perspectives'. *Bioscience Reports 30;40(4):BSR20200127.*

HIRSCH TOBIAS, TOBIAS ROTHOEFT, NORBERT TEIG, JOHANN W. BAUER, GRAZIELLA PELLEGRINI, LAURA DE ROSA, DAVIDE SCAGLIONE, et al. 2017. 'Regeneration of the Entire Human Epidermis Using Transgenic Stem Cells'. *Nature 551 (7680): 327–32.*

HOPKINSON SUSAN B., KIRK FINDLAY, GREGORY W. DEHART, AND JONATHAN C.R. JONES. 1998. 'Interaction of BP180 (Type XVII Collagen) and CC6 Integrin Is Necessary for Stabilization of Hemidesmosome Structure'. *Journal of Investigative Dermatology 111 (6): 1015–22.*

HOPKINSON SUSAN B., KEVIN J. HAMILL, YVONNE WU, JESSICA L. EISENBERG, SHO HIROYASU, AND JONATHAN C.R. JONES. 2014. 'Focal Contact and Hemidesmosomal Proteins in Keratinocyte Migration and Wound Repair'. *Advances in Wound Care 3 (3): 247–63*.

HORNUNG VEIT, AND EICKE LATZ. 2010. 'Intracellular DNA Recognition'. *Nature Reviews Immunology 10:123–130.*

HOWDEN SARA E., JOHN P. MAUFORT, BRET M. DUFFIN, ANDREW G. ELEFANTY, EDOUARD G. STANLEY, AND JAMES A. THOMSON. 2015. 'Simultaneous Reprogramming and Gene Correction of Patient Fibroblasts'. *Stem Cell Reports 5 (6): 1109–18*.

HOWDEN SARA E., JAMES A. THOMSON, AND MELISSA H. LITTLE. 2018. 'Simultaneous Reprogramming and Gene Editing of Human Fibroblasts'. *Nature Protocols 13 (5): 875–98*.

HOWE STEVEN J, MARC R MANSOUR, KERSTIN SCHWARZWAELDER, CYNTHIA BARTHOLOMAE, MICHAEL HUBANK, HELENA KEMPSKI, MARTIJN H BRUGMAN, et al. 2008. 'Insertional Mutagenesis Combined with Acquired Somatic Mutations Causes Leukemogenesis Following Gene Therapy of SCID-X1 Patients.' *The Journal of Clinical Investigation 118 (9): 3143–50*.

HSIAU TIM, TRAVIS MAURES, KELSEY WAITE, JOYCE YANG, REED KELSO, KEVIN HOLDEN, AND RICH STONER. 2018. 'Inference of CRISPR Edits from Sanger Trace Data'. *BioRxiv 251082*.

HSU PATRICK D, DAVID A SCOTT, JOSHUA A WEINSTEIN, F ANN RAN, SILVANA KONERMANN, VINEETA AGARWALA, YINQING LI, et al. 2013. 'DNA Targeting Specificity of RNA-Guided Cas9 Nucleases.' *Nature Biotechnology 31 (9): 827–32.*

HSU YA CHIEH, LISHI LI, AND ELAINE FUCHS. 2014. 'Emerging Interactions between Skin Stem Cells and Their Niches'. *Nature Medicine 20(8):847-56.*

HSU, YA CHIEH, H. AMALIA PASOLLI, AND ELAINE FUCHS. 2011. 'Dynamics between Stem Cells, Niche, and Progeny in the Hair Follicle'. *Cell 144 (1): 92–105.*

HUANG, HAI JUN, QI SHUANG GAO, BI FEI TAO, AND SI WEN JIANG. 2008. 'Long-Term Culture of Keratinocyte-like Cells Derived from Mouse Embryonic Stem Cells'. *In Vitro Cellular and Developmental Biology - Animal 44 (7): 193–203*.

HUANGFU DANWEI, RENÉ MAEHR, WENJUN GUO, ASTRID EIJKELENBOOM, MELINDA SNITOW, ALICE E. CHEN, AND DOUGLAS A. MELTON. 2008. 'Induction of Pluripotent Stem Cells by Defined Factors Is Greatly Improved by Small-Molecule Compounds'. *Nature Biotechnology 26 (7): 795–97.*

IGOUCHEVA OLGA, VITALI ALEXEEV, AND JOUNI UITTO. 2011. 'Gene Expression Signatures of Mouse Bone Marrow-Derived Mesenchymal Stem Cells in the Cutaneous Environment and Therapeutic Implications for Blistering Skin Disorder'. *Cytotherapy 13: 30–45.*

INMAN GARETH J., JUN WANG, AI NAGANO, LUDMIL B. ALEXANDROV, KARIN J. PURDIE, RICHARD G. TAYLOR, VICTORIA SHERWOOD et al. 2018. 'The Genomic Landscape of Cutaneous SCC Reveals Drivers and a Novel Azathioprine Associated Mutational Signature'. *Nature Communications* 9(1): 1–14.

INOUE H., N. NAGATA, H. KUROKAWA, AND S. YAMANAKA. 2014. 'IPS Cells: A Game Changer for Future Medicine'. *The EMBO Journal 33 (5): 409–17*.

ISHIDA KENTARO, HUAIGENG XU, NORIKO SASAKAWA, MANDY SIU YU LUNG, JULIA ALEXANDRA KUDRYASHEV, PETER GEE, AND AKITSU HOTTA. 2018. 'Site-Specific Randomization of the Endogenous Genome by a Regulatable CRISPR-Cas9 PiggyBac System in Human Cells'. *Scientific Reports 8 (1): 1–12.*

ISHINO Y, H SHINAGAWA, K MAKINO, M AMEMURA, AND A NAKATA. 1987. 'Nucleotide Sequence of the Iap Gene, Responsible for Alkaline Phosphatase Isozyme Conversion in Escherichia Coli, and Identification of the Gene Product.' *Journal of Bacteriology 169 (12): 5429–33*.

ITO, MAYUMI, YAPING LIU, ZAIXIN YANG, JANE NGUYEN, FAN LIANG, REBECCA J. MORRIS, AND GEORGE COTSARELIS. 2005. 'Stem Cells in the Hair Follicle Bulge Contribute to Wound Repair but Not to Homeostasis of the Epidermis'. *Nature Medicine 11 (12): 1351–54.*

ITOH MUNENARI, MAIJA KIURU, MITCHELL S. CAIRO, AND ANGELA M. CHRISTIANO. 2011. 'Generation of Keratinocytes from Normal and Recessive Dystrophic Epidermolysis Bullosa-Induced Pluripotent Stem Cells'. *Proceedings of the National Academy of Sciences of the United States of America 108 (21): 8797–8802.*

ITOH MUNENARI, NORIKO UMEGAKI-ARAO, ZONGYOU GUO, LIANG LIU, CLAIRE A. HIGGINS, AND ANGELA M. CHRISTIANO. 2013. 'Generation of 3D Skin Equivalents Fully Reconstituted from Human Induced Pluripotent Stem Cells (IPSCs)'. *PLoS ONE 8 (10): e77673.*

IUCHI SHIRO, SALLY DABELSTEEN, KAREN EASLEY, JAMES G. RHEINWALD, AND HOWARD GREEN. 2006. 'Immortalized Keratinocyte Lines Derived from Human Embryonic Stem Cells'. *Proceedings of the National Academy of Sciences of the United States of America 103 (6): 1792–97*.

IZMIRYAN A, MEGANUCLEASE-MEDIATED COLA GENE CORRECTION, HEATHER FAWCETT, JONATHAN F WING, SHEHLA MOHAMMED, IAN M FRAYLING, PAUL G NORRIS, DAVID MCGIBBON, P E SARKANY, AND ALAN R LEHMANN. 2016. 'Meganuclease-Mediated COL7A1 Gene Correction for Recessive Dystrophic Epidermolysis Bullosa'. *J Invest Dermatol 136(4):872-875.*

IZMIRYAN ARAKSYA, CLARISSE GANIER, MATTEO BOVOLENTA, ALAIN SCHMITT, FULVIO MAVILIO, AND ALAIN HOVNANIAN. 2018. 'Ex Vivo COL7A1 Correction for Recessive Dystrophic Epidermolysis Bullosa Using CRISPR/Cas9 and Homology-Directed Repair'. *Molecular Therapy 7;12:554-56.*

J O'KEEFFE AHERN, LARA-SÁEZ I, ZHOU D, MURILLAS R, BONAFONT J, MENCÍA Á, GARCÍA M, et al. 2021. 'Non-Viral Delivery of CRISPR-Cas9 Complexes for Targeted Gene Editing via a Polymer Delivery System'. *Gene Therapy*.

JACKÓW JOANNA, ZONGYOU GUO, COREY HANSEN, HASAN E. ABACI, YANNE S. DOUCET, JUNG U. SHIN, RYOTA HAYASHI, et al. 2019. 'CRISPR/Cas9-Based Targeted Genome Editing for Correction of Recessive Dystrophic Epidermolysis Bullosa Using IPS Cells'. *Proceedings of the National Academy of Sciences of the United States of America 116 (52): 26846–52.*

JERIHA JAKOB, NIKOLA KOLUNDZIC, PREETI KHURANA, ANDREA PEREZ-DOMINGUEZ, AND DUSKO ILIC. 2020. 'mRNA-Based Reprogramming Under Xeno-Free and Feeder-Free Conditions'. *Methods in Molecular Biology, 1–10. https://doi.org/10.1007/7651_2020_302.*

JIN SHUAI, YUAN ZONG, QIANG GAO, ZIXU ZHU, YANPENG WANG, PENG QIN, CHENGZHI LIANG, et al. 2019. 'Cytosine, but Not Adenine, Base Editors Induce Genome-Wide off-Target Mutations in Rice'. *Science 364 (6437): 292–95.*

JINEK M., K. CHYLINSKI, I. FONFARA, M. HAUER, J. A. DOUDNA, AND E. CHARPENTIER. 2012. 'A Programmable Dual-RNA-Guided DNA Endonuclease in Adaptive Bacterial Immunity'. *Science 337 (6096): 816–21.*

JONES PHILIP H., AND FIONA M. WATT. 1993. 'Separation of Human Epidermal Stem Cells from Transit Amplifying Cells on the Basis of Differences in Integrin Function and Expression'. *Cell 73 (4): 713–24.*

JONKMAN MARCEL F., AND ANNA M.G. PASMOOIJ. 2009. 'Revertant Mosaicism — Patchwork in the Skin'. *New England Journal of Medicine 360 (16): 1680–82.*

KAJI KEISUKE, KATHERINE NORRBY, AGNIESZKA PACA, MARIA MILEIKOVSKY, PARIA MOHSENI, AND KNUT WOLTJEN. 2009. 'Virus-Free Induction of Pluripotency and Subsequent Excision of Reprogramming Factors'. *Nature 458 (7239): 771–75*.

KATAYAMA MASAHIKO, AND KIYOTOSHI SEKIGUCHI. 2004. 'LAMININ-5 IN EPITHELIAL TUMOUR INVASION.' *Journal of Molecular Histology 35 (3): 277–86*.

KAWASAKI HIROSHI, KENJI MIZUSEKI, SATOMI NISHIKAWA, SATOSHI KANEKO, YOSHIHISA KUWANA, SHIGETADA NAKANISHI, SHIN ICHI NISHIKAWA, AND YOSHIKI SASAI. 2000. 'Induction of Midbrain Dopaminergic Neurons from ES Cells by Stromal Cell-Derived Inducing Activity'. *Neuron 28 (1): 31–40.*

KELLER GORDON. 2005. 'Embryonic Stem Cell Differentiation: Emergence of a New Era in Biology and Medicine'. *Genes Dev 15;19(10):1129-55*.

KERN JOHANNES S, STEFAN LOECKERMANN, ANJA FRITSCH, INGRID HAUSSER, WERA ROTH, THOMAS M MAGIN, CLAUDIA MACK, et al. 2009. 'Mechanisms of Fibroblast Cell Therapy for Dystrophic Epidermolysis Bullosa: High Stability of Collagen VII Favors Long-Term Skin Integrity'. *Molecular Therapy 17 (9): 1605–15.*

KIM DAESIK, SANGSU BAE, JEONGBIN PARK, EUNJI KIM, SEOKJOONG KIM, HYE RYEONG YU, JINHA HWANG, JONG-IL KIM, AND JIN-SOO KIM. 2015. 'Digenome-Seq : Genome-Wide Profiling of CRISPR-Cas9 off-Target Effects in Human Cells'. *Nat Methods 12 (3): 237–44*.

KIM K., A. DOI, B. WEN, K. NG, R. ZHAO, P. CAHAN, J. KIM, et al. 2010. 'Epigenetic Memory in Induced Pluripotent Stem Cells'. *Nature 467 (7313): 285–90*.

KIM KYOUNGMI, SEUK MIN RYU, SANG TAE KIM, GAYOUNG BAEK, DAESIK KIM, KAYEONG LIM, EUGENE CHUNG, SUNGHYUN KIM, AND JIN SOO KIM. 2017. 'Highly Efficient RNA-Guided Base Editing in Mouse Embryos'. *Nature Biotechnology 35 (5): 435–37.*

KIM SOJUNG, DAESIK KIM, SEUNG WOO CHO, JUNGEUN KIM, AND JIN SOO KIM. 2014. 'Highly Efficient RNA-Guided Genome Editing in Human Cells via Delivery of Purified Cas9 Ribonucleoproteins'. *Genome Research 24 (6): 1012–19*.

KIM Y. BILL, ALEXIS C. KOMOR, JONATHAN M. LEVY, MICHAEL S. PACKER, KEVIN T. ZHAO, AND DAVID R. LIU. 2017. 'Increasing the Genome-Targeting Scope and Precision of Base Editing with Engineered Cas9-Cytidine Deaminase Fusions'. *Nature Biotechnology 35 (4): 371–76.*

KIM Y G, J CHA, AND S CHANDRASEGARAN. 1996. 'Hybrid Restriction Enzymes: Zinc Finger Fusions to Fok I Cleavage Domain.' *Proceedings of the National Academy of Sciences of the United States of America 93 (3): 1156–60.*

KIM YENA, NARAE PARK, YERI ALICE RIM, YOOJUN NAM, HYERIN JUNG, KIJUN LEE, AND JI HYEON JU. 2018. 'Establishment of a Complex Skin Structure via Layered Co-Culture of Keratinocytes and Fibroblasts Derived from Induced Pluripotent Stem Cells'. *Stem Cell Research and Therapy Stem Cell Res Ther 13;9(1):217* 9 (1).

KIVISAARI A. K., M. KALLAJOKI, T. MIRTTI, J. A. MCGRATH, J. W. BAUER, F. WEBER, R. KÖNIGOVÁ, et al. 2008. 'Transformation-Specific Matrix Metalloproteinases (MMP)-7 and MMP-13 Are Expressed by Tumour Cells in Epidermolysis Bullosa-Associated Squamous Cell Carcinomas'. *British Journal of Dermatology 158 (4): 778–85.*

KLEINSTIVER BENJAMIN P., VIKRAM PATTANAYAK, MICHELLE S. PREW, SHENGDAR Q. TSAI, NHU T. NGUYEN, ZONGLI ZHENG, AND J. KEITH JOUNG. 2016. 'High-Fidelity CRISPR–Cas9 Nucleases with No Detectable Genome-Wide off-Target Effects'. *Nature 529 (7587): 490–95.*

KNIPPING FRIEDERIKE, MARK J. OSBORN, KARL PETRI, JAKUB TOLAR, HANNO GLIMM, CHRISTOF VON KALLE, MANFRED SCHMIDT, AND RICHARD GABRIEL. 2017. 'Genome-Wide Specificity of Highly Efficient TALENs and CRISPR/Cas9 for T Cell Receptor Modification'. *Molecular Therapy - Methods and Clinical Development 12;4:213-224.*

KOCHER THOMAS, JOHANNES BISCHOF, SIMONE ALEXANDRA HAAS, OLIVER PATRICK MARCH, BERNADETTE LIEMBERGER, STEFAN HAINZL, JULIA ILLMER et al. 2021. 'A Non-Viral and Selection-Free COL7A1 HDR Approach with Improved Safety Profile for Dystrophic Epidermolysis Bullosa'. *Molecular Therapy - Nucleic Acids* 25:237–50.

KOCHER THOMAS, ROLAND N. WAGNER, ALFRED KLAUSEGGER, CHRISTINA GUTTMANN-GRUBER, STEFAN HAINZL, JOHANN W. BAUER, JULIA REICHELT, AND ULRICH KOLLER. 2019. 'Improved Double-Nicking Strategies for COL7A1-Editing by Homologous Recombination'. *Molecular Therapy - Nucleic Acid 6;18:496-507.*

KOGUT IGOR, DENNIS R. ROOP, AND GANNA BILOUSOVA. 2013. 'Differentiation of Human Induced Pluripotent Stem Cells into a Keratinocyte Lineage'. *Methods Mol Biol 1195:1-12.*

KOLUNDZIC NIKOLA, PREETI KHURANA, LIANI DEVITO, MATTHEW DONNE, CARL HOBBS, JAKOB JERIHA, XUAN FEI COLIN CORNELIUS WONG, et al. 2019. 'Induced Pluripotent Stem Cell Line Heterozygous for p.R2447X Mutation in Filaggrin: KCLi002-A'. *Stem Cell Research 38:10146238.*

KOMOR ALEXIS C., YONGJOO B. KIM, MICHAEL S. PACKER, JOHN A. ZURIS, AND DAVID R. LIU. 2016. 'Programmable Editing of a Target Base in Genomic DNA without Double-Stranded DNA Cleavage'. *Nature 533 (7603): 420–24*.

KOMOR ALEXIS C., KEVIN T. ZHAO, MICHAEL S. PACKER, NICOLE M. GAUDELLI, AMANDA L. WATERBURY, LUKE W. KOBLAN, Y. BILL KIM, AHMED H. BADRAN, AND DAVID R. LIU. 2017. 'Improved Base Excision Repair Inhibition and Bacteriophage Mu Gam Protein Yields C:G-to-T:A Base Editors with Higher Efficiency and Product Purity'. *Science Advances 3 (8): 1–9.*

KONDRASHOV ALEXANDER, MINH DUC HOANG, JAMES G.W. SMITH, JAMIE R. BHAGWAN, GARY DUNCAN, DIOGO MOSQUEIRA, MARIA BARBADILLO MUNOZ, NGUYEN T.N. VO, AND CHRIS DENNING. 2018. 'Simplified Footprint-Free Cas9/CRISPR Editing of Cardiac-Associated Genes in Human Pluripotent Stem Cells'. *Stem Cells and Development 27 (6): 391–404.*

KÖNIG A, L BRUCKNER-TUDERMAN. 1992. 'Transforming Growth Factor-Beta Stimulates Collagen VII Expression by Cutaneous Cells in Vitro.' *The Journal of Cell Biology 117 (3): 679–85.*

KOSTER MARANKE I., SOEUN KIM, ALEA A. MILLS, FRANCESCO J. DEMAYO, AND DENNIS R. ROOP. 2004. 'P63 Is the Molecular Switch for Initiation of an Epithelial Stratification Program'. *Genes and Development 18 (2): 126–31.*

KOWALEWSKI CEZARY, KATARZYNA WERTHEIM-TYSAROWSKA, AGNIESZKA SOBCZY, ANNA KUTKOWSKA-KA, AND KATARZYNA WO. 2011. 'The COL7A1 Mutation Database'. *Hum Mutat 33(2):327-31.*

KRUGLIKOV ILJA L., AND PHILIPP E. SCHERER. 2016. 'Dermal Adipocytes: From Irrelevance to Metabolic Targets?' *Trends in Endocrinology and Metabolism 27(1):1-10.*

KÜHL TOBIAS, MARKUS MEZGER, INGRID HAUSSER, RUPERT HANDGRETINGER, LEENA BRUCKNER-TUDERMAN, AND ALEXANDER NYSTRÖM. 2015. 'High Local Concentrations of Intradermal MSCs Restore Skin Integrity and Facilitate Wound Healing in Dystrophic Epidermolysis Bullosa'. *Molecular Therapy 23 (8): 1368–79.*

KUMAR DINENDER, AND BAIMING SUN. 2005. 'Transforming Growth Factor-B2 Enhances Differentiation of Cardiac Myocytes from Embryonic Stem Cells'. *Biochemical and Biophysical Research Communications* 332 (1): 135–41.

KUSCU CEM, MAHMUT PARLAK, TURAN TUFAN, JIEKUN YANG, KAROL SZLACHTA, XIAOLONG WEI, RASHAD MAMMADOV, AND MAZHAR ADLI. 2017. 'CRISPR-STOP: Gene Silencing through Base-Editing-Induced Nonsense Mutations'. *Nature Methods 14 (7): 710–12.*

KWART DYLAN, DOMINIK PAQUET, SHAUN TEO, AND MARC TESSIER-LAVIGNE. 2017. 'Precise and Efficient Scarless Genome Editing in Stem Cells Using CORRECT'. *Nature Protocols 12 (2): 329–54.*

LANGDON ROBERT C., CHARLES B. CUONO, NICHOLAS BIRCHALL, JOSEPH A. MADRI, ELIZABETH KUKLINSKA, JOSEPH MCGUIRE, AND GISELA E. MOELLMANN. 1988. 'Reconstitution of Structure and Cell Function in Human Skin Grafts Derived from Cryopreserved Allogeneic Dermis and Autologous Cultured Keratinocytes'.

Journal of Investigative Dermatology 91 (5): 478–85.

LATELLA MARIA CARMELA, FABIENNE COCCHIARELLA, LAURA DE ROSA, GIANDOMENICO TURCHIANO, MANUEL A.F.V. GONÇALVES, FERNANDO LARCHER, MICHELE DE LUCA, AND ALESSANDRA RECCHIA. 2017. 'Correction of Recessive Dystrophic Epidermolysis Bullosa by Transposon-Mediated Integration of COL7A1 in Transplantable Patient-Derived Primary Keratinocytes'. *Journal of Investigative Dermatology 137 (4): 836–44.*

LATTANZI ANNALISA, VASCO MENEGHINI, GIULIA PAVANI, FATIMA AMOR, SOPHIE RAMADIER, TRISTAN FELIX, CHIARA ANTONIANI, et al. 2019. 'Optimization of CRISPR/Cas9 Delivery to Human Hematopoietic Stem and Progenitor Cells for Therapeutic Genomic Rearrangements'. *Molecular Therapy 27 (1): 137–50.*

LECHLER TERRY, AND ELAINE FUCHS. 2005. 'Asymmetric Cell Divisions Promote Stratification and Differentiation of Mammalian Skin'. *Nature 437 (7056): 275–80.*

LEE HYE KYUNG, MICHAELA WILLI, SHANNON M. MILLER, SOJUNG KIM, CHENGYU LIU, DAVID R. LIU, AND LOTHAR HENNIGHAUSEN. 2018. 'Targeting Fidelity of Adenine and Cytosine Base Editors in Mouse Embryos'. *Nature Communications 9 (1): 4804.*

LEWIS D A, J B TRAVERS, A-K SOMANI, AND D F SPANDAU. 2010. 'The IGF-1/IGF-10 Signaling Axis in the Skin: A New Role for the Dermis in Aging-Associated Skin Cancer'. *Oncogene 29: 1475–85.*

LI KAI, GANG WANG, TROELS ANDERSEN, PINGZHU ZHOU, AND WILLIAM T. PU. 2014. 'Optimization of Genome Engineering Approaches with the CRISPR/Cas9 System'. Edited by Kefei Yu. *PLoS ONE 9 (8): e105779*.

LI LINGJIE, YONG WANG, JESSICA L. TORKELSON, GAUTAM SHANKAR, JILLIAN M. PATTISON, HANSON H. ZHEN, FENGQIN FANG, et al. 2019. 'TFAP2C- and P63-Dependent Networks Sequentially Rearrange Chromatin Landscapes to Drive Human Epidermal Lineage Commitment'. *Cell Stem Cell 24 (2): 271–284.e8.*

LI LINGYU, CHANG LIU, STEFFEN BIECHELE, QINGQING ZHU, LU SONG, FREDRIK LANNER, NAIHE JING, AND JANET ROSSANT. 2013. 'Location of Transient Ectodermal Progenitor Potential in Mouse Development'. *Development 140 (22): 4533–43.*

LI WENLIN, WEI WEI, SAIYONG ZHU, JINLIANG ZHU, YAN SHI, TONGXIANG LIN, ERGENG HAO, ALBERTO HAYEK, HONGKUI DENG, AND SHENG DING. 2009. 'Generation of Rat and Human Induced Pluripotent Stem Cells by Combining Genetic Reprogramming and Chemical Inhibitors'. *Cell Stem Cell 9;4(1):16-9.*

LI XIAO LAN, GUO HUA LI, JUAN FU, YA WEN FU, LU ZHANG, WANQIU CHEN, CAMERON ARAKAKI, et al. 2018. 'Highly Efficient Genome Editing via CRISPR–Cas9 in Human Pluripotent Stem Cells Is Achieved by Transient BCL-XL Overexpression'. *Nucleic Acids Research 46 (19): 10195–215.*

LIANG F, M HAN, P J ROMANIENKO, AND M JASIN. 1998. 'Homology-Directed Repair Is a Major Double-Strand Break Repair Pathway in Mammalian Cells.' *Proceedings of the National Academy of Sciences of the United States of America 95 (9): 5172–77.*

LIANG PUPING, HONGWEI SUN, YING SUN, XIYA ZHANG, XIAOWEI XIE, JINRAN ZHANG, ZHEN ZHANG, et al. 2017. 'Effective Gene Editing by High-Fidelity Base Editor 2 in Mouse Zygotes'. *Protein and Cell 8 (8): 601–11.*

LIEBER MICHAEL R. 2010. 'The Mechanism of Double-Strand DNA Break Repair by the Nonhomologous DNA End-Joining Pathway.' *Annual Review of Biochemistry* 79:181-211.

LIEBER MICHAEL R, YUNMEI MA, ULRICH PANNICKE, AND KLAUS SCHWARZ. 2003. 'Mechanism and Regulation of Human Non-Homologous DNA End-Joining.' *Nature Reviews. Molecular Cell Biology 4 (9): 712–20.*

LIN STEVEN, BRETT T STAAHL, RAVI K ALLA, AND JENNIFER A DOUDNA. 2014. 'Enhanced Homology-Directed Human Genome Engineering by Controlled Timing of CRISPR/Cas9 Delivery'. *ELife* 15;3:e04766.

LIU HAISONG, FANGFANG ZHU, JUN YONG, PENGBO ZHANG, PINGPING HOU, HONGGANG LI, WEI JIANG, et al. 2008. 'Generation of Induced Pluripotent Stem Cells from Adult Rhesus Monkey Fibroblasts'. *Cell Stem Cell 4;3(6):587-90.*

LIU JIA, THOMAS GAJ, YIFENG YANG, NAN WANG, SAILAN SHUI, SOJUNG KIM, CHIDANANDA NAGAMANGALA KANCHISWAMY, JIN SOO KIM, AND CARLOS F. BARBAS. 2015. 'Efficient Delivery of Nuclease Proteins for Genome Editing in Human Stem Cells and Primary Cells'. *Nature Protocols 10 (11): 1842–59.*

LIU LI PING, YU MEI LI, NING NING GUO, SHU LI, XIAOLONG MA, YI XUAN ZHANG, YIMENG GAO, et al. 2019. 'Therapeutic Potential of Patient IPSC-Derived Melanocytes in Autologous Transplantation'. *Cell Reports 27 (2): 455–466.e5*.

LIU ZHEN, ZONGYANG LU, GUANG YANG, SHISHENG HUANG, GUANGLEI LI, SONGJIE FENG, YAJING LIU, et al. 2018. 'Efficient Generation of Mouse Models of Human Diseases via ABE- and BE-Mediated Base Editing'. *Nature Communications 9 (1): 1–8.*

LIU ZHIQUAN, MAO CHEN, SIYU CHEN, JICHAO DENG, YUNING SONG, LIANGXUE LAI, AND ZHANJUN LI. 2018. 'Highly Efficient RNA-Guided Base Editing in Rabbit'. *Nature Communications 13;9(1):2717.*

LWIN SU M., FARHATULLAH SYED, WEI LI DI, TENDAI KADIYIRIRE, LU LIU, ALYSON GUY, ANASTASIA PETROVA, et al. 2019. 'Safety and Early Efficacy Outcomes for Lentiviral Fibroblast Gene Therapy in Recessive Dystrophic Epidermolysis Bullosa'. *JCI Insight 6;4(11):e126243*.

MA YUNQING, JIAYUAN ZHANG, WEIJIE YIN, ZHENCHAO ZHANG, YAN SONG, AND XING CHANG. 2016. 'Targeted AID-Mediated Mutagenesis (TAM) Enables Efficient Genomic Diversification in Mammalian Cells'. *Nature Methods 13 (12): 1029–35.*

MAHERALI NIMET, TIM AHFELDT, ALESSANDRA RIGAMONTI, JOCHEN UTIKAL, CHAD COWAN, AND KONRAD HOCHEDLINGER. 2008. 'A High-Efficiency System for the Generation and Study of Human Induced Pluripotent Stem Cells'. *Cell Stem Cell*

3 (3): 340–45.

MARINKOVICH M. PETER, DOUGLAS R. KEENE, CLYTIE S. RIMBERG, AND ROBERT E. BURGESON. 1993. 'Cellular Origin of the Dermal-epidermal Basement Membrane'. *Developmental Dynamics 197 (4): 255–67*.

MARSON ALEXANDER, RUTH FOREMAN, BRETT CHEVALIER, STEVE BILODEAU, MICHAEL KAHN, RICHARD A. YOUNG, AND RUDOLF JAENISCH. 2008. 'Wnt Signaling Promotes Reprogramming of Somatic Cells to Pluripotency'. *Cell Stem Cell 7;3(2):132-5.*

MARTIN RENATA M., KAZUYA IKEDA, M. KYLE CROMER, NOBUKO UCHIDA, TOSHINOBU NISHIMURA, ROSA ROMANO, ANDREW J. TONG, et al. 2019. 'Highly Efficient and Marker-Free Genome Editing of Human Pluripotent Stem Cells by CRISPR-Cas9 RNP and AAV6 Donor-Mediated Homologous Recombination'. *Cell Stem Cell 24 (5): 821–828.*

MAVILIO FULVIO, GRAZIELLA PELLEGRINI, STEFANO FERRARI, FRANCESCA DI NUNZIO, ENZO DI IORIO, ALESSANDRA RECCHIA, GIULIETTA MARUGGI, et al. 2006. 'Correction of Junctional Epidermolysis Bullosa by Transplantation of Genetically Modified Epidermal Stem Cells'. *Nature Medicine 12 (12): 1397–1402.*

MCGRATH ERICA, HYUNSU SHIN, LINYI ZHANG, JE NIE PHUE, WELLS W. WU, RONG FONG SHEN, YOON YOUNG JANG, JAVIER REVOLLO, AND ZHAOHUI YE. 2019. 'Targeting Specificity of APOBEC-Based Cytosine Base Editor in Human IPSCs Determined by Whole Genome Sequencing'. *Nature Communications 10 (1): 1–9.*

MEHTA ADITI, OLIVIA M. MERKEL. 2020. 'Immunogenicity of Cas9 Protein'. *Journal of Pharmaceutical Sciences*. *J Pharm Sci 109(1):62-67.*

MERCURIO A. M., I. RABINOVITZ, AND L. M. SHAW. 2001. 'The A6β4 Integrin and Epithelial Cell Migration'. *Current Opinion in Cell Biology*. *56(4): 443–452.*

MERIENNE NICOLAS, GABRIEL VACHEY, LUCIE DE LONGPREZ, CÉCILE MEUNIER, VIRGINIE ZIMMER, GUILLAUME PERRIARD, MATHIEU CANALES, et al. 2017. 'The Self-Inactivating KamiCas9 System for the Editing of CNS Disease Genes'. *Cell Reports 20 (12): 2980–91.*

MERKLE FLORIAN T., SULAGNA GHOSH, NOLAN KAMITAKI, JANA MITCHELL, YISHAI AVIOR, CURTIS MELLO, SEVA KASHIN, et al. 2017. 'Human Pluripotent Stem Cells Recurrently Acquire and Expand Dominant Negative P53 Mutations'. *Nature 545 (7653): 229–33.*

MERRILL B. J., U. GAT, R. DASGUPTA, AND E. FUCHS. 2001. 'Tcf3 and Lef1 Regulate Lineage Differentiation of Multipotent Stem Cells in Skin'. *Genes and Development 15 (13): 1688–1705.*

METALLO CHRISTIAN M., SAMIRA M. AZARIN, LAUREL E. MOSES, LIN JI, JUAN J. DE PABLO, AND SEAN P. PALECEK. 2010. 'Human Embryonic Stem Cell-Derived Keratinocytes Exhibit an Epidermal Transcription Program and Undergo Epithelial Morphogenesis in Engineered Tissue Constructs'. *Tissue Engineering - Part A 16 (1): 213–23*.

METALLO CHRISTIAN M., LIN JI, JUAN J. DE PABLO, AND SEAN P. PALECEK. 2008. 'Retinoic Acid and Bone Morphogenetic Protein Signaling Synergize to Efficiently Direct Epithelial Differentiation of Human Embryonic Stem Cells'. *Stem Cells 26 (2): 372–80.*

METALLO CHRISTIAN M., LIN JI, JUAN J. DE PABLO, AND SEAN P. PALECEK. 2010. 'Directed Differentiation of Human Embryonic Stem Cells to Epidermal Progenitors.' *Methods in Molecular Biology 585:83–92.*

MILLS ALEA A., BINHAI ZHENG, XIAO JING WANG, HANNES VOGEL, DENNIS R. ROOP, AND ALLAN BRADLEY. 1999. 'P63 Is a P53 Homologue Required for Limb and Epidermal Morphogenesis'. *Nature 398 (6729): 708–13.*

MOJICA F J, C DÍEZ-VILLASEÑOR, E SORIA, AND G JUEZ. 2000. 'Biological Significance of a Family of Regularly Spaced Repeats in the Genomes of Archaea, Bacteria and Mitochondria.' *Molecular Microbiology 36 (1): 244–46.*

MOJICA FJ DÍEZ-VILLASEÑOR C, GARCÍA-MARTÍNEZ J, SORIA E. 2005. 'Intervening Sequences of Regularly Spaced Prokaryotic Repeats Derive from Foreign Genetic Elements'. *Journal of Molecular Evolution 60 (2): 174–82*.

MOLL ROLAND, WERNER W. FRANKE, DOROTHEA L. SCHILLER, BENJAMIN GEIGER, AND REINHARD KREPLER. 1982. 'The Catalog of Human Cytokeratins: Patterns of Expression in Normal Epithelia, Tumors and Cultured Cells'. *Cell 31(1):11-24.*

MORRIS JOHN, JAHAN RAHMAN, XINYI GUO, AND NEVILLE SANJANA. 2020. 'Automated Design of CRISPR Prime Editors for Thousands of Human Pathogenic Variants'. *BioRxiv https://doi.org/10.1101/2020.05.07.083444*.

MORRIS R. J., AND C. S. POTTEN. 1994. 'Slowly Cycling (Label-retaining) Epidermal Cells Behave like Clonogenic Stem Cells in Vitro'. *Cell Proliferation 27 (5): 279–89*.

MOULIN V. 1995. 'Growth Factors in Skin Wound Healing'. *European Journal of Cell Biology 68(1):1-7*.

MURAUER EVA M., YANNICK GACHE, IRIS K. GRATZ, ALFRED KLAUSEGGER, WOLFGANG MUSS, CHRISTINA GRUBER, GUERRINO MENEGUZZI, HELMUT HINTNER, AND JOHANN W. BAUER. 2011. 'Functional Correction of Type VII Collagen Expression in Dystrophic Epidermolysis Bullosa'. *Journal of Investigative Dermatology 131 (1): 74–83*.

MUSSOLINO CLAUDIO, AND TONI CATHOMEN. 2012. 'TALE Nucleases: Tailored Genome Engineering Made Easy.' *Current Opinion in Biotechnology 23 (5): 644–50*.

NAGY NIKOLETTA, NOOR ALMAANI, AKIO TANAKA, JOEY E LAI-CHEONG, TANASIT TECHANUKUL, JEMIMA E MELLERIO, AND JOHN A MCGRATH. 2011. 'HB-EGF Induces COL7A1 Expression in Keratinocytes and Fibroblasts: Possible Mechanism Underlying Allogeneic Fibroblast Therapy in Recessive Dystrophic Epidermolysis Bullosa'. *Journal of Investigative Dermatology 131: 1771–74.*

NAKAGAWA MASATO, MICHIYO KOYANAGI, KOJI TANABE, KAZUTOSHI TAKAHASHI, TOMOKO ICHISAKA, TAKASHI AOI, KEISUKE OKITA, YUJI MOCHIDUKI, NANAKO TAKIZAWA, AND SHINYA YAMANAKA. 2008. 'Generation of Induced Pluripotent Stem Cells without Myc from Mouse and Human Fibroblasts'. *Nature Biotechnology 26 (1): 101–6.*

NASHUN BUHE, PETER WS HILL, AND PETRA HAJKOVA. 2015. 'Reprogramming of Cell Fate: Epigenetic Memory and the Erasure of Memories Past'. *The EMBO Journal 34 (10): 1296–1308.*

NASO GAETANO, AND ANASTASIA PETROVA. 2019. 'CRISPR/Cas9 Gene Editing for Genodermatoses: Progress and Perspectives'. *Emerging Topics in Life Sciences*, *https://doi.org/10.1042/ETLS20180148.*

NELSON ERIC E, AND AMANDA E GUYER. 2012. 'Rational Design of Highly Active SgRNAs for CRISPR-Cas9-Mediated Gene Inactivation'. *Nat Biotechnol 32(12):1262-7.*

NELSON W. G., AND T. T. SUN. 1983. 'The 50- and 58-Kdalton Keratin Classes as Molecular Markers for Stratified Squamous Epithelia: Cell Culture Studies'. *Journal of Cell Biology 97 (1): 244–51.*

NIGHTINGALE SARAH J., ROGER P. HOLLIS, KAREN A. PEPPER, DENISE PETERSEN, XIAO-JIN YU, CATHERINE YANG, INGRID BAHNER, AND DONALD B. KOHN. 2006. 'Transient Gene Expression by Nonintegrating Lentiviral Vectors'. *Molecular Therapy 13 (6): 1121–32.*

NISHIDA KEIJI, TAKAYUKI ARAZOE, NOZOMU YACHIE, SATOMI BANNO, MIKA KAKIMOTO, MAYURA TABATA, MASAO MOCHIZUKI, et al. 2016. 'Targeted Nucleotide Editing Using Hybrid Prokaryotic and Vertebrate Adaptive Immune Systems'. *Science 16;353(6305):aaf8729.*

NISHIMASU HIROSHI, F ANN RAN, PATRICK D HSU, SILVANA KONERMANN, SORAYA I SHEHATA, NAOSHI DOHMAE, RYUICHIRO ISHITANI, FENG ZHANG, AND OSAMU NUREKI. 2014. 'Crystal Structure of Cas9 in Complex with Guide RNA and Target DNA.' *Cell 156 (5): 935–49.*

NIWA HITOSHI, TOM BURDON, IAN CHAMBERS, AND AUSTIN SMITH. 1998. 'Self-Renewal of Pluripotent Embryonic Stem Cells Is Mediated via Activation of STAT3'. *Genes and Development 12 (13): 2048–60.*

NIWA HITOSHI, JUN ICHI MIYAZAKI, AND AUSTIN G. SMITH. 2000. 'Quantitative Expression of Oct-3/4 Defines Differentiation, Dedifferentiation or Self-Renewal of ES Cells'. *Nature Genetics 24 (4): 372–76.*

NYSTRÖM ALEXANDER, DANIELA VELATI, VENUGOPAL R. MITTAPALLI, ANJA FRITSCH, JOHANNES S. KERN, AND LEENA BRUCKNER-TUDERMAN. 2013. 'Collagen VII Plays a Dual Role in Wound Healing'. *Journal of Clinical Investigation 123 (8): 3498–3509.*

OHTA SHIGEKI, YOICHI IMAIZUMI, YOHEI OKADA, WADO AKAMATSU, REIKO KUWAHARA, MANABU OHYAMA, MASAYUKI AMAGAI, et al. 2013. 'Generation of Human Melanocytes from Induced Pluripotent Stem Cells'. *Methods Mol Biol 989:193-215*

OOST JOHN VAN DER, EDZE R WESTRA, RYAN N JACKSON, AND BLAKE WIEDENHEFT. 2014. 'Unravelling the Structural and Mechanistic Basis of CRISPR-Cas Systems.' *Nature Reviews. Microbiology 12 (7): 479–92.*

ORTIZ-URDA SUSANA, JOHN GARCIA, CHERYL L. GREEN, LEI CHEN, QUN LIN, DALLAS P. VEITCH, LYNN Y. SAKAI, HYANGKYU LEE, M. PETER MARINKOVICH, AND PAUL A. KHAVARI. 2005. 'Type VII Collagen Is Required for Ras-Driven Human Epidermal Tumorigenesis'. *Science 307 (5716): 1773–76.*

ORTIZ-URDA SUSANA, QUN LIN, CHERYL L GREEN, DOUGLAS R KEENE, M PETER MARINKOVICH, AND PAUL A KHAVARI. 2003. 'Injection of Genetically Engineered Fibroblasts Corrects Regenerated Human Epidermolysis Bullosa Skin Tissue.' *The Journal of Clinical Investigation 111 (2): 251–55.*

ORTIZ-URDA SUSANA, BHASKAR THYAGARAJAN, DOUGLAS R KEENE, QUN LIN, MIN FANG, MICHELE P CALOS, AND PAUL A KHAVARI. 2002. 'Stable Nonviral Genetic Correction of Inherited Human Skin Disease'. *Nat Med 8(10):1166-70.*

OSBORN MARK J., CHRISTOPHER J. LEES, AMBER N. MCELROY, SARAH C. MERKEL, CINDY R. EIDE, WENDY MATHEWS, COLBY J. FESER, et al. 2018. 'Crispr/Cas9-Based Cellular Engineering for Targeted Gene Overexpression'. *International Journal of Molecular Sciences 22;19(4):946.*

OSBORN MARK J., GREGORY A. NEWBY, AMBER N. MCELROY, FRIEDERIKE KNIPPING, SARAH C. NIELSEN, MEGAN J. RIDDLE, LILY XIA, et al. 2020. 'Base Editor Correction of COL7A1 in Recessive Dystrophic Epidermolysis Bullosa Patient-Derived Fibroblasts and IPSCs'. *Journal of Investigative Dermatology 140 (2): 338–347.*

OSBORN MARK J., COLBY G. STARKER, AMBER N. MCELROY, BEAU R. WEBBER, MEGAN J. RIDDLE, LILY XIA, ANTHONY P. DEFEO, et al. 2013. 'TALEN-Based Gene Correction for Epidermolysis Bullosa'. *Molecular Therapy 21 (6): 1151–59.*

OSBORN MARK J., BEAU R. WEBBER, FRIEDERIKE KNIPPING, CARA LIN LONETREE, NICOLE TENNIS, ANTHONY P. DEFEO, AMBER N. MCELROY, et al. 2016. 'Evaluation of TCR Gene Editing Achieved by TALENs, CRISPR/Cas9, and MegaTAL Nucleases'. *Molecular Therapy 24 (3): 570–81.*

OTT MARION G, MANFRED SCHMIDT, KERSTIN SCHWARZWAELDER, STEFAN STEIN, ULRICH SILER, ULRIKE KOEHL, HANNO GLIMM, et al. 2006. 'Correction of X-Linked Chronic Granulomatous Disease by Gene Therapy, Augmented by Insertional Activation of MDS1-EVI1, PRDM16 or SETBP1'. *Nature Medicine 12 (4): 401–9.*

OWARIBE KATSUSHI, JÜRGEN KARTENBECK, SABINE STUMPP, THOMAS M. MAGIN, THOMAS KRIEG, LUIS A. DIAZ, AND WERNER W. FRANKE. 1990. 'The Hemidesmosomal Plaque: I. Characterization of a Major Constituent Protein as a Differentiation Marker for Certain Forms of Epithelia'. *Differentiation 45 (3): 207–20.*

PALEARI YLENIA, FABIENNE COCCHIARELLA, RICCARDO MEZZADRA, FULVIO MAVILIO, ARIANNA MOIANI, DANIELA SARTORI, MARIA ROSA LIDONNICI, ANNARITA MICCIO, CLAUDIA CATTOGLIO, AND GIULIANA FERRARI. 2012. 'Lentiviral Vector Integration in the Human Genome Induces Alternative Splicing and Generates Aberrant Transcripts'. *Journal of Clinical Investigation 122 (5): 1653–66.*

PAQUET DOMINIK, DYLAN KWART, ANTONIA CHEN, ANDREW SPROUL, SAMSON JACOB, SHAUN TEO, KIMBERLY MOORE OLSEN, ANDREW GREGG, SCOTT NOGGLE, AND MARC TESSIER-LAVIGNE. 2016. 'Efficient Introduction of Specific Homozygous and Heterozygous Mutations Using CRISPR/Cas9'. *Nature 5;533(7601):125-9.*

PARENTE M. G., L. C. CHUNG, J. RYYNANEN, D. T. WOODLEY, K. C. WYNN, E. A. BAUER, M. G. MATTEI, M. L. CHU, AND J. UITTO. 1991. 'Human Type VII Collagen: CDNA Cloning and Chromosomal Mapping of the Gene'. *Proceedings of the National Academy of Sciences of the United States of America 88 (16): 6931–35*.

PARK IN HYUN, NATASHA ARORA, HONGGUANG HUO, NIMET MAHERALI, TIM AHFELDT, AKIKO SHIMAMURA, M. WILLIAM LENSCH, CHAD COWAN, KONRAD HOCHEDLINGER, AND GEORGE Q. DALEY. 2008. 'Disease-Specific Induced Pluripotent Stem Cells'. *Cell 134 (5): 877–86.*

PATTISON JILLIAN M., SANDRA P. MELO, SAMANTHA N. PIEKOS, JESSICA L. TORKELSON, ELIZAVETA BASHKIROVA, MAXWELL R. MUMBACH, CHARLOTTE RAJASINGH, et al. 2018. 'Retinoic Acid and BMP4 Cooperate with P63 to Alter Chromatin Dynamics during Surface Epithelial Commitment'. *Nature Genetics 50(12):1658-1665*.

PEARSON ROGER W. 1962. 'Studies on the Pathogenesis of Epidermolysis Bullosa'. *Journal of Investigative Dermatology 39:551-75.*

PELLEGRINI GRAZIELLA, ELENA DELLAMBRA, OSVALDO GOLISANO, ENRICA MARTINELLI, IVANA FANTOZZI, SERGIO BONDANZA, DIEGO PONZIN, FRANK MCKEON, AND MICHELE DE LUCA. 2001. 'P63 Identifies Keratinocyte Stem Cells'. *Proceedings of the National Academy of Sciences of the United States of America 98 (6): 3156–61*.

PELLEGRINI GRAZIELLA, OSVALDO GOLISANO, PATRIZIA PATERNA, ALESSANDRO LAMBIASE, STEFANO BONINI, PAOLO RAMA, AND MICHELE DE LUCA. 1999. 'Location and Clonal Analysis of Stem Cells and Their Differentiated Progeny in the Human Ocular Surface'. *The Journal of Cell Biology 145 (4): 769–82.*

PELLEGRINI GRAZIELLA, ROSARIO RANNO, GIORGIO STRACUZZI, SERGIO BONDANZA, LILIANA GUERRA, GIOVANNA ZAMBRUNO, GIOVANNI MICALI, AND MICHELE DE LUCA. 1999. 'The Control of Epidermal Stem Cells (Holoclones) in the Treatment of Massive Full-Thickness Burns with Autologous Keratinocytes Cultured on Fibrin'. *Transplantation 68 (6): 868–79.*

PENDARIES VALÉRIE, GÉRALDINE GASC, MATTHIAS TITEUX, LAURE TONASSO, JOSÉ ENRIQUE MEJÍA, AND ALAIN HOVNANIAN. 2012. 'SiRNA-Mediated Allele-Specific Inhibition of Mutant Type VII Collagen in Dominant Dystrophic Epidermolysis Bullosa'. *Journal of Investigative Dermatology 132 (6): 1741–43.*

PERDONI CHRISTOPHER, JOHN A. MCGRATH, AND JAKUB TOLAR. 2014. 'Preconditioning of Mesenchymal Stem Cells for Improved Transplantation Efficacy in Recessive Dystrophic Epidermolysis Bullosa'. *Stem Cell Research and Therapy* 5 (6): 1–12.

PETROF G., M. MARTINEZ-QUEIPO, J.E. MELLERIO, P. KEMP, AND J.A. MCGRATH. 2013. 'Fibroblast Cell Therapy Enhances Initial Healing in Recessive Dystrophic Epidermolysis Bullosa Wounds: Results of a Randomized, Vehicle-Controlled Trial'. *British Journal of Dermatology 169 (5): 1025–33.*

PETROF GABRIELA, SU M. LWIN, MAGDALENA MARTINEZ-QUEIPO, ALYA ABDUL-WAHAB, SIMON TSO, JEMIMA E. MELLERIO, INEKE SLAPER-CORTENBACH, et al. 2015. 'Potential of Systemic Allogeneic Mesenchymal Stromal Cell Therapy for Children with Recessive Dystrophic Epidermolysis Bullosa'. *Journal of Investigative Dermatology 135 (9): 2319–21.*

PETROVA A., D. ILIC, AND J.A. MCGRATH. 2010. 'Stem Cell Therapies for Recessive Dystrophic Epidermolysis Bullosa'. *British Journal of Dermatology 163 (6): 1149–56.*

PETROVA ANASTASIA, ANNA CELLI, LAUREEN JACQUET, DIMITRA DAFOU, DEBRA CRUMRINE, MELANIE HUPE, MATTHEW ARNO, et al. 2014. '3D In Vitro Model of a Functional Epidermal Permeability Barrier from Human Embryonic Stem Cells and Induced Pluripotent Stem Cells'. *Stem Cell Reports 2 (5): 675–89.*

PETROVA ANASTASIA, CHRISTOS GEORGIADIS, ROLAND A. FLECK, LEANNE ALLISON, JOHN A. MCGRATH, FRANCESCO DAZZI, WEI LI DI, AND WASEEM QASIM. 2020. 'Human Mesenchymal Stromal Cells Engineered to Express Collagen VII Can Restore Anchoring Fibrils in Recessive Dystrophic Epidermolysis Bullosa Skin Graft Chimeras'. *Journal of Investigative Dermatology 140 (1): 121–131.*

PINNEL S. R. 1987. 'Induction of Collagen Synthesis by Ascorbic Acid. A Possible Mechanism'. *Archives of Dermatology 123 (12): 1684–86.*

PORTEUS MATTHEW. 2016. ‘Genome Editing: A New Approach to Human Therapeutics’. *Annual Review of Pharmacology and Toxicology 56 (1): 163–90.*

POURREYRON CELINE, GEORGIE COX, XIN MAO, ANDREAS VOLZ, NUZHAT BAKSH, TRACY WONG, HIVA FASSIHI, et al. 2007. ‘Patients with Recessive Dystrophic Epidermolysis Bullosa Develop Squamous-Cell Carcinoma Regardless of Type VII Collagen Expression’. *Journal of Investigative Dermatology 127 (10): 2438–44.*

PREECE ROLAND, AND CHRISTOS GEORGIADIS. 2019. ‘Emerging CRISPR/Cas9 Applications for T-Cell Gene Editing’. *Emerging Topics in Life Sciences https://doi.org/10.1042/ETLS20180144.*

RAGHAVAN SRIKALA, CHRISTOPH BAUER, GINA MUNDSCHAU, QINGQIN LI, AND ELAINE FUCHS. 2000. ‘Conditional Ablation of B1 Integrin in Skin: Severe Defects in Epidermal Proliferation, Basement Membrane Formation, and Hair Follicle Invagination’. *Journal of Cell Biology 150 (5): 1149–60.*

RAMI AVINA, ŁUKASZ ŁACZMAŃSKI, JAGODA JACKÓW-NOWICKA, AND JOANNA JACKÓW. 2021. ‘Reprogramming and Differentiation of Cutaneous Squamous Cell Carcinoma Cells in Recessive Dystrophic Epidermolysis Bullosa’. *International Journal of Molecular Sciences 22 (1): 1–14*.

RAMSHAW JOHN A.M., NAINA K. SHAH, AND BARBARA BRODSKY. 1998. ‘Gly-X-Y Tripeptide Frequencies in Collagen: A Context for Host-Guest Triple-Helical Peptides’. *Journal of Structural Biology 122 (1–2): 86–91.*

RAN F. ANN, PATRICK D. HSU, CHIE-YU LIN, JONATHAN S. GOOTENBERG, SILVANA KONERMANN, ALEXANDRO E. TREVINO, DAVID A. SCOTT, et al. 2013. ‘Double Nicking by RNA-Guided CRISPR Cas9 for Enhanced Genome Editing Specificity’. *Cell 154 (6): 1380–89.*

RAN F. ANN, LE CONG, WINSTON X. YAN, DAVID A. SCOTT, JONATHAN S. GOOTENBERG, ANDREA J. KRIZ, BERND ZETSCHE, et al. 2015. ‘In Vivo Genome Editing Using Staphylococcus Aureus Cas9’. *Nature 520 (7546): 186–91.*

RANGANATHAN VINOD, KARL WAHLIN, JULIEN MARUOTTI, AND DONALD J. ZACK. 2014. 'Expansion of the CRISPR-Cas9 Genome Targeting Space through the Use of H1 Promoter-Expressed Guide RNAs'. *Nature Communications 5:4516 1–8.*

RASHIDGHAMAT ELLIE, TENDAI KADIYIRIRE, SALMA AYIS, GABRIELA PETROF, LU LIU, VENU PULLABHATLA, CHRYSANTHI AINALI, et al. 2020. 'Phase I/II Open-Label Trial of Intravenous Allogeneic Mesenchymal Stromal Cell Therapy in Adults with Recessive Dystrophic Epidermolysis Bullosa'. *Journal of the American Academy of Dermatology 83(2):447-454.*

RAVIN SUK SEE DE, LINHONG LI, XIAOLIN WU, UIMOOK CHOI, CORNELL ALLEN, SHERRY KOONTZ, JANET LEE, et al. 2017. 'CRISPR-Cas9 Gene Repair of Hematopoietic Stem Cells from Patients with X-Linked Chronic Granulomatous Disease'. *Science Translational Medicine 11;9(372): 3480.*

REES HOLLY A., AND DAVID R. LIU. 2018. 'Base Editing: Precision Chemistry on the Genome and Transcriptome of Living Cells'. *Nature Reviews Genetics 19 (12): 770–88.*

REMY SÉVERINE, LAURENT TESSON, SÉVERINE MENORET, CLAIRE USAL, ANNE DE CIAN, VIRGINIE THEPENIER, REYNALD THINARD, et al. 2014. 'Efficient Gene Targeting by Homology-Directed Repair in Rat Zygotes Using TALE Nucleases'. *Genome Research 24 (8): 1371–83.*

RENAUD, JEAN BAPTISTE, CHARLOTTE BOIX, MARINE CHARPENTIER, ANNE DE CIAN, JULIEN COCHENNEC, EVELYNE DUVERNOIS-BERTHET, LOÏC PERROUAULT, et al. 2016. 'Improved Genome Editing Efficiency and Flexibility Using Modified Oligonucleotides with TALEN and CRISPR-Cas9 Nucleases'. *Cell Reports 14 (9): 2263–72.*

RHEINWALD JAMES G. 2013. 'The Quest to Derive Keratinocytes from Pluripotent Stem Cells'. *Current Pathobiology Reports (2): 119–28.*

RHEINWALD JAMES G., AND HOWARD GREEN. 1975. 'Formation of a Keratinizing Epithelium in Culture by a Cloned Cell Line Derived from a Teratoma'. *Cell 6 (3): 317–30.*

RHEINWATD JAMES G., AND HOWARD GREEN. 1975. 'Serial Cultivation of Strains of Human Epidermal Keratinocytes: The Formation of Keratinizing Colonies from Single Cells.' *Cell 6 (3): 331–43.*

RICARD-BLUM SYLVIE, AND FLORENCE RUGGIERO. 2005. 'The Collagen Superfamily: From the Extracellular Matrix to the Cell Membrane'. *Pathologie Biologie* 5*3 (7): 430–42.*

RICHARDSON CHRISTOPHER D, GRAHAM J RAY, MARK A DEWITT, GEMMA L CURIE, AND JACOB E CORN. 2016. 'Enhancing Homology-Directed Genome Editing by Catalytically Active and Inactive CRISPR-Cas9 Using Asymmetric Donor DNA'. *Nature Biotechnology 34 (3): 339–44.*

RM LAVKER, TT SUN 1982. 'Heterogeneity in Epidermal Basal Keratinocytes: Morphological and Functional Correlations'. *Science* 215(4537).

ROCHAT ARIANE, KOJI KOBAYASHI, AND YANN BARRANDON. 1994. 'Location of Stem Cells of Human Hair Follicles by Clonal Analysis'. *Cell* 76 *(6): 1063–73.*

ROTH THEODORE L., CRISTINA PUIG-SAUS, RUBY YU, ERIC SHIFRUT, JULIA CARNEVALE, P. JONATHAN LI, JOSEPH HIATT, ET AL. 2018. 'Reprogramming Human T Cell Function and Specificity with Non-Viral Genome Targeting'. *Nature 559 (7714): 405–9.*

ROUET P, F SMIH, AND M JASIN. 1994. 'Expression of a Site-Specific Endonuclease Stimulates Homologous Recombination in Mammalian Cells.' *Proceedings of the National Academy of Sciences of the United States of America 91 (13): 6064–68.*

ROUSSELLE PATRICIA, DOUGLAS R. KEENE, FLORENCE RUGGIERO, MARIE FRANCE CHAMPLIAUD, MICHEL DER VAN REST, AND ROBERT E. BURGESON. 1997. 'Laminin 5 Binds the NC-1 Domain of Type VII Collagen'. *Journal of Cell Biology 138 (3): 719–28.*

SAKUMA TOSHIE, MICHAEL A BARRY, AND YASUHIRO IKEDA. 2012. 'Lentiviral Vectors: Basic to Translational.' *The Biochemical Journal 443 (3): 603–18.*

SAN FILIPPO JOSEPH, PATRICK SUNG, AND HANNAH KLEIN. 2008. 'Mechanism of Eukaryotic Homologous Recombination.' *Annual Review of Biochemistry* 77:229–57.

SANDER JEFFRY D, AND J KEITH JOUNG. 2014. 'CRISPR-Cas Systems for Editing, Regulating and Targeting Genomes.' *Nature Biotechnology 32 (4): 347–55.*

SASAKI MIKAKO, RIICHIRO ABE, YASUYUKI FUJITA, SATOMI ANDO, DAISUKE INOKUMA, AND HIROSHI SHIMIZU. 2008. 'Mesenchymal Stem Cells Are Recruited into Wounded Skin and Contribute to Wound Repair by Transdifferentiation into Multiple Skin Cell Type.' *Journal of Immunology 180 (4): 2581–87.*

SCHAFER IRWIN A., MAUREEN PANDY, RODERICK FERGUSON, AND BRYAN R. DAVIS. 1985. 'Comparative Observation of Fibroblasts Derived from the Papillary and Reticular Dermis of Infants and Adults: Growth Kinetics, Packing Density at Confluence and Surface Morphology'. *Mechanisms of Ageing and Development 31 (3): 275–938.*

SCHUMANN KATHRIN, STEVEN LIN, ERIC BOYER, DIMITRE R. SIMEONOV, MEENA SUBRAMANIAM, RACHEL E. GATE, GENEVIEVE E. HALIBURTON, et al. 2015. 'Generation of Knock-in Primary Human T Cells Using Cas9 Ribonucleoproteins'. *Proceedings of the National Academy of Sciences* 112(33):10437–42.

SEBASTIANO VITTORIO, HANSON HUI ZHEN, BAHAREH HADDAD DERAFSHI, ELIZAVETA BASHKIROVA, SANDRA P. MELO, PEI WANG, THOMAS L. LEUNG, et al. 2014. 'Human COL7A1-Corrected Induced Pluripotent Stem Cells for the Treatment of Recessive Dystrophic Epidermolysis Bullosa'. *Science Translational Medicine 6 (264): 1–12*.

SEBBAN SHULAMIT, AND YOSEF BUGANIM. 2016. 'Nuclear Reprogramming by Defined Factors: Quantity Versus Quality'. *Trends in Cell Biology 26(1):65-75.*

SELEKMAN JOSHUA A., NICHOLAS J. GRUNDL, JOSHUA M. KOLZ, AND SEAN P. PALECEK. 2013. 'Efficient Generation of Functional Epithelial and Epidermal Cells from Human Pluripotent Stem Cells under Defined Conditions'. *Tissue Engineering - Part C: Methods 19 (12): 949–60.*

SENOO MAKOTO, FILIPA PINTO, CHRISTOPHER P. CRUM, AND FRANK MCKEON. 2007. 'P63 Is Essential for the Proliferative Potential of Stem Cells in Stratified Epithelia'. *Cell 129 (3): 523–36.*

SHALOM-FEUERSTEIN RUBY, LAURA SERROR, EDITH ABERDAM, FRANZ JOSEF MÜLLER, HANS VAN BOKHOVEN, KLAS G. WIMAN, HUIQING ZHOU, DANIEL ABERDAM, AND ISABELLE PETIT. 2013. 'Impaired Epithelial Differentiation of Induced Pluripotent Stem Cells from Ectodermal Dysplasia-Related Patients Is Rescued by the Small Compound APR-246/PRIMA-1MET'. *Proceedings of the National Academy of Sciences of the United States of America 110 (6): 2152–56*.

SHAMIS YULIA, KYLE J. HEWITT, SUSAN E. BEAR, ALT HOLLAND ADDY, HIBA QARI, MARIAM MARGVELASHVILLI, ELANA B. KNIGHT, AVI SMITH, AND JONATHAN A. GARLICK. 2012. 'IPSC-Derived Fibroblasts Demonstrate Augmented Production and Assembly of Extracellular Matrix Proteins'. *In Vitro Cellular and Developmental Biology - Animal 48 (2): 112–22.*

SHEN MAX W., MANDANA ARBAB, JONATHAN Y. HSU, DANIEL WORSTELL, SANNIE J. CULBERTSON, OLGA KRABBE, CHRISTOPHER A. CASSA, DAVID R. LIU, DAVID K. GIFFORD, AND RICHARD I. SHERWOOD. 2018. 'Predictable and Precise Template-Free CRISPR Editing of Pathogenic Variants'. *Nature 563(7733):646-651.*

SHIMIZU H, A ISHIKO, T MASUNAGA, Y KURIHARA, M SATO, L BRUCKNER-TUDERMAN, AND T NISHIKAWA. 1997. 'Most Anchoring Fibrils in Human Skin Originate and Terminate in the Lamina Densa.' *Laboratory Investigation; a Journal of Technical Methods and Pathology 76 (6): 753–63.*

SHINKUMA SATORU, ZONGYOU GUO, AND ANGELA M. CHRISTIANO. 2016. 'Site-Specific Genome Editing for Correction of Induced Pluripotent Stem Cells Derived from Dominant Dystrophic Epidermolysis Bullosa'. *Proceedings of the National Academy of Sciences 113 (20): 5676–81.*

SHUKLA AKASH, HARDIK PARIKH, TEJAS MODI, PHILIP ABRAHAM, SWATI KAMBLE, DIPENDU MAJUMDER, AND SHOBNA BHATIA. 2010. 'Long-Term Type VII Collagen Restoration to Human Epidermolysis Bullosa Skin Tissue'. *Annals of Gastroenterology 28 (1): 130–34.*

SILVA GEORGE, LAURENT POIROT, ROMAN GALETTO, JULIANNE SMITH, GUILLERMO MONTOYA, PHILIPPE DUCHATEAU, AND FREDERIC PAQUES. 2011. 'Meganucleases and Other Tools for Targeted Genome Engineering: Perspectives and Challenges for Gene Therapy'. *Current Gene Therapy 11 (1): 11–27*.

SIPRASHVILI ZURAB, NGON T. NGUYEN, MARIA Y. BEZCHINSKY, M. PETER MARINKOVICH, ALFRED T. LANE, AND PAUL A. KHAVARI. 2010. 'Long-Term Type VII Collagen Restoration to Human Epidermolysis Bullosa Skin Tissue'. *Human Gene Therapy 21 (10): 1299–1310.*

SIPRASHVILI ZURAB, NGON T. NGUYEN, EMILY S. GORELL, KYLIE LOUTIT, PHUONG KHUU, LOUISE K. FURUKAWA, H. PETER LORENZ, et al. 2016. 'Safety Andwound Outcomes Following Genetically Corrected Autologous Epidermal Grafts in Patients with Recessive Dystrophic Epidermolysis Bullosa'. *JAMA - Journal of the American Medical Association 316 (17): 1808–17.*

SKOTTMAN HELI, MILLA MIKKOLA, KAROLINA LUNDIN, CIA OLSSON, ANNE-MARIE STRÖMBERG, TIMO TUURI, TIMO OTONKOSKI, OUTI HOVATTA, AND RIITTA LAHESMAA. 2005. 'Gene Expression Signatures of Seven Individual Human Embryonic Stem Cell Lines'. *Stem Cells 23 (9): 1343–56.*

SLUIS MARJOLEIN VAN, AND BRIAN MCSTAY. 2015. 'A Localized Nucleolar DNA Damage Response Facilitates Recruitment of the Homology-Directed Repair Machinery Independent of Cell Cycle Stage'. *Genes and Development 29 (11): 1151–63.*

SMITH R. S., T. J. SMITH, T. M. BLIEDEN, AND R. P. PHIPPS. 1997. 'Fibroblasts as Sentinel Cells. Synthesis of Chemokines and Regulation of Inflammation.' *The American Journal of Pathology 151(2): 317–322*.

SMOLLER B R, J KRUEGER, N S MCNUTT, AND A HSU. 1990. '"Activated" Keratinocyte Phenotype Is Unifying Feature in Conditions Which Predispose to Squamous Cell Carcinoma of the Skin.' *Modern Pathology : An Official Journal of the United States and Canadian Academy of Pathology 3 (2): 171–75.*

SMOLLER BRUCE A., N. SCOTT MCNUTT, D. MARTIN CARTER, ALICE B. GOTTLIEB, AMY HSU, AND JAMES KRUEGER. 1990. 'Recessive Dystrophic Epidermolysis Bullosa Skin Displays a Chronic Growth-Activated Immunophenotype: Implications for Carcinogenesis'. *Archives of Dermatology 126 (1): 78–83.*

SOLDNER FRANK, DIRK HOCKEMEYER, CAROLINE BEARD, QING GAO, GEORGE W. BELL, ELIZABETH G. COOK, GUNNAR HARGUS, et al. 2009. 'Parkinson's Disease Patient-Derived Induced Pluripotent Stem Cells Free of Viral Reprogramming Factors'. *Cell 136 (5): 964–77.*

SOMMER CESAR A., ANDREIA GIANOTTI SOMMER, TYLER A. LONGMIRE, CONSTANTINA CHRISTODOULOU, DOLLY D. THOMAS, MONICA GOSTISSA, FRED W. ALT, GEORGE J. MURPHY, DARRELL N. KOTTON, AND GUSTAVO MOSTOSLAVSKY. 2010. 'Excision of Reprogramming Transgenes Improves the Differentiation Potential of IPS Cells Generated with a Single Excisable Vector'. *Stem Cells 28 (1): 64–74.*

SOMMER CESAR A, MATTHIAS STADTFELD, GEORGE J MURPHY, KONRAD HOCHEDLINGER, DARRELL N KOTTON, AND GUSTAVO MOSTOSLAVSKY. 2009. 'IPS Cell Generation Using a Single Lentiviral Stem Cell Cassette HHS Public Access'. *Stem Cells 27 (3): 543–49.*

STADTFELD MATTHIAS, KRISTEN BRENNAND, AND KONRAD HOCHEDLINGER. 2008. 'Reprogramming of Pancreatic β Cells into Induced Pluripotent Stem Cells'. *Current Biology 18 (12): 890–94.*

STADTFELD MATTHIAS, NIMET MAHERALI, DAVID T. BREAULT, AND KONRAD HOCHEDLINGER. 2008. 'Defining Molecular Cornerstones during Fibroblast to IPS Cell Reprogramming in Mouse'. *Cell Stem Cell 2 (3): 230–40.*

STANLEY JOHN R., NURIT RUBINSTEIN, AND VERA KLAUS-KOVTUN. 1985. 'Epidermolysis Bullosa Acquisita Antigen Is Synthesized by Both Human Keratinocytes and Human Dermal Fibroblasts'. *Journal of Investigative Dermatology 85 (6): 542–45*.

STRASSBURG SANDRA, STEPHEN M. RICHARDSON, ANTHONY J. FREEMONT, AND JUDITH A. HOYLAND. 2010. 'Co-Culture Induces Mesenchymal Stem Cell Differentiation and Modulation of the Degenerate Human Nucleus Pulposus Cell Phenotype'. *Regenerative Medicine 5 (5): 701–11.*

TAKAHASHI KAZUTOSHI, KOJI TANABE, MARI OHNUKI, MEGUMI NARITA, TOMOKO ICHISAKA, KIICHIRO TOMODA, AND SHINYA YAMANAKA. 2007. 'Induction of Pluripotent Stem Cells from Adult Human Fibroblasts by Defined Factors'. *Cell 131 (5): 861–72.*

TAKAHASHI KAZUTOSHI, AND SHINYA YAMANAKA. 2006. 'Induction of Pluripotent Stem Cells from Mouse Embryonic and Adult Fibroblast Cultures by Defined Factors'. *Cell 126 (4): 663–76.*

TAKASHIMA SHOTA, SATORU SHINKUMA, YASUYUKI FUJITA, TOSHIFUMI NOMURA, HIDEYUKI UJIIE, KEN NATSUGA, HIROAKI IWATA, et al. 2019. 'Efficient Gene Reframing Therapy for Recessive Dystrophic Epidermolysis Bullosa Using CRISPR/Cas9'. *Journal of Investigative Dermatology 139(8):1711-1721.*

TAMAI KATSUTO, TAKEHIKO YAMAZAKI, TAKENAO CHINO, MASARU ISHII, SATORU OTSURU, YASUSHI KIKUCHI, SHIN IINUMA, et al. 2011. 'PDGFRalpha-Positive Cells in Bone Marrow Are Mobilized by High Mobility Group Box 1 (HMGB1) to Regenerate Injured Epithelia.' *Proceedings of the National Academy of Sciences of the United States of America 108 (16): 6609–14*.

TANG JEAN YUH, M. PETER MARINKOVICH, ELEANOR LUCAS, EMILY GORELL, ALBERT CHIOU, YING LU, JODIE GILLON, DIPEN PATEL, AND DAN RUDIN. 2021. 'A Systematic Literature Review of the Disease Burden in Patients with Recessive Dystrophic Epidermolysis Bullosa'. *Orphanet Journal of Rare Diseases* 16(1):1–25.

TAPIA NATALIA, AND HANS R. SCHÖLER. 2016. 'Molecular Obstacles to Clinical Translation of IPSCs'. *Cell Stem Cell 1;19(3):298-309.*

TITEUX MATTHIAS, VALÉRIE PENDARIES, MARIA A ZANTA-BOUSSIF, AUDREY DÉCHA, NATHALIE PIRONON, LAURE TONASSO, JOSÉ E MEJIA, AGNES BRICE, OLIVIER DANOS, AND ALAIN HOVNANIAN. 2010. 'SIN Retroviral Vectors Expressing COL7A1 Under Human Promoters for Ex Vivo Gene Therapy of Recessive Dystrophic Epidermolysis Bullosa'. *Molecular Therapy 18 (8): 1509–18.*

TOCKNER B., T. KOCHER, S. HAINZL, J. REICHELT, J. W. BAUER, U. KOLLER, AND E. M. MURAUER. 2016. 'Construction and Validation of an RNA Trans-Splicing Molecule Suitable to Repair a Large Number of COL7A1 Mutations'. *Gene Therapy 23 (11): 775–84.*

TOGO SHINSAKU, TADASHI SATO, HISATOSHI SUGIURA, XINGQI WANG, HESHAM BASMA, AMY NELSON, XIANGDE LIU, TOM W. BARGAR, JOHN G. SHARP, AND STEPHEN I. RENNARD. 2011. 'Differentiation of Embryonic Stem Cells into Fibroblast-like Cells in Three-Dimensional Type i Collagen Gel Cultures'. *In Vitro Cellular and Developmental Biology - Animal 47 (2): 114–24.*

TOLAR JAKUB, ISHIDA YAMAMOTO AKEMI, MEGAN RIDDLE, RON T. MCELMURRY, MARK OSBORN, LILY XIA, TROY LUND, et al. 2009. 'Amelioration of Epidermolysis Bullosa by Transfer of Wild-Type Bone Marrow Cells'. *Blood 113 (5): 1167–74.*

TOLAR JAKUB, JOHN A. MCGRATH, LILY XIA, MEGAN J. RIDDLE, CHRIS J. LEES, CINDY EIDE, DOUGLAS R. KEENE, et al. 2014. 'Patient-Specific Naturally Gene-Reverted Induced Pluripotent Stem Cells in Recessive Dystrophic Epidermolysis Bullosa'. *Journal of Investigative Dermatology 134 (5): 1246–54.*

TOLAR JAKUB, LILY XIA, CHRIS J. LEES, MEGAN RIDDLE, AMBER MCELROY, DOUGLAS R. KEENE, TROY C. LUND, et al. 2013. 'Keratinocytes from Induced Pluripotent Stem Cells in Junctional Epidermolysis Bullosa'. *Journal of Investigative Dermatology 133(2):562-5.*

TOLAR JAKUB, LILY XIA, MEGAN J RIDDLE, CHRIS J LEES, CINDY R EIDE, RON T MCELMURRY, MATTHIAS TITEUX, et al. 2011. 'Induced Pluripotent Stem Cells from Individuals with Recessive Dystrophic Epidermolysis Bullosa'. *Journal of Investigative Dermatology 131 (4): 848–56*.

TORKELSON J.L., C. HANSEN, J. JACKOW, Z. GUO, H. HUI-ZHEN, R. HAYASHI, B. SALLEE, ET AL. 2019. 'Scalable Production of CRISPR-Corrected Autologous IPSC Derived Skin Grafts to Treat Epidermolysis Bullosa'. *Journal of Investigative Dermatology 139 (5): S179.*

TROY, TAMMY CLAIRE, AND KURSAD TURKSEN. 2005. 'Commitment of Embryonic Stem Cells to an Epidermal Cell Fate and Differentiation in Vitro'. *Developmental Dynamics 232 (2): 293–300.*

TSAI SHENGDAR Q, NHU T NGUYEN, JOSE MALAGON-LOPEZ, VED V TOPKAR, MARTIN J ARYEE, AND J KEITH JOUNG. 2017. 'CIRCLE-Seq: A Highly Sensitive in Vitro Screen for Genome-Wide CRISPR–Cas9 Nuclease off-Targets'. *Nature Methods 14 (6): 607–14.*

TSAI SHENGDAR Q, ZONGLI ZHENG, NHU T NGUYEN, MATTHEW LIEBERS, VED V TOPKAR, VISHAL THAPAR, NICOLAS WYVEKENS, et al. 2015. 'GUIDE-Seq Enables Genome-Wide Profiling of off-Target Cleavage by CRISPR-Cas Nucleases' *Nat Biotechnol 33(2):187-197.*

TURCHIANO GIANDOMENICO, GEOFFROY ANDRIEUX, JULIA KLERMUND, GEORGES BLATTNER, VALENTINA PENNUCCI, MELINA EL GAZ, GIANNI MONACO, et al. 2021. 'Quantitative Evaluation of Chromosomal Rearrangements in Gene-Edited Human Stem Cells by CAST-Seq'. *Cell Stem Cell 18;S1934-5909(21)00052-7.*

TURCZYNSKI SANDRINA, MATTHIAS TITEUX, LAURE TONASSO, AUDREY DÉCHA, AKEMI ISHIDA-YAMAMOTO, AND ALAIN HOVNANIAN. 2016. 'Targeted Exon Skipping Restores Type VII Collagen Expression and Anchoring Fibril Formation in an In Vivo RDEB Model'. *Journal of Investigative Dermatology 136 (12): 2387–95.*

TWAROSKI K., C. EIDE, M.J. RIDDLE, L. XIA, C.J. LEES, W. CHEN, W. MATHEWS, D.R. KEENE, J.A. MCGRATH, AND J. TOLAR. 2019. 'Revertant Mosaic Fibroblasts in Recessive Dystrophic Epidermolysis Bullosa'. *British Journal of Dermatology 181(6):1247-1253*.

UCHIDA NAOYA, RASHIDAH GREEN, JOSIAH BALLANTINE, LUKE P. SKALA, MATTHEW M. HSIEH, AND JOHN F. TISDALE. 2016. 'Kinetics of Lentiviral Vector Transduction in Human CD34+ Cells'. *Experimental Hematology 44 (2): 106–15.*

UMEGAKI-ARAO NORIKO, ANNA M.G. PASMOOIJ, MUNENARI ITOH, JANE E. CERISE, ZONGYOU GUO, BRYNN LEVY, ANTONI GOSTYÑSKI, LISA R. ROTHMAN, MARCEL F. JONKMAN, AND ANGELA M. CHRISTIANO. 2014. 'Induced Pluripotent Stem Cells from Human Revertant Keratinocytes for the Treatment of Epidermolysis Bullosa'. *Science Translational Medicine 26;6(264):264ra164*.

URNOV FYODOR D., EDWARD J. REBAR, MICHAEL C. HOLMES, H. STEVE ZHANG, AND PHILIP D. GREGORY. 2010. 'Genome Editing with Engineered Zinc Finger Nucleases'. *Nature Reviews Genetics 11 (9): 636–46.*

UTIKAL JOCHEN, NIMET MAHERALI, WARAKORN KULALERT, AND KONRAD HOCHEDLINGER. 2009. 'Sox2 Is Dispensable for the Reprogramming of Melanocytes and Melanoma Cells into Induced Pluripotent Stem Cells'. *Journal of Cell Science 122 (19): 3502–10.*

VENUGOPAL SUPRIYA S., WENFEI YAN, JOHN W. FREW, HEATHER I. COHN, LESLEY M. RHODES, KIM TRAN, WEI MELBOURNE, et al. 2013. 'A Phase II Randomized Vehicle-Controlled Trial of Intradermal Allogeneic Fibroblasts for Recessive Dystrophic Epidermolysis Bullosa'. *Journal of the American Academy of Dermatology 69 (6): 898–908.e7.*

VUONG TUAN ANH, SANG JIN LEE, YOUNG EUN LEEM, JAE RIN LEE, GYU UN BAE, AND JONG SUN KANG. 2019. 'SGTb Regulates a Surface Localization of a Guidance Receptor BOC to Promote Neurite Outgrowth'. *Cellular Signalling 55: 100–108.*

WAGNER JOHN E., AKEMI ISHIDA-YAMAMOTO, JOHN A. MCGRATH, MARIA HORDINSKY, DOUGLAS R. KEENE, DAVID T. WOODLEY, MEI CHEN, et al. 2010. 'Bone Marrow Transplantation for Recessive Dystrophic Epidermolysis Bullosa'. *New England Journal of Medicine 363 (7): 629–39.*

WALKO GERNOT, MARIA J. CASTAÑÓN, AND GERHARD WICHE. 2015. 'Molecular Architecture and Function of the Hemidesmosome'. *Cell and Tissue Research 360(2):363-78.*

WARREN LUIGI, PHILIP D. MANOS, TIM AHFELDT, YUIN HAN LOH, HU LI, FRANK LAU, WATARU EBINA, et al. 2010. 'Highly Efficient Reprogramming to Pluripotency and Directed Differentiation of Human Cells with Synthetic Modified MRNA'. *Cell Stem Cell 7 (5): 618–30.*

WASIK AGATA M., JERZY GRABAREK, ALEKSANDAR PANTOVIC, ARTUR CIEŚLAR-POBUDA, HAMID R. ASGARI, CASPAR BUNDGAARD-NIELSEN, MEHRDAD RAFAT, IAN M.C. DIXON, SAEID GHAVAMI, AND MAREK J. ŁOS. 2014. 'Reprogramming and Carcinogenesis-Parallels and Distinctions'. In *International Review of Cell and Molecular Biology*, *308:167–203.*

WATABE TETSURO, AND KOHEI MIYAZONO. 2009. 'Roles of TGF-β Family Signaling in Stem Cell Renewal and Differentiation'. *Cell Research 19(1):103-15.*

WATERMAN ELIZABETH A., NORIYASU SAKAI, NGON T. NGUYEN, BASIL A.J. HORST, DALLAS P. VEITCH, CLARA N. DEY, SUSANA ORTIZ-URDA, PAUL A. KHAVARI, AND M. PETER MARINKOVICH. 2007. 'A Laminin-Collagen Complex Drives Human Epidermal Carcinogenesis through Phosphoinositol-3-Kinase Activation'. *Cancer Research 67 (9): 4264–70*.

WEBB ANGELA, AMY LI, AND PRITINDER KAUR. 2004. 'Location and Phenotype of Human Adult Keratinocyte Stem Cells of the Skin'. *Differentiation 72 (8): 387–95.*

WEBBER BEAU R., KYLE T. O'CONNOR, RON T. MCELMURRY, ELISE N. DURGIN, CINDY R. EIDE, CHRISTOPHER J. LEES, MEGAN J. RIDDLE, et al. 2017. 'Rapid Generation of COL7A1 Mouse Model of Recessive Dystrophic Epidermolysis Bullosa and Partial Rescue via Immunosuppressive Dermal Mesenchymal Stem Cells'. *Laboratory Investigation 97 (10): 1218–24.*

WEBBER BEAU R, MARK J OSBORN, AMBER N MCELROY, KIRK TWAROSKI, CARA-LIN LONETREE, ANTHONY P DEFEO, LILY XIA, et al. 2016. 'CRISPR/Cas9-Based Genetic Correction for Recessive Dystrophic Epidermolysis Bullosa'. *NPJ Regenerative Medicine 1 (1): 16014.*

WERNER SABINE, AND HANS SMOLA. 2001. ‘Paracrine Regulation of Keratinocyte Proliferation and Differentiation’. *Trends in Cell Biology 11(4):143-6.*

WERTHEIM-TYSAROWSKA KATARZYNA, AGNIESZKA SOBCZYŃSKA-TOMASZEWSKA, CEZARY KOWALEWSKI, MICHAŁ SKROŃSKI, GRZEGORZ ŚWIĘĆKOWSKI, ANNA KUTKOWSKA-KAŹMIERCZAK, KATARZYNA WOZŃIAK, AND JERZY BAL. 2012. ‘The COL7A1 Mutation Database’. *Human Mutation 33(2):327-31.*

WILGUS TRACI A., AND BRIAN C. WULFF. 2014. ‘The Importance of Mast Cells in Dermal Scarring’. *Advances in Wound Care 3 (4): 356–65.*

WILSON LAURENCE O W, AIDAN R O BRIEN, AND DENIS C BAUER. 2018. ‘The Current State and Future of CRISPR-Cas9 GRNA Design Tools’. *Front Pharmacol 12;9:749*.

WONG TRACY, LUKE GAMMON, LU LIU, JEMIMA E. MELLERIO, PATRICIA J.C. DOPPING-HEPENSTAL, JOHN PACY, GEORGE ELIA, et al. 2008. ‘Potential of Fibroblast Cell Therapy for Recessive Dystrophic Epidermolysis Bullosa’. *Journal of Investigative Dermatology 128 (9): 2179–89.*

WOODLEY DAVID T., TOM ATHA, YI HUANG, MEI CHEN, GERALD G. KRUEGER, CYNTHIA M. JORGENSEN, JANET A. FAIRLEY, LAWRENCE CHAN, AND DOUGLAS R. KEENE. 2003. ‘Normal and Gene-Corrected Dystrophic Epidermolysis Bullosa Fibroblasts Alone Can Produce Type VII Collagen at the Basement Membrane Zone’. *Journal of Investigative Dermatology 121 (5): 1021–28.*

WOODLEY DAVID T., DOUGLAS R. KEENE, TOM ATHA, YI HUANG, RAMIN RAM, NORIYUKI KASAHARA, AND MEI CHEN. 2004. ‘Intradermal Injection of Lentiviral Vectors Corrects Regenerated Human Dystrophic Epidermolysis Bullosa Skin Tissue in Vivo’. *Molecular Therapy 10 (2): 318–26.*

WOODLEY DAVID T, JENNIFER REMINGTON, YI HUANG, YINGPING HOU, WEI LI, DOUGLAS R KEENE, AND MEI CHEN. 2007. ‘Intravenously Injected Human Fibroblasts Home to Skin Wounds, Deliver Type VII Collagen, and Promote Wound Healing’. *Molecular Therapy 15 (3): 628–35.*

WU QIUSHUANG, SANTIAGO GERARDO MEDINA, GOPAL KUSHAWAH, MICHELLE LYNN DEVORE, LUCIANA A. CASTELLANO, JACQELYN M. HAND, MATTHEW WRIGHT, AND ARIEL ALEJANDRO BAZZINI. 2019. 'Translation Affects MRNA Stability in a Codon-Dependent Manner in Human Cells'. *ELife 23;8:e45396.*

WU WENBO, ZHIWEI LU, FEI LI, WENJIE WANG, NANNAN QIAN, JINZHI DUAN, YU ZHANG, FENGCHAO WANG, AND TING CHEN. 2017. 'Efficient in Vivo Gene Editing Using Ribonucleoproteins in Skin Stem Cells of Recessive Dystrophic Epidermolysis Bullosa Mouse Model'. *Proceedings of the National Academy of Sciences 114 (7): 1660–65.*

XIN HUHU, TAO WAN, AND YUAN PING. 2019. 'Off-Targeting of Base Editors: BE3 but Not ABE Induces Substantial off-Target Single Nucleotide Variants'. *Signal Transduction and Targeted Therapy 12;4:9.*

XU CHUNHUI, JIANJIE JIANG, VIRGINIE SOTTILE, JIM MCWHIR, JANE LEBKOWSKI, MELISSA K CARPENTER 2004. 'Immortalized Fibroblast-Like Cells Derived from Human Embryonic Stem Cells Support Undifferentiated Cell Growth'. *Stem Cells 22 (6): 972–80.*

XU HAN, TENGFEI XIAO, CHEN HAO CHEN, WEI LI, CLIFFORD A. MEYER, QIU WU, DI WU, et al. 2015. 'Sequence Determinants of Improved CRISPR SgRNA Design'. *Genome Research 25 (8): 1147–57.*

XU XIAOYUN, DONGBING GAO, PING WANG, JIAN CHEN, JINXUE RUAN, JIE XU, AND XIAOFENG XIA. 2018. 'Efficient Homology-Directed Gene Editing by CRISPR/Cas9 in Human Stem and Primary Cells Using Tube Electroporation'. *Scientific Reports 8 (1): 1–11.*

YANG ANNIE, RONEN SCHWEITZER, DEQIN SUN, MOURAD KAGHAD, NANCY WALKER, RODERICK T. BRONSON, CLIFF TABIN, et al. 1999. 'P63 Is Essential for Regenerative Proliferation in Limb, Craniofacial and Epithelial Development'. *Nature 398 (6729): 714–18.*

YANG LEI, XIAOHUI ZHANG, LIREN WANG, SHUMING YIN, BIYUN ZHU, LING XIE, QIUHUI DUAN, et al. 2018. 'Increasing Targeting Scope of Adenosine Base Editors in Mouse and Rat Embryos through Fusion of TadA Deaminase with Cas9 Variants'. *Protein and Cell 9 (9): 814–19.*

YANG LUHAN, MARC GUELL, SUSAN BYRNE, JOYCE L. YANG, ALEJANDRO DE LOS ANGELES, PRASHANT MALI, JOHN AACH, et al. 2013a. 'Optimization of Scarless Human Stem Cell Genome Editing'. *Nucleic Acids Research 41 (19): 9049–61.*

YANG RUIFENG, YING ZHENG, MICHELLE BURROWS, SHUJING LIU, ZHI WEI, ARBEN NACE, WEI GUO, SURESH KUMAR, GEORGE COTSARELIS, AND XIAOWEI XU. 2014. 'Generation of Folliculogenic Human Epithelial Stem Cells from Induced Pluripotent Stem Cells'. *Nature Communications 5:3071.*

YEH WEI HSI, HAO CHIANG, HOLLY A. REES, ALBERT S.B. EDGE, AND DAVID R. LIU. 2018. 'In Vivo Base Editing of Post-Mitotic Sensory Cells'. *Nature Communications 9 (1): 1–10.*

YU JUNYING, MAXIM A. VODYANIK, KIM SMUGA-OTTO, JESSICA ANTOSIEWICZ-BOURGET, JENNIFER L. FRANE, SHULAN TIAN, JEFF NIE, et al. 2007. 'Induced Pluripotent Stem Cell Lines Derived from Human Somatic Cells'. *Science 318 (5858): 1917–20.*

YU YI, THOMAS C. LEETE, DAVID A. BORN, LAUREN YOUNG, LUIS A. BARRERA, SEUNG JOO LEE, HOLLY A. REES, GIUSEPPE CIARAMELLA, AND NICOLE M. GAUDELLI. 2020. 'Cytosine Base Editors with Minimized Unguided DNA and RNA Off-Target Events and High on-Target Activity'. *Nature Communications 11 (1): 1–10.*

YY LI, HANNA GJ, LAGA AC, HADDAD RI, LORCH JH, HAMMERMAN PS. 2015. 'Genomic Analysis of Metastatic Cutaneous Squamous Cell Carcinoma'. *Clinical Cancer Research : An Official Journal of the American Association for Cancer Research* 21 (6): 1447–56.

ZAFRA MARIA PAZ, EMMA M. SCHATOFF, ALYNA KATTI, MIGUEL FORONDA, MARCO BREINIG, ANABEL Y. SCHWEITZER, AMBER SIMON, et al. 2018. 'Optimized Base Editors Enable Efficient Editing in Cells, Organoids and Mice'. *Nature Biotechnology 36 (9): 888–96*

ZENG MING, FATMA ALSHEHRI, DEZHONG ZHOU, IRENE LARA-SAÉZ, XI WANG, XIAOLIN LI, QIAN XU, JING ZHANG, AND WENXIN WANG. 2019. 'Efficient and Robust Highly Branched Poly(β-Amino Ester)/Minicircle COL7A1 Polymeric Nanoparticles for Gene Delivery to Recessive Dystrophic Epidermolysis Bullosa Keratinocytes'. *ACS Appl. Mater. Interfaces* 11:30661–72.

ZHANG JIAN-PING, XIAO-LAN LI, AMANDA NEISES, WANQIU CHEN, LIN-PING HU, GUANG-ZHEN JI, JUN-YAO YU, et al. 2016. 'Different Effects of SgRNA Length on CRISPR-Mediated Gene Knockout Efficiency'. *Scientific Reports 24;6:28566*.

ZHAO YANGBING, ZHILI ZHENG, CYRILLE J. COHEN, LUCA GATTINONI, DOUGLAS C. PALMER, NICHOLAS P. RESTIFO, STEVEN A. ROSENBERG, AND RICHARD A. MORGAN. 2006. 'High-Efficiency Transfection of Primary Human and Mouse T Lymphocytes Using RNA Electroporation'. *Molecular Therapy 13 (1): 151–59*.

ZHOU CHANGYANG, YIDI SUN, RUI YAN, YAJING LIU, ERWEI ZUO, CHAN GU, LINXIAO HAN, ET AL. 2019. 'Off-Target RNA Mutation Induced by DNA Base Editing and Its Elimination by Mutagenesis'. *Nature 571 (7764): 275–78.*

ZHOU HONGYAN, SHILI WU, JIN YOUNG JOO, SAIYONG ZHU, DONG WOOK HAN, TONGXIANG LIN, SUNIA TRAUGER, et al. 2009. 'Generation of Induced Pluripotent Stem Cells Using Recombinant Proteins'. *Cell Stem Cell 8;4(5):381-4*.

ZUO ERWEI, YIDI SUN, WU WEI, TANGLONG YUAN, WENQIN YING, HAO SUN, LIYUN YUAN, LARS M. STEINMETZ, YIXUE LI, AND HUI YANG. 2019. 'Cytosine Base Editor Generates Substantial Off-Target Single-Nucleotide Variants in Mouse Embryos'. *Science 364 (6437): 289–92.*